Uncertainty Propagation, Control, and Estimation of Stochastic Dynamic Systems Using Generalized Polynomial Chaos Expansion

by

RAJNISH BHUSAL

Presented to the Faculty of the Graduate School of
The University of Texas at Arlington in Partial Fulfillment
of the Requirements
for the Degree of

DOCTOR OF PHILOSOPHY

THE UNIVERSITY OF TEXAS AT ARLINGTON

August 2021

To

my parents,

Meena and Baikuntha Bhusal,

my uncle, Moti Bhusal,

and my little sister, Deepti,

who have always been my emotional anchor.

Acknowledgements

This dissertation is the culmination of my journey as a Ph.D. student, which has been indeed a life-changing experience. This would not have been possible without the support and guidance I received from several individuals. First of all, I am sincerely thankful and indebted to my advisor, Dr. Kamesh Subbarao, for believing in me and bringing me up academically. He has taught me everything I know today in this field, and my work would not have been possible without his patience and support. His guidance, which is often beyond the scope of academia, has been an invaluable asset to me and is the one I will always treasure.

I am thankful to my committee members Dr. Alan P. Bowling, Dr. Bo P Wang, Dr. Animesh Chakravarthy, and Dr. Andrzej Korzeniowski, for their academic lessons and advice. I have been very fortunate to have them and many other teachers and professors advise me and inspire in me a drive to do well since my early years in grade school through graduate school. My Ph.D. research has been funded in part by the Office of Naval Research (award no. N00014-18-1-2215), and I am grateful for the support.

Moreover, I would like to extend my sincere thanks to the administrative staff of the Mechanical and Aerospace Engineering Department, especially Debi Barton, Lanie Gordon, Wendy Ryan, and Ayesha Fatima, for their unwavering support and dedication.

I would also like to thank my colleagues, Pengkai, Paul, Murali, Denish, Roopak, Karan, Ameya, Mitchell, Abel, Katiyayni, Baris, Cem, Kashish, Shobhit, and Saina from Aerospace Systems Laboratory (ASL) in particular for their discussions, advice,

and friendship over the years. Further, it is important for me to mention my lab mate, Diganta Bhattacharjee, from ASL separately. Diganta has helped me develop a better understanding of mathematics and controls during our many conversations about my research. I am also thankful to two of my dearest friends, Vedant and Rahul, for all the fun times we had during my time at UTA. I would like to thank my cousin brother, Raju Bhusal, for lending a shoulder to lean on whenever I needed one. Further, it is important for me to mention Pawan and Sudipt, who have been brothers to me and have always extended their unconditional support and friendship for all these years. I feel privileged to have the company of Sudip, Manoj, Puja, Bhuwan, Richa, Luna, Karuna, Keshav, and Manish, who made these five years an enjoyable and memorable experience. Especially, Anveshika, Shreya, Sadiksha, and Abhishek, I feel fortunate to have come across you in Reva; thank you for always being there for me.

My family was always there for me to cheer me up and help me figure life out as I faced new challenges, and my utmost gratitude goes to them. This degree would have been unattainable without the love, faith, and patience from my grandparents, my parents, my aunt, and my sister. Most importantly, I am thankful to my little brother, Mission Bhusal, whose love for me has been a constant source of inspiration for all these years. I should apologize to him for being thousands of miles away and not playing cricket with him. And, lastly, I am greatly indebted to my uncle, Moti Prasad Bhusal, who planted and nurtured my love for science, without whom this dissertation would have never come into existence.

July 23, 2021

Abstract

Uncertainty Propagation, Control, and Estimation of Stochastic Dynamic Systems Using Generalized Polynomial Chaos Expansion

Rajnish Bhusal, Ph.D.

The University of Texas at Arlington, 2021

Supervising Professor: Kamesh Subbarao

In recent years, uncertainty propagation has emerged as an important research area in the field of dynamical systems. The growing interest in this area arises out of the need to develop computationally efficient approaches to predict the evolution of a system subject to uncertainties. To this end, this dissertation is focused on developing computational frameworks for uncertainty propagation, control, and state estimation of stochastic dynamical systems using the generalized polynomial chaos (gPC) expansion technique.

In the first part of this dissertation, the construction of gPC expansion is presented in general. The novelty of this dissertation lies in developing a mixed sparse grid quadrature technique to carry out computationally efficient uncertainty propagation in dynamical systems wherein the random variables are governed by different (or a mixture of) probability distribution types. Additionally, the proposed quadrature technique in the gPC expansion framework is utilized to study the sensitivity of the system output to the uncertain input variables. Subsequently, this work integrates the idea of uncertainty propagation with those of model data-fusion and optimal con-

trol theory for state estimation and robust control, respectively, of stochastic systems subject to parametric uncertainties.

Furthermore, the stability margin of a group of cooperative unmanned vehicles is examined in a multi-agent system setting. In this regard, a unified framework is proposed to study the consensus of multi-agent systems with multiplicative uncertainties in the feedback path of agents. The proposed technique provides performance indices that measure the robustness of the networked group of agents to gain, phase, and input delay perturbations. Finally, the dissertation studies the consensus problems in multi-agent systems wherein the information exchange between the agents is affected by non-uniform time-varying delays in the network.

The proposed frameworks are applied to various benchmark problems and real-world applications, including the motion of satellites in low-Earth orbits, aeroelastic systems, hypersonic reentry of a spacecraft to Earth, synchronization in the states of short-period dynamics of aircraft, among others.

Table of Contents

List of Illustrations

List of Tables

Chapter 1

Introduction

Mathematical models that simulate real-world physical processes are playing an increasingly crucial role in many branches of science and engineering. These mathematical models often comprise a set of differential and/or integral equations and can be used to understand the evolution of the state of the physical system. Regardless of the underlying mathematical formalism, the computational results from these models always depend on inputs that are uncertain and rely on approximations that introduce errors. With the advancement in technology and a push towards increased automation, quantification and propagation of the uncertainties through models of these dynamical systems have become indispensable to aid the decision-making process. Further, to mitigate the risks associated with the uncertainties, the demand for robust optimization, robust control, and probabilistic estimation has increased. This dissertation provides a computational black-box to carry out the aforementioned tasks in a computationally efficient way. Further, this dissertation focuses on the uncertainty quantification and propagation in the computational models of a group of systems, namely multi-agent systems. In addition, a framework is provided to characterize the stability margins of the multi-agent systems, which quantifies the measure of cooperative robustness of the systems to the external perturbations and time-delays.

1.1 Objectives

The key objectives of this research are summarized as follows:

1. The first objective of this dissertation is to develop a computationally efficient non-intrusive uncertainty propagation technique for general non-linear stochastic systems with initial condition and parametric uncertainties which are characterized by different probability distribution types. In order to achieve this objective, we utilize the approach of pseudospectral collocation in generalized polynomial chaos (gPC) expansion framework. A further goal of this research is to develop an efficient multidimensional quadrature rule in sparse grid setting to handle the mixed distribution of uncertainties.
2. The second objective is to carry out a sensitivity analysis of the response distribution of the stochastic system to the underlying uncertain variables. With regards to this task, gPC expansion-based Sobol' indices are derived using Analysis of Variance (ANOVA) approach.
3. The third objective is to design robust optimal control strategies for stochastic systems with linear dynamics. In order to fulfill this objective, stochastic linear quadratic regulator problems involving expectation performance indices are studied. To that end, a single controller is designed for all possible variations of the random variables within the domain of their probability density functions.
4. Our next objective is to utilize the efficacy of pseudospectral collocation-based gPC expansion technique to develop a state estimator/filter for nonlinear systems. The uncertainties in the system are propagated using gPC expansion technique for the filter. Further, the measurement update is carried out in ensemble Kalman filtering framework. In addition to that, the sensitivity of the posterior density function to the underlying random variables is characterized.
5. Subsequently, this dissertation aims to carry out probabilistic analysis of cooperative control protocols to study the effect of random inputs in the system

of multiple agents. Additionally, the objective is to study the sensitivity of networked multi-agent systems to cyber attacks from malicious intruders.

6. The final objective is to develop a unified framework to characterize the stability margins (gain margin and phase margin) and uniform input delay margin of a general linear multi-agent system for consensus. Moreover, the delay margin of a linear multi-agent system with non-uniform time-varying communication delays is computed.

1.2 Background and Motivation

In this section, the background and motivation of various components of the research are summarized.

1.2.1 Uncertainty Propagation Using Generalized Polynomial Chaos Expansion

This research presents the use of generalized polynomial chaos expansion for the propagation of uncertainties that are inherent in various dynamic system models in different forms. These stochastic dynamic models are pertinent in various engineering fields which include space situational awareness (tracking and data association related to resident space objects, conjunction assessment), relative navigation scenarios (target tracking, formation flying among aircraft, and autonomous rendezvous and docking of spacecraft), among others. In order to make informed decisions in preventing hazards and to mitigate the risks, it is of utmost importance to accurately characterize the uncertainties, study their evolution through probabilistic/statistical approaches, and analyze their impact on model response. To that end, a general framework that highlights the steps involved in uncertainty study of stochastic dynamical systems is illustrated in Figure 1.1.

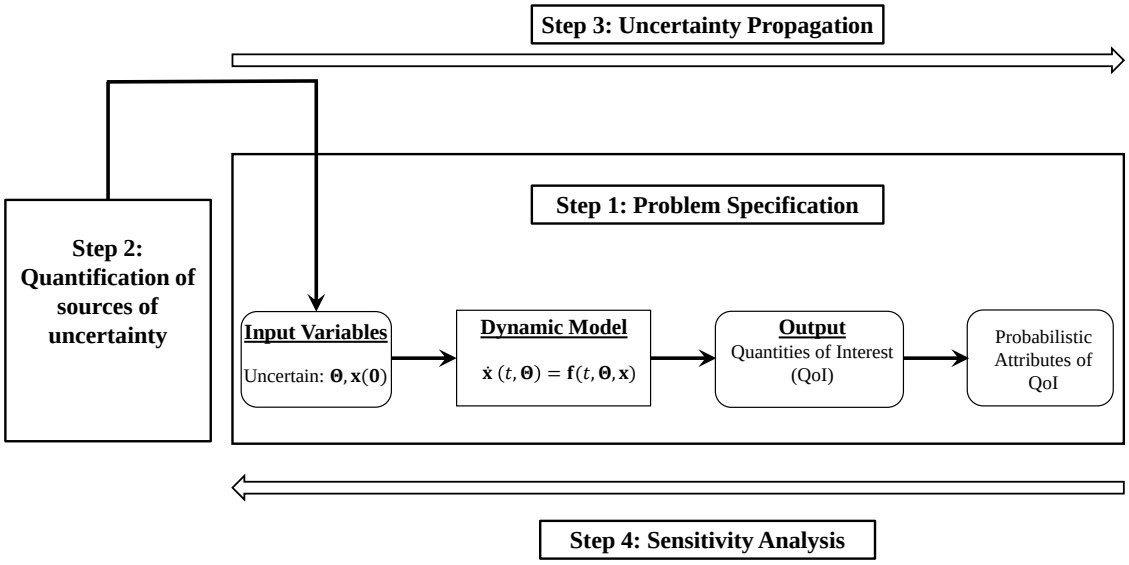

Figure 1.1: Framework for uncertainty study in stochastic systems

As shown in Figure 1.1, the first step towards uncertainty study in stochastic systems involves developing a mathematical model for the system in the form of differential equations. Additionally, the quantities of interest (QoI) are chosen whose probabilistic content needs to be determined.

Next step is that of *uncertainty quantification*, which helps in determining the sources and distribution of the uncertainties and underlying random variables, respectively. In general, uncertainty quantification can be defined as the process of quantifying uncertainties associated with model calculations of true, physical quantities of interest, with the goals of accounting for all relevant sources of uncertainty and quantifying the contributions of specific sources to overall uncertainty [1]. Common sources of uncertainty include uncertainties in the model parameters, uncertainties in the model initial conditions, as well as uncertainties in the mathematical form of the models. Further, reliable probabilistic models of the input random variables are also built based on the available information from various sources (e.g., expert

judgment on the problem, data bases and literature, physical arguments, and existing measurements/observations).

Moreover, the consideration of uncertainty in the mathematical model makes the model stochastic and therefore, the governing differential equations with uncertainties are termed as stochastic differential equations (SDEs). Next step towards uncertainty study involves *uncertainty propagation*, which is essential to transform the uncertainty measure associated with the input random variables onto a measure of uncertainty for the QoI of the model. In this step, the SDEs governing the stochastic system are propagated in time and the probabilistic content of QoI is characterized in the form of

(i) confidence intervals on the QoI,

(ii) quantile of the QoI,

(iii) probabilities of exceedance of a safety threshold or of an event of interest,

(iv) mean, variance and higher order moments of the QoI,

(v) probability density function of the QoI.

The sensitivity analysis step refers to the computation of so-called sensitivity or importance indices of the components of the random variable with respect to a given probabilistic content of the QoI. In other words, the sensitivity analysis studies the contribution of uncertainty of each model input to the uncertainty of the QoI and identifies the dominant contributors.

In this dissertation, we focus on uncertainty propagation and sensitivity analysis aspects for the study of uncertainties and their impacts in stochastic dynamical systems. The most general approach to study the propagation of uncertainties in dynamical systems is through the solutions of SDEs. Unlike ordinary differential equations (ODEs) for deterministic models, which have a unique solution for each appropriate initial condition, the solution to SDEs are stochastic processes. Prob-

ability density function (PDF) is generally used to characterize each realization of these stochastic processes [2]. The most commonly employed approach to simulate an SDE is the Monte Carlo simulation (MCS) technique, which relies on sampling a finite number (say, equal to N) of random variables from their PDFs. The Monte Carlo simulation method, while being highly accurate to estimate statistical moments as well as PDFs of QoI, has an error convergence rate which is inversely proportional to the square root of the number of samples drawn (i.e., $O(1/\sqrt{N})$). Hence, this method can become intractable for computationally demanding models [3]. Alternatively, Fokker-Planck (FP) equations provide means to accurately capture the time evolution of the PDF of the SDEs; solution, however FP equations are only applicable to Brownian [4] or Lévy [5] diffusion type of SDEs. Perturbation approach and weighted integral method are among few other efficient techniques that have been developed in literature to solve the problem of uncertainty propagation, but are limited to estimating first two statistical moments of the distribution [6]. Though moment equations approach can be used to estimate higher order moments, statistical moment equations suffer from the well-known closure problem and require closure approximations which may induce huge errors in estimating moments for systems with high nonlinearities [7].

In this context, meta-modeling is a very relevant approach which involves building a surrogate of the model that makes it more feasible to create large number of samples for MCS and improve the accuracy of the solution without incurring a huge computational burden. In recent years, the polynomial chaos expansion framework has been extensively used as a meta-modeling technique to carry out uncertainty quantification and propagation [8–10]. The polynomial chaos expansion technique was originally developed by Norbert Wiener [11] in 1938. Using Hermite polynomials, Wiener constructed an orthonormal random basis for expanding nonlinear functionals

of the Brownian motion (homogeneous chaos), and used it to study problems in statistical mechanics. Wiener's homogeneous chaos was further refined by Cameron and Martin [12] in 1947 by expanding nonlinear functionals in terms of Fourier-Hermite functionals, and Itô [13] in 1951 by introducing Itô integrals. Moreover, Ghanem and Spanos [14] in 1991 pioneered the polynomial chaos expansion technique by designing a new numerical method for solving nonlinear functionals with random coefficients. Using Karhunen-Loeve expansion, they first expanded the random coefficients as a series of Gaussian random variables, followed by representing the random solution as a Hermite expansion of the Gaussian random variables. While the approach of expanding random coefficients using Hermite polynomials guarantees optimal convergence rate for Gaussian and near Gaussian random fields, representing non-Gaussian processes with Hermite polynomials cause difficulties with convergence.

As a remedy to this problem, gPC expansion was introduced by Xiu and Karniadakis [15] in 2002. The gPC expansion is based on the principle of projecting the random solution onto a basis of polynomials which are orthogonal to the PDF of the input random variables. The orthogonal polynomials for the random variables are selected from the Askey scheme [15] based on the distribution of the random variables. Therefore, the problem of generating solutions for stochastic differential equations is reduced to computing the coefficients of the expansion. Ghanem et al. introduced the concept of Stochastic Galerkin projection-based polynomial chaos expansion which are suited to various stochastic engineering problems [14]. However, the Galerkin projection technique always requires specific algebraic developments to formulate the system of equations for each new class of problems and can not be used as a black box simulator; hence it is often labeled as "intrusive". Another approach to compute the coefficients required for gPC expansion is the sampling-based non-intrusive gPC expansion. Xiu et al. [16] proposed a class of non-intrusive techniques called stochastic

collocation method that combines the strengths of Monte Carlo methods and stochastic Galerkin methods. The major challenge in the case of stochastic collocation is the selection of collocation nodes which in turn requires efficient quadrature techniques to compute the coefficients of the polynomials for the expansion. Gaussian quadrature tensor grids which are formed by tensor products of one-dimensional quadrature rules are inefficient to use as the number of points increases exponentially with number of dimensions, an issue that is often termed as the *curse of dimensionality* [17]. The Sparse grid (SG)-based cubature rules proposed by Smolyak [18] alleviates the issue of curse of dimensionality and is often used in the literature for computational efficiency. Congedo et al. [19] have compared the computational cost and accuracy of several sparse grid-based techniques for evaluating the coefficients of the polynomial chaos expansion for multi-dimensional stochastic problems. Similarly, Jones et al. introduced the gPC expansion approach based on Gaussian Hermite tensor grid and sparse grid collocation nodes in the nonlinear propagation of orbit uncertainty [20]. Propagation and sensitivity analysis of the uncertainties affecting the lifetime of an object in low Earth orbit (LEO) using polynomial interpolation-based gPC expansion was carried out by Dell'Elce and Kerschen [21]. Recently, Adurthi et al. [22] proposed the concept of conjugate unscented transform (CUT)-based quadrature technique and Madankan et al. [23] made use of CUT-based quadrature for developing gPC expansion-based minimum variance estimator.

While the gPC technique provides corresponding basis of expansion for various known distributions, relevant works in the literature are centered around the problem where all the random inputs are governed by a single distribution function, either uniform or normal. In many cases, it is erroneous to assume a single distribution function type for all the random variables in the SDE under consideration. For instance, in the context of satellite orbit propagation in low Earth orbits where the

motion of satellites are perturbed by atmospheric drag forces, the frontal area-to-mass ratio in the drag model varies within a certain range, and thus, it is appropriate to model this with a uniform distribution function. On the other hand, initial condition uncertainties can be suitably modeled with normal distribution functions. It is trivial to incorporate independent random variables governed by different probability distributions in gPC expansion framework using the intrusive Galerkin projection and similar work has been carried out by Fisher in [24]. However, using the state of the art in existing literature, this can be only carried out non-intrusively by employing the approach of repetitive simulations with samples generated from random sampling techniques like Monte Carlo, Latin hypercube, etc. which are computationally expensive. Alternatively, solving the aforementioned problem in gPC expansion framework non-intrusively would demand an efficient quadrature technique which can provide quadrature nodes characterizing the joint PDF generated from the mixture of distributions. This motivates us to develop mixed sparse grid-based multi-variable quadrature technique, which is one of the key objectives of this research.

Moreover, it is intuitive to understand that different variables influence the response PDF of a stochastic system in different ways. Out of all the variables, some have insignificant influence on the response of the system and these parameters can be modeled less precisely than the ones which generate significant effects. However, the relevant variables need to be distinguished and estimated with high accuracy. Sensitivity analysis is generally carried out using *variance-based global methods*, also known as ANOVA (ANalysis Of VAriance) [25]. The analysis aids us to make informed decisions about the sensitivity of the system to the parameters involved [26]. The Sobol' indices, which are obtained through the use of the Sobol decomposition by separating out different contributions from the associated variables (both individual and collective) serve as determinants for sensitivity analysis [27]. To that end,

polynomial chaos-based Sobol' indices for sensitivity analysis were introduced by Sudret [6]. This further motivates us to carry out sensitivity analysis in the context of uncertainty propagation problems with mixed distribution types.

1.2.2 Stochastic Optimal Control of Linear Systems With Probabilistic Uncertainties

As stated in the previous section, dynamical systems often have to deal with uncertainties in the environment and even suffer from modeling-based uncertainties. This motivates us to consider the problem of designing robust feedback controllers for linear dynamical systems with parametric uncertainties in the stochastic linear quadratic regulator (LQR) framework. Based on the class of uncertainties, robust control formulations can be categorized into being either deterministic or stochastic. A vast majority of the robust control literature relies on deterministic set-based uncertainty descriptions (see [28, 29] and references therein). In this deterministic approach, the controller is designed and analyzed based on worst-case uncertainties, which may lead to sluggish/conservative closed-loop performance if the worst-case realizations have a small probability of occurrence [30, 31]. This has led to a growing interest in considering stochastic robust control approaches, which exploit the probability distribution of the uncertain parameters to design control strategies.

In the literature, the most commonly used stochastic control techniques are suited to deterministic systems with stochastic forcing (or Brownian disturbance) (see [32, 33]). On the other hand, the problem of stochastic control for systems with parametric uncertainties is solved using random sampling (for example, MCS)-based techniques [34, 35]. As stated earlier in the previous section, the computational cost of the MCS-based random sampling approaches can be prohibitively expensive if the uncertainty space is high dimensional. This motivates us to develop a stochastic

control formulation for linear systems using generalized polynomial chaos expansion framework.

In recent years, gPC expansion has been quite extensively used to develop control strategies for stochastic systems. In [36, 37], linear quadratic regulators are designed for stochastic systems with parametric uncertainties using gPC expansion. Similarly, [38] considers the design of H_2 optimal static output feedback control for linear systems using the gPC expansion framework. Further, the gPC expansion approach has also been used to design model predictive control strategies for stochastic systems (see [30,31]). However, all of these works develop the control formalism using the Galerkin projection method to compute the coefficients of gPC expansion. In [39], the parameters in the linear-parameter varying systems are assumed to be uncertain, and parameter-dependent feedback controllers are designed using the gPC expansion technique. Different from the aforementioned works, [39] considers the computation of the coefficients of the gPC expansion using the Lagrange interpolation approach in the framework of stochastic collocation. To the best of our knowledge, stochastic control of linear systems using the pseudospectral collocation-based gPC expansion has not been formulated in the existing literature.

1.2.3 Generalized Polynomial Chaos-Based Ensemble Kalman Filtering

Precise estimation of the system states plays a vital role in many engineering applications, for example, robot navigation [40], spacecraft tracking [41], process monitoring [42], among others. State estimation involves both estimation and filtering using the governing system of equations and noisy observations of the system from available sensors [43]. In real world situations, both the dynamical model and measurement model are significantly nonlinear. Often, the parameters of the sys-

tem are also not known precisely, and the uncertain parameters have non-Gaussian distributions.

In the context of linear systems with Gaussian assumptions on noise, the Kalman filter is the optimal and it provides recursive equations for a finite set of parameters (e.g., means and covariances) that capture the time evolution of the conditional distribution of the state given the measurements. The filtering problem for nonlinear systems is considerably more difficult, and the evolution of the conditional distribution cannot be captured by a finite set of parameters. Further, the solution to the general nonlinear filtering problem requires solving infinite-dimensional stochastic evolution equations. In literature, one can find various algorithms to generate solutions to the nonlinear filtering problem using numerical approximations to the infinite-dimensional problem. Extended Kalman filter (EKF), Unscented Kalman filter (UKF) [44], and Ensemble Kalman filter (EnKF) [45] are some of the widely used Kalman-type nonlinear filters in the Gaussian paradigm. In the EKF, the PDF of the state is approximated by a Gaussian random variable, which is then propagated analytically through the first-order linearization of the nonlinear system. In the presence of severe nonlinearities and high noise intensities, the EKF can suffer from divergence of the state estimates which is a major drawback of the algorithm [46]. In the UKF, a set of sigma sample points produced by the unscented transformation captures the Gaussian random variable, which approximates the state distribution. These sigma points completely capture the true mean and covariance of the random variable, and when propagated through the true nonlinear system, captures the posterior mean and covariance accurately upto the third order (Taylor series expansion) for all nonlinearities. In EnKF, sets of ensemble realizations are generated using the Monte Carlo (MC) sampling for the initial state, process noise, and measurement noise. Ensemble members are then propagated in time by solving the nonlinear model equations to

obtain the predicted state estimates and are corrected by an approximate Kalman filter scheme upon arrival of measurements. Though EnKF avoids the linearization of the model dynamics and observation model, it leads to inaccuracies due to numerical errors from random MC sampling [47]. Note that the aforementioned nonlinear filters have difficulties dealing with the non-Gaussian probability distributions of the random variable.

In recent years, stochastic estimation of nonlinear and non-Gaussian dynamical systems has received considerable attention in the literature. One of the extensively used nonlinear filters to solve state estimation problems with non-Gaussian uncertainties is the Gaussian sum filter (GSF) [48, 49]. GSF is able to account for large deviations from Gaussianity and approximates the non-Gaussian conditional density function as a weighted sum of Gaussian mixture model (GMM) [46]. However, for highly nonlinear systems, suitable adaptation techniques need to be developed to update the weights of the Gaussian mixture model to better approximate the posterior density function, which may further incur high computational cost [50, 51]. Another technique for solving the nonlinear filtering problem is that of *particle filter* (PF) [52]. Here, a cloud of randomly generated particles is propagated using nonlinear system dynamics, and finally, a weighted sum of the propagated particles are used to obtain the state estimates. Like EnKF, particle filters are ensemble-based sequential estimation methods and generally demand a large number of particles be propagated to produce reasonably accurate estimates [53]. Unlike other Gaussian-based filters, particle filters can deal with non-Gaussian probabilities but are not adapted to high-dimensional systems because of particle degeneracy, which leads to higher computational costs [53, 54].

The major challenge with the filters mentioned above lies in the efficient propagation of uncertainties in the filtering process, which can be addressed by developing a

nonlinear filter in the gPC expansion framework. Recently, the use of gPC expansion to develop nonlinear filtering technique has found significant attention. Blanchard et al. [55] developed an EKF-based gPC filter for a nonlinear system with a linear measurement model to estimate the parameters of mechanical systems, in which the state uncertainty propagation was carried out using polynomial chaos expansion, and the Kalman-based update was utilized to obtain the corrected state estimates. Dutta et al. [56] proposed a gPC expansion-based filter in the Bayesian framework for a general nonlinear system by approximating the prior PDF using maximum-entropy estimation theory under GMM approximation. Recently, gPC-based nonlinear filter in the Schmidt-Kalman filter framework has been proposed in [57,58] to solve the state estimation problem under non-Gaussian parametric uncertainties. In literature, various variants of gPC-based ensemble Kalman filters have also been proposed [47, 59, 60]. Computationally efficient ensemble square root Kalman filter and parallelized ensemble Kalman filter in the gPC expansion framework have been developed to estimate the states of a nonlinear system in [47] and [59], respectively. However, the formulations developed in [47, 59] are limited to systems with linear measurement models. In [60], a polynomial chaos-based ensemble Kalman filter has been proposed for nonlinear systems with nonlinear measurement models to estimate the trajectory of a vehicle entering the Mars atmosphere. However, the filter in [60] uses a random sampling technique in an MC-based stochastic collocation framework to compute the coefficients of gPC expansion. This approach demands a large number of random collocation points be generated to obtain gPC solutions for large dimensional systems [61] and thus, reduces the efficacy of the filtering technique. This motivates us to develop ensemble Kalman filter-based state estimator in the pseudospectral collocation-based gPC expansion framework.

1.2.4 Probabilistic Analysis of Consensus Protocols for Uncertain Edge Weights in Multi-Agent Systems

The study of collective behavior of multi-agent systems has drawn significant attention in recent years and is a major focus of current research. Over the past years, a variety of distributed control protocols have been proposed to guarantee the desired coordination among a group of multiple agents. Surveys of most recent advances on these problems can be found in [62–65]. The distributed control protocols proposed in the recent years find their applications in formation control [66], flocking [67], rendezvous of unmanned aerial vehicles [68], attitude synchronization among multiple spacecrafts [69], among others. Moreover, consensus among the group of homogeneous agents has been one of the prime objectives in designing network based local control strategies for the multiple agents. Most of the existing work on distributed coordination of networks of dynamic agents assume that each agent exchanges exact information through an ideal communication channel. Thus, the cooperative control strategies for asymptotic consensus are designed based on deterministic analysis of the problem.

Realistically though, the group of agents interact with each other in a communication constrained environment, prone to uncertainties, and the analysis of the collective behavior of the multi-agent systems in such a context needs to be carried out from the probabilistic point of view. In recent years, there has been some interest in solving consensus problems for the stochastic variants of the networked dynamical system. In [70, 71], consensus seeking protocols have been proposed in an uncertain environment where the agents receive noisy measurements of the states of neighboring agents. For Langrangian networked systems with parametric uncertainties under a directed graph, a distributed adaptive control method with sliding-mode estimators for containment is developed in [72]. However, in the aforementioned studies,

the uncertainty is considered either in the measurement process or in the dynamics of the agents and the parameters governing information flow among the agents are considered to be deterministic. In [73], Hatano et al. provide necessary and sufficient conditions for consensus among stochastic discrete-time linear dynamical systems, assuming a randomly varying network topology which is modeled through the Erdös-Rèyi random graph. Kan et al. [74] have studied the multi-agent consensus problem in a leader-follower architecture where the leaders maintain a constant desired state and the interactions among the follower agents are dictated by a two-state Markov model.. Similar to [73, 74], most of the recent works in multi-agent coordinated control under uncertain interaction environment have been carried out using randomly switching network topology [75, 76]. In contrast, the analysis of consensus protocols for a fixed network topology (among the agents) with uncertain interaction parameters is non-existent to the best of our knowledge. To this end, we provide probabilistic analysis of the consensus control protocols in the scenario where the interaction parameters in a system of interconnected cooperative agents are susceptible to uncertainties.

Related to this is the problem of security in networked systems. With advancements in the communication technologies, multi-agent systems, like all distributed systems, are vulnerable to cyber-attacks. Security of networked systems is a topic which has attracted considerable interest in recent times [77,78]. In a typical scenario, the multi-agent system is susceptible to "command injection" attacks that provide conflicting control commands causing the agents to diverge from desired consensus. These attacks can be cyber attacks via reference signal generated from malicious intruder agents or from any other command generator ground stations. In the presence of such intruders, a huge threat is imposed on the agents, impacting the physical operation of all the agents and/or impairing the outcome of any sensitive operation being carried out by the agents. This motivates us to examine the impact of such

intelligent intruders on the consensus performance of the agents using the same probabilistic analysis framework.

1.2.5 Stability Margin and Uniform Input Delay Margin of Linear Multi-Agent Systems

With increasing applications, studies on the stability and robustness aspects of multi-agent systems are imperative. This dissertation in particular, provides a framework for calculation of stability margin and input delay margin for a group of multiple agents in the networked interconnection. For a single-input single-output (SISO) system, classical input-output stability criteria based on Nyquist, Popov and circle theorems [79] aid to characterize the allowable gain and phase variation (stability margin) in the loop at each frequency and tolerable limits of open-loop modeling errors. Generalizations of the aforementioned theorems to multi-input multi-output (MIMO) systems are not straightforward, and several works such as [80–83] suitably characterize the MIMO stability margins. In the context of multi-agent systems, the stability margin serves as a robustness measure against gain and phase variations for a group of agents. A networked multi-agent system is a multiloop feedback system and with suitable analysis, the aforementioned works to characterize the multiloop stability margin can be extended to the context of multi-agent systems. On that note, Kim [84] characterized the stability margin of SISO multi-agent systems based on the minimum singular value of the loop transfer function matrix and the results of [81]. In [85], the gain margin of SISO multi-agent systems is computed using the Nyquist stability criterion and small-gain theorem [86] while considering additive uncertainty on one of the edge weights of the graph structure. Apart from these works, stability margin-based design strategies have been formulated in the literature to achieve robust consensus in the multi-agent systems. Tonetti and Murray [87] have consid-

ered disturbance rejection-based graph topology-design strategies for continuous-time linear SISO multi-agent systems by calculating gain and phase margins of the interconnected systems upon analyzing the Nyquist curve of the networked sensitivity function matrix. Partitioning a directed networked dynamical system into smaller networks to improve the stability margin of the original network is proposed in [88] for multi-agent systems with SISO agents. Consensus protocols based on dynamic feedback controllers have been designed in [89] and [90] for discrete-time single-input linear multi-agent systems considering gain-phase margin optimization problem. The gain-phase margin optimization problem is solved using an analytic interpolation approach via conformal mappings [91]. Note that all the aforementioned works stem from assuming that each agent is either a SISO system or a single-input system. On the other hand, there have been a limited number of works in the literature to characterize the stability margins of multi-agent systems where underlying agents are governed by high-order MIMO dynamics. The disk margin of discrete-time linear multi-agent systems with MIMO agents has been computed in [92, 93]. However, determining the gain and phase margins of the multi-agent systems where each agent has a general linear dynamics still requires further investigation.

Moreover, multi-agent systems need to exchange information among agents over a communication network, which is invariably prone to time delays. The presence of time delay may significantly degrade closed-loop performance, and even cause instability. As mentioned in [62], two types of time delays, input delay and communication delay, have been considered in the literature. Input delay is related to processing and connecting time for the packets arriving at each agent while communication delay refers to the time for transferring information between agents. As discussed in [94], for integrator dynamics, when certain connectivity conditions are satisfied by the topology graph, the consensusability conditions are independent of communication

delays, but dependent on input delays. Therefore stability criteria for multi-agent systems with input delays have been attracting attention recently [95, 96].

For integrator dynamics of agents, the time delay problem has been discussed in [97] which provides necessary and sufficient conditions for the maximum delay such that the multi-agent system reaches consensus from arbitrary initial conditions. Stability conditions in terms of linear matrix inequalities (LMIs) using Lyapunov-Krasovskii techniques for single integrator dynamics of agents under consensus protocol with input delays are provided in [98]. For first-order multi-agent systems under undirected graph topology, [99] derives the analytical expression for the input delay margin by solving a univariate convex optimization problem. In [100], robust consensus conditions for multi-agent system consisting of SISO agents in an undirected network subject to heterogeneous feedback delays are derived from frequency-dependent and delay-dependent convex sets. Furthermore in [95], the input delay margin for consensus among agents under undirected graph topology with scalar dynamics and single input vector dynamics with a single unstable open-loop pole is derived. Recently in [101], static consensus protocols under undirected graph topology have been derived for multi-agent systems with nonuniform input delays. Although, most of the works in the literature for high-order multi-agent systems with input delay are restricted to undirected graphs, some of the recent works for multi-agent systems with input delay under directed graph topology can be found in [102, 103].

To the best of our knowledge, a unified framework to characterize the gain margin, phase margin and uniform input delay margin of the multi-agent systems has not been established in the literature and it serves as the motivation of the current work. This research focuses on characterizing the stability margins as a direct multivariable generalization of the complex units used in SISO gain and phase analysis. More specifically, we are concerned with the stability of the collective dynamics of

the agents subject to complex perturbations. The application of such perturbation analysis is significant in the areas where any errors such as signal interference introduce significant gain and phase shifts, affecting the collective stability of networked agents. The overall effect of such errors can be modeled as a complex perturbation in the feedback loop [84]. On the other hand, it is well-known that frequency-based representation of the time delay links it with the phase lag in the system with no gain change. This motivates us to obtain the input delay margin of a multi-agent system based on the unitary phase perturbation of the system's loop transfer function in the feedback path.

1.2.6 Delay Margin for Linear Multi-Agent Systems With Non-Uniform Time-Varying Communication Delays

In addition to the uniform input delay margin computation discussed in the previous section, this research also addresses the consensus control problems of high-order linear multi-agent systems with non-uniform time-varying communication delays. In the literature, the consensus problem in first-order ($n = 1$), second-order ($n = 2$), and high-order ($n \geq 2$) linear multi-agent systems with delays have been solved using frequency-domain and time-domain (Lyapunov)-based approaches. For multi-agent systems of order $n = 1$ under undirected graph topology, [99] derives an analytical expression for the delay margin by solving a univariate convex optimization problem. Similarly, the delay margins for multi-agent systems of order $n = 2$ under undirected and directed graph topology are deduced using frequency-domain analysis in [104] and [105], respectively. Further, in [106], exact delay stability bounds are computed for linear multi-agent systems of order $n \geq 2$ using *cluster treatment of characteristic roots* (CTCR) approach. However, all of these works derive the delay bounds and consensus conditions for the multi-agent systems subject to uniform de-

lays (same time-delay for each communication link in the graph). Taking a different route, [107, 108] derive the consensus conditions for linear multi-agent systems with $n \geq 2$ under undirected graph and non-uniform delays.

In the real-time communication processes, time delays are not constant and usually change over time. However, most of the works carried out in the literature of multi-agent systems, including the aforementioned ones, do not consider the time-varying nature of delays. In [109], a consensus condition for linear ($n \geq 2$) multi-agent systems under undirected graph with time-varying delays, which are assumed to be uniform for all the agents in the network, is derived. The consensus problem in multi-agent systems of order $n = 2$ under directed graph topology and non-uniform time-varying delays has been studied in [110]. For linear ($n \geq 2$) multi-agent systems with time-varying non-uniform delays under directed graph topology, [111] provides a delay-dependent stability criterion using an adaptive control protocol and Lyapunov-Krasovskii method. However, the formulation in [111] requires the system matrices to be in a controllable-canonical form. Also, the setups in [110, 111] assume the delays between the two neighboring agents (say, i and j) in a bi-directional communication channel (if it exists) to be symmetrical ($\tau_{ij} = \tau_{ji}$).

To our concern, most of the works carried out in the literature for linear multi-agent systems assume the time-delay to be uniform among the agents or constant in time. Moreover, the assumptions on the system dynamics and underlying graph topology are restrictive. This motivates us to study the problem of multi-agent systems with non-uniform time-varying delays for general high-order linear multi-agent systems. In this dissertation, we utilize the Lyapunov-Krasovskii stability criteria and develop LMI-based approach to characterize the delay margin for multi-agent systems.

1.3 Contributions

This section summarizes the major contributions of this research. The technical approach and the contribution for each component of the research are highlighted in the following subsections.

1.3.1 Uncertainty Propagation Using Generalized Polynomial Chaos Expansion

An efficient numerical framework to quantify and propagate uncertainties characterized by different distribution functions in a nonlinear stochastic system is proposed. The uncertainty propagation is carried out using pseudospectral collocation in gPC expansion framework. A novel quadrature-sampling technique, namely *Mixed Sparse Grid* (MSG) quadrature, is proposed to compute the collocation nodes for stochastic differential equations with underlying joint density function of Gaussian and uniform distributions. Nested one-dimensional quadrature rules are used for high-dimensional problems to further improve the efficacy of the proposed technique. This work also studies the long term degeneracy problem typically observed with gPC expansions of high order systems as indicated in [10, 112]. It is shown that the proposed numerical framework can mitigate this problem by selecting suitable accuracy level of MSG quadrature for a given order of gPC expansion. The proposed framework is shown to be computationally more efficient than the existing Conjugated Unscented Transform [22] and Monte Carlo-based sampling techniques.

1.3.2 Stochastic Optimal Control of Linear Systems with Probabilistic Uncertainties

We present new theoretical results for synthesizing robust optimal state-feedback controller for systems with probabilistic uncertainties in the gPC expansion framework. The control formalism is developed to minimize two expectation performance indices: (i) an infinite horizon and (ii) a finite horizon. We first recast these per-

formance indices in terms of the coefficients of the gPC expansion. Different from the works in the open literature, we use the pseudospectral collocation method (also known as discrete projection) proposed in [16] to compute the coefficients of the gPC expansion. To that end, the coefficients of gPC expansion are expressed in terms of the solution of the system at suitably selected collocation (quadrature) nodes. The equivalent performance indices are minimized to obtain a single feedback control gain matrix which stabilizes the stochastic system for all possible variations of the uncertain variable within the domain of its probability distribution function.

1.3.3 Generalized Polynomial Chaos-Based Ensemble Kalman Filtering

We propose a gPC expansion-based nonlinear filter for a system with continuous-time nonlinear dynamics and discrete-time nonlinear measurement model with uncertain initial states and parameters. The filter is developed in a prediction-correction form such that the predicted state estimates are computed using the gPC expansion-based uncertainty propagation. Aslo, upon arrival of the measurements, the predicted estimates are corrected in an ensemble Kalman filter setting. Using mixed-sparse grid-based pseudospectral collocation, the proposed filter can carry out state estimation for a nonlinear system with non-Gaussian uncertainties in the parameters and states. In contrast to [60], we use collocation nodes generated via deterministic quadrature-based sampling to compute the gPC coefficients. Subsequently, a framework is proposed to carry out sensitivity analysis to compute the sensitivity of the posterior distribution of the state estimates as a function of underlying uncertain variables (initial states and model parameters). To the best of our knowledge, this is the first attempt to carry out gPC expansion-based sensitivity analysis for a filtering problem.

1.3.4 Probabilistic Analysis of Consensus Protocols for Uncertain Edge Weights in Multi-Agent Systems

We provide a probabilistic analysis of the consensus protocols developed for multi-agent systems with single integrator dynamics in a scenario where the edge weights governing the interaction among the agents are uncertain with known probability density functions. In addition to that, this work carries out probabilistic analysis of the effect of stealth attack from malicious intruders on the consensus value of coordinating agents. We specifically show that the agents diverge from the desired location of synchronization in the presence of an intruder in the communication network. The framework of gPC expansion is utilized to obtain numerical solution of multi-agent systems for the scenario where interaction parameters among the agents are uncertain. Finally, sensitivity analysis based on gPC expansion is carried out to study the significance of edge weights on response distribution of the states of agents to answer the following question: "Who is the weakest link?"

1.3.5 Stability Margin and Uniform Input Delay Margin of Linear Multi-Agent Systems

We develop a unified framework to compute the gain margin, phase margin, and input delay margin for multi-agent systems to achieve consensus. The problem of calculating the stability margins and input delay margin is converted into finding eigenvalues of multiplicative perturbation in the feedback paths of a set of MIMO loop transfer functions, which involves solving a constrained minimization problem. We do not impose any restrictions on the dynamics of agents and on the graph topology, except that the graph structure should have atleast a directed spanning tree which is imperative for consensus. The closed loop stability of a general MIMO system independent of gain and phase perturbations, and input delay can be treated as a

robust stability problem and suitable small gain conditions can be derived for stability. To that end, we develop necessary and sufficient conditions for gain-independent, phase-independent and delay-independent stability of multi-agent systems. These conditions can be regarded as extended *small gain conditions*. The gain margin and phase margin of the multi-agent system obtained from the proposed framework are less conservative than the conventional disk-based gain margin and disk-based phase margin [113, 114], respectively . Further, the approach to compute the input delay margin proposed in this work produces a less conservative delay margin as compared to the Lyapunov Krasovskii-based approach discussed in [115].

1.3.6 Delay Margin for Linear Multi-Agent Systems With Non-Uniform Time-Varying Communication Delays

We propose a consensus control protocol for the multi-agent systems with time-varying non-uniform communication delays. In contrast to other works in the literature, we do not impose any restrictions on the system dynamics of the agents and the underlying graph topology. The consensus problem in multi-agent systems is converted to an equivalent MIMO stability problem. A new Lyapunov-Krasovskii functional for analyzing the delay-dependent stability of multi-agent system with time-varying nonuniform communication delay is proposed. The cross-product terms that emerge from the time derivative of the Lyapunov-Krasovskii functional is dealt with tighter integral inequalities, based on Jensen's integral inequality [116]. Hence, the results obtained are less conservative. Finally, a novel delay-dependent stability criterion is derived in the form of a LMI to obtain the delay margin for the high-order multi-agent system with non-uniform time-varying input delays.

List of Publications

Journal Publications

1. Rajnish Bhusal and Kamesh Subbarao, "Uncertainty Quantification Using Generalized Polynomial Chaos Expansion for Nonlinear Dynamical systems with Mixed State and Parameter Uncertainties," *ASME Journal of Computational and Nonlinear Dynamics*, Vol. 14, No. 2, 2019. DOI: 10.1115/1.4041473 (reference [61])
2. Rajnish Bhusal and Kamesh Subbarao, "Generalized Polynomial Chaos Expansion Approach for Uncertainty Quantification in Small Satellite Orbital Debris Problems," *The Journal of the Astronautical Sciences*, Vol. 67, No. 1, pp. 225-253, 2020. DOI: 10.1007/s40295-019-00176-1 (reference [117])
3. Baris Taner, Rajnish Bhusal, and Kamesh Subbarao, "Nested Robust Controller Design for Interconnected Linear Parameter Varying Aerial Vehicles," *AIAA Journal of Guidance, Control, and Dynamics*, Vol. 44, No. 8, pp. 1454-1468, 2021. DOI: 10.2514/1.G005323 (reference [118])
4. Rajnish Bhusal and Kamesh Subbarao, "Robust Stability Margin of Continuous-Time Cooperative Unmanned Systems," Submitted to *AIAA Journal of Guidance, Control, and Dynamics*, 2021 (Under review).

Refereed Conference Proceedings

1. Rajnish Bhusal and Kamesh Subbarao, "Uncertainty Quantification Using Non-Intrusive Generalized Polynomial Chaos Expansion for Orbital Debris Studies," *2018 AAS/AIAA Astrodynamics Specialist Conference*, AAS-18-438, pp. 1921-1940, Snowbird, UT, August 2018.
2. Rajnish Bhusal and Kamesh Subbarao, "Sensitivity Analysis of Cooperating Multi-agent Systems with Uncertain Connection Weights," *2019 American*

Control Conference (ACC), IEEE, pp: 4024-4029, Philadelphia, PA, July 2019. DOI: 10.23919/ACC.2019.8815336 (reference [119])

3. Rajnish Bhusal, Baris Taner, and Kamesh Subbarao, "Performance Analysis of a Team of Highly Capable Individual Unmanned Aerial Systems," *2020 AIAA Scitech Forum*, Orlando, FL, January 2020. DOI: 10.2514/6.2020-2070 (reference [120])
4. Baris Taner, Rajnish Bhusal, and Kamesh Subbarao, "A Nested Robust Controller Design for Interconnected Vehicles," *2020 AIAA Scitech Forum*, Orlando, FL, January 2020. DOI: 10.2514/6.2020-0602 (reference [121])
5. Rajnish Bhusal, Baris Taner, and Kamesh Subbarao, "On the Phase Margin of Networked Dynamical Systems and Fabricated Attacks of an Intruder," *2020 American Control Conference (ACC)*, IEEE, pp. 3279-3284, Denver, CO, July 2020. DOI: 10.23919/ACC45564.2020.9147500 (reference [122])
6. Rajnish Bhusal and Kamesh Subbarao, "Nonlinear State Estimation of Reentry Vehicle using Polynomial Chaos-based Ensemble Filtering," *2020 AAS/AIAA Astrodynamics Specialist Conference*, AAS-18-438, pp. 2193-2209, South Lake Tahoe, CA, August 2020.
7. Rajnish Bhusal and Kamesh Subbarao, "Generalized Polynomial Chaos Expansion-based Stochastic Linear Quadratic Regulator for Multi-agent Systems," *2021 AIAA Scitech Forum*, Nashville, TN, January 2021. DOI: 10.2514/6.2021-0979 (reference [123])
8. Rajnish Bhusal and Kamesh Subbarao, "Generalized Polynomial Chaos-based Ensemble Kalman Filtering for Orbit Estimation," *2021 American Control Conference (ACC)*, IEEE, pp. 4280-1285, New Orleans, LA, May 2021. DOI: 10.23919/ACC50511.2021.9482961 (*Invited presentation*) (reference [124])

9. Rajnish Bhusal and Kamesh Subbarao, "Robust Stability Margin of Continuous-Time Cooperative Unmanned Systems," Submitted to *2022 AIAA Scitech Forum* (Accepted for publication).
10. Rajnish Bhusal and Kamesh Subbarao, "Consensus of Cooperative Unmanned Systems with Non-uniform Time-varying Delays," Submitted to *2022 AIAA Scitech Forum* (Accepted for publication).
11. Rajnish Bhusal, Diganta Bhattacharjee, and Kamesh Subbarao, "Stochastic Model Predictive Control of Discrete-time Cooperative Unmanned System," Submitted to *2022 AIAA Scitech Forum* (Accepted for publication).

1.4 Outline of the Dissertation

The dissertation is divided into 8 chapters. Chapter 2 addresses the problem of uncertainty propagation using non-intrusive collocation-based generalized polynomial expansion technique. Stochastic control of linear systems subject to probabilistic parametric uncertainties is discussed in Chapter 3. The generalized polynomial chaos expansion-based nonlinear filter is developed in Chapter 4. Subsequently, Chapter 5 carries out probabilistic analysis of cooperative consensus control protocols in multi-agent systems with single-integrator dynamics. Further, Chapter 6 studies the robust stability margin and uniform delay margin of multi-agent systems, followed by the characterization of non-uniform time-varying delay margin in Chapter 7. Finally, the concluding remarks of this dissertation are presented in Chapter 8.

Chapter 2

Uncertainty Propagation Using Generalized Polynomial Chaos Expansion *

This chapter presents the mathematical details for the generalized polynomial chaos expansion methodology to solve the problem of uncertainty propagation in stochastic dynamical systems. We consider a general dynamical system subject to uncertainties in the model parameters and initial conditions characterized by their respective probability density functions. Specifically, a sampling-based non-intrusive approach using pseudospectral stochastic collocation is employed to obtain the coefficients required for the generalized polynomial chaos expansion. Various recently developed quadrature techniques are employed within the generalized polynomial chaos expansion framework in order to illustrate their efficacy. In addition to that, we provide an efficient numerical quadrature technique which can be used in pseudospectral collocation framework and can handle different distribution types of random variables. Besides the uncertainty propagation, stochastic sensitivity analysis is performed to gain insight into the impact of uncertain variables on the evolution of the quantities of interest.

*Part of the material reported in this chapter is reprinted with permission from the following: (i) Rajnish Bhusal and Kamesh Subbarao, "Uncertainty Quantification Using Generalized Polynomial Chaos Expansion for Nonlinear Dynamical systems with Mixed State and Parameter Uncertainties," *ASME Journal of Computational and Nonlinear Dynamics*, Vol. 14, No. 2, 2019, DOI: 10.1115/1.4041473, Copyright © 2019 by ASME (reference [61]) (ii) Rajnish Bhusal and Kamesh Subbarao, "Generalized Polynomial Chaos Expansion Approach for Uncertainty Quantification in Small Satellite Orbital Debris Problems," *The Journal of the Astronautical Sciences*, Vol. 67, No. 1, pp. 225-253, 2020, DOI: 10.1007/s40295-019-00176-1, Copyright © 2019 by American Astronautical Society (reference [117]).

The chapter is organized as follows. First, we provide fundamentals of probability theory in Section 2.1. Next, we review the basics of the orthogonal polynomials and their properties in Section 2.2. Section 2.3 gives an overview of the generalized polynomial chaos expansion technique for a random process. The methodology of generalized polynomial chaos expansion for a general stochastic dynamical system is presented in Section 2.4. Further, Section 2.5 discusses various quadrature techniques and their applicability. Subsequently, numerical examples are presented to illustrate the application of gPC surrogate modeling to stochastic systems in Section 2.6. Further, we provide a brief discussion on the findings of this chapter in Section 2.7. Finally, Section 2.8 gives the concluding remarks.

2.1 Preliminary Concepts from Probability Theory

This section provides the fundamental concepts from the probability theory which are essential to understand any stochastic system in general.

2.1.1 Probability Space, Random Variable, and Probability Density Function

Let us consider a random experiment and define Ω as the sample space associated with the experiment. The sample space Ω is the set of all possible distinct outcomes from the experiment. Collections of outcomes from the experiment are called as events. Therefore, each event is a subset of the sample space. In order to account for the relationship between the events, we define a field, namely σ-field (also known as σ-algebra) as follows.

Definition 2.1.1. *A σ-field is a field, which is closed with respect to countable unions and countable intersections of its members [125]. In other word, a set $\mathcal{F}$ of subsets of Ω is called a σ-field or σ-algebra if the following three properties are satisfied:*

(i) $\varnothing, \Omega \in \mathcal{F}$,

(ii) if $A \in \mathcal{F}$, then the complement of A, $\bar{A} \in \mathcal{F}$,

(iii) if $A_1, A_2, \ldots \in \mathcal{F}$ then $\bigcup_{i=1}^{\infty} A_i \in \mathcal{F}$ and $\bigcap_{i=1}^{\infty} A_i \in \mathcal{F}$.

Further, a pair $(\Omega, \mathcal{F})$ for which $\mathcal{F}$ is a σ-field in Ω is called a measurable space. Next, we define a probability space within which we can define the random variables associated with a random experiment.

Definition 2.1.2. *Given a measurable space $(\Omega, \mathcal{F})$. A function $\mathcal{P}$ defined on the subsets of Ω is called a probability measure and $(\Omega, \mathcal{F}, \mathcal{P})$ is called a probability space if the following axioms (known as Kolmogorov's axioms) are satisfied [126]:*

(i) $\mathcal{P}[\varnothing] = 0$,

(ii) Probabilities are non-negative, i.e., $\mathcal{P}[A] \geq 0$ for all $A \in \mathcal{F}$,

(iii) The entire sample space Ω is called the sure event, and its probability is one, i.e., $\mathcal{P}[\Omega] = 1$,

(iv) If $A_1, A_2, \ldots, \in \mathcal{F}$ are mutually exclusive events, i.e., $A_i \bigcap A_j = \varnothing$ for $i \neq j$, then

$$\mathcal{P}\left(\bigcup_{i=1}^{\infty} A_i\right) = \sum_{i=1}^{\infty} \mathcal{P}(A_i). \tag{2.1}$$

Now, we are ready to define the random variable for any random experiment. The functional relationship, which assigns real numbers $z(\omega)$ to each point ω in a sample space Ω is called a random variable. Therefore, random variables provide a compact way of referring to events of a random experiment via their numerical attributes. We will use the notation Z to denote the random variable and $z = z(\omega)$ to denote a particular value of the random variable.

A random variable may be discrete or continuous. A discrete random variable can take only on a countable number of distinct values. We say Z is a discrete random variable if there exist distinct real values Z_i such that

$$\sum_{i} \mathcal{P}(Z = Z_i) = 1. \tag{2.2}$$

On the other hand, a continuous random variable can assume any value within one or more intervals on the real line. In order to define a continuous random variable, let us introduce a special function, namely indicator function as follows.

Definition 2.1.3. *Given a set* $\Gamma \in \mathbb{R}$*, the indicator function of* Γ*, denoted by* $I_\Gamma(x)$*, is defined by*

$$I_\Gamma(x) := \begin{cases} 1, & x \in \Gamma, \\ 0, & x \notin \Gamma. \end{cases} \tag{2.3}$$

Given some integrable function $f(\cdot)$, we say Z is a continuous random variable if $\mathcal{P}(Z \in \Gamma)$ has the following form

$$\mathcal{P}(Z \in \Gamma) = \int_\Gamma f(s)ds := \int_{-\infty}^{\infty} I_\Gamma(s)f(s)ds. \tag{2.4}$$

Note that, since $\mathcal{P}(Z \in \mathbb{R}) = 1$, the function $f(\cdot)$ must be such that $\int_{-\infty}^{\infty} f(s)ds = 1$. Any such nonnegative function that integrates to one is called a probability density function (PDF). In this dissertation, we limit our work to continuous random variables. Next, we provide the properties of PDF $f_Z(z)$ which characterizes a continuous random variable Z as follows:

(i) $f_Z(z) \geq 0, \quad -\infty < z < \infty$

(ii) $\int_{-\infty}^{\infty} f_Z(z)\, dz = 1$

(iii) $\mathcal{P}(Z \leq a) = F_Z(a) = \int_{-\infty}^{a} f_Z(z)\, dz$

where $F_Z(z)$ is called the cumulative distribution function (CDF) of Z such that $\dfrac{dF_Z(z)}{d(z)} = f_Z(z)$.

2.1.2 Statistical Moments, Expectation, and Covariance

In probability theory, moments are the statistical parameters to measure a distribution. In order to define the moments, we first introduce the notion of expectation for a random variable. The definition of a expectation is motivated by the conven-

tional idea of numerical average. The expectation of a continuous random variable Z, whose probability density function is described by $f_Z(z)$ is given by

$$\mathbb{E}[Z] = \int_{-\infty}^{\infty} Z f_Z(z) dz. \tag{2.5}$$

Similarly, any function $g(Z)$ of the random variable Z has following expectation

$$\mathbb{E}[g(Z)] = \int_{-\infty}^{\infty} g(Z) f_Z(z) dz. \tag{2.6}$$

Now, we can define the moments of a random variable as follows. The nth moments, $n \geq 1$, of a real-valued random variable Z is defined to be $\mathbb{E}[Z^n]$. The first moment of the random variable Z is denoted by $\mathbb{E}[Z]$ and is also known as the mean of the random variable. The mean of the continuous random variable Z can be computed using (2.5). Similarly, one can compute the higher order moments (raw moments) $\mathbb{E}[Z^2], \mathbb{E}[Z^3], \ldots$ using (2.6) with $g(Z) = Z^2, Z^3, \ldots$, respectively. Further, one can define the nth central moment of the random variable Z as $\mathbb{E}[(Z - E[Z])^n]$. The second order central moment is also known as the variance, and can be defined as

$$\text{var}(Z) := \mathbb{E}[(Z - E[Z])^2]. \tag{2.7}$$

Let us now consider two random variables Y and Z. The random variables Y and Z are independent if and only if

$$\mathbb{E}[h(Y)g(Z)] = \mathbb{E}[h(Y)]\,\mathbb{E}[g(Z)] \tag{2.8}$$

for all functions $h(Y)$ and $g(Z)$ [126]. Further, we can define the covariance between Y and Z as follows

$$\text{cov}(Y, Z) := \mathbb{E}\left[(Y - E[Y])(Z - E[Z])\right]. \tag{2.9}$$

The covariance between two random variables gives a measure of correlation or dependence between the random variables. Therefore, Y and Z are uncorrelated if and only if $\text{cov}(Y, Z) = 0$.

2.1.3 Random Vector

In order to extend the idea of a random variable to the case of probability spaces with multiple random variables, the notion of random vector is quite useful. For the d-dimensional probability space with random variables $Z_1, Z_2, \ldots, Z_d$, $\mathbf{Z} = [Z_1, Z_2, \ldots, Z_d]^{\mathrm{T}} \in \mathbb{R}^d$ denotes a random vector. The expected value or mean of the random vector $\mathbf{Z}$ is denoted by $\mathbb{E}[\mathbf{Z}]$ whose elements are the expected values of the respected random variables such that

$$\mathbb{E}[\mathbf{Z}] = [\mathbb{E}[Z_1], \mathbb{E}[Z_2], \ldots, \mathbb{E}[Z_d]]^{\mathrm{T}}. \tag{2.10}$$

In the case of random vectors, we define the covariance matrix as the second order central moment. Mathematically, the covariance matrix $\mathbf{P_{ZZ}} \in \mathbb{R}^{d\times d}$ of a random vector $\mathbf{Z} \in \mathbb{R}^d$ is a matrix whose (i, j)th element is the covariance between the ith and the jth random variables and is given by

$$\mathbf{P_{ZZ}} = \mathbb{E}\left[(\mathbf{Z} - \mathbb{E}[Z])(\mathbf{Z} - \mathbb{E}[Z])^{\mathrm{T}}\right] \tag{2.11}$$

2.1.4 Random Processes

The notion of random or stochastic process is important while discussing uncertainty in physical or engineering systems. In dynamical systems, randomness varies continuously over time; therefore, it is essential to study the evolution of the random variables that describe the randomness as a function of time. A continuous time random process or stochastic process is a family of random variables $\{Z_t\}$ where t ranges over a specified interval of time defined on some space Ω [125, 126]. For example, $\{Z_t, t \geq 0\}$, $\{Z_t, t_1 \leq t \leq t_2\}$ are the continuous time random processes. Brownian motion or Wiener process is one of the examples of continuous-time random process.

Definition 2.1.4. *A family of random variables $\{Z_t\}$ for which each $\mathbb{E}[Z_t^2] < \infty$ for all t is known as a second-order random process.*

Next, we introduce the concept of orthogonal polynomials and present some of their properties.

2.2 Fundamentals of Orthogonal Polynomials

In this section, we introduce the concept of orthogonal polynomials and present some of their properties.

Consider a set of polynomials, $\{Q_n(x), n \in \mathbb{N}\}$ where $\mathbb{N} = 0, 1, 2, \ldots$ and $Q_n(x)$ is a polynomial in x of degree n of the following form

$$Q_n(x) = a_n x^n + a_{n-1}x^{n-1} + \cdots + a_1 x + a_0, \quad a_n \neq 0. \tag{2.12}$$

Now the system of polynomials $\{Q_n(x), n \in \mathbb{N}\}$ is called an orthogonal system of polynomials with respect to a weight function $w(x)$ on (a, b) if it satisfies following orthogonality relation

$$\int_a^b Q_n(x)Q_m(x)w(x)dx = \gamma_n \delta_{mn}, \quad m, n \in \mathbb{N} \tag{2.13}$$

where δ_{mn} is the Kronecker delta function ($\delta_{mn} = 0$ if $m \neq n$ and $\delta_{mn} = 1$ if $m = n$) and $\gamma_n > 0$ are the normalization constants given by

$$\gamma_n = \int_a^b Q_n^2(x)w(x)dx. \tag{2.14}$$

One of the most important characteristics of classical orthogonal system of polynomials $\{Q_n(x)\}$ is that any three consecutive polynomials in the system satisfy the following recurrence relation, well known as three-term recurrence relation in the technical literature [127]

$$Q_{n+1}(x) = (A_n x + B_n)Q_n(x) - C_n Q_{n-1}(x), \quad n \geq 0 \tag{2.15}$$

where A_n, B_n, and C_n are arbitrary sequences of real numbers such that $A_n \neq 0$, $C_n \neq 0$, and $C_n A_n A_{n-1} > 0$ for all $n \in \mathbb{N}$. Throughout this dissertation, we extensively use two of the most widely used orthogonal polynomials, namely Hermite and

Legendre polynomials. Some of the important properties of these polynomials have been highlighted in Appendix B.

2.3 Generalized Polynomial Chaos Expansion of a Random Process

Let $(\Omega, \mathcal{F}, \mathcal{P})$ be a probability space, where Ω is the sample space, $\mathcal{F}$ is the σ-algebra of the subsets of Ω, and $\mathcal{P}$ is the probability measure. For a random event $\omega \in \Omega$, let $Z = Z(\omega)$ be a continuous random variable. To that end, we consider a general second order process $\zeta(\omega) \in \mathcal{L}_2(\Omega, \mathcal{F}, \mathcal{P})$. As demonstrated in [128], we can express any such second order process as a infinite sum of weighted orthogonal polynomials, and such an expansion is known as generalized polynomial chaos (gPC) expansion. The gPC expansion of the random process $\zeta(\omega)$ can be written as

$$\zeta(\omega) = \sum_{r=0}^{\infty} \zeta_r^c \Phi_r(Z) \tag{2.16}$$

where ζ^c denotes the coefficients of expansion, and $\Phi(Z)$ is the basis of expansion in terms of random variable Z. The gPC expansion requires polynomial basis to be orthogonal with respect to the probability density function of the underlying random variable and satisfy the orthogonality relation in (2.13). The gPC expansion chooses the basis of expansion from the Askey-scheme of polynomials [129], which forms a complete basis in the Hilbert space determined by corresponding support [15]. Table 2.1 provides the correspondence of gPC orthogonal polynomials to different distributions of random variable Z. In this research, the distribution functions of the random variables are restricted to continuous distributions, which suffices for most applications.

Table 2.1: Link between type of gPC basis polynomials and their underlying Random Variables

Distribution of Z	Orthogonal polynomials	Support
Gaussian	Hermite	$Z \in (-\infty, \infty)$
Gamma	Laguerre	$Z \in [0, \infty)$
Beta	Jacobi	$Z \in [0,1]$
Uniform	Legendre	$Z \in [-1,1]$

2.4 Stochastic Dynamical System and Generalized Polynomial Chaos Expansion

Let us consider a general stochastic dynamical system which can be modeled with following stochastic differential equation (SDE)

$$\dot{\mathbf{x}}(t, \mathbf{Z}) = \mathbf{f}(t, \mathbf{x}, \mathbf{p}, \mathbf{Z}), \quad \mathbf{x}_0 = \mathbf{x}(0, \mathbf{Z}_{x_0}) \tag{2.17}$$

where $\mathbf{x} \in \mathbb{R}^n$ is the state vector, $t \in [0, T]$ is the temporal variable, $\mathbf{p} \in \mathbb{R}^p$ is the vector of model parameters, and $\mathbf{x}_0$ is the initial state vector at time $t = 0$. Here $\mathbf{Z} \in \mathbb{R}^d$, $d \leq n + n_p$ denotes the random vector which represents the uncertainties in the the system (2.17).

In this chapter, we consider the uncertainties in the initial conditions and parameters of the system. We consider the random vector $\mathbf{Z}$ in the form, $\mathbf{Z} = [\mathbf{Z}_{x_0}, \mathbf{Z}_p]$ where $\mathbf{Z}_{x_0}$ and $\mathbf{Z}_p$ represent a vector of uncertain initial conditions of the state and model parameters of the system with known stationary probability density functions, respectively. *The problems modeled here correspond to those, when the random variables pertaining to the uncertain initial conditions and parameters have different distribution types.* Specifically, this research solves SDEs whose random inputs are modeled such that,

$$\begin{aligned} \mathbf{Z}_{x_0} &\sim \mathcal{N}(\mu, \sigma^2) \\ \mathbf{Z}_p &\sim \mathcal{U}[a, b] \end{aligned}$$

Here, the initial condition uncertainties are governed by normal distribution with mean μ and variance σ^2. On the other hand, the parametric uncertainties are governed by uniform distribution with a and b as lower and upper bounds respectively.

For the system in (2.17), assuming the solution $\mathbf{x}(t, \mathbf{Z}) = [x_1(t, \mathbf{Z}), \ldots, x_n(t, \mathbf{Z})]^{\mathrm{T}}$ to be a second-order process, the gPC expansion of $x_i(t, \mathbf{Z})$ for each $i = 1, \ldots, n$ can be written as,

$$x_i\left(t, \mathbf{Z}\right) = \sum_{|\mathbf{r}|=0}^{\infty} x_{i,\mathbf{r}}^{c}(t)\Phi_{\mathbf{r}}\left(\mathbf{Z}\right), \qquad \Phi_{\mathbf{r}}\left(\mathbf{Z}\right) = \prod_{j=1}^{d} \Phi_{r_j}(z_j) \tag{2.18}$$

where $x_{i,\mathbf{r}}^{c}(t)$ is the coefficient of the multidimensional basis $\Phi_{\mathbf{r}}\left(\mathbf{Z}\right)$, $\Phi_{r_j}(z_j)$, $j = 1, \ldots, d$ is the jth univariate basis in random variable z_j , and $\mathbf{r} = (r_1, \ldots, r_d)$ is the ordered set of multi-indices with $|\mathbf{r}| = r_1 + \cdots + r_d$. For computational feasibility, the infinite summation in (2.18) needs to be truncated at the finite term P. The truncated gPC expansion is given by,

$$x_i\left(t, \mathbf{Z}\right) = \sum_{|\mathbf{r}|=0}^{P} x_{i,\mathbf{r}}^{c}(t)\Phi_{\mathbf{r}}\left(\mathbf{Z}\right). \tag{2.19}$$

The total number of basis functions is given by $N + 1 = \begin{pmatrix} d+P \\ d \end{pmatrix}$. Now, the solution in (2.19) with multidimensional index $\mathbf{r}$ can be written in terms of a single index k as follows

$$x_i\left(t, \mathbf{Z}\right) = \sum_{k=0}^{N} x_{i,k}^{c}(t)\Phi_{k}\left(\mathbf{Z}\right) = \mathbf{\Phi}(\mathbf{Z})^{\mathrm{T}}\mathbf{x}_i^{c}(t) \tag{2.20}$$

where $\mathbf{x}_i^{c}(t) = [x_{i,0}^{c}(t), x_{i,1}^{c}(t), \ldots, x_{i,N}^{c}(t)] \in \mathbb{R}^{N+1}$ is the vector of time-varying gPC coefficients and $\mathbf{\Phi}(\mathbf{Z}) = [\Phi_0(\mathbf{Z}), \Phi_1(\mathbf{Z}), \ldots, \Phi_N(\mathbf{Z})]^{\mathrm{T}} \in \mathbb{R}^{N+1}$ is the vector of gPC basis. The coefficients of gPC expansion can be computed using the following relation

$$x_{i,k}^{c} = \frac{1}{\gamma_k}\,\mathbb{E}\left[x_i(\mathbf{Z})\Phi_k(\mathbf{Z})\right] \tag{2.21}$$

where $\gamma_k = \mathbb{E}\left[\Phi_k^2\right] > 0$ is the normalization factor.

Generalized polynomial chaos approach reduces the problem of solving stochastic differential equation to solving for the coefficients of the gPC expansion. There are two widely used techniques for computing the gPC expansion coefficients: *Stochastic Galerkin Projection* and *Non-intrusive Stochastic Collocation*.

2.4.1 Stochastic Galerkin Projection

In the stochastic Galerkin projection-based gPC expansion technique, the coefficients of the gPC expansion can be computed by performing a Galerkin projection of the error of the truncation of governing SDE onto polynomial space spanned by finite dimensional basis $\mathbf{\Phi}_k$. Using the orthogonality of the polynomial basis, the given stochastic differential equation reduces to a system of coupled $d(N+1)$ deterministic ordinary differential equations (ODEs) for the coefficients of gPC expansion. Further details on stochastic Galerkin projection for stochastic dynamical systems, please refer to [15, 128]. Although Galerkin projection ensures that the residue of the SDE is orthogonal to the linear space spanned by the polynomials corresponding to the distribution of random variable, the system of equations needs to be re-derived in terms of polynomial moments for each new system of SDEs. Therefore, the approach of Galerkin projection is quite intrusive and can not be used as a black-box simulator [61, 128]. Further, with an increasing order of expansion, stochastic Galerkin projection requires to solve higher order inner products which increases the computational time required to obtain the coefficients of gPC expansion and in the cases of highly nonlinear systems, it takes almost the same computational time as the Monte Carlo simulation [130].

2.4.2 Non-Intrusive Stochastic Collocation

In order to avoid the difficulties in implementing the intrusive Galerkin projection approach of gPC expansion, and implement the gPC expansion as a black-box, non-intrusive approach for computing the coefficients of polynomial basis needs to be considered. The stochastic collocation is a widely used non-intrusive numerical technique in gPC framework to compute the coefficients required for the expansion. It combines the strength of the stochastic Galerkin method resulting from polynomial approximations in random spaces and the ease of implementation of sampling-based Monte Carlo technique [16].

The main idea behind the stochastic collocation is to generate ensemble of solution by solving the system of SDEs for finite number of realizations of the random vector $\mathbf{Z}$. These realizations can be obtained by randomly drawing independent samples from the given density function of the random variable or using deterministic nodes given by a specific quadrature technique. These nodal points are generally termed as collocation points. At these sampled collocation nodes, the system of SDEs can be solved deterministically. Polynomial interpolation in multi-dimensional random space is the natural choice to perform stochastic collocation [128]. Once the solution ensemble is obtained by solving the deterministic system of equations at the nodes, a polynomial approximation of the solution based on the ensemble is constructed. The major difficulty in conducting the interpolation approach of gPC arises when the stochastic dimension is high. It is quite difficult to construct an interpolation basis on an arbitrary set of nodes to interpolate any data in high dimensions.

The *pseudospectral approach*, also termed as *discrete projection*, is the approach of applying numerical quadrature to the notion of the stochastic collocation. The orthogonal gPC projection is given by (2.19), where the expansion coefficients are

given by (2.21). It is customary to express the expectation of a random function as an integral under the PDF of the random variable. Moreover, if $\boldsymbol{\rho}(\mathbf{Z})$ represents the joint PDF of the random vector $\mathbf{Z}$ with support $\Gamma \subset \mathbb{R}^d$, the expansion coefficients can be written as,

$$x_{i,k}^c = \frac{1}{\gamma_k} \mathbb{E}\left[x_i(\mathbf{Z})\Phi_k(\mathbf{Z})\right] = \frac{1}{\gamma_k} \int_\Gamma x_i(\mathbf{Z})\Phi_k(\mathbf{Z})\boldsymbol{\rho}(\mathbf{Z})d\mathbf{Z} \tag{2.22}$$

where $\gamma_k = \mathbb{E}\left[\Phi_k^2\right] > 0$ is the normalization factor. The notion behind the pseudospectral technique is to approximate the above integral in (2.22) using the numerical quadrature technique by collocating $x_i(\mathbf{Z})$ on pre-determined quadrature nodes. Based on the numerical quadrature technique, the approximation to an integral of any function $f(\mathbf{Z})$ in the form of (2.22) can be expressed as,

$$\int_\Gamma f(\mathbf{Z})\ \boldsymbol{\rho}(\mathbf{Z})\ d\mathbf{Z} \approx \sum_{q=1}^{M} f\left(\mathbf{Z}_q\right) w_q \tag{2.23}$$

where, $\mathbf{Z}_q$ are the quadrature node, w_q are the corresponding nodal weights and M is the number of quadrature nodes used. Further details on quadrature rules and approaches would be discussed in Section 2.5. Meanwhile, the expansion coefficients from (2.22) can be written as,

$$x_{i,k}^c = \frac{1}{\gamma_k} \int_\Gamma x_i(\mathbf{Z})\ \boldsymbol{\Phi}_k(\mathbf{Z})\ \boldsymbol{\rho}(\mathbf{Z})\ d\mathbf{Z} \approx \frac{1}{\gamma_k} \sum_{q=1}^{M} x_i\left(\mathbf{Z}_q\right) \boldsymbol{\Phi}_k\left(\mathbf{Z}_q\right) w_q \tag{2.24}$$

It is evident that the convergence of the solution obtained from the pseudospectral approach is completely dependent on the convergence behavior of the quadrature-based integral approximation. The higher the accuracy of the quadrature technique, the less would be the difference between the discrete projection and the orthogonal gPC projection, which in turn decides the convergence of the gPC expanded approximation to the true solution [61].

2.4.3 gPC Expansion-Based Approximate Statistics

Given the estimates of the gPC coefficients, the approximate statistics i.e. mean and variance of $x_i(\mathbf{Z})$ can be computed as,

$$\begin{aligned}
\mathbb{E}\left[x_i(t,\mathbf{Z})\right] &\approx \mathbb{E}\left[\sum_{k=0}^{N} x_{i,k}^{c}(t)\Phi_k\left(\mathbf{Z}\right)\right] = x_{i,0}^{c}(t) \\
\mathrm{var}\left[x_i(t,\mathbf{Z})\right] &\approx \mathbb{E}\left[\left(\sum_{k=0}^{N} x_{i,k}^{c}(t)\Phi_k\left(\mathbf{Z}\right) - \mathbb{E}\left[x_i(t,\mathbf{Z})\right]\right)^2\right] = \sum_{k=1}^{N} \gamma_k \left(x_{i,k}^{c}(t)\right)^2
\end{aligned} \tag{2.25}$$

where $\mathbb{E}[\cdot]$ represents the expectation operator to compute mean and var$[\cdot]$ denotes the variance operator.

2.4.4 gPC Expansion-Based Sensitivity Analysis

In practice, the response PDF of the stochastic systems are influenced by different variables differently. Among all the variables, some of the variables have insignificant influence on the response of the system and these parameters can be modeled less precisely than the ones which generate significant effects. The relevant variables need to be distinguished and estimated with high accuracy while modeling the uncertainties. Sensitivity analysis generally carried out using *variance-based global methods*, also known as ANOVA (ANalysis Of VAriance) aids us to make informed decisions about the sensitivity of the system to the parameters involved [26]. It provides a measure of the contribution of each uncertain variables in the generation of the uncertainty of the quantities of interest. In this regard, the Sobol' indices obtained by carrying out Sobol decomposition serve as determinants for sensitivity analysis. The portion of the uncertainty in the QoI (measured through its variance) that can be attributed to the uncertainty in a random variable is termed as the sensitivity index. The sensitivity indices are often normalized with the variance of the quantity of interest and the dimensionless coefficients thus obtained are referred to as total-effect

Sobol' indices or total sensitivity indices. To that end, the gPC expansion provides a computationally efficient approach to compute these sensitivity indices for global sensitivity analysis [26].

For a given gPC expansion, the Sobol' indices at any order may be obtained by the combination of the squares of the suitable gPC coefficients. The gPC coefficients to be selected needs to be determined on the basis of order of sensitivity function required. For the sensitivity analysis, we use the gPC expansion in the multi-index form defined in (2.19). More specifically, to compute gPC-based Sobol' indices to carry out first order sensitivity analysis, the set of multi-indices $\mathbf{r}$ must be reordered to another set of multi-indices $\mathcal{I}_i$ which corresponds to the polynomials depending on random input Z_i only.

$$\mathcal{I}_i = \{\mathbf{r} \ \mid r_i > 0 \ \mid r_{j\neq i} = 0\}, \quad \forall i = 1, \ldots, d \tag{2.26}$$

where, r_i is the one-dimensional polynomial degree and d is the number of random variables. Now, the gPC-based first order sensitivity function can be obtained as,

$$\mathcal{S}_i(t) = \frac{\sum_{\alpha\in\mathcal{I}_i} \ x_{i,\alpha}^{c^2}(t)\,\mathbb{E}\left[\mathbf{\Phi}_\alpha^2\right]}{\sigma_{x_i}^2} \tag{2.27}$$

where $\sigma_{x_i}^2$ is the variance of $x_i(t)$ computed in (2.25). On the other hand, the total sensitivity function $\mathcal{S}_i^{tot}(t)$ of random input Z_i is given by,

$$\mathcal{S}_i^{tot}(t) = \frac{\sum_{\alpha\in\mathcal{I}_i^{tot}} \ x_{i,\alpha}^{c^2}(t)\,\mathbb{E}\left[\mathbf{\Phi}_\alpha^2\right]}{\sigma_{x_i}^2} \tag{2.28}$$

where, $\mathcal{I}_i^{tot} = \{\mathbf{r} \ \mid r_i > 0\}$ corresponds to the polynomials depending on random input Z_i and possibly on other random inputs as well.

To illustrate the idea, let us consider an example consisting of two random variables ($d = 2$) with known distribution functions. The set of multi-indices $\mathbf{r}$ to carry out gPC expansion can be obtained using graded lexicographical ordering. For the second order ($N = 3$) gPC expansion,

$$\mathbf{r} = \{(0,0),(1,0),(0,1),(2,0),(1,1),(0,2),(3,0),(2,1),(1,2),(0,3)\}$$

The set of indices $\mathcal{I}_i$ for first-order sensitivity function can be written as,

$$\mathcal{I}_1 = \{(1,0),(2,0),(3,0)\}, \quad \mathcal{I}_2 = \{(0,1),(0,2),(0,3)\}$$

On the other hand, the set of indices $\mathcal{I}_i^{tot}$ for total sensitivity function can be written as,

$$\begin{aligned} \mathcal{I}_1^{tot} &= \{(1,0),(2,0),(3,0),(1,1),(2,1),(1,2)\}, \\ \mathcal{I}_2^{tot} &= \{(0,1),(1,1),(0,2),(2,1),(1,2),(0,3)\} \end{aligned}$$

Hereafter, the sensitivity functions can be computed by calculating the coefficients of gPC expansion using the approach discussed in Section 2.4.2.

2.5 Quadrature Rules for Multi-dimensional Integration

Pseudospectral approach of gPC stochastic collocation requires efficient quadrature rules for approximating expectation integrals. As stated earlier and expressed in (2.22) and (2.23), expectation of any random function can be expressed as an integral under the joint PDF $\boldsymbol{\rho}(\mathbf{Z})$ of the random vector $\mathbf{Z}$, which in turn can be approximated with a quadrature rule. The ultimate aim of any quadrature rule is to provide a set of points $\mathbf{Z}_q = \left[Z_{1_q}, \ldots, Z_{d_q}\right]^T \in \mathbb{R}^d$ and weights $w_q \in \mathbb{R}$ such that, the d-dimensional integral I_d can be approximated as,

$$I_d = \int_\Gamma f(\mathbf{Z})\boldsymbol{\rho}(\mathbf{Z})d\mathbf{Z} \approx \sum_{q=1}^{M} f(\mathbf{Z}_q)w_q \tag{2.29}$$

under the support $\Gamma \subset \mathbb{R}^d$. While various choices of quadrature rules are available in the literature, this work focuses on some of the following quadrature techniques.

2.5.1 Gaussian Quadrature Tensor Grid

The natural choice for evaluating univariate integration are the Gaussian Quadrature methods. The Gaussian quadrature rule gives a minimal number of points in one dimensional space by choosing the set of points that maximizes the degree of the polynomial function that exactly evaluates the integral. With $\mathbb{N}$ as a set of natural numbers excluding 0, let us consider $A = \{A_\alpha : \alpha \in \mathbb{N}\}$ represents a sequence of univariate quadrature rules. Let each rule A_α provides m_α set of nodes $\boldsymbol{X}_\alpha$ and corresponding weight w_α such that each A_α is exact for all univariate polynomials of order $2m_\alpha - 1$ or less. The straightforward way to evaluate multivariate integrals is to perform a tensor product of sequence of univariate integrals. The d-dimensional tensor product of univariate quadrature rules with different accuracy levels in each dimension indicated by the multi-index $\boldsymbol{\alpha} = [\alpha_1, \ldots, \alpha_d]$ is defined as,

$$\left(A_{\alpha_1} \otimes \cdots \otimes A_{\alpha_d}\right)(f) = \sum_{x_1 \in \boldsymbol{X}_{\alpha_1}} \cdots \sum_{x_d \in \boldsymbol{X}_{\alpha_d}} f\left(x_1, \ldots, x_d\right) \prod_{i=1}^{d} w_{\alpha_i} \tag{2.30}$$

where, $\otimes$ represents the tensor product, $\boldsymbol{X}_{\alpha_i}$ is the point set and w_{α_i} is the weight implied by univariate quadrature rule A_{α_i} with accuracy level α_i [131]. This rule is often called the full tensor grid formula or the multivariate quadrature rule. If the univariate rule is developed using m number of points, then extending it to d-dimensions in a tensor product fashion would result in m^d number of quadrature points i.e. the number of functional evaluations increases exponentially which demands a huge computational cost. This makes the full tensor grid formulation inefficient and often infeasible in high dimensions i.e. it suffers from the *curse of dimensionality*.

2.5.2 Sparse Grid

The sparse grid quadrature is derived based on the Smolyak approach [18]. It was originally developed by Smolyak and is widely used to alleviate the *curse of dimensionality* of the tensor product rule. Smolyak's grid makes use of linear combination of lower-dimensional tensor products and the computational cost increases polynomially unlike the full tensor grid where the cost increases exponentially. If A_α represents the univariate Gaussian rule with accuracy level α, the difference of the approximation when increasing the level of accuracy from $\alpha - 1$ to α is given by,

$$\Delta_\alpha(f) = A_\alpha(f) - A_{\alpha-1}(f), \quad \forall \alpha \in \mathbb{N}, \quad A_0(f) = 0 \tag{2.31}$$

With multi-index $\boldsymbol{\alpha} = [\alpha_1, \ldots, \alpha_d] \in \mathbb{N}^d$, for any integer q, the set of accuracy level sequences can be defined as,

$$N_q^d = \begin{cases} \left\{ \boldsymbol{\alpha} \,\middle|\, \sum_{i=1}^d \alpha_i = d + q \right\}, & \text{for } q \geq 0 \\ \varnothing, & \text{for } q < 0 \end{cases}$$

The Smolyak rule for accuracy level $\gamma \in \mathbb{N}$ for d-dimensional integration of function f is given by,

$$I_{d,\gamma}(f) = \sum_{q=0}^{\gamma-1} \sum_{\boldsymbol{\alpha} \in \mathbb{N}_q^d} \left(\Delta_{\alpha_1} \otimes \cdots \otimes \Delta_{\alpha_d}\right)(f) \tag{2.32}$$

where, the tensor product operation represented with $\otimes$ is defined in (2.30). As discussed in [132], (2.32) can be expressed explicitly as,

$$I_{d,\gamma}(f) = \sum_{q=\gamma-d}^{\gamma-1} (-1)^{\gamma-1-q} \binom{d-1}{\gamma-1-q} \sum_{\boldsymbol{\alpha} \in \mathbb{N}_q^d} \left(A_{\alpha_1} \otimes \cdots \otimes A_{\alpha_d}\right)(f) \tag{2.33}$$

where, $\binom{d-1}{\gamma-1-q}$ represents the binomial coefficient. The nodes for the sparse grid quadrature are given by specific combinations of points of one-dimensional quadrature rules,

$$\boldsymbol{X}_{d,\gamma} = \bigcup_{q=\gamma-d}^{\gamma-1} \bigcup_{\boldsymbol{\alpha}\in\mathbb{N}_q^d} (\boldsymbol{X}_{\alpha_1} \otimes \cdots \otimes \boldsymbol{X}_{\alpha_d}) \tag{2.34}$$

where, $\bigcup$ denotes the union operator of the point sets. The corresponding weights for these nodes are $(-1)^{\gamma-1-q}\binom{d-1}{\gamma-1-q}\prod_{i=1}^{d} W_{\alpha_i}$. The algorithm to generate points and weights from the sparse grid technique can be traced to the work of Jia et al. in [133]. The number of nodes in the case of sparse grid increases polynomially and delays the *curse of dimensionality* to a great extent. Note that some of the weights generated by the sparse grid technique can be negative, which is the feature of various multivariate quadrature rules.

Further, classical Gaussian quadrature rules use completely different nodes for each accuracy level, i.e. using Gaussian quadrature rules for developing sparse grid adds distinct nodes to the sparse grid as $\boldsymbol{X}_m \cap \boldsymbol{X}_n = \varnothing$ if $m \neq n$. However, the use of nested sequences of quadrature rules i.e. the set of nodes used by some rule is a subset of those used by one with higher accuracy, increases the effectiveness of the quadrature rules in dimensions greater than 1. Among many others, Kronrod-Patterson (KP) rule with accuracy level α adds a number of points to the set of the nodes $\boldsymbol{X}_{\alpha-1}$ which increases the polynomial exactness of the approximation [131]. Though this results in more points in 1-D than the Gaussian quadrature rule, this property of nestedness makes the KP rule more efficient in higher dimensions for use in sparse grid quadrature as many of the sets share a substantial number of points. This results in further reduction in the number of points in the case of the sparse grid. Figure 2.1 illustrates the sparse grid (using nested KP univariate rules)-based quadrature nodes of accuracy level 5 for the random vector $\mathbf{Z}$ with independent

random variables $[Z_1, Z_2]^T$ for both uniformly and normally distributed cases. In the subsequent sections, the notation SG-γ would represent sparse grid of accuracy level γ. In this work, the concept of sparse grid would be extended to mixed sparse grid in the Section 2.5.4 to generate cubature points corresponding to the joint PDF, which is a product of different probability distributions.

2.5.3 Conjugate Unscented Transform

Conjugate Unscented Transform (CUT) is a non-product quadrature rule put forward by Adurthi et. al [22] which computes multidimensional expectation integrals involving Gaussian and uniform PDF. CUT is an extension of conventional Unscented Transform [134] to generate a fully symmetric cubature (sigma) point set, which satisfies higher order moment constraints. The CUT sigma points are equivalent to Stroud's cubature points [135, 136] for symmetric regions. The main idea behind CUT is to judiciously select appropriate axes called *Conjugate Axes* and constrain the sigma points to lie at appropriate locations on those axes such that they satisfy the *moment constraint equations*. The set of equations called as *moment constraint equations* can be written as,

$$\sum_{q=1}^{M} w_q \left\{ Z_{(q,1)}^{n_1} Z_{(q,2)}^{n_2} \cdots Z_{(q,d)}^{n_d} \right\} = \mathbb{E}[Z_1^{n_1} Z_2^{n_2} \cdots Z_d^{n_d}] \tag{2.35}$$

where, $n_1 + \cdots + n_d = n$ represents the order of the moment of the density function [22]. The major objective of the CUT is now to find sigma points that satisfy (2.35) up to a desired order of moments. The sigma points are constrained to lie symmetrically on well defined axes, which includes following set of axes [22]

(i) Principal axes (σ_i): In d-D space, the principal axes are the d-orthogonal axes centered at the origin.

(ii) Conjugate axes (c^m): mth-conjugate axes are constructed from all the all the combinations including sign permutations of the set of principal axes taken m ($m < d$) at a time

(iii) Scaled conjugate axes(s^m): mth-scaled conjugate axes are constructed from all the combinations including sign permutations of the set of principal axes such that in every combination exactly one principal axis is scaled by a scaling parameter h.

Each sigma point is scaled by a variable r_q and a weight w_q is assigned to each of those points. Based on the symmetrical property of sigma points, all the odd order moment constraint equations are automatically satisfied. Thus, one only needs to satisfy moment constraint equations of even orders. Solving these equations up to a desired order results in the values of $\{r_q\}$ and $\{w_q\}$. Different sigma points can be generated by considering different orders of moment constraint equations. Fourth-order CUT, sixth-order CUT, and eighth-order CUT exist in the literature which are labeled as CUT-4, CUT-6 and CUT-8 respectively. The way of constraining the points on various axes discussed above can be found in works by Adurthi et al. [22]. The weights obtained from the Conjugate Unscented Transform are positive upto certain dimensions for each CUT-order for each distribution. CUT-6 generates positive weights upto $d < 9$ while, CUT-8 generates positive weights only upto $d = 6$ for expectation integrals involving Gaussian distributions. Also, CUT-6 generates positive weights upto $d \leq 9$ while, CUT-8 generates positive weights only upto $d \leq 5$ for expectation integrals involving uniform distributions. Figure 2.2 illustrates the CUT-8-based sigma points for the random vector $\mathbf{Z}$ of independent random variables $[Z_1, Z_2]^T$ for both uniformly and normally distributed cases. Unlike sparse grid, conjugate unscented transform will not be extended in this research to incorporate random variables governed by different probability distributions. Extension of CUT

would require the prior calculation of higher order moments of the product of different probability distributions in order to solve the moment constraint equations, which is not trivial.

2.5.4 Mixed Sparse Grid Cubature Rule for Mixed Distribution Problems

The cubature rules discussed above in Sections 2.5.2 and 2.5.3 can provide the nodes for the expectation integral problems with random variables governed by a single distribution function (either uniform or normal). However, in practice, the random variables of a stochastic system can be governed by different distribution functions. This indeed demands for a cubature rule that can provide nodes and weights for the expectation integral problems governed by a mixture of distribution functions.

The concept of sparse grid discussed in Section 2.5.2 will be extended to generate nodes for the multi-dimensional expectation integral approximations where the underlying joint probability distribution is a product of different marginal distribution functions. The mixed sparse grid (MSG) can be generated by using a mixture of 1-D quadrature rules in different dimensions depending on the distribution of the random variables. To illustrate this idea consider the case of approximating a 2-dimensional expectation integral.

$$\int_{\Gamma} f(\mathbf{Z})\boldsymbol{\rho}(\mathbf{Z})\, d\mathbf{Z} \approx \sum_{q=1}^{M} w_q \; f(Z_{1_q}, Z_{2_q}) \tag{2.36}$$

where, $\mathbf{Z} = [Z_1, Z_2]^T$ is the random vector and $\boldsymbol{\rho}(\mathbf{Z})$ is the joint probability distribution function with support $\Gamma \subset \mathbb{R}^2$. Also, w_q and Z_{i_q} with $i \in \{1, 2\}$ are the weights and nodes of the mixed sparse grid cubature rule respectively. Let Z_1 and Z_2 be independent random variables and governed by uniform and normal distribution functions

respectively. In this case, the MSG nodes can be generated by performing a sparse tensor product (linear combination of lower-dimension tensor product) of univariate rules such that, A_{α_1} are 1-D Gaussian Legendre quadrature rules to integrate univariate Legendre polynomials and A_{α_2} are 1-D Gaussian Hermite quadrature rules to integrate univariate Hermite polynomials. Hence, MSG nodes can be generated using the sparse grid quadrature given in (2.34) using the selective combination of various univariate rules depending on the distribution characterizing the random variables. Figure 2.3 illustrates the quadrature nodes generated using the MSG of accuracy level 5 for a 2-dimensional random variable vector $\mathbf{Z} = [Z_1, Z_2]^T$, where the random variables are independent and distributed such that, Z_1 is uniformly distributed on $\mathcal{U}[-1, 1]$ and Z_2 is normally distributed on $\mathcal{N}(0, 1^2)$.

The main focus of this work is to provide an approximate solution to the SDE with random variables governed by different probability distribution functions. Hence, it is required to construct a polynomial basis which is orthogonal with respect to the joint probability distribution.

Consider a random vector $\mathbf{Z}$ of m independent random variables Z_1, Z_2, up to Z_m which are governed by marginal probability distributions ρ_{z_1}, ρ_{z_2}, up to ρ_{z_m} respectively, such that $\mathbf{Z} = [Z_1, Z_2, \ldots, Z_m]^T$. Since the random variables are independent, the joint probability distribution is given by,

$$\rho_{\mathbf{Z}} = \rho_{Z_1} \times \ \rho_{Z_2} \times \ldots \times \ \rho_{Z_m}$$

where, $\rho_{\mathbf{Z}}$ is the joint probability distribution of the random vector $\mathbf{Z}$. It can be easily shown that, such a joint probability distribution of different distribution functions exists by verifying the area under the joint distribution function (continuous) over the domain is unity. The basis orthogonal to the joint probability distribution ($\rho_{\mathbf{Z}}$) can be constructed in the similar fashion as that for the multi-variable case in gPC

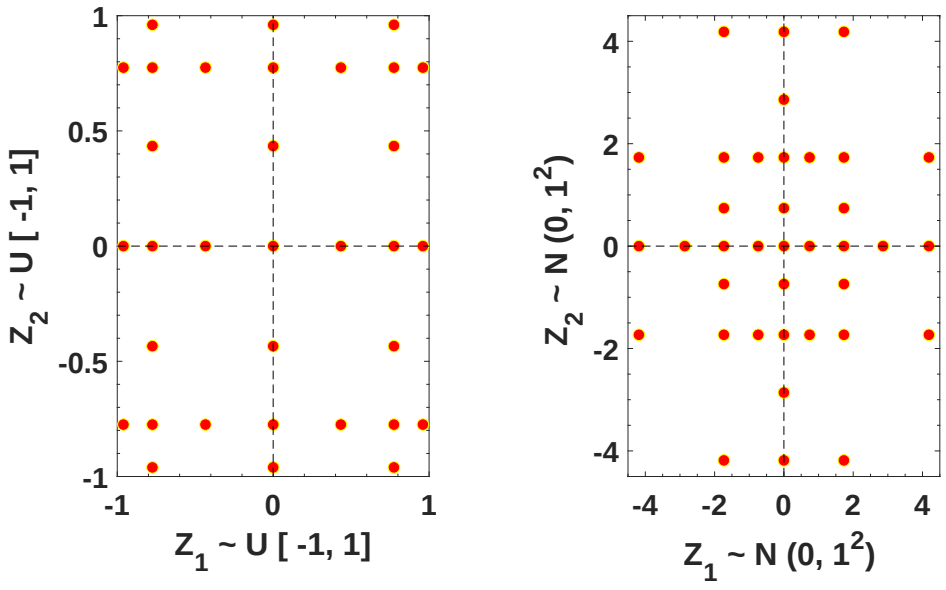

Figure 2.1: SG nodes for uniform and normal distribution random variable $\mathbf{Z} = [Z_1, Z_2]$

expansion using reverse graded lexicographic technique of multi-indexing [128] ; the only difference being the selection of different polynomial basis for different indexes. For instance, if Z_1 and Z_2 are uniformly distributed standard random variables and Z_3 is a normally distributed standard random variable then, the polynomials governing the univariate basis for Z_1 and Z_2 would be Legendre polynomials and for Z_3 would be Hermite polynomials.

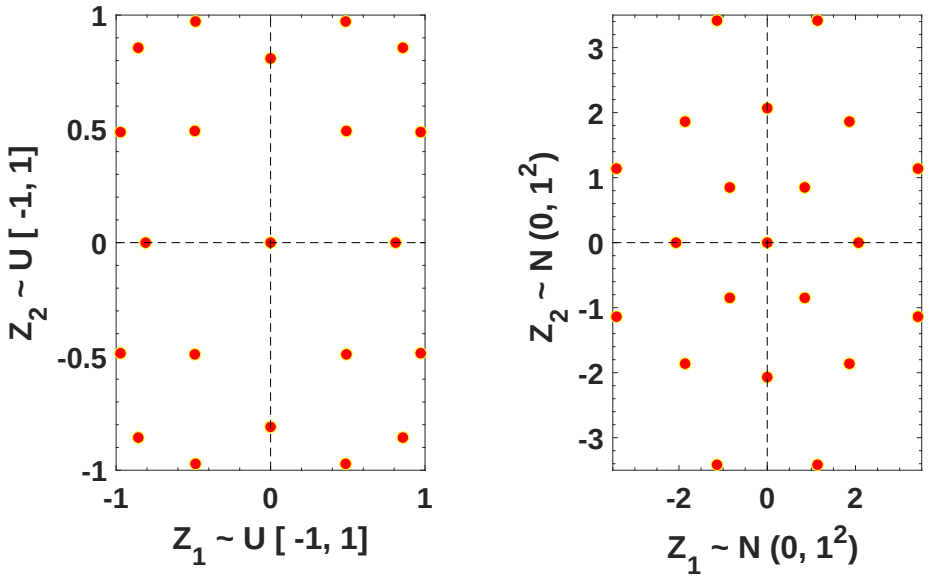

Figure 2.2: CUT nodes for uniform and normal distribution random variable $\mathbf{Z} = [Z_1, Z_2]$

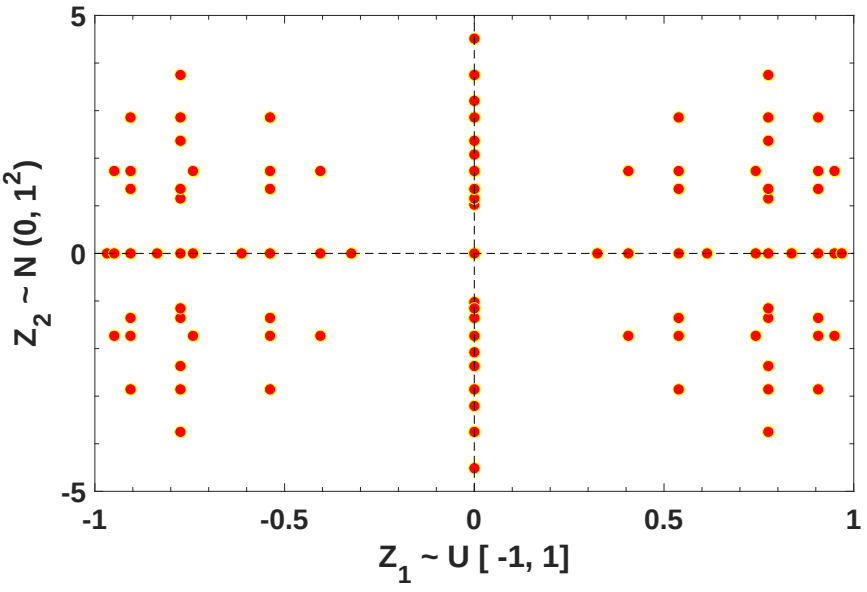

Figure 2.3: MSG nodes for random vector with mixture of distributions

2.6 Numerical Results

In this section, several test problems are considered to make comparisons between various quadrature techniques discussed in the Section 2.5. Numerical problems involving evaluation of an expectation integral and propagation of uncertainties in a damped oscillator using gPC expansion are considered to demonstrate the convergence criteria of sparse grid and conjugate unscented transform-based cubature techniques. Further, the validation of MSG-based gPC expansion is carried out in the context of orbital uncertainty propagation. All the simulations are performed in MATLAB environment on a computer with Intel Core i7 CPU 3.20 GHz.

2.6.1 Expectation Integral Evaluations

The problem of evaluating an expectation integral of a polynomial of different degrees in 6-dimensional space ($d = 6$) is considered. A similar problem was introduced in [22], where the eighth-degree polynomial function was considered. The results obtained from the case of expectation integral at various degrees would give a general idea about the efficacy of the quadrature rule at different degrees. The problem of expectation integral is,

$$I = \int 0.1 \sum_{i=1}^{d} x_i^{\alpha} \mathcal{N}\left(\boldsymbol{x} : 0, \boldsymbol{I}\right) d\boldsymbol{x} \tag{2.37}$$

where, α represents the degree of the polynomial. Results obtained from Gaussian Hermite (GH) quadrature-based full tensor grid is considered to be exact. It has been found that, GH tensor grid requires atleast 6 points along each dimension to exactly evaluate the integral for polynomial degree upto 10. The notation GH-6 refers for Gaussian Hermite tensor grid rule with a total of 6^d points. Sparse grid (produced using KP univariate rules) and CUT sampling techniques are employed for various values of α and the results are compared with the reference truth obtained from GH-

Table 2.2: Comparison of expectation integrals between SG and CUT-based cubature rule

Rule (# points)	$\alpha = 2$	$\alpha = 4$	$\alpha = 6$	$\alpha = 8$	$\alpha = 10$
SG-2 (13)	0.6 (0%)	1.8 (0%)	5.4 (40%)	16.2 (74.2 %)	48.6 (91.4 %)
SG-3 (73)	0.6 (0%)	1.8 (0%)	5.4 (40%)	16.2 (74.2 %)	48.6 (91.4 %)
SG-4 (257)	0.6 (0%)	1.8 (0%)	9 (0%)	92.0 (46 %)	141.6 (75.0 %)
SG-5 (749)	0.6 (0%)	1.8 (0%)	9 (0%)	63 (0 %)	567 (0 %)
CUT-4 (76)	0.6 (0%)	1.8 (0%)	6 (33.3%)	21.6 (65.7 %)	81.6 (85.6 %)
CUT-6 (137)	0.6 (0%)	1.8 (0%)	9 (0%)	60.5 (3.8 %)	464.0 (18.1 %)
CUT-8 (745)	0.6 (0%)	1.8 (0%)	9 (0%)	63 (0 %)	545.18 (3.8 %)
* GH-6 (46656)	0.6	1.8	9	63	567

* signifies the reference rule used to evaluate exact value of integral

6. Table 2.2 provides the numerical value of the integral approximated by various accuracy levels and orders of SG and CUT respectively, along with the number of cubature points used by each rule for approximation.

In Table 2.2, the % value inside the brackets represents % of relative error in the corresponding approach w.r.to Gaussian Hermite quadrature (GH-6). It can be observed from Table 2.2 that SG requires fewer points to exactly evaluate the integral than CUT upto the polynomial degree of 4. For polynomial of degree 6, CUT-6 converges with fewer points than corresponding SG rule (SG-4). Subsequently, for the polynomial with degree 8, only SG-5 and CUT-8 can exactly evaluate the integral. Both of the techniques require similar number of points; SG-5 requires 4 points more than CUT-8. The % of relative error in the case of $\alpha = 8$ is much smaller in the case of CUT than SG of corresponding orders and accuracy levels respectively. However, when the order of polynomial is further increased above 8, CUT-8 fails to converge. Contrarily, the sparse grid of corresponding accuracy level (SG-5) can still exactly evaluate the integral. On further increasing the polynomial degree (not shown in Table 2.2, it is observed that SG-5 can exactly evaluate this integral problem to a

degree of 12 with just 749 points. However, CUT-8 with almost similar number of points fails to converge after the polynomial degree of 8.

For this example, we also note that the integral value in this problem should always be positive as the integrand is always positive. In [22] it was shown that, HCKF-5 i.e. High-degree Cubature Kalman Filter of order 5 proposed in [137] gives negative integral value when the value of $\alpha = 8$ with 73 nodes. It was also concluded in [22] that the negative integral value possibly occurs due to the presence of negative weights. However, the case of negative integral evaluation is not observed for any accuracy level of sparse grid with negative weights generated from nested Kronrod Patterson univariate rules. Hence, negative weights would not necessarily be an issue if the suitable number of sample points are used to capture the moments of the distribution.

2.6.2 Rosenbrock Function

As a second example, the Rosenbrock function is used in this work to demonstrate pseudospectral approach-based gPC expansion using the cubature rules discussed in Section 2.5. The Rosenbrock function, also referred to as the Valley function is a benchmark test function often encountered in numerical optimization [138] and to evaluate nonintrusive gPC approaches [139]. The multi-dimensional Rosenbrock function is given by

$$f(\boldsymbol{x}) = \sum_{i=1}^{d-1} 100 \left(x_{i+1} - x_i^2\right)^2 + (1 - x_i)^2 \tag{2.38}$$

where, $\boldsymbol{x}$ is a d-dimensional vector.

For the analysis, fifth-dimensional ($d = 5$) Rosenbrock function is considered. In this study, the cumulative distribution function (CDF) probability levels are com-

Table 2.3: Distribution of random variables with corresponding gPC basis

Random variable	Distribution	gPC basis
x_1	$\mathcal{U}[-2, 2]$	Legendre
x_2	$\mathcal{U}[-2, 2]$	Legendre
x_3	$\mathcal{U}[-2, 2]$	Legendre
x_4	$\mathcal{U}[-2, 2]$	Legendre
x_5	$\mathcal{U}[-2, 2]$	Legendre

puted at different specified response levels ($r = 1, 50, 100, 500, 1000, 2500$) of the $f(\boldsymbol{x})$ using pseudospectral approach of gPC expansion.

2.6.2.1 Case I: All random variables are uniformly distributed

Let us consider a case where, x_i for all $i = 1, \ldots, 5$ are distributed uniformly. The bounds of uncertainty for the random variables are presented in the Table 2.3. The CDF obtained from repetitive simulations using 10^4 Latin hypercube samples is considered to be the reference solution. As the random variables have same distribution function, samples generated using sparse grid (SG) and conjugated unscented transform (CUT) are used as the collocation nodes to compute the coefficients of gPC expansion using pseudospectral approach. The gPC solution ensemble generated by evaluating the gPC expansion at 10^4 random grid points is analyzed to obtain the Nth order gPC-approximated response CDF.

Figure 2.4 depicts the computational results obtained from SG-based gPC expansion. The CDF probabilities are mapped at various response levels of $f(\boldsymbol{x})$ for increasing levels of accuracy of SG (for fourth order of gPC expansion) and increasing orders of gPC expansion (for fifth accuracy level of SG). Clearly, fourth order gPC expansion with fifth accuracy level of SG is exact and pseudospectral collocation carried out using samples from lower accuracy levels of SG produce highly inaccurate solution statistics. Also, with fixed accuracy level of SG, the convergence of gPC ex-

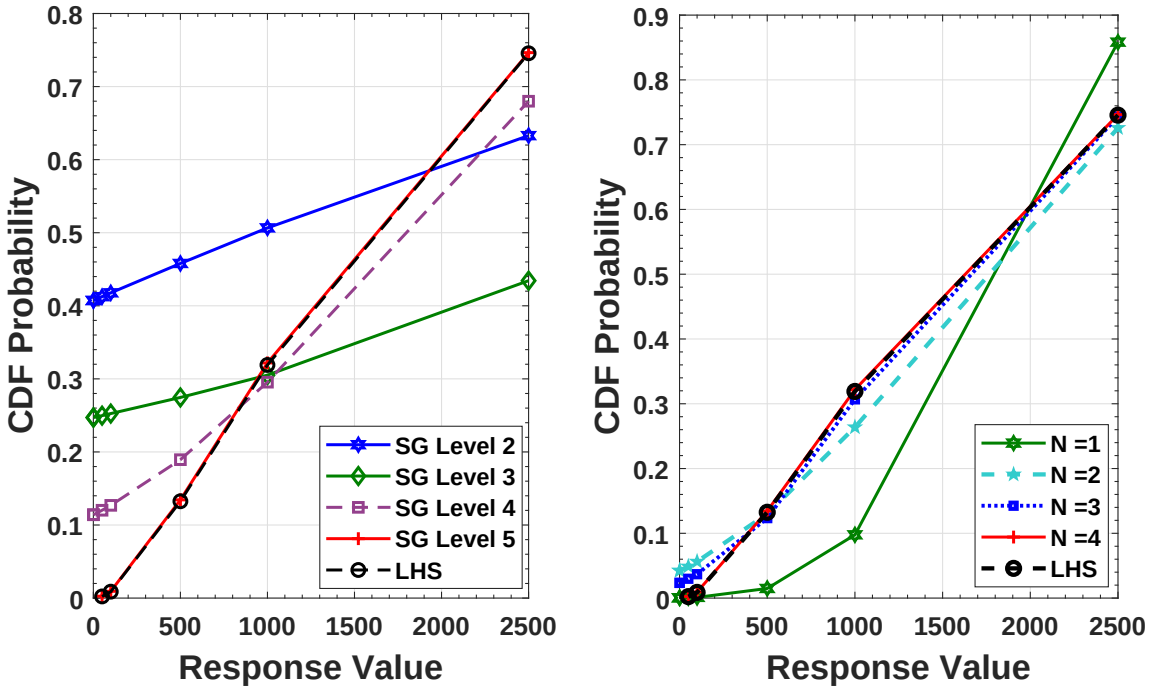

Figure 2.4: Computational results obtained from SG-based gPC expansion

pansion to the reference CDF statistics improves with increasing order of expansion and the gPC expanded solution is exact at fourth order of gPC expansion along with collocation points generated from SG approach of accuracy level 5.

Figure 2.5 depicts the computational results obtained from CUT-based gPC expansion. The CDF probabilities are mapped at various response levels of $f(\boldsymbol{x})$ for increasing CUT-orders (for fourth order of gPC expansion) and increasing orders of gPC expansion (for CUT-8). The convergence of gPC expansion to the reference CDF statistics improves with increasing CUT orders at fixed order of expansion and also with increasing order of expansion at fixed CUT-order. As in the case of sparse grid, fourth order gPC expansion with collocation nodes obtained from CUT-8 is exact along with collocation points generated from CUT approach as a result of satisfying eighth order moment constraint equation (CUT-8).

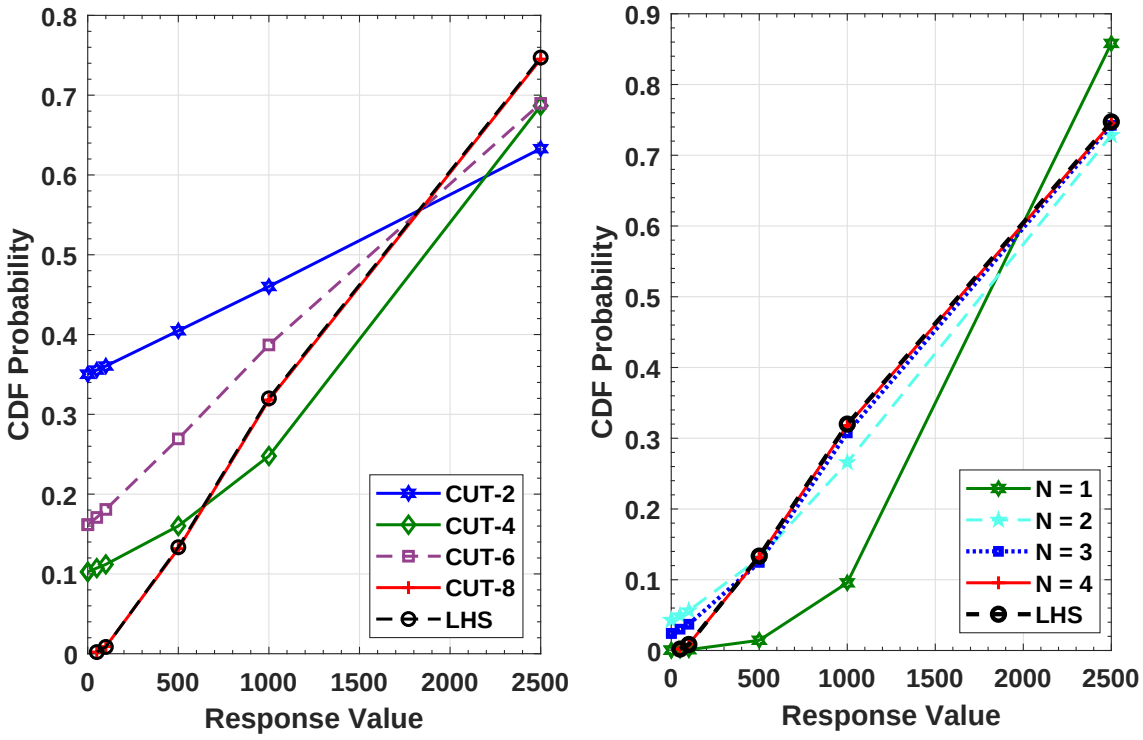

Figure 2.5: Computational results obtained from CUT-based gPC expansion

In order to compare the efficacy of SG and CUT, sum of squared residuals (SSR), which is the sum of squares of residual errors is considered as the comparison metric. SSR in approximated CDF probability levels with SG and CUT-based gPC expansion are computed and plotted on a log-linear graph against the number of collocation samples, as shown in Fig. 2.6. In the case of SG-based gPC expansion, the SSR decreases with increasing number of collocation samples. However, CUT-based gPC expansion shows inconsistencies in convergence with increasing number of collocation samples. Further, it can be inferred that SG-based gPC expansion requires fewer nodes for obtaining higher accuracy as compared to CUT-based gPC expansion.

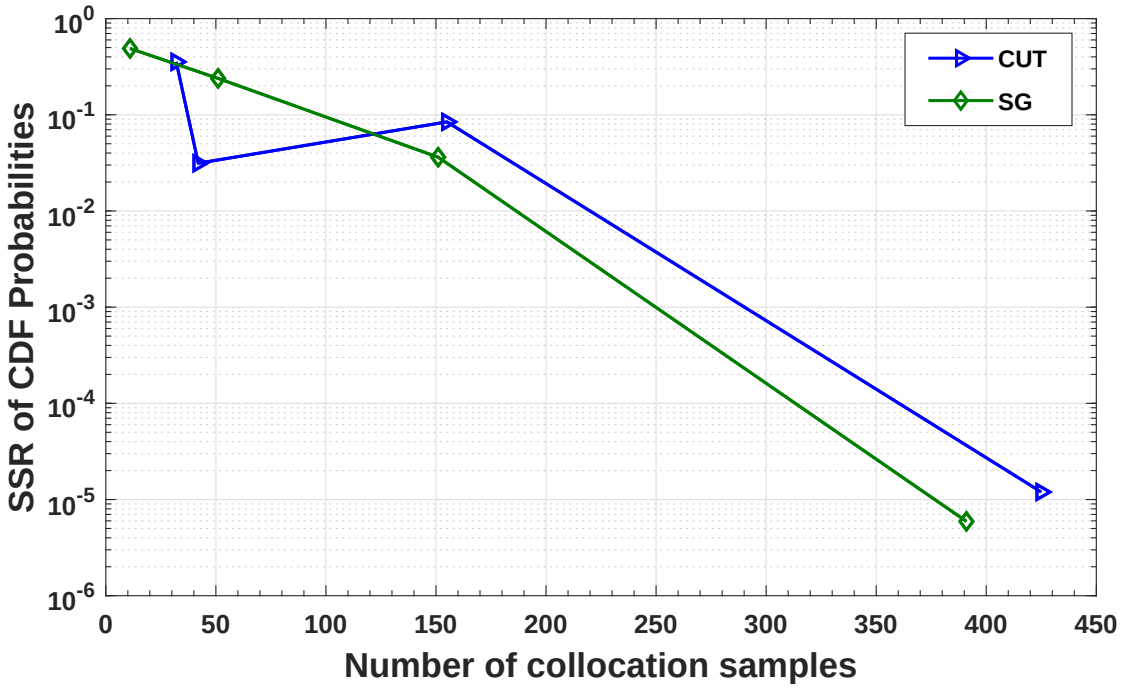

Figure 2.6: Convergence behavior of SG and CUT-based gPC expansion with increasing number of samples in log-linear scale

2.6.2.2 Case II: Random variables are governed by different distribution functions

The governing distribution functions with corresponding supports for the random variables are presented in the Table 2.4. Collocation nodes generated using MSG sampling technique are used to carry out the gPC expansion.

The computational results corresponding to the MSG-based gPC expansion is shown in Fig. 2.7 for increasing levels of accuracy of MSG (for fourth order of gPC ex-

Table 2.4: Distribution of random variables with corresponding gPC basis

Random variable	Distribution	gPC basis
x_1	$\mathcal{U}[-2, 2]$	Legendre
x_2	$\mathcal{U}[-2, 2]$	Legendre
x_3	$\mathcal{U}[-2, 2]$	Legendre
x_4	$\mathcal{N}(0, 0.5^2)$	Hermite
x_5	$\mathcal{N}(0, 0.5^2)$	Hermite

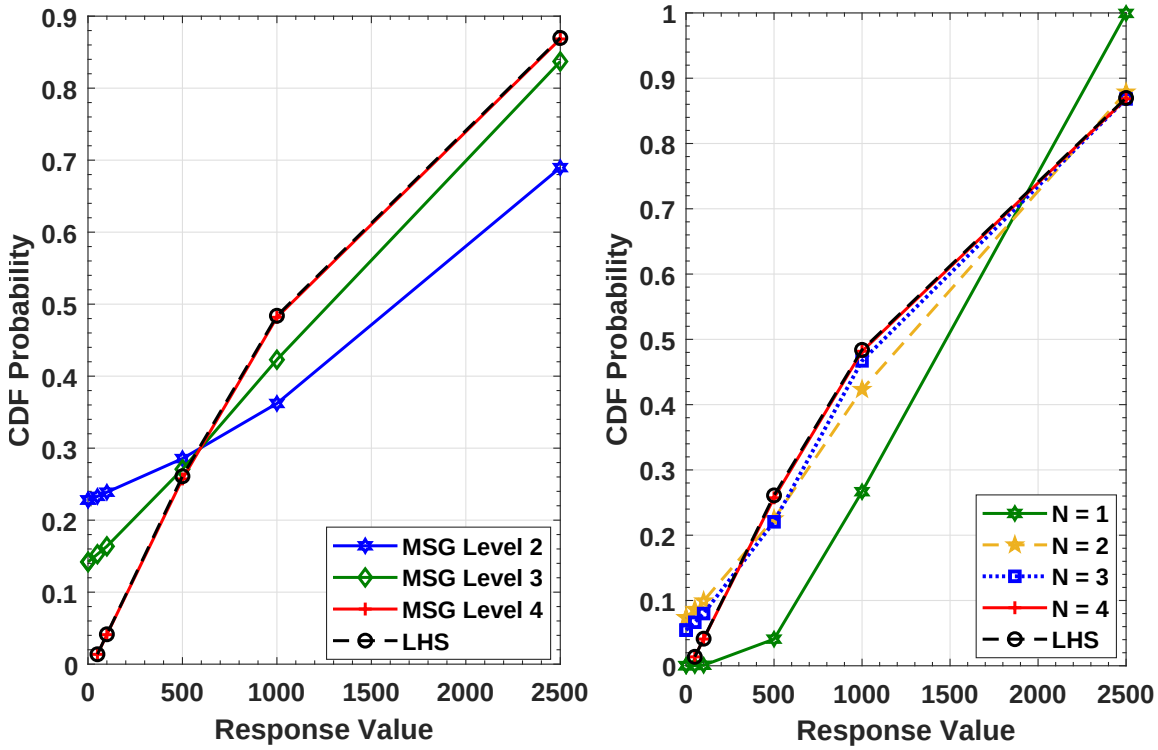

Figure 2.7: Computational results obtained from MSG-based gPC expansion

pansion) and increasing orders of gPC expansion (for fourth accuracy level of MSG). For fourth order of expansion, number of samples generated using MSG of accuracy level lower than 4 is not sufficient to exhibit convergence. Further, with increasing order of gPC expansion, the gPC-approximated CDF statistics shows higher resemblance to the reference statistics as obtained from LHS-based sampling and is exact at fourth order of expansion for collocation nodes generated from fourth accuracy level of MSG. The number of sample points required for MSG-based gPC expansion to converge to reference truth is 881 points which is much fewer than 10,000 samples of LHS-based sampling.

2.6.3 Uncertainty Propagation in a Simple Harmonic Oscillator

Next, we consider the problem of uncertainty propagation in an unforced oscillator system subject to initial condition and parametric uncertainties exhibiting a simple harmonic motion (SHM). The governing equations of motion of the oscillator system is considered to be as follows

$$\ddot{\mathbf{x}}(t, \mathbf{Z}) = -\omega^2 \mathbf{x} \tag{2.39}$$

where $\mathbf{x} = [x_1, x_2]^{\mathrm{T}}$ is the state vector and ω represents the angular frequency for the SHM. For the stochastic process $\mathbf{x}(t, \mathbf{Z})$, which varies randomly as a function of random vector $\mathbf{Z}$ and time t, the SDE in (2.39) can be rewritten in terms of state (x_1 as position and x_2 as velocity) equations as follows

$$\begin{aligned} \frac{dx_1}{dt}(t, \mathbf{Z}) &= x_2 \\ \frac{dx_2}{dt}(t, \mathbf{Z}) &= -\omega^2 x_1. \end{aligned}$$

The angular frequency for SHM is assumed to be uncertain which is governed by uniform probability distribution function. On the other hand, the uncertainties in both the initial states of the oscillator are assumed to be normally distributed. The bounds of uncertainty are presented in the Table 2.5 along with corresponding gPC basis.

Table 2.5: Uncertainty bounds of the random variables

Random Variable	Distribution	gPC basis
$x_1(0)$	$\mathcal{N}(10, 0.1^2)$	Hermite
$x_2(0)$	$\mathcal{N}(0, 0.1^2)$	Hermite
ω	$\mathcal{U}[0.4, 0.8]$	Legendre

The governing SDE has a quadratic term in one of the random input, ω and can treated as the product of two random variables, both having same bounds of

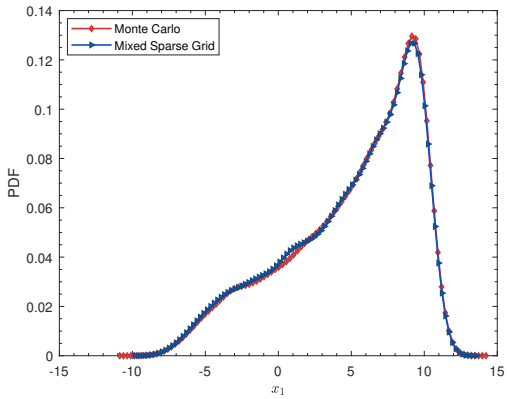

(a) Response PDF of x_1 at $t = 10$ s

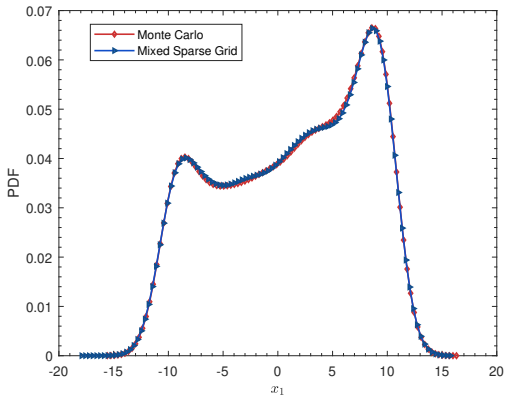

(b) Response PDF of x_1 at $t = 15$ s

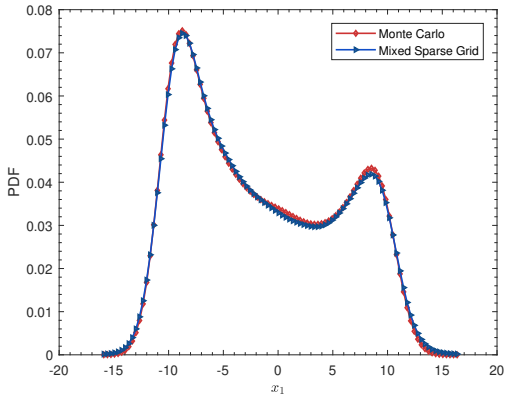

(c) Response PDF of x_1 at $t = 25$ s

Figure 2.8: Probability density estimate of position of the system at various time instants

uncertainty. Thus, the dimension of the uncertainty is four in the stochastic problem under consideration.

As the random variables in the SDE have different probability distribution functions, MSG collocation nodes are generated in order to perform stochastic collocation in gPC expansion framework. Fourth level of accuracy ($\gamma = 4$) is selected to produce MSG collocation nodes. Variable time step Runge-Kutta (4,5) method is employed as the numerical integrator for this problem.

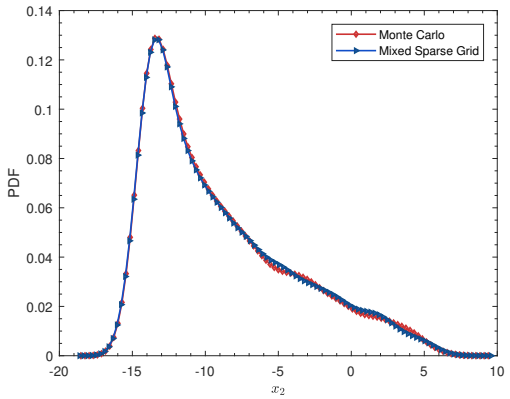

(a) Response PDF of x_2 at $t = 10$ s

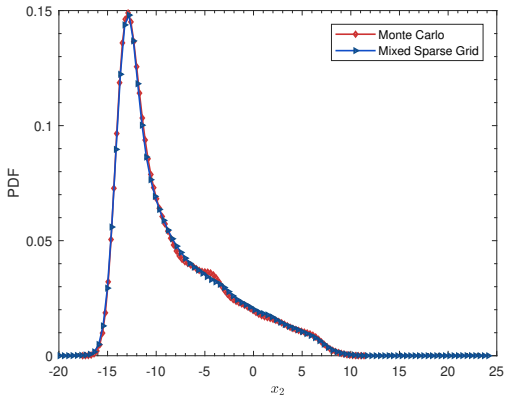

(b) Response PDF of x_2 at $t = 15$ s

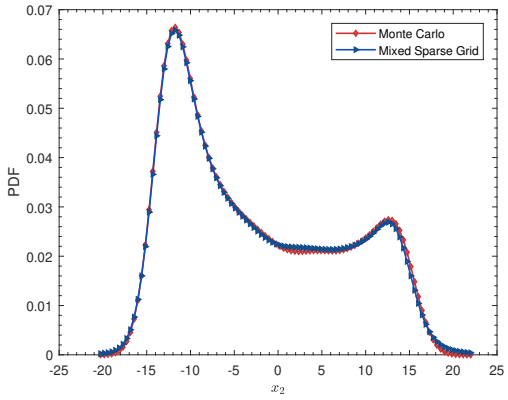

(c) Response PDF of x_2 at $t = 25$ s

Figure 2.9: Probability density estimate of velocity of the system at various time instants

The response distribution obtained from $10,000$ random samples of Monte Carlo simulation is considered to be the reference truth. In order to obtain response PDF from gPC expansion, the coefficients of expansion need to be computed using MSG-based collocation nodes in pseudospectral framework. Once the coefficients are obtained, the solution ensemble is generated by performing eighth order gPC expansion evaluated at $10,000$ random grid points. Once the solution ensemble is generated, the response PDF are obtained using the kernel smoothing density estimate [140] at various time instants.

Figures 2.8 and 2.9 demonstrate the response PDF of position and velocity of the system under SHM at various time instants. A good match with Monte Carlo Simulation (MCS) is seen for MSG-based pseudospectral approach of gPC expansion of eighth order. Table 2.6 depicts the comparison between Monte Carlo simulation (MCS) and MSG-based gPC expansion. To obtain the response PDFs, the number of realizations of solutions along with the total simulation time required to carry out the integration are shown in Table 2.6. It can be inferred that, the number of realizations and hence the simulation time can be reduced by using gPC expansion with MSG collocation nodes.

Table 2.6: Comparison of MSG-based gPC expansion with MCS

Approach	Number of realizations	Simulation Time
MCS	10,000	3217 s
MSG-gPC	1209	254 s

2.6.4 CubeSat Uncertainty Propagation

In recent years, the increased population of resident space objects (RSOs) is a huge challenge for space situational awareness (SSA) [141]. This problem worsens with the presence of uncertainties in the complex dynamics which describe the motion of RSOs. This section presents the use of MSG-based gPC collocation approach to approximate the probability density function of the states of a defunct satellite.

A dynamical model containing perturbations acting on a defunct 2U CubeSat orbiting in low Earth orbit (LEO) as space debris is considered. Aerodynamic drag is considered as the major non-gravitational perturbation and other non-gravitational perturbations are assumed to be negligible. Gravity perturbations due to irregularities

Table 2.7: Uncertainty bounds of the drag parameters influencing the CubeSat

Random variable	Distribution	gPC basis
$\frac{A_{\text{ref}}}{m}$ (Area to mass ratio)	$\mathcal{U}[0.005, 0.014]\ m^2/kg$	Legendre
C_D (Coefficient of Drag)	$\mathcal{U}[2, 4]$	Legendre

in the Earth's geometry and its mass distribution are also considered. In Earth-centered inertial (ECI) frame, the dynamics of the satellite can be written as,

$$\ddot{\mathbf{r}} \;=\; -\frac{\mu}{r^3}\mathbf{r} + \mathbf{a}_D + \mathbf{a}_g \tag{2.40}$$

where $\mathbf{a}_D = -\frac{1}{2}\rho \dot{r}_{rel} \left(\frac{C_D A_{\text{ref}}}{m}\right) \dot{\mathbf{r}}_{\text{rel}}$. Here, $\mathbf{r}$, μ, C_D, A_{ref}, m, and ρ represent the inertial position vector of the CubeSat, drag coefficient, the reference frontal area of the CubeSat, the mass of the CubeSat, and the air density at LEO, respectively. Further, $\dot{\mathbf{r}}_{rel} = \dot{\mathbf{r}} - \boldsymbol{\omega_E} \times \mathbf{r}$ denotes the velocity of the CubeSat relative to the Earth's atmosphere with $\boldsymbol{\omega_E}$ as the angular velocity of the rotation of the Earth and $\dot{r}_{rel}$ is the magnitude of $\dot{\mathbf{r}}_{rel}$. In (2.40), $\mathbf{a}_g$ represent the acceleration of the CubeSat due to gravity perturbations. The expression for the acceleration due to gravity perturbation can be computed by taking the gradient of the aspherical potential function provided in [142].

The Earth is assumed to have an equatorial radius of 6378.137 Km and the gravitational parameter (μ) of the Earth is considered to be 398600.441 Km^3/s^2. The atmosphere around the Earth is considered to be rotating about the rotational axis of the Earth at an angular speed of 7.2921159×10^{-5} rad/s. The *U.S. Standard Atmosphere Model 1976* along with the exponential interpolation is employed to model the density of the atmosphere in LEO. Earth's gravity perturbation incorporates a 200×200 spherical harmonics model as given by GRACE GGM02C gravity model [143].

Table 2.8: Initial orbital elements for the CubeSat in LEO

a	e	i	Ω	ω	θ
6955 km	0.052	65.1 deg	339.94 deg	58 deg	332 deg

Table 2.9: Standard deviation in the initial position uncertainty

Random variable	Distribution	Standard Deviation	gPC basis
X_0 (Initial Position along ECI-x)	Normal	10 m	Hermite
Y_0 (Initial Position along ECI-y)	Normal	10 m	Hermite
Z_0 (Initial Position along ECI-z)	Normal	10 m	Hermite

The uncertainties are considered in the parameters of the drag model and the three initial position states of the CubeSat. The ODE in (2.40) becomes SDE in the presence of the uncertain variables. The parameters of drag model are assumed to be uniformly distributed and the bounds of uncertainty are presented in Table 2.7.

The uncertainty in the position of the satellite are considered to be normally distributed. The mean of the initial positions and the deterministic initial velocities for the 2U-CubeSat can be calculated from the six orbital elements given in the Table 2.8 which are taken from [144]. In this context, six orbital elements: a, e, i, Ω, ω, and θ represent semi-major axis, eccentricity, inclination, right ascension of the node, argument of perigee, and true anomaly respectively. The standard deviation in the position uncertainty of the CubeSat along with corresponding gPC basis is given in the Table 2.9.

The states of the CubeSat are propagated for 10 days using a Runge-Kutta-Fehlberg 7(8) method of integration with a tolerance of 10^{-12}. The response distribution of quantities of interest (QoI) obtained from 100,000 random samples of Monte Carlo simulation is considered to be the reference truth. The response PDFs are also approximated using pseudospectral collocation-based gPC expansion technique. To that end, collocation nodes are generated using MSG sampling technique with

accuracy level of 4 such that, samples on two of the stochastic dimensions (for coefficient of drag and frontal area to mass ratio uncertainties) are generated using Gaussian Legendre-based univariate quadrature rule and the samples on remaining three stochastic dimension (for initial position uncertainties) are generated using Gaussian Hermite-based univariate quadrature rule. Once the coefficients are obtained using MSG-based psuedospectral approach, the solution ensemble of QoI is generated by performing a fifth order gPC expansion evaluated at 100,000 random grid points.

2.6.4.1 Probability density estimate

Figures 2.10, 2.11 and 2.12 depict the posterior distribution of position of the CubeSat after 2.5, 7.5 and 10 days of propagation. The PDF estimates are obtained by applying the kernel density estimation (KDE) technique [140] using the solution ensembles generated from Monte Carlo simulation and gPC expansion. For PDF estimation and plotting, normalized system of units called as canonical units are utilized; where, the units of distance are normalized with respect to mean radius of the Earth resulting in Distance unit (DU).

As can be observed from the Figs. 2.10, 2.11 and 2.12, the PDF estimate produced using fourth level MSG-based pseudospectral approach of gPC expansion shows a close resemblance with that produced from Monte Carlo simulation. Further, it can be observed that, a bimodal behavior in the PDF of the position of CubeSat is just seen to be emerging, despite the fact that the distribution of position was assumed to be Gaussian at an initial epoch. It is well known that, a Gaussian PDF remains Gaussian if the dynamics of the system are linear, the proof of which is trivial (please refer to [145]). This property no longer holds true when the dynamics are non-linear. The bimodal behavior in the PDF can be clearly observed after 10 days of propagation in the ECI-Y position and is evident in ECI-X position of the

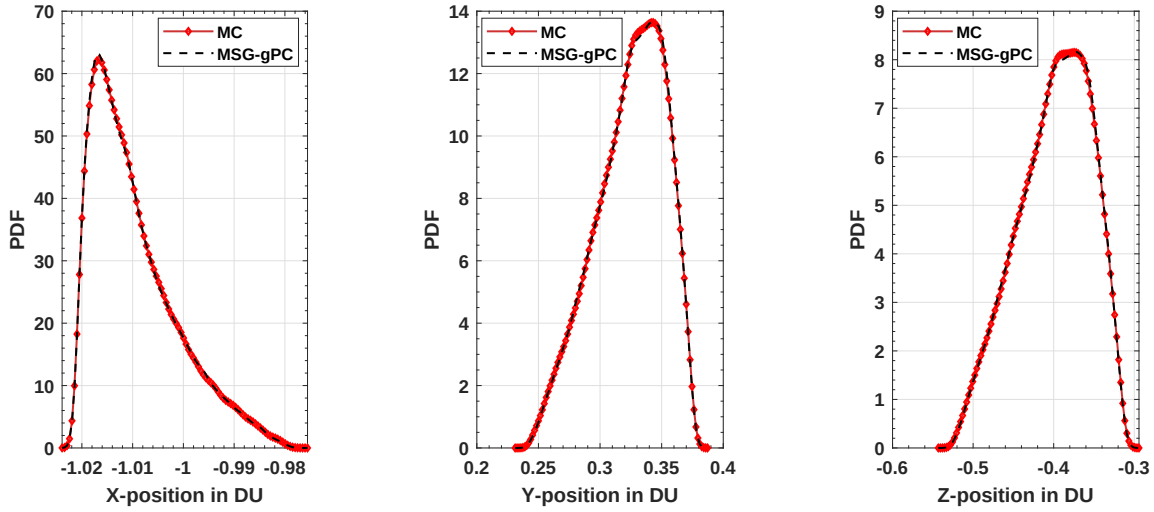

Figure 2.10: Distribution of Monte Carlo and gPC solutions for the position of the CubeSat after 2.5 days

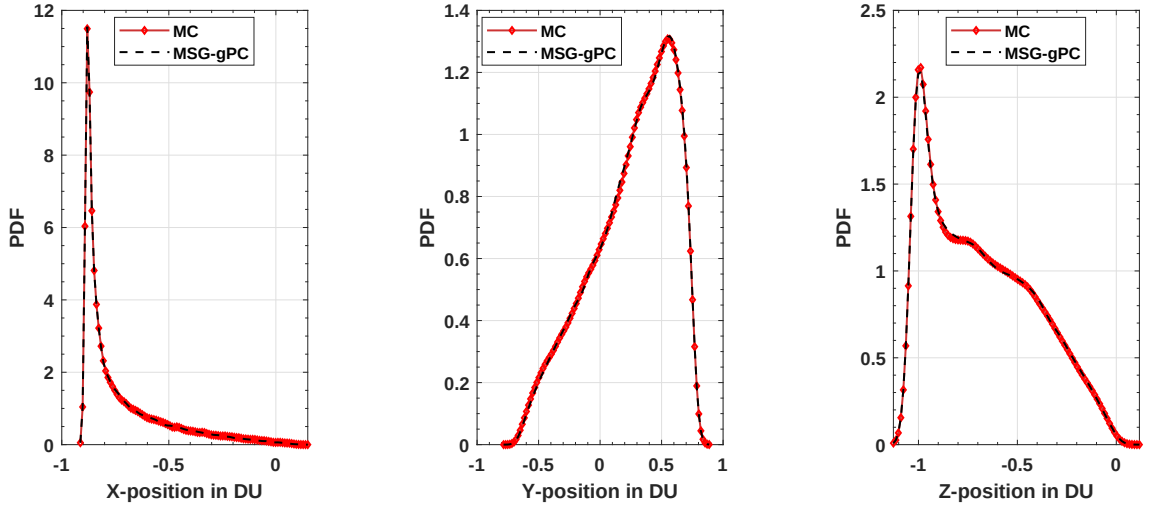

Figure 2.11: Distribution of Monte Carlo and gPC solutions for the position of the CubeSat after 7.5 days

CubeSat. The MSG-based collocation in gPC expansion framework can accurately approximate this bimodality in the PDF.

Table 2.10 illustrates the convergence behavior of the MSG-based gPC expansion as compared to that of Monte Carlo simulation. As mentioned earlier, response

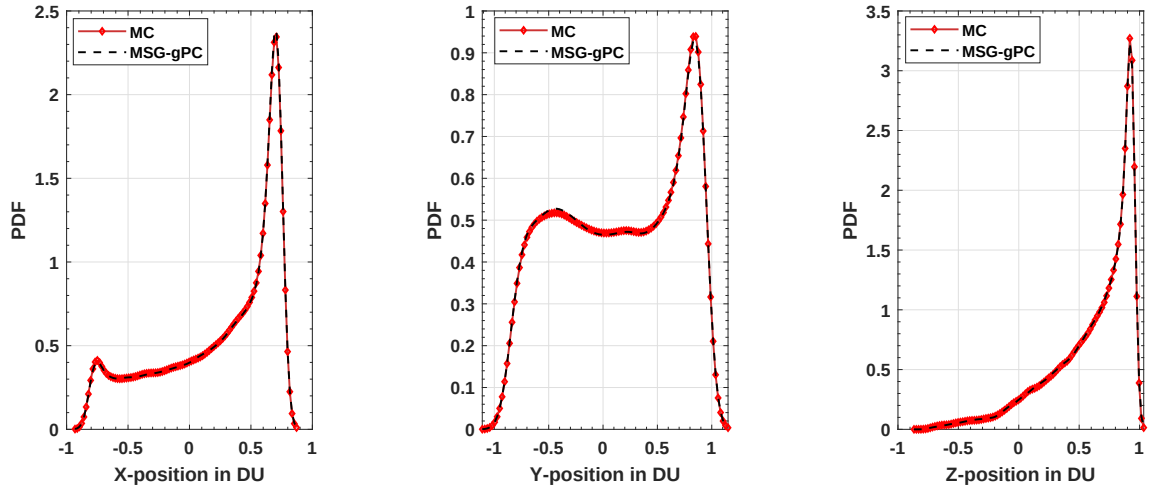

Figure 2.12: Distribution of Monte Carlo and gPC solutions for the position of the CubeSat after 10 days

Table 2.10: Convergence of MSG-based gPC expansion as compared to that of MCS

Candidate approach	Number of samples	Computational time	$\mathcal{D}$
MCS	1000	196 s	0.0920
	2500	492 s	0.0612
	10000	1967 s	0.0291
	50000	9878 s	0.0030
	100000	26264 s	- (Reference)
MSG-based gPC	635	125 s	0.0028
	2702	532 s	0.0001

PDF obtained from 10^5 MCS is considered to be the reference truth. Kullback-Leibler (KL) distance is considered as the measure that can be used to gauge the similarity between the reference solution and the candidate solution. KL-distance is the most frequently used statistical distance measure between two probability distribution functions [146]. If p_0 and p_1 are the two probability densities, the Kullback-Leibler distance is defined as,

$$\mathcal{D}\left(p_1 \mid\mid p_0\right) = \int p_1(x)\ ln\ \left(\frac{p_1(x)}{p_0(x)}\right) dx \tag{2.41}$$

where, $ln(\cdot)$ denotes natural logarithm. As can be observed from Table 2.10, the KL-distance for third level MSG-based gPC expansion (fifth order) with 635 samples is smaller than 50000 Monte Carlo (MC) samples. However, the computational time required for 50000 MC samples is almost 80 folds greater than that required for third level MSG-based gPC expansion. The KL-distance is much higher for MC samples fewer than 50000. In order to estimate the response PDF with KL-distance of order 10^{-4} when compared with 100000 MC realizations, MSG-based gPC expansion requires a nominal 2702 realizations. The number of realizations required for MSG with same order of accuracy can be further reduced by selecting nested univariate rules such as, Kronrod-Patterson and Clenshaw-Curtis based rules [147].

2.6.4.2 Sensitivity analysis

SSA requires estimation of the space object's state and uncertainties to be known accurately. Hence, sensitivity analysis to characterize the influence of the uncertain inputs on the propagated state of the object is very essential. Once the gPC coefficients are obtained, variance-based sensitivity functions for the five random parameters are computed according to (2.28). Figure 2.13 represent the temporal variation of gPC expansion-based total sensitivity on radial position variability of the CubeSat with respect to the five random variables whose distribution attributes are provided in Tables 2.7, 2.8 and 2.9.

As can be observed from Fig. 2.13, for the first few epochs, the most influential random variables on the radial position variability of the CubeSat are the initial conditions of the states of the CubeSat (X_0, Y_0 and Z_0) and the effect of drag parameters (frontal area to mass ratio $\left(\frac{A_{ref}}{m}\right)$ and coefficient of drag (C_D)) is negligible. However, as time progresses, the states of the CubeSat in LEO are quite sensitive to the drag parameters and the effect of initial position uncertainties eventually becomes

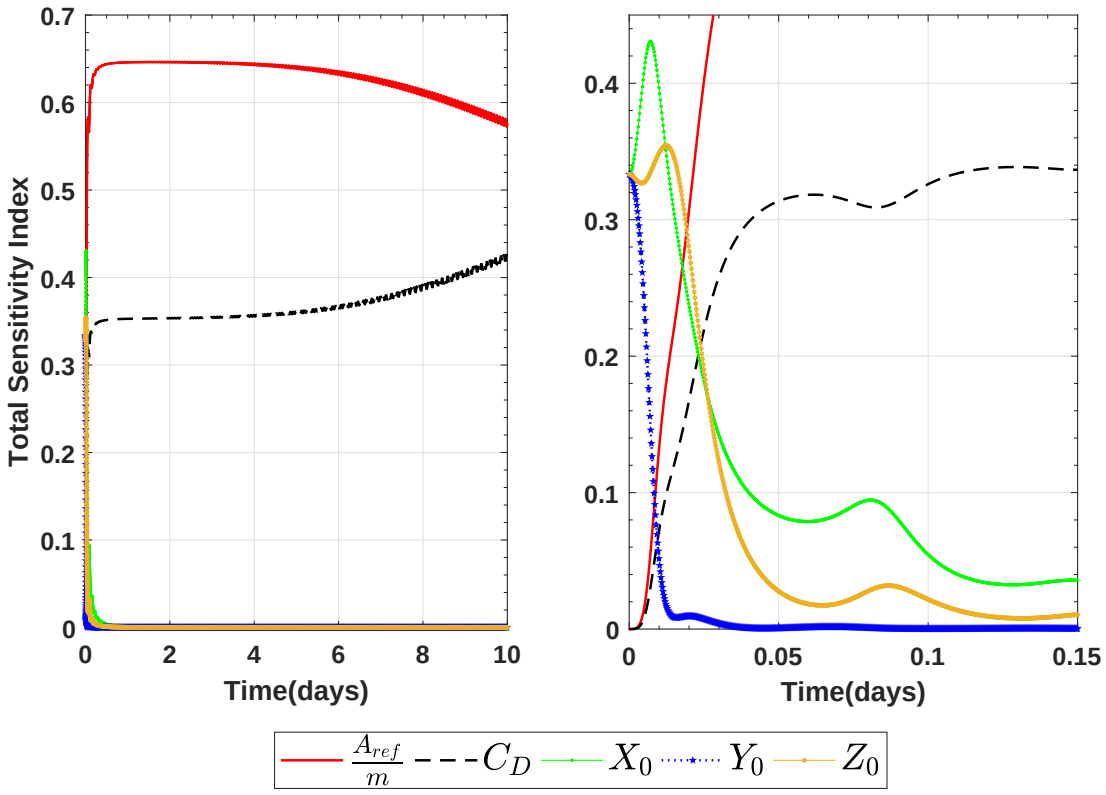

Figure 2.13: Temporal variation of gPC-based total sensitivity of random inputs on radial position of the CubeSat

negligible. Further, it can be clearly observed that, frontal area to mass ratio of the CubeSat is the most significant parameter affecting the radial position of the CubeSat for the time of propagation considered in the simulation.

The high sensitivity index values for the drag parameters agree with the intuition that, effects of atmospheric drag and gravitational perturbations are significant in LEO. As discussed by Eelco [148], smaller satellites and space debris fragments are more sensitive to drag accelerations than large satellites that are otherwise similarly constructed beacuse of larger area to mass ratio. This is in accordance with the results depicted in Fig. 2.13, where the frontal area to mass ratio is by far the most important contributor to the radial position of the CubeSat. As the CubeSat

is propagated further in time, the significance of the coefficient of drag is observed to be increased, while that of frontal area to mass ratio is observed to be decreased.

This result also suggests that more information about object's geometry (instantaneous projected area) and drag coefficient is essential to evaluate and improve the thermospheric models for the objects in LEO and thus to accurately estimate the object's orbital motion. The results presented are also in accordance with the discussion presented in literature [21, 148, 149] regarding effect of drag parameters on orbital determination and orbital lifetime study of objects in LEO.

2.6.5 Nonlinear Coupled Two-Degree-of-Freedom Aeroelastic System

A coupled two-degree-of-freedom aeroelastic system with a cubic stiffness nonlinearity in both degrees of freedom is considered. Few parameters and the initial conditions of the system are considered to be uncertain, hence, the dynamic model of the system is governed by a stochastic differential equation. Pseudospectral approach in gPC collocation framework with MSG nodes is applied to obtain the response distribution of the SDE at various time instants.

Figure 2.14 provides a schematic representation of an airfoil oscillating in pitch and plunge. Fung derived the aeroelastic equations of motion for linear springs [150]. The governing equations of motion for a coupled two-degree-of-freedom system with a cubic stiffness nonlinearity in both pitch and plunge was derived by Lee et al. [151]. The equations of motion involving such nonlinear restoring forces can be written as:

$$\xi'' + x_\alpha \alpha'' + 2\zeta_\xi \frac{\omega_r}{V_r}\xi' + \left(\frac{\omega_r}{V_r}\right)^2 \left(\xi + \beta_\xi \xi^3\right) = p(\tau) \tag{2.42}$$

$$\frac{x_\alpha}{r_\alpha^2}\xi'' + \alpha'' + 2\frac{\zeta_\alpha}{V_r}\alpha' + \frac{1}{V_r^2}\left(\alpha + \beta_\alpha \alpha^3\right) = r(\tau) \tag{2.43}$$

where $\xi = \dfrac{\text{plunge (h)}}{\text{midchord (b)}}$ is the non-dimensional displacement of the hinge point or elastic axis point, α is the pitch angle which is positive nose up about the elastic axis

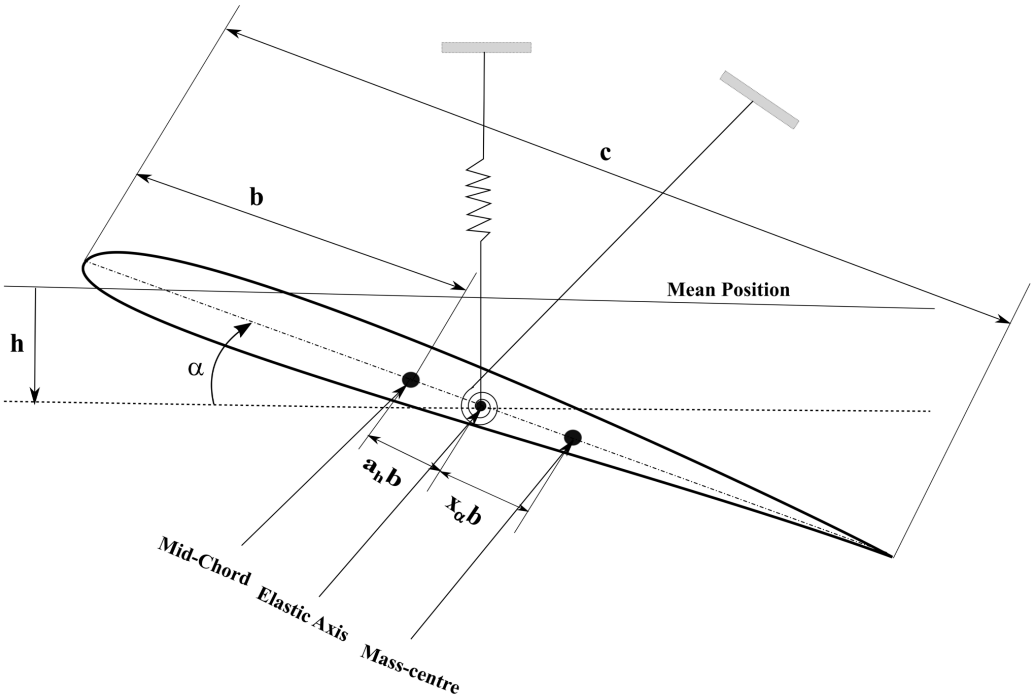

Figure 2.14: Schematic representation of two-degree-of-freedom airfoil

and c is the chord of the airfoil. The elastic axis is located at a distance $a_h b$ from the midchord , while the mass centre is located at a distance $x_a b$ from the elastic axis . Both distances are positive when measured towards the trailing edge of the airfoil. ω_ξ, ζ_ξ, ω_α, and ζ_α are the natural frequencies and damping ratios in uncoupled plunging and pitching modes, respectively. Here, β_α and β_ξ are the nonlinear spring constants which control the amount of structural nonlinearity. Further, r_α is the radius of gyration about the elastic axis, x_α is the non-dimensional distance from the hinge point to the center of mass of airfoil and

$$p(\tau) = -\frac{1}{\pi\mu}C_L(\tau) + \frac{P(\tau)b}{mV_\infty^2} \tag{2.44}$$

$$r(\tau) = \frac{2}{\pi\mu r_\alpha^2}C_M(\tau) + \frac{Q(\tau)}{mV_\infty^2 r_\alpha^2} \tag{2.45}$$

where $P(\tau)$ and $Q(\tau)$ are the external applied force and moment. Various non-dimensional parameters involved in above mathematical expressions are defined as follows:

$$\omega_r = \frac{\omega_\xi}{\omega_\alpha}, \quad V_r = \frac{V_\infty}{b\omega_\alpha}, \quad \tau = \frac{V_\infty t}{b}, \quad \mu = \frac{m}{\pi\rho_\infty b^2}$$

where ω_r, V_r, τ and μ are the frequency ratio, reduced velocity, non-dimensional time and airfoil air mass ratio respectively. Here, m is the airfoil mass per unit length, V_∞ is the free-stream velocity and ρ_∞ is the free-stream density. The expressions for lift and pitching moment coefficients, $C_L(\tau)$ and $C_M(\tau)$ are provided in [151] based on an incompressible flow model given in [150], and are as follows

$$\begin{aligned}
C_L(\tau) =& \pi\left(\xi'' - a_h\alpha'' + \alpha'\right) + 2\pi\left\{\alpha(0) + \xi'(0) + \left(\frac{1}{2} - a_h\right)\alpha'(0)\right\}\phi(\tau) \\
&+ 2\pi\int_0^\tau \phi(\tau-\sigma)\left[\alpha'(\sigma) + \xi''(\sigma) + \left(\frac{1}{2} - a_h\right)\alpha''(\sigma)\right]\mathrm{d}\sigma \\
C_M(\tau) =& \pi\left(\frac{1}{2} + a_h\right)\left\{\alpha(0) + \xi'(0) + \left(\frac{1}{2} - a_h\right)\alpha'(0)\right\}\phi(\tau) \\
&+ \pi\left(\frac{1}{2} + a_h\right)\int_0^\tau \phi(\tau-\sigma)\left\{\alpha'(\sigma) + \xi''(\sigma) + \left(\frac{1}{2} - a_h\right)\alpha''(\sigma)\right\}\mathrm{d}\sigma \\
&+ \frac{\pi}{2}a_h\left(\xi'' - a_h\alpha''\right) - \left(\frac{1}{2} - a_h\right)\frac{\pi}{2}\alpha' - \frac{\pi}{16}\alpha'',
\end{aligned} \tag{2.46}$$

where the Wagner function $\phi(\tau)$ is given by

$$\phi(\tau) = 1 - \Psi_1 \mathrm{e}^{-\varepsilon_1\tau} - \Psi_2 \mathrm{e}^{-\varepsilon_2\tau} \tag{2.47}$$

and $\Psi_1 = 0.165, \Psi_2 = 0.335, \varepsilon_1 = 0.0455$ and $\varepsilon_2 = 0.3$ are the constants [152].

The expressions for $C_L(\tau)$ and $C_M(\tau)$ contain indicial integral forms in terms of Wagner's functions. To that end, Lee et al. transformed equations of motion given in Eqns. (2.42) and (2.43) into a set of eight first-order ordinary differential equations by introducing a set of new variables w_1, w_2, w_3, w_4 which are given by

$$\begin{aligned}
w_1 &= \int_0^\tau \mathrm{e}^{-\varepsilon_1(\tau-\sigma)}\alpha(\sigma)\mathrm{d}\sigma, \quad w_2 = \int_0^\tau \mathrm{e}^{-\varepsilon_2(\tau-\sigma)}\alpha(\sigma)\mathrm{d}\sigma \\
w_3 &= \int_0^\tau \mathrm{e}^{-\varepsilon_1(\tau-\sigma)}\xi(\sigma)\mathrm{d}\sigma, \quad w_4 = \int_0^\tau \mathrm{e}^{-\varepsilon_2(\tau-\sigma)}\xi(\sigma)\mathrm{d}\sigma
\end{aligned} \tag{2.48}$$

Now, the equations (2.42) and (2.43) can be written in terms of Wagner's functions as follows

$$\begin{aligned} c_0\xi'' + c_1\alpha'' + c_2\xi' + c_3\alpha' + c_4\xi + c_5\xi^3 + c_6\alpha + c_7w_1 + c_8w_2 + c_9w_3 + c_{10}w_4 = f(\tau) \\ d_0\xi'' + d_1\alpha'' + d_2\alpha' + d_3\alpha + d_4\alpha^3 + d_3\xi' + d_6\xi + d_7w_1 + d_8w_2 + d_9w_3 + d_{10}w_4 = g(\tau) \end{aligned} \tag{2.49}$$

where the coefficients c_i and d_i, $i = 0, 1, \ldots, 10$, and the forcing functions $f(\tau)$ and $g(\tau)$ are provided in the Appendix D. Finally, the equations of motion of the nonlinear aeroelastic system in (2.49) are rewritten in terms of state variables $x_1 = \alpha$, $x_2 = \dot{\alpha}$, $x_3 = \xi$, $x_4 = \dot{\xi}$, $x_5 = w_1$, $x_6 = w_2$, $x_7 = w_3$ and $x_8 = w_4$ as follows

$$\begin{aligned} \dot{x}_1 &= x_2 \\ \dot{x}_2 &= (c_0H - d_0P) / (d_0c_1 - c_0d_1) \\ \dot{x}_3 &= x_4 \\ \dot{x}_4 &= (-c_1H + d_1P) / (d_0c_1 - c_0d) \\ \dot{x}_5 &= x_1 - \varepsilon_1x_5 \\ \dot{x}_6 &= x_1 - \varepsilon_2x_6 \\ \dot{x}_7 &= x_3 - \varepsilon_1x_7 \\ \dot{x}_8 &= x_3 - \varepsilon_2x_8 \end{aligned} \tag{2.50}$$

where

$$\begin{aligned} P &= c_2x_4 + c_3x_2 + c_4x_3 + c_5x_3^3 + c_6x_1 + c_7x_5 + c_8x_6 + c_9x_7 + c_{10}x_8 - f(\tau) \\ H &= d_2x_2 + d_3x_1 + d_4x_1^3 + d_5x_4 + d_6x_3 + d_7x_5 + d_8x_6 + d_9x_7 + d_{10}x_8 - g(\tau). \end{aligned} \tag{2.51}$$

The aeroelastic system as discussed above involves fluid-structure interaction governed by the coupling of inertial, elastic, and aerodynamic forces. This coupling results in the onset of a flutter phenomena in the aeroelastic system. To that end, a linear aeroelastic system undergoes a change from stable stationary motion to divergent unbounded motion at some critical reduced velocity. The critical point at which

this transformation occurs is called flutter point or Hopf bifurcation point. However, a nonlinear aeroelastic system may enter into a periodic motion called as limit cycle oscillation (LCO) beyond the flutter point. Flutter point is determined numerically by setting the cubic spring constant β_α to be zero. Millman et al. [153] has reported the Hopf bifurcation point to be located at $V_r = 6.279$.

Depending on the value of β_α, the aeroelastic system shows two different types of dynamic responses namely, supercritical and subcritical. For the hard spring with positive β_α, the aeroelastic system demonstrates a supercritical response with a stable periodic solution for reduced velocity greater than the flutter point. On the other hand, subcritical response has a dynamically unstable response at reduced velocities above the flutter point. Lee et al. [154] demonstrated that dynamically unstable subcritical response is generally observed for soft spring where the value of cubic spring constant (β_α) is negative.

Table 2.11: Values of parameters used for simulation

Variable	Values
μ	100
a_h	-0.5
ω_r	0.2
x_α	0.25
β_z	0
r_α	0.5
ζ_α	0
ζ_ξ	0

2.6.5.1 Uncertainty Propagation in Supercritical Regime of the Aeroelastic System

Aeroelastic system operating in supercritical regime demonstrates periodic solution above the flutter point. Hence, the accuracy of MSG-based gPC expansion

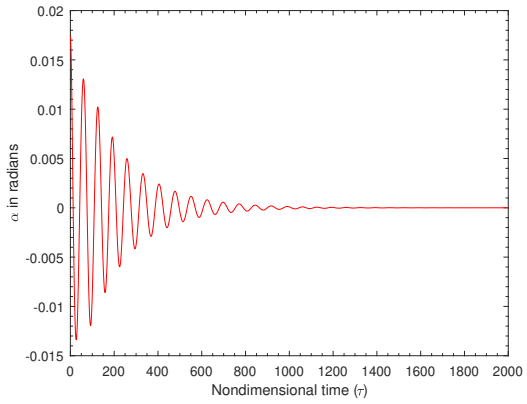

(a) $V_r = 6.2$, $\beta_\alpha = 3$

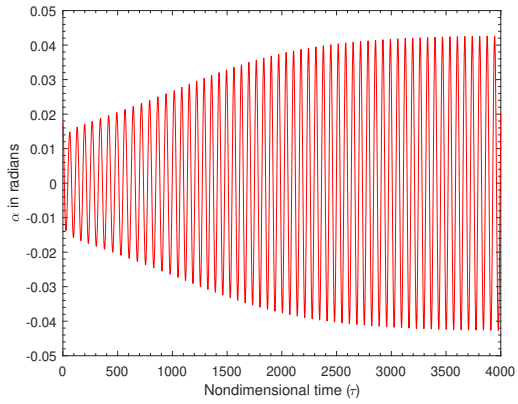

(b) $V_r = 6.3$, $\beta_\alpha = 3$

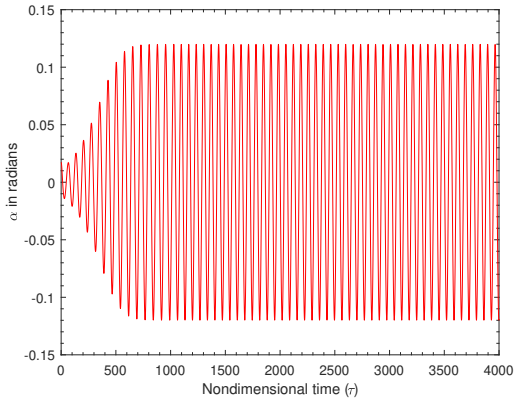

(c) $V_r = 6.4$, $\beta_\alpha = 3$

Figure 2.15: Pitch response of the aeroelastic system with deterministic initial conditions and parameters

is studied in supercritical regime of airfoil above the flutter point. The pitch angle response of the aeroelastic system at different values of reduced velocity around the supercritical Hopf bifurcation point can be observed in Figs.2.15 for the values of the parameters listed in Table 2.11 which are taken from [154]. The initial pitch angle, $\alpha(0)$ is considered to be 1 degree and initial conditions of all the other states are assumed to be zero. The values of the constants in Wagner function, $\psi_1 = 0.165$, $\psi_2 = 0.335$, $\epsilon_1 = 0.0455$ and $\epsilon_2 = 0.3$ are taken from Jones [152].

The initial pitch angle ($\alpha(0)$) and cubic spring constant (β_α) show significant effects on the dynamic behavior of the aeroelastic system as discussed in [153] and [154] and therefore, are considered to be the two stochastic inputs in this work. The initial pitch angle is considered to be normally distributed and the cubic spring constant of the model is considered to be uniformly distributed. The domain of the distribution of random variables along with their corresponding gPC basis for gPC expansion are given in Table 2.12.

Table 2.12: Uncertainty bounds of the random variables

Variable	Distribution	gPC basis
$\alpha(0)$	$\alpha(0) \sim \mathcal{N}\ \left(1 \times \frac{\pi}{180}\text{rad}, (0.2\text{rad})^2\right)$	Hermite
β_α	$\beta_\alpha \sim \mathcal{U}\ [1.5,\ 4.5]$	Legendre

The simulation is carried out for a reduced velocity of 6.5. Fourth-order fixed step Runge Kutta integrator is used to carry out the numerical integration. The time step ($\Delta\tau$) used for the integration is 0.1.

The response distribution obtained from $10,000$ random samples of Monte Carlo simulation (MCS) is considered to be the reference truth. In order to obtain response PDF from gPC expansion, the coefficients of expansion need to be computed using MSG-based collocation nodes in pseudospectral framework. The collocation nodes are generated using MSG sampling technique (with accuracy level, $\gamma = 6$) such that, samples on one of the two stochastic dimensions are generated using Gaussian Legendre univariate quadrature nodes and the samples on the second stochastic dimension are generated using Gaussian Hermite univariate quadrature nodes. The weights corresponding to the sparse grid nodes are obtained for each nodal set in multidimension. Once the coefficients are obtained, the solution ensemble is generated by

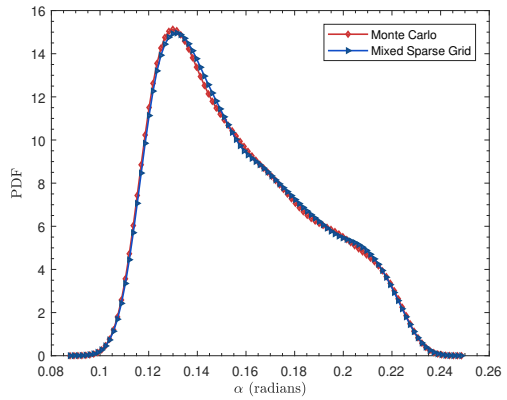

(a) Probability density estimate of α at $\tau = 2000$

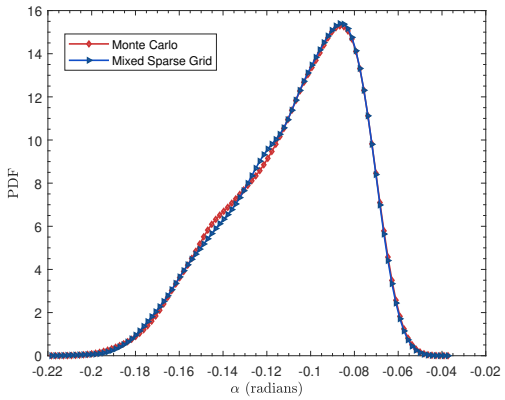

(b) Probability density estimate of α at $\tau = 5000$

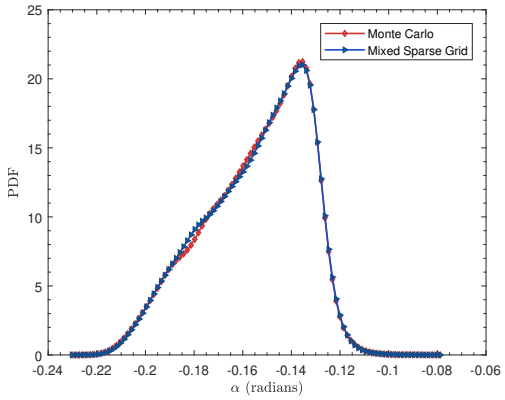

(c) Probability density estimate of α at $\tau = 8000$

Figure 2.16: Probability density estimate of pitch angle α at various non-dimensional time (supercritical regime)

performing eighth order gPC expansion evaluated at $10,000$ random grid points. The probability density estimate based on normal kernel function of pitch angle (α) and non-dimensional plunge (ξ) are obtained using solution ensemble generated from gPC expansion at various non-dimensional time.

The response PDF for pitch and non-dimensional plunge at three different non-dimensional time (τ) are shown in Fig.2.16 and Fig.2.17. The PDF plotted using a MSG-based gPC expansion shows a close resemblance with that of the MCS. Eighth-

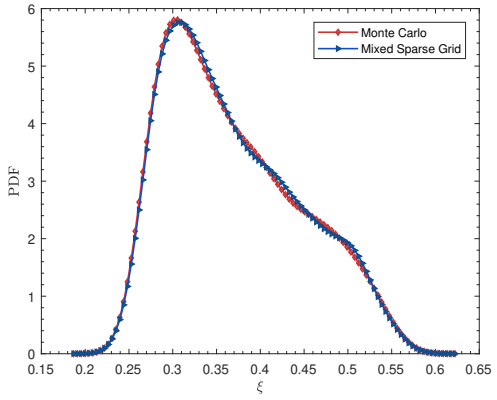

(a) Probability density estimate of ξ at $\tau = 2000$

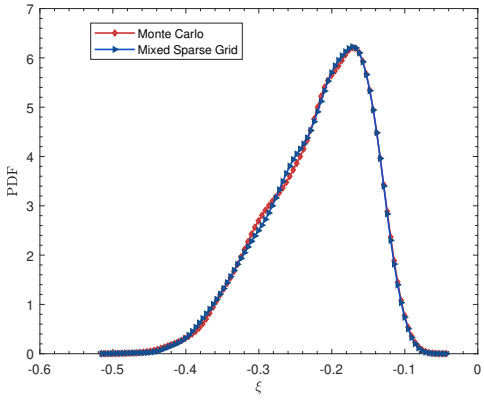

(b) Probability density estimate of ξ at $\tau = 5000$

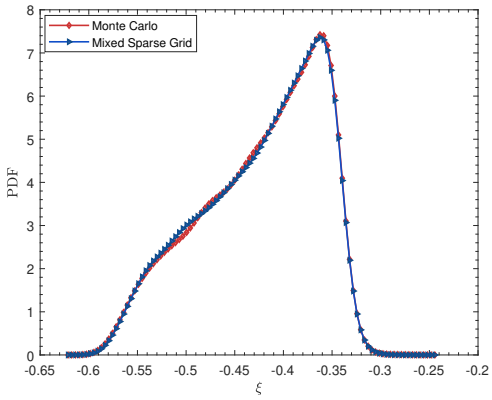

(c) Probability density estimate of ξ at $\tau = 8000$

Figure 2.17: Probability density estimate of non-dimensional plunge ξ at various non-dimensional time (supercritical regime)

order gPC expansion is sufficient enough to capture the response PDF with MSG-based collocation nodes. Moreover, the MSG-based gPC expansion uses much fewer nodes as compared to the MCS which can be observed in Table 2.13. The comparison based on simulation time is also tabulated in Table 2.13 which clearly illustrates that, MSG-based gPC expansion requires less computational time as compared to MCS.

Table 2.13: Comparison of MSG-based gPC with MCS

Approach	Number of realizations	Simulation Time
MCS	10,000	5951 s
MSG-gPC	341	151 s

2.6.5.2 Uncertainty Propagation in Subcritical Regime of Aeroelastic System

In the case when a negative value of cubic spring constant is used, the airfoil exhibits a divergent flutter for any initial pitch angle except $\alpha(0) = 0$ at reduced velocities above the flutter point [153] and the airfoil is said to be operating under subcritical regime. However, if the reduced velocity is less than the flutter point, the airfoil may stabilize after certain duration. In order to illustrate the accuracy of the proposed approach, the uncertainty propagation is also carried out in stable subcritical regime of the aeroelastic system.

The simulation is carried out for a reduced velocity of 6.2 in order to obtain a stable solution. The stability region for subcritical response of aeroelastic system can be obtained from the bifurcation diagram provided by Millman et al. [153]. Distributions of random variables along with their corresponding gPC basis are provided in Table 2.14. Note the domain of the distribution β_α in the negative range which causes the airfoil to operate in subcritical regime.

Table 2.14: Uncertainty bounds of the random variables

Variable	Distribution	gPC basis
$\alpha(0)$	$\mathcal{N}\ \left(1 \times \frac{\pi}{180}\text{rad}, (0.2\text{rad})^2\right)$	Hermite
β_α	$\mathcal{U}\ [-4.5,\ -1.5]$	Legendre

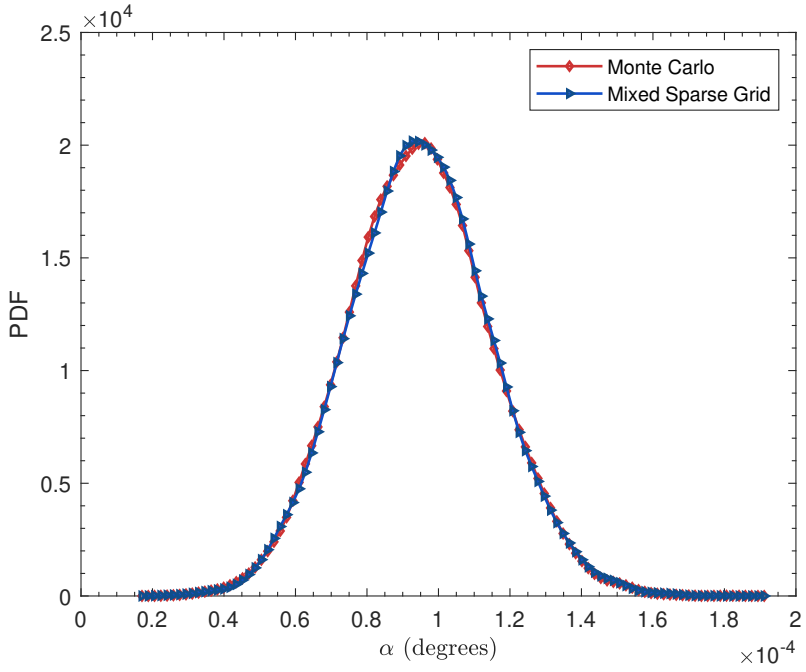

Figure 2.18: Probability density estimate of α at $\tau = 1000$ (subcritical regime)

The response PDF for pitch using 10,000 MCS and MSG ($\gamma = 5$)-based gPC expansion at $\tau = 1000$ is illustrated in Fig. 2.18. Alike in the supercritical regime, the proposed technique is equally accurate in the subcritical regime. The range of the PDF in the order of 10^{-4} suggests that, the initial pitch angle of 1 radians is found to be decaying to zero with time. Further, the estimated distribution of the pitch angle in the subcritical regime is observed to be approximately Gaussian, which is the behavior of the systems which stabilize to a steady state value.

2.6.6 Issue of Long Term Degeneracy With gPC Expansions

The issue of increased nonlinearity of the response surface with increasing integration times for the pitch response of the aeroelastic system has been discussed in [112] and [155]. It was concluded that Gaussian tensor grid-based pseudospectral approach of gPC expansion fails to converge for stochastic models which demonstrate

oscillatory response when integrated for a large period of time, even with very high order of expansion. This issue has been termed as the *long term degeneracy* problem. However, the response PDFs for pitch response of airfoil operating in supercritical regime obtained in Fig. 2.16 using MSG-based gPC expansion do not exhibit this long term degeneracy upon integrating to $\tau = 8000$. Investigation has been carried out in this section to enumerate the possible reasons behind the issue of long term degeneracy in [112] and [155] for the same nonlinear aeroelastic system.

Gaussian tensor grid uses full tensor product of 1D Gaussian rules as been discussed in Section 2.5. The number of nodes increases exponentially in the case of Gaussian tensor grid with increase in number of dimensions. Hence, the use of Gaussian tensor grid in the pseudospectral approach demands huge number of sample points for convergence. If less number of sample nodes are used, higher order moments of the PDF cannot be captured effectively by the sample nodes and results in degeneracy issue. Further, one dimensional quadrature rules are efficient to exactly integrate the polynomials only upto a degree of $2m - 1$, where m is the number of nodes as discussed in Section 2.5. Hence, the tensor grid obtained from the tensor product of these rules are also efficient to integrate polynomials only up to a certain order with the given number of nodes. Thus, it is quite evident that the issue of degeneracy would worsen if fewer samples are used as collocation nodes in the pseudospectral approach of gPC expansion to integrate expectation integrals involving high degree of polynomials.

The response PDF in Fig.2.16 has been obtained using MSG-based sample nodes produced using an accuracy level (γ) of 6 in the sparse grid algorithm. However, the same convergence cannot be obtained if MSG nodes with lower accuracy level are used. The accuracy level of sparse grid algorithm has a proportionate relationship with the number of sparse grid nodes. Table 2.15 gives the number of MSG samples

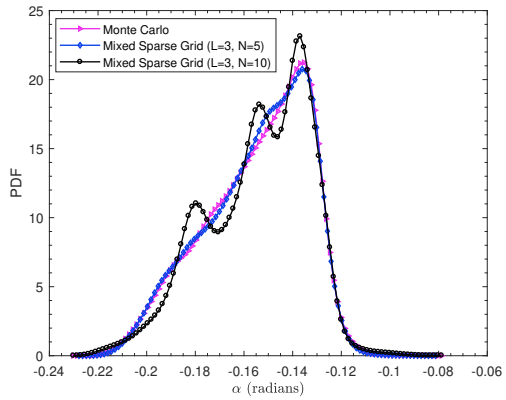

(a) Probability density estimate of α at $\tau = 8000$

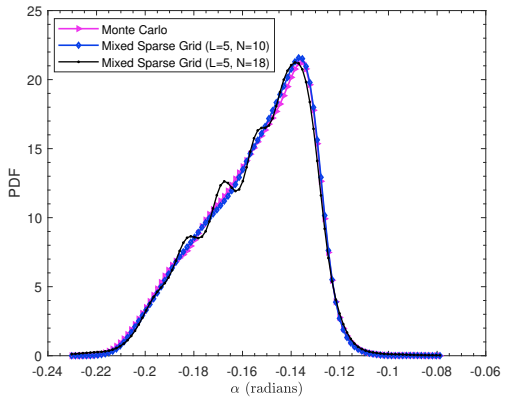

(b) Probability density estimate of α at $\tau = 8000$

Figure 2.19: Estimated response PDF of pitch angle when different accuracy levels of sparse grid are used with different orders of gPC expansion

for stochastic dimension of 2 such that, one of the two random variables is governed by uniform distribution and the other random variable is governed by normal distribution. Hence, the number of MSG points would be fewer when the accuracy level of sparse grid algorithm is reduced below 6, which reduces the convergence behavior of gPC approximated solution if the number of samples are not sufficient enough to capture all the higher order moments of the distribution.

Table 2.15: Number of MSG nodes for stochastic dimension of 2

Accuracy level (γ)	Number of sample nodes
3	54
4	113
5	206
6	341

Figure 2.19 illustrates the response PDF estimate at non-dimensional time, $\tau = 8000$ when MSG nodes of lower accuracy levels ($\gamma < 6$) are used with different orders of gPC expansion. It can be observed from Fig.2.19a that, MSG nodes generated

from sparse grid algorithm with accuracy level of 3 cannot capture the response PDF of the solution accurately with a gPC expansion upto fifth-order. Further increase in gPC expansion order to level 10 further deteriorates the convergence behavior. On increasing the accuracy level of MSG algorithm to 5 improves the convergence of response PDF estimate. The tenth order gPC expansion approximated solution matches quite closely to the reference Monte Carlo simulated solution PDF. However, on further increasing the order of gPC expansion to 18 induces nonlinearity in the response PDF surface.

It is to be noted that, the convergence of the solution obtained from pseudospectral approach is entirely dependent on the convergence behaviour of the quadrature-based integral approximation. Higher the accuracy of the quadrature technique, less would be the difference between the discrete pseudospectral projection and the orthogonal gPC projection, which in turn decides the convergence of the gPC expanded approximation to the true solution. Hence, special care must be taken to select proper type and order of quadrature rule for approximating the expectation integrals. The increased nonlinearity in the response surface can be possibly observed when the number of collocation nodes are not sufficient enough to capture all the higher order moments of the probability distribution function. However, the increase in the number of sample points also increases computational burden. MSG-based stochastic collocation uses fewer samples as compared to Gaussian quadrature with increase in number of stochastic dimensions as discussed in Section 2.5. Hence, the issue of long term degeneracy can be efficiently mitigated by using the proposed algorithm of MSG-based gPC expansion.

2.7 Discussion

As discussed in earlier sections, the major contribution of the research lies in developing MSG-based gPC expansion which can be specifically used in solving SDEs where random variables are characterized by different distribution functions. The only approach available in the literature is the Monte Carlo-based repetitive simulation which can solve such SDEs and hence, MCS is used as the reference method to evaluate the efficiency of MSG-based gPC expansion.

Moreover, the order of the gPC expansion greatly affects the overall accuracy and convergence of the approximation. As discussed in Section 2.6.6, convergence cannot be achieved only by increasing the order of gPC expansion or the number of collocation nodes. For a given number of collocation nodes, the accuracy of the gPC expansion can be improved only by increasing the gPC order to a certain limit, after which the error keeps accumulating and results in the issue of degeneracy in oscillatory systems as shown in Fig. 2.19. Higher order of gPC expansion demands higher number of collocation nodes for improved accuracy. Thus, better convergence can be guaranteed by considering the synchronized increment in both.

2.8 Chapter Summary

This chapter demonstrated the use of the generalized polynomial chaos surrogate modeling technique to approximate the solution of stochastic differential equation and also discussed the efficacy of sparse grid (SG) and conjugate unscented transform (CUT) in solving the problem of uncertainty quantification and propagation. The numerical examples of expectation integral evaluation and uncertainty quantification of Rosenbrock test function illustrated the applicability of the conjugate unscented transform and regular sparse grid techniques which are computationally less burden-

some than Gaussian tensor grids. It can be inferred that, both SG and CUT provide excellent and computationally efficient set of nodes to perform stochastic collocation in gPC framework; however, the accuracy of the latter is limited by the order of CUT to which it can be increased. Higher accuracy in approximation requires more number of quadrature nodes used in collocation; but the number of nodes are limited in CUT of order 8 (CUT-8). On the contrary, the number of collocation nodes can be increased to much higher accuracy level in the context of sparse grid to obtain higher accuracy, but at the cost of computational power.

Further, a numerical non-intrusive approach for solving stochastic differential equations where the underlying random variables are governed by different probability distribution functions was also proposed. The numerical results obtained in all the numerical examples demonstrated the accuracy of proposed mixed sparse grid technique in gPC framework. The results also demonstrated that the mixed sparse grid-based gPC expansion is much more computationally efficient than the random sampling techniques (LHS and MCS). In the problem of orbital uncertainty propagation, sensitivity analysis revealed that the drag parameters i.e. frontal area to mass ratio and coefficient of drag are the most influential parameters to the object's position in the low Earth orbits. Moreover, in the case of uncertain oscillatory systems, the issue of long term degeneracy can be observed with the application of gPC expansion. The mixed sparse grid-based stochastic collocation in gPC expansion framework can mitigate this issue by suitably selecting the number of collocation samples and order of gPC expansion. Although the numerical examples presented in this work consider stochastic problems with random variables governed only by normal and uniform distribution functions, this approach can be easily applied to stochastic problems governed by any form of distribution functions.

Chapter 3

Stochastic Optimal Control of Linear Systems With Probabilistic Uncertainties

This chapter considers the synthesis of minimum expectation optimal trajectories of continuous-time linear systems subject to parametric uncertainties. We present a new theoretical framework for designing the state feedback controller for stochastic systems in the gPC expansion framework. Quadrature-based pseudospectral collocation formulated in Chapter 2 is used to obtain the coefficients required for the gPC expansion. Moreover, the stochastic performance index for optimization involving expectation is converted to a deterministic cost function using the pseudospectral collocation technique. The optimization problem is solved to obtain theoretical control laws for both finite and infinite horizon control problems. A numerical example is presented to demonstrate the accuracy of the proposed approach.

The chapter is organized as follows. We first formulate the problem under consideration in Section 3.1. The gPC expansion of the stochastic linear system is provided in Section 3.2. The theoretical developments to solve minimum expectation optimal control problems for stochastic linear systems using gPC expansion are shown next in Section 3.3. Simulation results are illustrated in Section 3.4, and the concluding remarks are presented in Section 3.5.

3.1 Problem Formulation

Consider a stochastic linear dynamical system of the form

$$\dot{\mathbf{x}}(t,\mathbf{z}) = \mathbf{A}(\mathbf{z})\mathbf{x}(t,\mathbf{z}) + \mathbf{B}(\mathbf{z})\mathbf{u}(t,\mathbf{z}) \tag{3.1}$$

where $\mathbf{x} \in \mathbb{R}^n$ is the state vector, $\mathbf{u} \in \mathbb{R}^m$ is the control input, and $\mathbf{A} \in \mathbb{R}^{n\times n}$ and $\mathbf{B} \in \mathbb{R}^{n\times m}$ are the system matrices. The random vector $\mathbf{z} = [z_1, z_2, \cdots, z_d]^{\mathrm{T}} \in \mathbb{R}^d$ represents uncertainties in system parameters. We assume the probability distribution function of the random variables z_i, $i = 1, \ldots, d$ are stationary and known.

In this work, we consider the design of an optimal state feedback controller that minimizes a finite horizon performance index given by

$$J_1 = \mathbb{E}\left[\frac{1}{2}\mathbf{x}^{\mathrm{T}}(t_f, \mathbf{z})\ \mathbf{P}(t_f)\ \mathbf{x}(t_f, \mathbf{z}) + \frac{1}{2}\int_0^{t_f} \big(\mathbf{x}^{\mathrm{T}}(t, \mathbf{z})\mathbf{Q}\ \mathbf{x}(t, \mathbf{z}) + \mathbf{u}^{\mathrm{T}}(t, \mathbf{z})\mathbf{R}\mathbf{u}(t, \mathbf{z})\big)dt\right], \tag{3.2}$$

and an infinite horizon performance index given by

$$J_2 = \mathbb{E}\left[\frac{1}{2}\int_0^{\infty} \big(\mathbf{x}^{\mathrm{T}}(t, \mathbf{z})\ \mathbf{Q}\ \mathbf{x}(t, \mathbf{z}) + \mathbf{u}^{\mathrm{T}}(t, \mathbf{z})\mathbf{R}\mathbf{u}(t, \mathbf{z})\big)dt\right] \tag{3.3}$$

where $\mathbf{Q} = \mathbf{Q}^{\mathrm{T}} \in \mathbb{R}^{n\times n} > 0$ and $\mathbf{R} = \mathbf{R}^{\mathrm{T}} \in \mathbb{R}^{m\times m} > 0$ are the standard LQR weighting matrices for both the performance indices in (3.2) and (3.3). For the performance index in (3.2), t_f is the final time and $\mathbf{P}(t_f) = \mathbf{P}^{\mathrm{T}}(t_f) \in \mathbb{R}^{n\times n} \geq 0$ is the terminal cost.

3.2 Generalized Polynomial Chaos Expansion of Stochastic Linear System

For the system in (3.1), assuming the solution $\mathbf{x}(t, \mathbf{z}) = [x_1(t, \mathbf{z}), \ldots, x_n(t, \mathbf{z})]^{\mathrm{T}}$ to be a second-order process [128], the gPC expansion of $x_i(t, \mathbf{z})$ for each $i = 1, \ldots, n$ can be written as,

$$x_i\,(t, \mathbf{z}) = \sum_{|\mathbf{r}|=0}^{P} x^c_{i,\mathbf{r}}(t)\Phi_{\mathbf{r}}\,(\mathbf{z}) \tag{3.4}$$

where $x^c_{i,\mathbf{r}}(t)$ is the coefficient of the multidimensional basis $\Phi_{\mathbf{r}}\,(\mathbf{z})$, and $\mathbf{r} = (r_1, \ldots, r_d)$ is the ordered set of multi-indices with $|\mathbf{r}| = r_1 + \cdots + r_d$. As discussed in Chapter 2, the total number of basis functions is given by $N + 1 = \begin{pmatrix} d + P \\ d \end{pmatrix}$. Now, the solution

in (3.4) with multidimensional index $\mathbf{r}$ can be written in terms of a single index k as follows

$$x_i(t, \mathbf{z}) = \sum_{k=0}^{N} x_{i,k}^c(t)\Phi_k(\mathbf{z}) = \mathbf{\Phi}(\mathbf{z})^{\mathrm{T}}\mathbf{x}_i^c(t) \tag{3.5}$$

where $\mathbf{x}_i^c(t) = [x_{i,0}^c(t), x_{i,1}^c(t), \ldots, x_{i,N}^c(t)] \in \mathbb{R}^{N+1}$ is the vector of time-varying gPC coefficients and $\mathbf{\Phi}(\mathbf{z}) = [\Phi_0(\mathbf{z}), \Phi_1(\mathbf{z}), \ldots, \Phi_N(\mathbf{z})]^{\mathrm{T}} \in \mathbb{R}^{N+1}$ is the vector of gPC basis. Moreover, the expansion coefficients can be written as,

$$x_{i,k}^c = \frac{1}{\gamma_k}\mathbb{E}\left[x_i(\mathbf{z})\Phi_k(\mathbf{z})\right] = \frac{1}{\gamma_k}\int_{\Gamma} x_i(\mathbf{z})\Phi_k(\mathbf{z})\boldsymbol{\rho}(\mathbf{z})d\mathbf{z} \tag{3.6}$$

where $\boldsymbol{\rho}(\mathbf{z})$ represents the joint PDF of the random variable vector $\mathbf{z}$ with support $\Gamma \subset \mathbb{R}^d$, and $\gamma_k = \mathbb{E}\left[\Phi_k^2\right] > 0$ is the normalization factor.

3.3 Control Design

In this section, we illustrate the methodology of designing a state feedback controller for the stochastic system described in (3.1) using the gPC expansion framework presented in Section 3.2. In this work, we wish to design a single controller for all the possible variations of the random parameter within the domain of its probability density function. We present the methodology of designing the controller for minimizing the finite horizon performance index provided in (3.2), which can be readily extended to the case of infinite horizon performance index provided in (3.3).

We first rewrite the expectation performance index in terms of gPC coefficients using the gPC solution of the stochastic differential equation in (3.1).

3.3.1 Expectation Performance Index in Terms of Deterministic gPC Coefficients

The control input is designed to be of the following form

$$\mathbf{u}(t, \mathbf{z}) = \mathbf{K}(t)\mathbf{x}(t, \mathbf{z}) \tag{3.7}$$

where $\mathbf{K}(t) \in \mathbb{R}^{m\times n}$ is the time-varying state feedback controller. With the control action in (3.7), the performance index in (3.2) can be written as

$$J_1 = \mathbb{E}\left[\frac{1}{2}\mathbf{x}^{\mathrm{T}}(t_f,\mathbf{z})\ \mathbf{P}(t_f)\ \mathbf{x}(t_f,\mathbf{z}) + \frac{1}{2}\int_0^{t_f} \mathbf{x}^{\mathrm{T}}(t,\mathbf{z})\ \left(\mathbf{Q}+\mathbf{K}^{\mathrm{T}}(t)\mathbf{R}\mathbf{K}(t)\right)\ \mathbf{x}(t,\mathbf{z})\ dt\right]. \tag{3.8}$$

Given (3.5), we can write the gPC expanded solution of (3.1) as

$$\mathbf{x}(t,\mathbf{z}) = \left[\mathbf{I}_n \otimes \mathbf{\Phi}(\mathbf{z})^{\mathrm{T}}\right]\mathbf{x}^c(t) \tag{3.9}$$

where $\mathbf{x}^c = \mathrm{col}(x_1^c, x_2^c, \ldots, x_n^c) \in \mathbb{R}^{(N+1)n}$. To that end, we can write the following

$$\begin{aligned}\mathbb{E}[\mathbf{x}(t)^{\mathrm{T}}\mathbf{x}(t)] =&\ \mathbb{E}\left[\mathbf{x}^c(t)^{\mathrm{T}}\left(\mathbf{I}_n \otimes \mathbf{\Phi}(\mathbf{z})\mathbf{\Phi}(\mathbf{z})^{\mathrm{T}}\right)\mathbf{x}^c(t)\right]\\ =&\ \mathbf{x}^c(t)^{\mathrm{T}}\left(\mathbf{I}_n \otimes \mathbb{E}\left[\mathbf{\Phi}(\mathbf{z})\mathbf{\Phi}(\mathbf{z})^{\mathrm{T}}\right]\right)\mathbf{x}^c(t).\end{aligned} \tag{3.10}$$

As the gPC polynomials are orthogonal such that $\mathbb{E}[\Phi_i(\mathbf{z})\Phi_j(\mathbf{z})] = 0$ for all $i \neq j$ and $\mathbb{E}[\Phi_i^2(\mathbf{z})] = \gamma_i$, we can rewrite (3.10) as

$$\mathbb{E}[\mathbf{x}(t)^{\mathrm{T}}\mathbf{x}(t)] = \mathbf{x}^c(t)^{\mathrm{T}}\left(\mathbf{I}_n \otimes \mathbf{\Gamma}\right)\mathbf{x}^c(t). \tag{3.11}$$

where $\mathbf{\Gamma} = \mathrm{diag}\left(\gamma_0, \gamma_1, \ldots, \gamma_N\right) > 0 \in \mathbb{R}^{(N+1)\times(N+1)}$ is the diagonal matrix of normalization factors. Using (3.11), we obtain

$$\mathbb{E}[\mathbf{x}^{\mathrm{T}}(t_f,\mathbf{z})\mathbf{P}(t_f)\mathbf{x}(t_f,\mathbf{z})] = \mathbf{x}^{\mathrm{c}}(t_f)^{\mathrm{T}}[\mathbf{P}(t_f)\otimes\mathbf{\Gamma}]\mathbf{x}^{\mathrm{c}}(t_f) \tag{3.12}$$

and

$$\mathbb{E}[\mathbf{x}^{\mathrm{T}}(t,\mathbf{z})(\mathbf{Q}+\mathbf{K}^{\mathrm{T}}\mathbf{R}\mathbf{K})\mathbf{x}(t,\mathbf{z})] = \mathbf{x}^{\mathrm{c}}(t)^{\mathrm{T}}[(\mathbf{Q}+\mathbf{K}^{\mathrm{T}}\mathbf{R}\mathbf{K})\otimes\mathbf{\Gamma}]\mathbf{x}^{\mathrm{c}}(t). \tag{3.13}$$

Using (3.12) and (3.13), we can recast the performance index in (3.8) in terms of gPC coefficients as follows

$$J_1 = \frac{1}{2}\mathbf{x}^{\mathrm{c}}(t_f)^{\mathrm{T}}[\mathbf{P}(t_f)\otimes\mathbf{\Gamma}]\ \mathbf{x}^{\mathrm{c}}(t_f) + \frac{1}{2}\int_0^{t_f}\mathbf{x}^{\mathrm{c}}(t)^{\mathrm{T}}\left[(\mathbf{Q}+\mathbf{K}^{\mathrm{T}}(t)\mathbf{R}\mathbf{K}(t))\otimes\mathbf{\Gamma}\right]\ \mathbf{x}^{\mathrm{c}}(t)\ dt. \tag{3.14}$$

Similarly, with the control input $\mathbf{u} = \mathbf{K}\mathbf{x}$ where $\mathbf{K}$ is a constant gain matrix, we can recast the infinite horizon performance index in (3.3) in terms of gPC coefficients as follows

$$J_2 = \frac{1}{2}\int_0^\infty \mathbf{x}^{\mathrm{c}}(t)^{\mathrm{T}}\left[(\mathbf{Q} + \mathbf{K}^{\mathrm{T}}\mathbf{R}\mathbf{K}) \otimes \mathbf{\Gamma}\right]\, \mathbf{x}^{\mathrm{c}}(t)\, dt. \tag{3.15}$$

Using the gPC expansion approach, we have transformed the expectation performance index in terms of coefficients of the gPC expansion. In order to design the feedback controller, we first need to compute these coefficients. We consider the synthesis of optimal state feedback controller using gPC-based pseudospectral collocation approach discussed in Chapter 2.

3.3.2 gPC Expansion-Based Pseudospectral Collocation

As discussed in Chapter 2, the expansion coefficients from (3.6) can be rewritten in the following form using the quadrature approximation,

$$x^c_{i,k}(t) = \frac{1}{\gamma_k}\sum_{q=1}^{N_q} x_i(t, z_q)\Phi_k(z_q)w_q \tag{3.16}$$

where z_q are the quadrature nodes, w_q are the corresponding nodal weights, $x_i(t, z_q)$ is the ith state variable at the quadrature node, and N_q is the number of quadrature nodes used. Let us define $\bar{\mathbf{x}}_i(t) = [x_i(t, z_1), x_i(t, z_2), \cdots, x_i(t, z_{N_q})]^{\mathrm{T}} \in \mathbb{R}^{N_q}$ and $\bar{\mathbf{x}}(t) = \mathrm{col}(\bar{\mathbf{x}}_1(t), \bar{\mathbf{x}}_2(t), \ldots, \bar{\mathbf{x}}_n(t)) \in \mathbb{R}^{nN_q}$. Using (3.16), we can obtain the gPC coefficient $\mathbf{x}^c(t)$ in (3.14) as follows

$$\mathbf{x}^{\mathrm{c}}(t) = \left[\mathbf{I}_n \otimes \mathbf{\Gamma}^{-1}\right]\, [\mathbf{I}_n \otimes \bar{\mathbf{\Phi}}][\mathbf{I}_n \otimes \mathbf{W}]\bar{\mathbf{x}}(t) \tag{3.17}$$

where $\mathbf{W} = \text{diag}(w_1, \cdots, w_{N_q}) \in \mathbb{R}^{N_q \times N_q}$ and

$$\bar{\mathbf{\Phi}} = \begin{bmatrix} \Phi_0(z_1) & \Phi_0(z_2) & \cdots & \Phi_0(z_{N_q}) \\ \Phi_1(z_1) & \Phi_1(z_2) & \cdots & \Phi_1(z_{N_q}) \\ \vdots & \vdots & \cdots & \vdots \\ \Phi_N(z_1) & \Phi_N(z_2) & \cdots & \Phi_N(z_{N_q}) \end{bmatrix} \in \mathbb{R}^{(N+1)\times N_q}. \tag{3.18}$$

Using the Kronecker identities, we can express (3.17) as

$$\mathbf{x}^c(t) = \left[\mathbf{I}_n \otimes \mathbf{\Gamma}^{-1}\bar{\mathbf{\Phi}}\mathbf{W}\right] \bar{\mathbf{x}}(t). \tag{3.19}$$

3.3.3 Feedback Solution

In order to compute $\bar{\mathbf{x}}(t, \mathbf{z})$ at each time instant, the stochastic system in (3.1) is solved at the collocation nodes. The stochastic system (3.1) at the collocation nodes can be rewritten as

$$\dot{\bar{\mathbf{x}}}(t) = \bar{\mathbf{A}}\bar{\mathbf{x}}(t) + \bar{\mathbf{B}}\bar{\mathbf{u}}(t) \tag{3.20}$$

where $\bar{\mathbf{A}}$ and $\bar{\mathbf{B}}$ are defined as follows

$$\bar{\mathbf{A}} = \begin{bmatrix} \mathbf{A}_{11}(z_1) & \mathbf{0} & \cdots & \mathbf{0} & \cdots & \mathbf{A}_{1n}(z_1) & \mathbf{0} & \cdots & \mathbf{0} \\ \mathbf{0} & \mathbf{A}_{11}(z_2) & \cdots & \mathbf{0} & \cdots & \mathbf{0} & \mathbf{A}_{1n}(z_2) & \cdots & \mathbf{0} \\ \vdots & \vdots & \ddots & \vdots & \cdots & \vdots & \vdots & \ddots & \vdots \\ \mathbf{0} & \mathbf{0} & \cdots & \mathbf{A}_{11}(z_{N_q}) & \cdots & \mathbf{0} & \mathbf{0} & \cdots & \mathbf{A}_{1n}(z_{N_q}) \\ \vdots & \vdots & \vdots & \vdots & \vdots & \vdots & \vdots & \vdots & \vdots \\ \mathbf{A}_{n1}(z_1) & \mathbf{0} & \cdots & \mathbf{0} & \cdots & \mathbf{A}_{nn}(z_1) & \mathbf{0} & \cdots & \mathbf{0} \\ \mathbf{0} & \mathbf{A}_{n1}(z_2) & \cdots & \mathbf{0} & \cdots & \mathbf{0} & \mathbf{A}_{nn}(z_2) & \cdots & \mathbf{0} \\ \vdots & \vdots & \ddots & \vdots & \cdots & \vdots & \vdots & \ddots & \vdots \\ \mathbf{0} & \mathbf{0} & \cdots & \mathbf{A}_{n1}(z_{N_q}) & \cdots & \mathbf{0} & \mathbf{0} & \cdots & \mathbf{A}_{nn}(z_{N_q}), \end{bmatrix} \tag{3.21}$$

$$\bar{\mathbf{B}} = \begin{bmatrix} \mathbf{B}_{11}(z_1) & \mathbf{0} & \cdots & \mathbf{0} & \cdots & \mathbf{B}_{1m}(z_1) & \mathbf{0} & \cdots & \mathbf{0} \\ \mathbf{0} & \mathbf{B}_{11}(z_2) & \cdots & \mathbf{0} & \cdots & \mathbf{0} & \mathbf{B}_{1m}(z_2) & \cdots & \mathbf{0} \\ \vdots & \vdots & \ddots & \vdots & \cdots & \vdots & \vdots & \ddots & \vdots \\ \mathbf{0} & \mathbf{0} & \cdots & \mathbf{B}_{11}(z_{N_q}) & \cdots & \mathbf{0} & \mathbf{0} & \cdots & \mathbf{B}_{1m}(z_{N_q}) \\ \vdots & \vdots & \vdots & \vdots & \vdots & \vdots & \vdots & \vdots & \vdots \\ \mathbf{B}_{n1}(z_1) & \mathbf{0} & \cdots & \mathbf{0} & \cdots & \mathbf{B}_{nm}(z_1) & \mathbf{0} & \cdots & \mathbf{0} \\ \mathbf{0} & \mathbf{B}_{n1}(z_2) & \cdots & \mathbf{0} & \cdots & \mathbf{0} & \mathbf{B}_{nm}(z_2) & \cdots & \mathbf{0} \\ \vdots & \vdots & \ddots & \vdots & \cdots & \vdots & \vdots & \ddots & \vdots \\ \mathbf{0} & \mathbf{0} & \cdots & \mathbf{B}_{n1}(z_{N_q}) & \cdots & \mathbf{0} & \mathbf{0} & \cdots & \mathbf{B}_{nm}(z_{N_q}). \end{bmatrix} \tag{3.22}$$

Moreover, the control input in (3.7) at each collocation nodes can be computed as

$$\bar{\mathbf{u}}(t) = \left[\mathbf{K}(t) \otimes \mathbf{I}_{N_q}\right] \bar{\mathbf{x}}(t). \tag{3.23}$$

Substituting (3.23) in (3.20), we obtain the following

$$\dot{\bar{\mathbf{x}}}(t) = \left[\bar{\mathbf{A}} + \bar{\mathbf{B}}\left(\mathbf{K}(t) \otimes \mathbf{I}_{N_q}\right)\right] \bar{\mathbf{x}}(t). \tag{3.24}$$

Using the solution of the gPC coefficients in (3.19) and Kronecker identities, we can write

$$\mathbf{x}^{\mathrm{c}}(t_f)^{\mathrm{T}}[\mathbf{P}(t_f) \otimes \mathbf{\Gamma}]\ \mathbf{x}^{\mathrm{c}}(t_f) = \bar{\mathbf{x}}^{\mathrm{T}}(t_f)\left[\mathbf{P}(t_f) \otimes \mathbf{F}\right]\bar{\mathbf{x}}(t_f) \tag{3.25}$$

and

$$\mathbf{x}^{\mathrm{c}}(t)^{\mathrm{T}}\left[(\mathbf{Q} + \mathbf{K}^{\mathrm{T}}(t)\mathbf{R}\mathbf{K}(t)) \otimes \mathbf{\Gamma}\right]\ \mathbf{x}^{\mathrm{c}}(t) = \bar{\mathbf{x}}^{\mathrm{T}}(t)\left[(\mathbf{Q} + \mathbf{K}^{\mathrm{T}}(t)\mathbf{R}\mathbf{K}(t)) \otimes \mathbf{F}\right]\bar{\mathbf{x}}(t) \tag{3.26}$$

where $\mathbf{F} = \mathbf{W}\bar{\mathbf{\Phi}}^{\mathrm{T}}\mathbf{\Gamma}^{-1}\bar{\mathbf{\Phi}}\mathbf{W} \in \mathbb{R}^{N_q \times N_q}$.

Remark 3.3.1. *In order to obtain a stabilizing feedback solution, we require* $\mathbf{F}$ *to be a positive definite matrix. Note that,* $\mathbf{W}\bar{\mathbf{\Phi}}^{T}$ *is a* $N_q \times (N+1)$ *matrix, and* $\mathbf{\Gamma}$ *is a*

$(N+1)\times(N+1)$ *positive-definite matrix. To that end,* $\mathbf{F}$ *is a positive definite matrix if rank*$(\mathbf{W}\bar{\mathbf{\Phi}}^T) = N_q$ *[156]. By restricting* $N_q \leq (N+1)$*, we obtain* $F > 0$*. Further, using the properties of Kronecker product, we also obtain* $\mathbf{P}(t) \otimes \mathbf{F} > 0$*,* $\mathbf{Q} \otimes \mathbf{F} > 0$*, and* $\mathbf{R} \otimes \mathbf{F} > 0$*.*

Next, we provide a Lemma to derive a stabilizing state feedback controller for the system (3.1) or equivalently the system (3.20).

Lemma 3.3.2. *With the state feedback control law in* (3.7)*, the control gain matrix* $\mathbf{K}$ *stabilizes the stochastic system* (3.1) *asymptotically for all the variations of the random variable* $\mathbf{z}$ *within the domain of its probability density function if the following matrix inequality holds*

$$\big[\bar{\mathbf{A}} + \bar{\mathbf{B}}(\mathbf{K}\otimes\mathbf{I})\big]^T(\mathbb{X}\otimes\mathbf{F}) + (\mathbb{X}\otimes\mathbf{F})\big[\bar{\mathbf{A}} + \bar{\mathbf{B}}(\mathbf{K}\otimes\mathbf{I})\big] < 0 \tag{3.27}$$

where $\mathbb{X} = \mathbb{X}^T \in \mathbb{R}^{n\times n} > 0$*.*

Based on the gPC-based pseudospectral collocation approach, the closed-loop stochastic system is devised in (3.24). Let us consider $V = \bar{\mathbf{x}}^{\mathrm{T}}(t)\,(\mathbb{X}\otimes\mathbf{F})\,\bar{\mathbf{x}}(t)$ as the Lyapunov function. Computing the derivative of the Lyapunov function along the state trajectory of system (3.24), one can obtain the matrix inequality in (3.27).

Moreover, substituting (3.25) and (3.26) in (3.14), the modified finite horizon performance index (cost function) can be written as

$$J_1 = \frac{1}{2}\bar{\mathbf{x}}(t_f)^{\mathrm{T}}\bar{\mathbf{P}}(t_f)\bar{\mathbf{x}}(t_f) + \frac{1}{2}\int_0^{t_f}\bar{\mathbf{x}}(t)^{\mathrm{T}}\big[(\mathbf{Q}+\mathbf{K}^{\mathrm{T}}(t)\mathbf{R}\mathbf{K}(t))\otimes\mathbf{F}\big]\;\bar{\mathbf{x}}(t)\;dt. \tag{3.28}$$

where $\bar{\mathbf{P}}(t_f) = \bar{\mathbf{P}}(t_f)\otimes\mathbf{F} \in \mathbb{R}^{nN_q\times nN_q}$.

Similarly, the modified infinite horizon performance index can be written as

$$J_2 = \frac{1}{2}\int_0^{t_f}\bar{\mathbf{x}}(t)^{\mathrm{T}}\big[(\mathbf{Q}+\mathbf{K}^{\mathrm{T}}\mathbf{R}\mathbf{K})\otimes\mathbf{F}\big]\;\bar{\mathbf{x}}(t)\;dt. \tag{3.29}$$

Note that, Lemma 3.3.2 only provides a stabilizing feedback solution, but doesn't necessarily optimize the performance index in (3.28) and (3.29). To that

end, we present the following Theorems to compute the optimal stabilizing controller. Also, it should be noted that, the expressions in (3.5) and (3.16) are not exact, but approximations required for computational feasibility; thus, the designed controllers are sub-optimal.

Theorem 3.3.3. *The performance index J_1 in* (3.28) *subject to the closed-loop system in* (3.24) *is minimized for a matrix $\mathbf{K}(t)$ solving the following continuous-time Riccati differential equation*

$$-\dot{\bar{\mathbf{P}}}(t) = \big[\bar{\mathbf{A}}+\bar{\mathbf{B}}(\mathbf{K}(t)\otimes\mathbf{I})\big]^T\bar{\mathbf{P}}(t)+\bar{\mathbf{P}}(t)\big[\bar{\mathbf{A}}+\bar{\mathbf{B}}(\mathbf{K}(t)\otimes\mathbf{I})\big]+\big[\mathbf{Q}+\bar{\mathbf{K}}^T(t)\mathbf{R}\mathbf{K}(t)\big]\otimes\mathbf{F}. \tag{3.30}$$

where $\bar{\mathbf{P}}(t)=\bar{\mathbf{P}}(t)>0$ for a given $\bar{\mathbf{P}}(t_f)$ is the solution of (3.30). *The gain matrix $\mathbf{K}(t)$ for all $t\in[0,t_f]$ can be obtained from the following matrix inequality*

$$\big[\bar{\mathbf{A}}+\bar{\mathbf{B}}(\mathbf{K}(t)\otimes\mathbf{I})\big]^T\bar{\mathbf{P}}(t)+\bar{\mathbf{P}}(t)\big[\bar{\mathbf{A}}+\bar{\mathbf{B}}(\mathbf{K}(t)\otimes\mathbf{I})\big]<0. \tag{3.31}$$

Proof. The Hamiltonian of the optimal control problem can be written as

$$\mathcal{H}=\frac{1}{2}\bar{\mathbf{x}}^{\mathrm{T}}(t)\big[(\mathbf{Q}+\mathbf{K}^{\mathrm{T}}(t)\mathbf{R}\mathbf{K}(t))\otimes\mathbf{F}\big]\bar{\mathbf{x}}(t)+\boldsymbol{\lambda}^{\mathrm{T}}\big[\bar{\mathbf{A}}+\bar{\mathbf{B}}(\mathbf{K}(t)\otimes\mathbf{I})\big]\bar{\mathbf{x}}(t) \tag{3.32}$$

where $\boldsymbol{\lambda}\in\mathbb{R}^{nN_q}$ are the vector of costates. The necessary and transversality conditions for optimality are

$$\begin{aligned}\dot{\boldsymbol{\lambda}}(t) &= -\big[(\mathbf{Q}+\mathbf{K}^{\mathrm{T}}(t)\mathbf{R}\mathbf{K}(t))\otimes\mathbf{F}\big]\bar{\mathbf{x}}(t)-\big[\bar{\mathbf{A}}+\bar{\mathbf{B}}(\mathbf{K}(t)\otimes\mathbf{I})\big]^{\mathrm{T}}\boldsymbol{\lambda}(t),\\ \boldsymbol{\lambda}(t_f) &= \bar{\mathbf{P}}(t_f)\bar{\mathbf{x}}(t_f),\end{aligned} \tag{3.33}$$

respectively; where $\bar{\mathbf{P}}=\mathbf{P}\otimes\mathbf{F}$. Let us assume the solution of the system of costate in (3.33) is given by

$$\boldsymbol{\lambda}(t)=\bar{\mathbf{P}}(t)\bar{\mathbf{x}}(t). \tag{3.34}$$

Upon differentiating (3.34) and using (3.33), the continuous-time Riccati differential equation in (3.30) can be obtained. Given $\bar{\mathbf{Q}}+\bar{\mathbf{K}}^{\mathrm{T}}(t)\bar{\mathbf{R}}\bar{\mathbf{K}}(t)>0$, and with Lyapunov analysis the matrix inequality in (3.31) can be obtained. □

Theorem 3.3.4. *The performance index J_2 in* (3.29) *subject to the closed-loop system in* (3.24) *is minimized for a constant matrix* $\mathbf{K}$ *solving the following algebraic Riccati equation*

$$\mathbf{0} = \big[\bar{\mathbf{A}} + \bar{\mathbf{B}}(\mathbf{K} \otimes \mathbf{I})\big]^T \bar{\mathbf{P}} + \bar{\mathbf{P}}\big[\bar{\mathbf{A}} + \bar{\mathbf{B}}(\mathbf{K} \otimes \mathbf{I})\big] + \big[\mathbf{Q} + \bar{\mathbf{K}}^T \mathbf{R}\mathbf{K}\big] \otimes \mathbf{F}. \tag{3.35}$$

where $\bar{\mathbf{P}} = \bar{\mathbf{P}}^T = \mathbf{P} \otimes \mathbf{F} > 0$. *The gain matrix* $\mathbf{K}$ *can be obtained from the following matrix inequality*

$$\big[\bar{\mathbf{A}} + \bar{\mathbf{B}}(\mathbf{K} \otimes \mathbf{I})\big]^T \bar{\mathbf{P}} + \bar{\mathbf{P}}\big[\bar{\mathbf{A}} + \bar{\mathbf{B}}(\mathbf{K} \otimes \mathbf{I})\big] < 0. \tag{3.36}$$

The proof of Therorem 3.3.4 follows from that of Theorem 3.3.3. As $t_f \to \infty$, the solution to the Riccati equation in (3.30) converges to a unique positive definite solution $\bar{\mathbf{P}}(\infty)$ and $\dot{\bar{\mathbf{P}}} \to 0$.

Note that, for the finite-horizon case, the terminal $\bar{\mathbf{P}}(t)$, i.e. $\bar{\mathbf{P}}(t_f)$ is known. Therefore, the matrix inequality (3.31) and the Riccati differential equation can be solved simultaneously to obtain $\mathbf{K}(t)$ and $\bar{\mathbf{P}}(t)$ for all $t = [0, t_f]$. However, this is not the case with that of infinite-horizon performance index, and further, matrix inequality in (3.36) is a bilinear matrix inequality (BMI), which is not trivial to solve. To that end, we present the following corollary to obtain an equivalent linear matrix inequality (LMI).

Corollary 3.3.5. *Under the conditions of Theorem 3.3.4, the performance index J_2 in* (3.29) *is minimized for a constant matrix* $\mathbf{K} = \mathbf{L}\mathbf{S}^{-1}$ *where* $\mathbf{L} \in \mathbb{R}^{m \times n}$ *and* $\mathbf{S} = \mathbf{P}^{-1} \in \mathbb{R}^{n \times n}$ *satisfy following conditions:*

$$\begin{aligned}\big(\mathbf{S} \otimes \mathbf{F}^{-1}\big)\bar{\mathbf{A}}^T + \bar{\mathbf{A}}\big(\mathbf{S} \otimes \mathbf{F}^{-1}\big) + \big(\mathbf{L}^T \otimes \mathbf{F}^{-1}\big)\bar{\mathbf{B}}^T + \bar{\mathbf{B}}\big(\mathbf{L} \otimes \mathbf{F}^{-1}\big) \\ + \big(\mathbf{S}\mathbf{Q}\mathbf{S} + \mathbf{L}^T\mathbf{R}\mathbf{L}\big) \otimes \mathbf{F}^{-1} = 0\end{aligned} \tag{3.37}$$

and

$$\big(\mathbf{S} \otimes \mathbf{F}^{-1}\big)\bar{\mathbf{A}}^T + \bar{\mathbf{A}}\big(\mathbf{S} \otimes \mathbf{F}^{-1}\big) + \big(\mathbf{L}^T \otimes \mathbf{F}^{-1}\big)\bar{\mathbf{B}}^T + \bar{\mathbf{B}}\big(\mathbf{L} \otimes \mathbf{F}^{-1}\big) < 0. \tag{3.38}$$

Proof. From Theorem 3.3.4, we can rewrite (3.35) as

$$\begin{aligned}\bar{\mathbf{A}}^{\mathrm{T}}(\mathbf{P}\otimes\mathbf{F})+(\mathbf{P}\otimes\mathbf{F})\bar{\mathbf{A}}+(\mathbf{K}^{\mathrm{T}}\otimes\mathbf{I})\bar{\mathbf{B}}^{\mathrm{T}}(\mathbf{P}\otimes\mathbf{F})+(\mathbf{P}\otimes\mathbf{F})\bar{\mathbf{B}}(\mathbf{K}\otimes\mathbf{I})\\ +\left(\mathbf{Q}+\mathbf{K}^{\mathrm{T}}\mathbf{R}\mathbf{K}\right)\otimes\mathbf{F}=0.\end{aligned} \tag{3.39}$$

Pre and post-multiplying (3.39) by $(\mathbf{P}\otimes\mathbf{F})^{-1}$, and using the Kronecker product identities, we obtain

$$\begin{aligned}(\mathbf{P}^{-1}\otimes\mathbf{F}^{-1})\bar{\mathbf{A}}^{\mathrm{T}}+\bar{\mathbf{A}}(\mathbf{P}^{-1}\otimes\mathbf{F}^{-1})+(\mathbf{P}^{-1}\mathbf{K}^{\mathrm{T}}\otimes\mathbf{F}^{-1})\bar{\mathbf{B}}^{\mathrm{T}}+\bar{\mathbf{B}}(\mathbf{K}\mathbf{P}^{-1}\otimes\mathbf{F})\\ +\left(\mathbf{P}^{-1}\left(\mathbf{Q}+\mathbf{K}^{\mathrm{T}}\mathbf{R}\mathbf{K}\right)\mathbf{P}^{-1}\right)\otimes\mathbf{F}^{-1}=0.\end{aligned} \tag{3.40}$$

Using $\mathbf{P}^{-1}=\mathbf{S}$, we obtain

$$\begin{aligned}(\mathbf{S}\otimes\mathbf{F}^{-1})\bar{\mathbf{A}}^{\mathrm{T}}+\bar{\mathbf{A}}(\mathbf{S}\otimes\mathbf{F}^{-1})+(\mathbf{S}\mathbf{K}^{\mathrm{T}}\otimes\mathbf{F}^{-1})\bar{\mathbf{B}}^{\mathrm{T}}+\bar{\mathbf{B}}(\mathbf{K}\mathbf{S}\otimes\mathbf{F})\\ \left(\mathbf{S}\mathbf{Q}\mathbf{S}+\mathbf{S}\mathbf{K}^{\mathrm{T}}\mathbf{R}\mathbf{K}\mathbf{S}\right)\otimes\mathbf{F}^{-1}=0.\end{aligned} \tag{3.41}$$

Further, with $\mathbf{L}=\mathbf{K}\mathbf{S}$, one can obtain the equality (3.37). Following the similar procedure for (3.36), one can obtain the LMI in (3.38). □

3.3.4 Implementation

The schematic of the design of the feedback controller and its implementation is depicted in Fig. 3.1 for the case of the infinite horizon performance index. Note that the control gain matrix is designed offline, only once. The designed controller is also implemented to stabilize the plant for all variations of the random variable $\mathbf{z}$ within the domain of its probability density function. Also, the offline computation of the controller only requires the structure of the system matrices as a function of the random variable $\mathbf{z}$ and not the value of the random variable explicitly.

In order to compute the collocation nodes, one can use the quadrature rules available in the literature based upon the distribution of the random variable. For example, for normal and uniform random variables, one can use Gaussian Hermite

and Gaussian Legendre-based tensor grid rules, respectively. However, it should be noted that Gaussian tensor grids are computationally expensive for high-dimensional problems [117]. To reduce the cost of computation, we employ sparse grid-based quadrature nodes discussed in Chapter 2. Although the formulation in this chapter is carried out for linear systems with parametric uncertainties, the theoretical developments can also be used for systems with both parametric and initial condition uncertainties. Moreover, we can also use the results developed in this chapter to develop feedback solutions for systems with different probability distribution functions. For example, for systems with parametric uncertainties modeled as uniform distribution and initial condition uncertainties as normal distribution, we can employ mixed-sparse grid quadrature rules developed in Chapter 2.

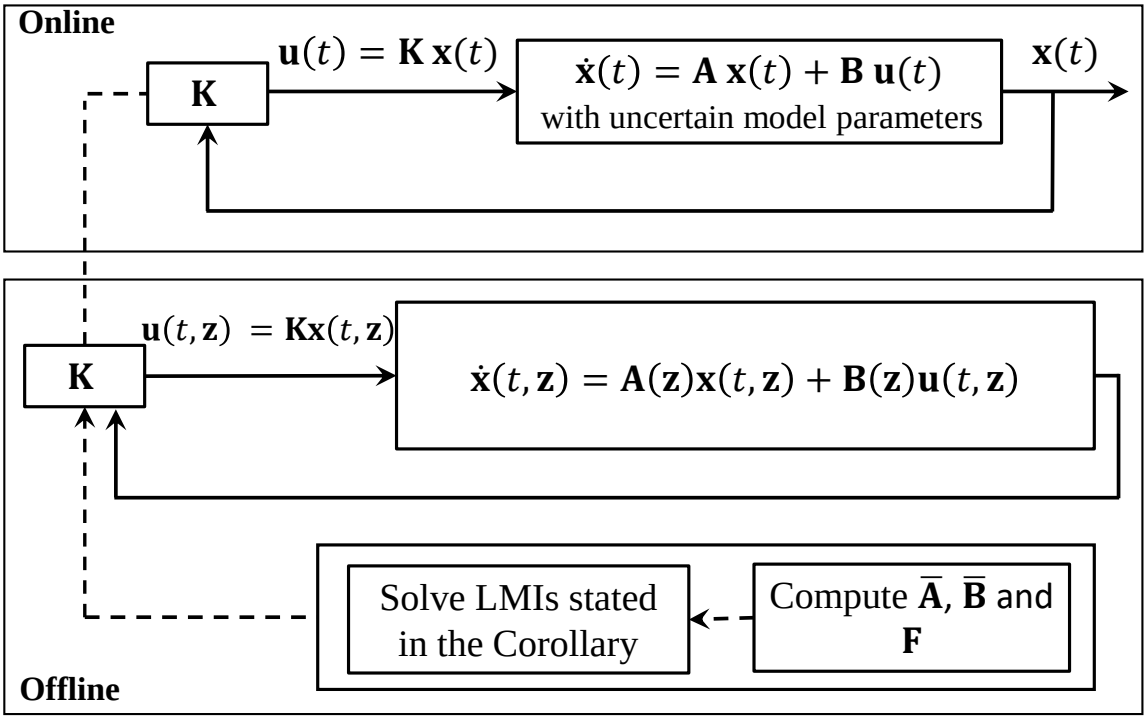

Figure 3.1: Offline computation of the controller and its implementation

3.4 Simulation Results

We consider an example used in [36] with following system matrices

$$\mathbf{A} = \begin{bmatrix} 2+z & 2 \\ -3 & -4 \end{bmatrix}, \quad \mathbf{B} = \begin{bmatrix} 1 \\ 1 \end{bmatrix} \tag{3.42}$$

where z is a uniformly distributed random parameter within the range [-1, 1]. The results obtained in [36] uses the control formulation, which is derived based on the Galerkin projection method for computing the gPC coefficients. Note that the open-loop system is stable only for $z < -0.5$.

For the case of infinite horizon performance index-based control design using gPC-based pseudospectral collocation technique, we use the following weighting matrices $\mathbf{Q} = \mathbf{I}_2$ and $\mathbf{R} = 1$. Using Corollary 3.3.5, we obtain the state feedback controller to be $\mathbf{K} = \begin{bmatrix} -2.3362 & -0.6276 \end{bmatrix}$ that minimizes the infinite horizon expectation performance index. To carry out similar analysis as in [36], we design two other LQR controllers: (i) $\mathbf{K}_{\text{nom}}$ with $z = 0$ (for the nominal system without any parametric uncertainty), and (ii) $\mathbf{K}_{\text{wc}}$ with $z = 1$ (for the worst-case uncertainty). We obtain the control gain matrices to be: $\mathbf{K}_{\text{nom}} = [-2.3289 - 0.7823]$ and $\mathbf{K}_{\text{wc}} = [-3.8570 - 1.1250]$.

To compare the performance of the three controllers for different values of uncertainty, z is varied from -1 to 1 in an interval of 0.05. Figure 3.2 depicts the plot of closed-loop eigenvalues for various values of z when the state feedback control strategy is applied with $\mathbf{K}$, $\mathbf{K}_{\text{nom}}$ and $\mathbf{K}_{\text{wc}}$. As pointed out by [36], implementation of $\mathbf{K}_{\text{nom}}$ results in substantial variation in the closed-loop damping and natural frequency with variation in z. It should be noted that, although the closed-loop eigenvalues are all in the left half of the complex-plane upon implementing $\mathbf{K}_{\text{nom}}$ for the example under consideration, this is not always the case (since the nominal controller is not guaranteed to stabilize the system with parametric uncertainties). Similar to the results

obtained from the Galerkin projection-based formulation in [36], there is considerably smaller variation in the nature of closed-loop eigenvalues upon implementing the controller ($\mathbf{K}$) derived from the pseudospectral collocation-based formulation. As observed, the closed-loop eigenvalues obtained from implementing the controller designed for worst-case uncertainty ($\mathbf{K}_{\text{wc}}$) are located on the far left of the complex plane. This depicts the conservative closed-loop performance of $\mathbf{K}_{\text{wc}}$.

Further, we compare the cost-to-go for different values of z with initial condition of $\mathbf{x}(0) = [1, 0.1]^{\text{T}}$ as illustrated in Fig. 3.3. We also compute the area under the three curves obtained in Fig. 3.3. The results are summarized as follows:

(i) As expected, the nominal controller $\mathbf{K}_{\text{nom}}$ achieves the lowest cost at $z = 0$. The area under the curve for the nominal controller is obtained to be $A_{\text{nom}} = 32.83$.

(ii) As expected, the controller designed for worst-case uncertainty $\mathbf{K}_{\text{wc}}$ achieves the lowest cost at $z = 1$. The area under the curve for the worst-case controller is obtained to be $A_{\text{wc}} = 36.19$.

(ii) The area under the curve from the implementation of gPC controller $\mathbf{K}$ is obtained to be $A_{\text{gPC}} = 31.40$. Since the gPC controller is designed to minimize the expectation (average) performance, we observe $A_{\text{gPC}} < A_{\text{nom}} < A_{\text{wc}}$.

In order to compare the performance of the designed controller, we compute the disk-based gain and phase margin [113] of the system for different values of $z \in [-1\ 1]$. The variation of the disk-based gain and phase margins with variation in z is plotted in Fig. 3.4. We observe that, the bounds of gain and phase margin decrease constantly as the value of z changes from -1 to 1.

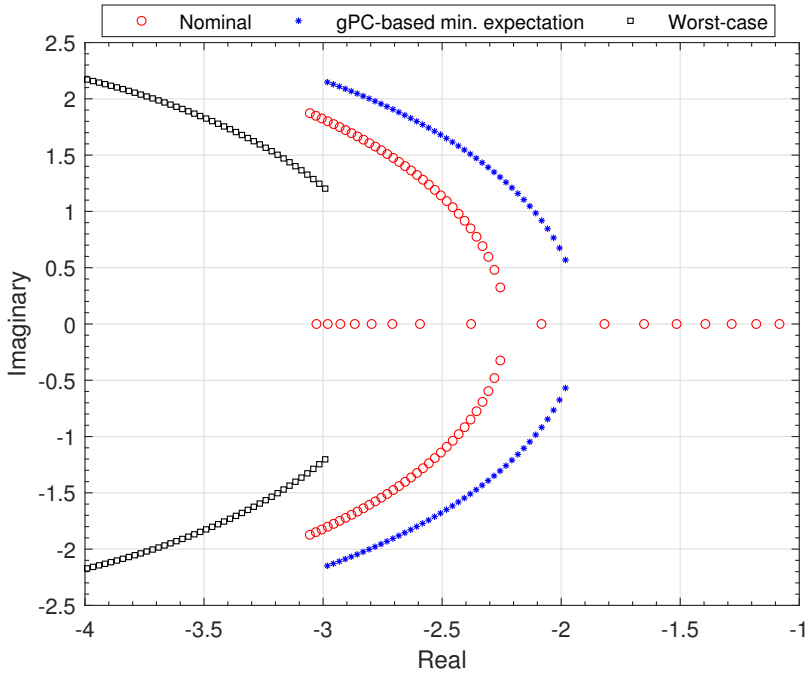

Figure 3.2: Eigenvalues of the closed-loop system with minimum expectation control, nominal optimal control, and optimal control designed for worst case uncertainties

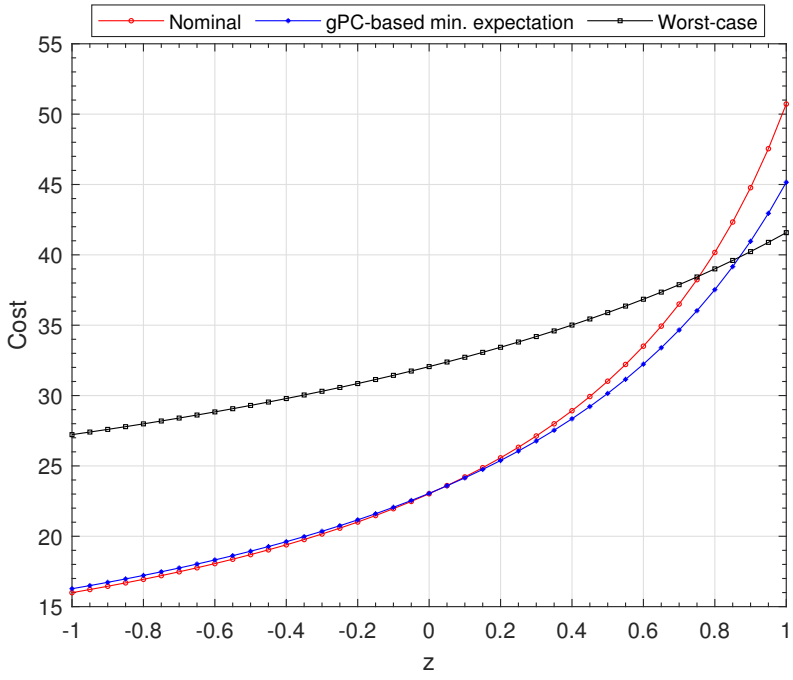

Figure 3.3: Comparison of cost-to-go with minimum expectation control, nominal optimal control, and optimal control designed for worst case uncertainties

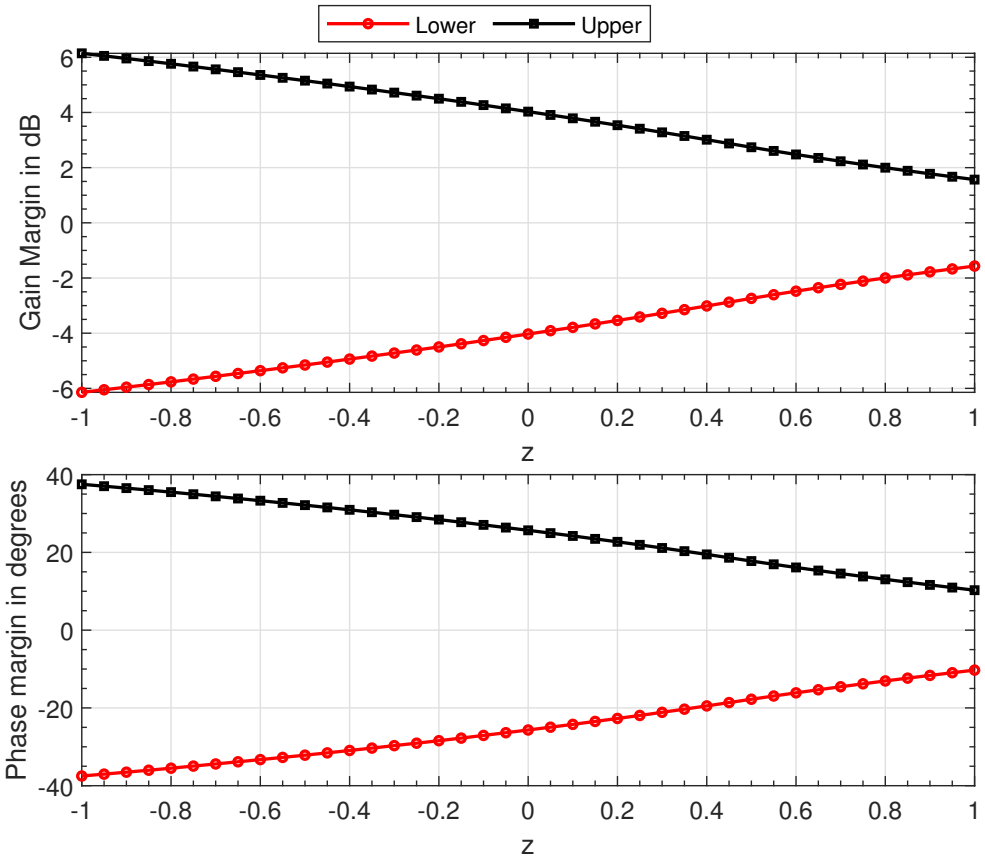

Figure 3.4: Variation of disk-based gain margin and phase margin with z

3.5 Chapter Summary

In this chapter, we have proposed a new method for designing of robust state feedback controllers for linear systems with time-invariant probabilistic parametric uncertainties. The controllers have been designed to minimize finite horizon and infinite horizon expectation performance indices. The theoretical results were developed by employing the pseudospectral collocation method in the generalized polynomial chaos expansion framework. Numerical results verify that a single robust controller can be derived from the proposed technique to regulate the stochastic system for all the variations of the random variable within its domain of PDF. Also, the proposed

gPC controller was found to be less conservative and optimal than the controller designed for worst-case uncertainty.

Chapter 4

Generalized Polynomial Chaos Expansion-Based Ensemble Filtering *

In this chapter, we use the gPC expansion technique to carry out state estimation in a nonlinear stochastic system subject to initial condition and parametric uncertainties. The filter is developed in a prediction-correction fashion. The uncertainties in the initial states and parameters are propagated using the generalized polynomial chaos expansion technique to compute the predicted estimates of states. Once the measurements are available, a nonlinear estimator is developed to update the predicted estimates in the ensemble Kalman filtering framework. The methodology is then applied to estimate the states of a hypersonic vehicle entering the Earth's atmosphere. The performance of the proposed filter is compared with those of the unscented Kalman filter and particle filter in terms of accuracy and computational efficiency.

The chapter is organized as follows. Section 4.1 provides the problem statement. The necessary preliminaries for the ensemble Kalman filter are provided in Section 4.2. Then, generalized polynomial chaos expansion-based ensemble Kalman filter is developed in Section 4.3 for the nonlinear system discussed in the problem statement. The developed filter is then applied to the navigation of a hypersonic vehicle during its atmospheric reentry to Earth in Section 4.4. Finally, the conclusions of the chapter are reported in Section 4.5.

*Part of the material reported in this chapter is reprinted with permission, from Rajnish Bhusal and Kamesh Subbarao, "Generalized Polynomial Chaos-based Ensemble Kalman Filtering for Orbit Estimation," *2021 American Control Conference (ACC)*, IEEE, pp. 4280-1285, New Orleans, LA, May 2021, DOI: 10.23919/ACC50511.2021.9482961, Copyright © 2021, IEEE (reference [124]).

4.1 Problem Formulation

Consider a general continuous-time dynamic system with uncertain initial conditions and parameters and a discrete-time measurement model. The measurement model is such that the observations are taken at discrete time instants $0 = t_0 < t_1 < \cdots < t_N \leq T$. The system and measurement model are given as

$$\begin{aligned} \dot{\mathbf{x}}(t) &= \mathbf{f}\left(\mathbf{x}(t), t\right) + \boldsymbol{\eta}(t), \quad 0 \leq t \leq T \\ \tilde{\mathbf{y}}_k &= \mathbf{h}\left(\mathbf{x}(t_k)\right) + \boldsymbol{\nu}_k, \quad k = 0, 1, \ldots, N \end{aligned} \tag{4.1}$$

where $\mathbf{x}(t) \in \mathbb{R}^n$ is the state vector, $\tilde{\mathbf{y}}_k \in \mathbb{R}^p$ is the measured output vector, $\boldsymbol{\eta}(t) \in \mathbb{R}^n$ is the process noise, and $\boldsymbol{\nu}_k \in \mathbb{R}^p$ is the measurement noise. In (4.1), $\mathbf{f} : \mathbb{R}^n \times [0, T] \to \mathbb{R}^n$ is the nonlinear state function and $\mathbf{h} : \mathbb{R}^n \to \mathbb{R}^p$ is the nonlinear output function. The noise vectors $\boldsymbol{\eta}$ and $\boldsymbol{\nu}$ are assumed to be zero mean Gaussian white noise vectors, which are uncorrelated with each other and satisfy following properties

$$\begin{aligned} \mathbb{E}\left[\boldsymbol{\eta}(t)\boldsymbol{\eta}^{\mathrm{T}}(\tau)\right] &= \mathbf{Q}\delta(t - \tau) \\ \mathbb{E}\left[\boldsymbol{\nu}_k\boldsymbol{\nu}_j^{\mathrm{T}}\right] &= \mathbf{R}\delta(k - j) \end{aligned} \tag{4.2}$$

where $\mathbf{Q} > \mathbf{0} \in \mathbb{R}^{n \times n}$ and $\mathbf{R} > \mathbf{0} \in \mathbb{R}^{p \times p}$ are the covariance matrices associated with process noise and measurement noise vectors, respectively.

We consider uncertainties in the initial conditions of the states and parameters of the system. Further, the uncertain parameters are assumed to be time-invariant. To that end, the uncertain initial states and parameters are considered to be a function of a random vector $\mathbf{z} = [z_1, z_2, \ldots, z_d]^{\mathrm{T}}$ with a joint probability density function $\boldsymbol{\rho}(\mathbf{z})$ on support Γ. Note that the uncertain parameters and initial conditions can have different marginal probability densities described by different probability distribution functions. Similar to the assumptions made in Chapter 2, the initial conditions of the states and parameters are considered to be characterized by Gaussian and uniform density functions, respectively.

In this work, the state estimation problem is to compute the estimates $\hat{\mathbf{x}}(t)$ of state $\mathbf{x}(t)$ governed by the system model in (4.1) subjected to initial condition and parametric uncertainties, such that the calculated measurements obtained as $\hat{\mathbf{y}}_k = \mathbf{h}\left(\hat{\mathbf{x}}(t_k)\right)$ for all $k = 0, 1, \ldots, N$ agrees with the actual measurements $\tilde{\mathbf{y}}_k$ in some probabilistic sense.

In order to generate state estimates given noisy measurements and different probability distributions of uncertain initial conditions and parameters, this research develops a nonlinear filtering technique by combining the generalized polynomial chaos (gPC) expansion technique with the ensemble Kalman filtering (EnKF) approach.

4.2 Preliminaries of Ensemble Kalman Filter

In this section, we provide a brief overview of the Ensemble Kalman filter technique to carry out state estimation of the nonlinear system in (4.1). Consider an ensemble of state estimates such that each $\hat{\mathbf{x}}^{(i)}(t)$, $i = 1, 2, \ldots, M$ denotes the ensemble member. The ensemble of initial state estimates $\hat{\mathbf{x}}^{(i)}(0)$ can be computed using MC-based random sampling technique with initial estimate $\hat{\mathbf{x}}(0)$ as the mean and $\mathbf{P}(0)$ as the initial covariance. The EnKF filter in the predictor-corrector form for the system in (4.1) can be written as [157]

$$\dot{\hat{\mathbf{x}}}^{(i)}(t) = \mathbf{f}\left(\hat{\mathbf{x}}^{(i)}(t), t\right) \tag{4.3}$$

$$\hat{\mathbf{x}}^{(i)}(t_k) = \hat{\mathbf{x}}^{(i)}(t_k^-) + \mathbf{K}_k\left(\tilde{\mathbf{y}}_k^{(i)} - \hat{\mathbf{y}}_k^{-(i)})\right) \tag{4.4}$$

where $\hat{\mathbf{x}}^{(i)}(t_k^-)$ and $\hat{\mathbf{x}}^{(i)}(t_k)$ are the propagated and corrected state ensembles, respectively at time step t_k at which the measurement arrives. The ensembles of the true measurement $\tilde{\mathbf{y}}_k^{(i)}$ and estimated measurement $\hat{\mathbf{y}}_k^{-(i)}$ are given by

$$\begin{aligned} \tilde{\mathbf{y}}_k^{(i)} &= \tilde{\mathbf{y}}_k + \boldsymbol{\nu}_k^{(i)} \\ \hat{\mathbf{y}}_k^{-(i)} &= \mathbf{h}\left(\hat{\mathbf{x}}^{(i)}(t_k^-)\right) \end{aligned} \tag{4.5}$$

where $\boldsymbol{\nu}^{(i)}$ is the ensemble obtained from the MC sampling of measurement noise with mean $\mathbf{0}_p$ and covariance $\mathbf{R}$. The Kalman gain matrix $\mathbf{K}$ at time instant t_k can be computed using

$$\mathbf{K}_k = \mathbf{P}^{\mathbf{e_x e_y}}(t_k^-)\left[\mathbf{P}^{\mathbf{e_y e_y}}(t_k^-)\right]^{-1}. \tag{4.6}$$

The predicted state error covariance $\mathbf{P}^{\mathbf{e_x e_x}}(t_k^-)$, measurement error covariance $\mathbf{P}^{\mathbf{e_y e_y}}(t_k^-)$ and cross-correlation matrices $\mathbf{P}^{\mathbf{e_x e_y}}(t_k^-)$ can be written as

$$\begin{aligned} \mathbf{P}^{\mathbf{e_x e_x}}(t_k^-) &= \frac{1}{M}\sum_{i=1}^{M}\left[\hat{\mathbf{x}}^{(i)}(t_k^-) - \hat{\mathbf{x}}(t_k^-)\right]\left[\hat{\mathbf{x}}^{(i)}(t_k^-) - \hat{\mathbf{x}}(t_k^-)\right]^{\mathrm{T}} \\ \mathbf{P}^{\mathbf{e_y e_y}}(t_k^-) &= \frac{1}{M}\sum_{i=1}^{M}\left[\hat{\mathbf{y}}_k^{-(i)} - \hat{\mathbf{y}}_k^-\right]\left[\hat{\mathbf{y}}_k^{-(i)} - \hat{\mathbf{y}}_k^-\right]^{\mathrm{T}} \\ \mathbf{P}^{\mathbf{e_x e_y}}(t_k^-) &= \frac{1}{M}\sum_{i=1}^{M}\left[\hat{\mathbf{x}}^{(i)}(t_k^-) - \hat{\mathbf{x}}(t_k^-)\right]\left[\hat{\mathbf{y}}_k^{-(i)} - \hat{\mathbf{y}}_k^-\right]^{\mathrm{T}}, \end{aligned} \tag{4.7}$$

where

$$\hat{\mathbf{x}}(t_k^-) = \frac{1}{M}\sum_{i=1}^{M}\hat{\mathbf{x}}^{(i)}(t_k^-), \quad \hat{\mathbf{y}}_k^- = \frac{1}{M}\sum_{i=1}^{N}\hat{\mathbf{y}}_k^{-(i)} \tag{4.8}$$

are the predicted mean state vector and predicted measurement vector, respectively. The corrected state estimate and state error covariance matrix can be similarly computed from the corrected state ensemble $\hat{\mathbf{x}}^{(i)}(t_k)$.

4.3 Generalized Polynomial Chaos Expansion-Based Ensemble Kalman Filter

This section provides an approach to combine the gPC expansion and EnKF to develop a filtering technique, namely gPC-EnKF for the system in (4.1).

Note that, the dynamic system in (4.1) is subject to parametric uncertainties. To handle these uncertainties, we consider an augmented state vector of the system by augmenting the uncertain parameters with the nominal state vector. It should be noted that the uncertain parameters are assumed to be time-invariant. For notational simplicity and ease of analysis, we retain the notation $\mathbf{x} \in \mathbb{R}^n$ for the augmented state vector. The initial state $\mathbf{x}(0)$ for the system in (4.1) with augmented parameter is assumed to be a function of a random vector $\mathbf{z} \in \mathbb{R}^d$ where d is the size of the augmented state vector.

The nonlinear filtering problem is solved in a prediction-correction fashion. In the prediction step, the stochastic system in (4.1) is propagated in time using the gPC expansion framework (see Chapter 2) to compute the predicted state estimates of the system. The prediction step is carried out until the measurements of the system are available. Upon arrival of the measurements, the predicted state estimates are corrected using the EnKF approach to compute the corrected state estimates.

4.3.1 Prediction Step

The filtering problem at the prediction step is to obtain an estimate of the state of the actual system at any time instant without taking measurements of the system into consideration. This resembles to the problem of uncertainty propagation in nonlinear stochastic system discussed in Chapter 2. To that end, we employ pseudospectral collocation-based gPC expansion framework to obtain the predicted state estimate $\hat{\mathbf{x}}(t^-)$.

4.3.1.1 Continuous-time Propagation Using gPC Expansion

We consider following continuous-time propagation of the state estimate $\hat{\mathbf{x}}(t)$ for the gPC-EnKF between the two consecutive discrete-time instants at which measurements arrive:

$$\dot{\hat{\mathbf{x}}}(t^-, \mathbf{z}) = \mathbf{f}\left(\hat{\mathbf{x}}(t^-, \mathbf{z}), t^-\right) \tag{4.9}$$

for all $t \in [t_k, t_{k+1})$ and for all $k = 0, 1, \ldots, N$. For the system in (4.9), assuming the solution $\hat{\mathbf{x}}(t^-, \mathbf{z}) = [\hat{x}_1(t^-, \mathbf{z}), \ldots, \hat{x}_n(t^-, \mathbf{z})]^{\mathrm{T}}$ to be a second-order process, the gPC expansion of $\hat{x}_i(t^-, \mathbf{z})$ for each $i = 1, \ldots, n$ can be written as,

$$\hat{x}_i\left(t^-, \mathbf{z}\right) = \sum_{|\mathbf{r}|=0}^{P} \hat{x}^c_{i,\mathbf{r}}(t^-)\Phi_{\mathbf{r}}\left(\mathbf{z}\right) \tag{4.10}$$

where $\hat{x}^c_{i,\mathbf{r}}(t^-)$ is the coefficient of the multidimensional basis $\Phi_{\mathbf{r}}\left(\mathbf{z}\right)$, and $\mathbf{r} = (r_1, \ldots, r_d)$ is the ordered set of multi-indices with $|\mathbf{r}| = r_1 + \cdots + r_d$. As discussed in Chapter 2, the total number of basis functions is given by $S + 1 = \begin{pmatrix} d+P \\ d \end{pmatrix}$. Now, the solution in (4.10) with multidimensional index $\mathbf{r}$ can be written in terms of a single index l as follows

$$\hat{x}_i\left(t^-, \mathbf{z}\right) = \sum_{l=0}^{S} \hat{x}^c_{i,l}(t^-)\Phi_l\left(\mathbf{z}\right) = \mathbf{\Phi}(\mathbf{z})^{\mathrm{T}}\hat{\mathbf{x}}^c_i(t^-) \tag{4.11}$$

where $\hat{\mathbf{x}}^c_i(t^-) = [\hat{x}^c_{i,0}(t^-), \hat{x}^c_{i,1}(t^-), \ldots, \hat{x}^c_{i,S}(t^-)] \in \mathbb{R}^{S+1}$ is the vector of time-varying gPC coefficients and $\mathbf{\Phi}(\mathbf{z}) = [\Phi_0(\mathbf{z}), \Phi_1(\mathbf{z}), \ldots, \Phi_S(\mathbf{z})]^{\mathrm{T}} \in \mathbb{R}^{S+1}$ is the vector of gPC basis. We know that, the expansion coefficients can be written as,

$$\hat{x}^c_{i,l} = \frac{1}{\gamma_l}\,\mathbb{E}\left[\hat{x}_i(\mathbf{z})\Phi_k(\mathbf{z})\right] = \frac{1}{\gamma_l}\int_{\Gamma} \hat{x}_i(\mathbf{z})\Phi_l(\mathbf{z})\boldsymbol{\rho}(\mathbf{z})d\mathbf{z} \tag{4.12}$$

where $\gamma_l = \mathbb{E}\left[\Phi_l^2\right] > 0$ is the normalization factor.

Given (4.11), we can write the gPC expanded solution of predicted state estimate vector as

$$\hat{\mathbf{x}}(t^-, \mathbf{z}) = \left[\mathbf{I}_n \otimes \mathbf{\Phi}(\mathbf{z})^{\mathrm{T}}\right]\hat{\mathbf{x}}^c(t^-) \tag{4.13}$$

where $\hat{\mathbf{x}}^c = \text{col}(\hat{\mathbf{x}}_1^c, \hat{\mathbf{x}}_2^c, \ldots, \hat{\mathbf{x}}_n^c) \in \mathbb{R}^{(S+1)n}$. Moreover, using the pseudospectral collocation technique, we can approximate (4.12) as

$$\hat{x}_{i,l}^c(t^-) = \frac{1}{\gamma_l} \sum_{q=1}^{N_q} \hat{x}_i(t^-, z_q)\Phi_l(z_q)w_q \tag{4.14}$$

where z_q are the quadrature nodes, w_q are the corresponding nodal weights, $\hat{x}_i(t^-, z_q)$ is the predicted estimate of the ith state variable at the quadrature node, and N_q is the number of quadrature nodes used. Further, using (4.14), we can obtain the lth gPC coefficient of the predicted state estimate $\hat{\mathbf{x}}_l^c(t^-)$ for $l = 0, 1, \ldots, S$ as follows

$$\hat{\mathbf{x}}_l^c(t^-) = \frac{1}{\gamma_l}[\mathbf{I}_n \otimes \bar{\mathbf{\Phi}}_l^{\mathrm{T}}][\mathbf{I}_n \otimes \mathbf{W}]\bar{\hat{\mathbf{x}}}(t^-) = \frac{1}{\gamma_l}\left[\mathbf{I}_n \otimes \bar{\mathbf{\Phi}}_l^{\mathrm{T}}\mathbf{W}\right]\bar{\hat{\mathbf{x}}}(t^-) \tag{4.15}$$

where $\bar{\hat{\mathbf{x}}}(t^-) = \text{col}\left(\bar{\hat{\mathbf{x}}}_1(t^-), \bar{\hat{\mathbf{x}}}_2(t^-), \ldots, \bar{\hat{\mathbf{x}}}_n(t^-)\right) \in \mathbb{R}^{nN_q}$ such that for all $i = 1, 2, \ldots, n$, $\bar{\hat{\mathbf{x}}}_i(t^-) = \left[\hat{x}_i(t^-, z_1), \hat{x}_i(t^-, z_2), \cdots, \hat{x}_i(t^-, z_{N_q})\right]^{\mathrm{T}} \in \mathbb{R}^{N_q}$.

In (4.15), $\mathbf{W} = \text{diag}(w_1, \cdots, w_{N_q}) \in \mathbb{R}^{N_q \times N_q}$ is the diagonal matrix of collocation weights and $\bar{\mathbf{\Phi}}_l = \left[\Phi_l(z_1), \Phi_l(z_2), \ldots, \Phi_l(z_{N_q})\right]^{\mathrm{T}} \in \mathbb{R}^{N_q \times 1}$.

4.3.1.2 Computation of Predicted State Estimates and Predicted State Error Covariance

Once the stochastic system in (4.9) is propagated using pseudospectral collocation-based gPC expansion, we approximate the mean $\hat{\mathbf{x}}(t^-)$ of the predicted state estimate and covariance matrix $\mathbf{P}^{\mathbf{xx}}(t^-)$ of the predicted state, for all $t \in [t_k, t_{k+1})$ using the coefficients of gPC expansion as follows

$$\begin{aligned} \hat{\mathbf{x}}(t^-) &\approx \hat{\mathbf{x}}_0^c(t^-) \\ \mathbf{P}^{\mathbf{xx}}(t^-) &\approx \sum_{l=1}^{S} \left[\gamma_{\mathbf{l}}\, \hat{\mathbf{x}}_l^c(t^-)\left(\hat{\mathbf{x}}_l^c(t^-)\right)^{\mathrm{T}}\right]. \end{aligned} \tag{4.16}$$

Similarly, one can compute the state error covariance matrix for the predicted estimate using the predicted state covariance matrix $\mathbf{P}^{\mathbf{xx}}(t^-)$ and the process noise covariance matrix $\mathbf{Q}$ as

$$\mathbf{P}^{\mathbf{e_x e_x}}(t^-) = \mathbf{P}^{\mathbf{xx}}(t^-) + \mathbf{Q}, \quad \forall t \in [t_k, t_{k+1}). \tag{4.17}$$

4.3.2 Correction Step

Once the predicted state estimates are computed using the gPC expansion technique, we utilize the EnKF procedure to correct the predicted estimates upon arrival of the measurements. Before carrying out the correction step, the predicted measurement outputs, predicted state ensembles, and measurement error covariance matrices need to be computed. In this regard, the gPC solution of the predicted output $\forall t \in [t_k, t_{k+1})$ can be calculated based upon the following output equation

$$\hat{\mathbf{y}}(t^-, \mathbf{z}) = \mathbf{h}\left(\hat{\mathbf{x}}(t^-, \mathbf{z})\right). \tag{4.18}$$

At each time instant t_k when the measurement arrives, let $\hat{\mathbf{y}}_k^-(\mathbf{z})$ be the gPC expansion of the predicted output $\hat{\mathbf{y}}_k^-(\mathbf{z}) = [\hat{y}_{1_k}^-(\mathbf{z}), \ldots, \hat{y}_{p_k}^-(\mathbf{z})]^{\mathrm{T}}$. Using the results obtained for the predicted state estimate in (4.13), the gPC expansion of the predicted output can be be written as

$$\hat{\mathbf{y}}_k^-(\mathbf{z}) = \left[\mathbf{I}_n \otimes \mathbf{\Phi}(\mathbf{z})^{\mathrm{T}}\right] \hat{\mathbf{y}}_k^{c^-} \tag{4.19}$$

where $\hat{\mathbf{y}}_k^{c^-}$ is the vector of gPC coefficients of the predicted output. Similar to the gPC coefficient for the predicted state estimate in (4.15), we can obtain the lth gPC coefficient of the predicted output $\hat{\mathbf{y}}_k^{c^-}$ for $l = 0, 1, \ldots, S$ as follows

$$\hat{\mathbf{y}}_{l_k}^{c^-} = \frac{1}{\gamma_l}\left[\mathbf{I}_p \otimes \bar{\mathbf{\Phi}}_l^{\mathrm{T}}\mathbf{W}\right] \bar{\hat{\mathbf{y}}}_k^- \tag{4.20}$$

where $\bar{\hat{\mathbf{y}}}_k^- = \mathrm{col}\left(\bar{\hat{\mathbf{y}}}_{1_k}^-, \bar{\hat{\mathbf{y}}}_{2_k}^-, \ldots, \bar{\hat{\mathbf{y}}}_{p_k}^-\right) \in \mathbb{R}^{pN_q}$ such that for all $i = 1, 2, \ldots, p$, $\bar{\hat{\mathbf{y}}}_{i_k}^- = \left[\hat{y}_{i_k}^-(z_1), \hat{y}_{i_k}^-(z_2), \cdots, \hat{y}_{i_k}^-(z_{N_q})\right]^{\mathrm{T}} \in \mathbb{R}^{N_q}$. Further, the mean and covariance of the predicted output at t_k can be computed as follows

$$\begin{aligned} \hat{\mathbf{y}}_k^- &\approx \hat{\mathbf{y}}_{0_k}^c \\ \mathbf{P}^{\mathbf{yy}}(t_k^-) &\approx \sum_{l=1}^{S} \left[\gamma_l \, \hat{\mathbf{y}}_{l_k}^{c^-} \left(\hat{\mathbf{y}}_{l_k}^{c^-}\right)^{\mathrm{T}}\right]. \end{aligned} \tag{4.21}$$

Moreover, the cross-correlation matrix between the predicted state and the predicted measurement output can be computed as

$$\mathbf{P}^{\mathbf{xy}}(t_k^-) \approx \sum_{l=1}^{S} \left[\gamma_l \, \hat{\mathbf{x}}_l^c(t_k^-) \left(\hat{\mathbf{y}}_{l_k}^{c^-}\right)^{\mathrm{T}}\right]. \tag{4.22}$$

Next, we follow the EnKF procedure to correct the predicted state estimate. To that end, one can generate an ensemble of solution realizations by randomly sampling the random vector $\mathbf{z}$ in (4.13). Let

$$\hat{\mathbf{x}}(t_k^-, \mathbf{z}^{(i)}) = \left[\mathbf{I}_n \otimes \mathbf{\Phi}(\mathbf{z}^{(i)})^{\mathrm{T}}\right] \hat{\mathbf{x}}^c(t_k^-) \quad i = 1, \ldots, M \tag{4.23}$$

be an ensemble of the M solution realizations of $\hat{\mathbf{x}}\left(t_k^-, \mathbf{z}\right)$, where $\mathbf{z}^{(i)}$ are the MC samples of the random vector $\mathbf{z}$ sampled from a Gaussian PDF with mean $\mathbf{0}$ and covariance matrix $\mathbf{I}$. Note that (4.23) involves only algebraic evaluations of the gPC solution at the sample points and does not incur additional computational burden to the filter.

Once the solution ensemble of the predicted state estimate is generated, the Kalman gain matrix is computed using (4.6) as

$$\mathbf{K}_k = \mathbf{P}^{\mathbf{e_x e_y}}(t_k^-) \left[\mathbf{P}^{\mathbf{e_y e_y}}(t_k^-)\right]^{-1} \tag{4.24}$$

Procedure 1 gPC-EnKF Algorithm

1: (Initialization) Given the initial PDF of state estimate: $\mathcal{N}(\hat{\mathbf{x}}(0), \mathbf{P}(0))$. Set $t_k = 0$ such that the initial PDF of the state estimate is $\mathcal{N}(\hat{\mathbf{x}}(t_k^-), \mathbf{P}(t_k^-))$. Choose mixed sparse grid-based quadrature rule of suitable accuracy level with nodes and weights $\{\mathbf{z}_q, w_q\}_{q=1}^{N_q}$. Select order P of the gPC-expansion.

2: gPC-EnKF Measurement Update :

- Compute $\hat{\mathbf{y}}_k^-(\mathbf{z}_q)$ at the collocation nodes using (4.19).
- Calculate $\hat{\mathbf{y}}_{l_k}^{c^-}$ using (4.20) for $l = 0, 1, \ldots, S$. Evaluate $\hat{\mathbf{y}}_k^-$ and $\mathbf{P}^{\mathbf{yy}}(t_k^-)$ using (4.21).
- Compute covariances $\mathbf{P}^{\mathbf{e_y e_y}}(t_k^-)$ and $\mathbf{P}^{\mathbf{e_x e_y}}(t_k^-)$ using (4.25).
- Evaluate the Kalman gain matrix $\mathbf{K}_k$ using (4.24).
- Generate $\mathbf{z}^{(i)}$, $i = 1, \ldots, M$ MC samples of $\mathbf{z}$ with mean $\mathbf{0}$ and covariance $\mathbf{I}$.
- Generate $\hat{\mathbf{x}}^{(i)}(t_k^-)$ using (4.23).
- Generate $\tilde{\mathbf{y}}_k^{(i)}$ and $\hat{\mathbf{y}}_k^{-(i)}$ using (4.5).
- Compute $\hat{\mathbf{x}}^{(i)}(t_k)$ using (4.4).
- Evaluate the gPC coefficients of the updated state using (4.27).
- Construct the gPC expansion for the updated state using (4.26).
- Evaluate the expanded updated states in (4.26) at the quadrature nodes $\mathbf{z}_q$ to obtain $\{\hat{\mathbf{x}}(t_k, \mathbf{z}_q)\}_{q=1}^{N_q}$.

3: Prediction of state estimate and state error covariance:

- Propagate the estimates at the collocation nodes $\{\hat{\mathbf{x}}(t_k, \mathbf{z}_q)\}_{q=1}^{N_q}$ to obtain $\{\hat{\mathbf{x}}(t_{k+1}^-, \mathbf{z}_q)\}_{q=1}^{N_q}$ using (4.9).
- Calculate $\hat{\mathbf{x}}_l^c(t_{k+1}^-)$ using (4.15) for $l = 0, 1, \ldots, S$. Evaluate $\hat{\mathbf{x}}(t_{k+1}^-)$ using (4.16).

4: Set $t_k = t_{k+1}$ and go to Step 2.

where $\mathbf{P}^{\mathbf{e_x e_y}}(t_k^-)$ and $\mathbf{P}^{\mathbf{e_y e_y}}(t_k^-)$ are the cross-correlation matrix between the state error estimate and the measurement error, and the measurement error covariance matrix, respectively. These matrices can be computed as follows

$$\begin{aligned} \mathbf{P}^{\mathbf{e_y e_y}}(t_k^-) &= \mathbf{P}^{\mathbf{yy}}(t_k^-) + \mathbf{R} \\ \mathbf{P}^{\mathbf{e_x e_y}}(t_k^-) &= \mathbf{P}^{\mathbf{xy}}(t_k^-). \end{aligned} \tag{4.25}$$

where $\mathbf{R}$ is the measurement noise covariance matrix. Now, the predicted state estimate obtained from the gPC approach can be updated using the correction step of the EnKF using (4.4) and (4.5). Next, the gPC expansion for the updated state estimate is computed as

$$\hat{\mathbf{x}}\left(t_k, \mathbf{z}\right) = \left[\mathbf{I}_n \otimes \mathbf{\Phi}(\mathbf{z})^{\mathrm{T}}\right] \hat{\mathbf{x}}^c(t_k) \tag{4.26}$$

where $\hat{\mathbf{x}}^c(t_k)$ is the vector of gPC coefficients of the updated state estimate. In this work, we compute the gPC coefficient vector of the updated state estimate using the method of averaging as follows

$$\hat{\mathbf{x}}_{\mathbf{r}}^c(t_k) \approx \frac{1}{M} \sum_{i=1}^{M} \hat{\mathbf{x}}^{(i)}(t_k) \mathbf{\Phi}_{\mathbf{r}}\left(\mathbf{z}^{(i)}\right). \tag{4.27}$$

In order to carry out the next step of prediction, the gPC expanded solution of the updated state estimates in (4.26) are evaluated at the quadrature nodes $\mathbf{z}_q$, $\forall q = 1, \ldots, N_q$ to obtain the updated state estimates. This completes one filtering step of the gPC-EnKF. The step-by-step procedure for gPC-EnKF are summarized in Procedure 1.

Note that the correction step of the proposed gPC-based EnKF filter only involves algebraic manipulations and does not incur additional computational burden. Besides, the computational complexity of the proposed filter depends upon the number of the collocation nodes used to compute the coefficients of gPC expansion. Thus, for a given order of gPC expansion, higher the efficacy of the quadrature rule, lower would be the computational cost of the proposed filtering algorithm.

4.4 Application to Atmospheric Reentry Problem

In this section, we consider a simulation example to study the accuracy and computational efficiency of the proposed filter. The proposed filter is applied to estimate the states of the vehicle entering the Earth's atmosphere.

4.4.1 Equations of Motion and Measurement Model

We assume that the planet is non-rotating and its atmosphere is stationary. The dynamics of the vehicle entering the atmosphere in the planet-centered planet-fixed

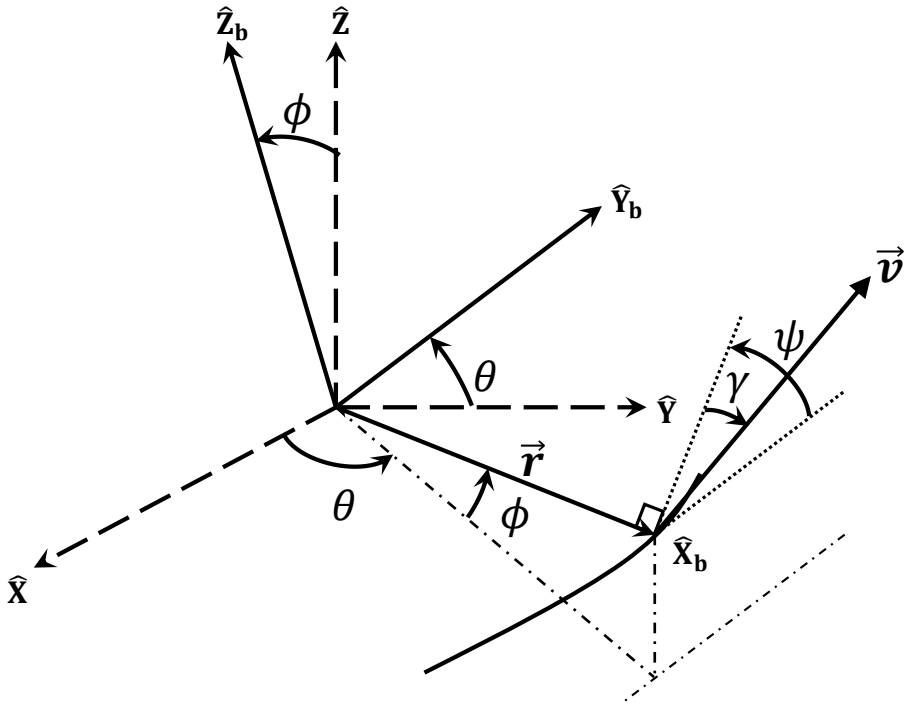

Figure 4.1: State variables in planet-fixed $(\hat{X}, \hat{Y}, \hat{Z})$ and vehicle-fixed $(\hat{X}_b, \hat{Y}_b, \hat{Z}_b)$ systems

coordinate system are represented by Vinh's equation [158] with six states: altitude h, velocity v, flight-path angle γ, geocentric longitude θ, geocentric latitude ϕ, and heading angle ψ, as illustrated in Fig. 4.1. The equations of motion of the vehicle can be written as

$$\begin{aligned}
\dot{h} &= v\sin(\gamma) \\
\dot{v} &= -\frac{\rho v^2}{2\beta} - g\sin(\gamma) \\
\dot{\gamma} &= \frac{1}{v}\left[\frac{\rho v^2}{2\beta}\left(\frac{L}{D}\right)\cos(\sigma) - \left(g - \frac{v^2}{r}\right)\cos(\gamma)\right] \\
\dot{\theta} &= \frac{v\cos(\gamma)\cos(\psi)}{r\cos(\phi)} \\
\dot{\phi} &= \frac{v\cos(\gamma)\sin(\psi)}{r} \\
\dot{\psi} &= \frac{1}{v}\left[\frac{\rho v^2}{2\beta}\left(\frac{L}{D}\right)\frac{\sin(\sigma)}{\cos(\gamma)} - \frac{v^2}{r}\cos(\gamma)\cos(\psi)\tan(\phi)\right]
\end{aligned} \tag{4.28}$$

where σ is the bank angle of the vehicle, ρ is the atmospheric density of the planet, β is the ballistic coefficient of the vehicle, and $\left(\frac{L}{D}\right)$ is the lift-to-drag ratio of the vehicle. Besides, $r = h + R$ is the radial distance from the center of the planet to the center of mass of the vehicle, R is the radius of the planet, $g = \frac{\mu}{r^2}$ is the acceleration due to gravity, and μ is the standard gravitational parameter of the planet. The density of the atmosphere is assumed to follow an exponential model given by $\rho = \rho_0 e^{(h_2-h)/h_1}$ where ρ_0 is the nominal reference density at the planet's surface, and h_1 and h_2 are the constant scale heights for the density computation.

To compute the filter estimates, we consider an integrated navigation scenario. Accelerometer measurements from the on-board inertial measurement unit (IMU)

and ground-based tracking data (range, azimuth and elevation) from the radar are considered. The measurements from the accelerometer are modeled as follows:

$$\tilde{\mathbf{y}}_a = \mathbf{y}_a + \boldsymbol{\nu}_a, \quad \mathbf{y}_a = \begin{bmatrix} -\dfrac{\rho v^2}{2\beta} \\ -\dfrac{\rho v^2}{2\beta}\left(\dfrac{L}{D}\right)\sin(\sigma) \\ \dfrac{\rho v^2}{2\beta}\left(\dfrac{L}{D}\right)\cos(\sigma) \end{bmatrix} \tag{4.29}$$

where $\mathbf{y}_a$ is the noise-free accelerometer reading and $\boldsymbol{\nu}_a$ is the noise associated with the accelerometer measurements. The radar-based range, azimuth, and elevation measurements are modeled as follows:

$$\begin{aligned} \tilde{y}_R &= \sqrt{(x_r - x)^2 + (y_r - y)^2 + (z_r - z)^2} + \nu_R \\ \tilde{y}_{az} &= \tan^{-1}\left(\frac{y - y_r}{x - x_r}\right) + \nu_{az} \\ \tilde{y}_{el} &= \tan^{-1}\left(\frac{z - z_r}{\sqrt{(x_r - x)^2 + (y_r - y)^2}}\right) + \nu_{el} \end{aligned} \tag{4.30}$$

where (x, y, z) and (x_r, y_r, z_r) are the Earth centered Cartesian coordinates of the vehicle and the radar position, respectively; ν_R, ν_{az}, and ν_{el} are the measurement noises associated with range, azimuth angle, and elevation angle measurements.

4.4.2 Simulation Results

The constant parameters used to simulate the vehicle's reentry to Earth's atmosphere are summarized in Table 4.1.

The true initial condition for the vehicle is considered to be as follows

$$\mathbf{x}(0) = [125 \times 10^3 \text{ m},\ 5900 \text{ m/s},\ -15.2^\circ,\ 0.1^\circ,\ 0.1^\circ,\ 0.1^\circ]^{\mathrm{T}}.$$

Here, the initial state uncertainty with Gaussian distribution is considered. The initial state estimate is generated randomly such that $\hat{\mathbf{x}}(0) \sim \mathcal{N}(\mathbf{x}_0, \sigma_0^2)$ with $\sigma_0 = \text{diag}(10^3 \text{ m}, 20 \text{ m/s}, 1^\circ, 0.01^\circ, 0.01^\circ, 0.01^\circ)$. The system parameters: ballistic

Table 4.1: Simulation Parameters

Parameters	Values
Standard gravitational parameter of Earth	$\mu = 3.986 \times 10^{14}$ m^3/s^2
Radius of Earth	$R = 6378.1363$ Km
Reference Density	$\rho_0 = 1.752$ Kg/m^3
Scale height 1	$h_1 = 6.7$ Km
Scale height 2	$h_2 = 0$ Km
Bank angle	$\sigma = 0^\circ$

coefficient and lift-to-drag are considered to be uniformly distributed such that $\beta \sim \mathcal{U}[60,\ 64]$ Kg/m^2 and $\left(\frac{L}{D}\right) \sim \mathcal{U}[0.20,\ 0.24]$.

For the simulation, the radar positioned at NASA Dryden Flight Research Center (FRC) in Edwards, California is considered to generate range, azimuth and elevation measurements. The location of the radar at FRC in spherical coordinates are $r = 6378.889$ Km$, \theta = 242.0885^\circ, \phi = 34.9607^\circ$, which in Earth centered Cartesian coordinates can be written as $x_r = -2447.163$ Km, $y_r = -4619.644$ Km and $z_r = 3655.203$ Km. The 3-σ magnitudes of the measurement noise are as follows:

$$\boldsymbol{\delta}_a = 0.1\ \mathbf{y}_a\ \text{m/s}^2, \quad \delta_R = 3\sqrt{50}\ \text{m}, \quad \delta_{az} = 0.03^\circ, \quad \delta_{el} = 0.03^\circ \tag{4.31}$$

where $\mathbf{y}_a$ is the true accelerometer reading and $\boldsymbol{\delta}_a$, δ_R, δ_{az}, and δ_{el} are the 3-σ magnitudes of the noises associated with accelerometer, range, azimuth, and elevation measurements, respectively.

All the simulations are performed in MATLAB environment on a computer with Intel Core i7 CPU 3.20 GHz. For numerical integrations, 'ode45' integration routine in MATLAB is utilized. Figure 4.2 illustrates the estimation error in h, v, and γ and Fig. 4.3 illustrates the estimation error in θ, ϕ, and ψ using the gPC-based EnKF approach with third order of expansion and 2193 mixed sparse grid-based collocation nodes. Clearly, the estimation error in the corrected states are observed to be close to zero and well within the 3-σ bounds.

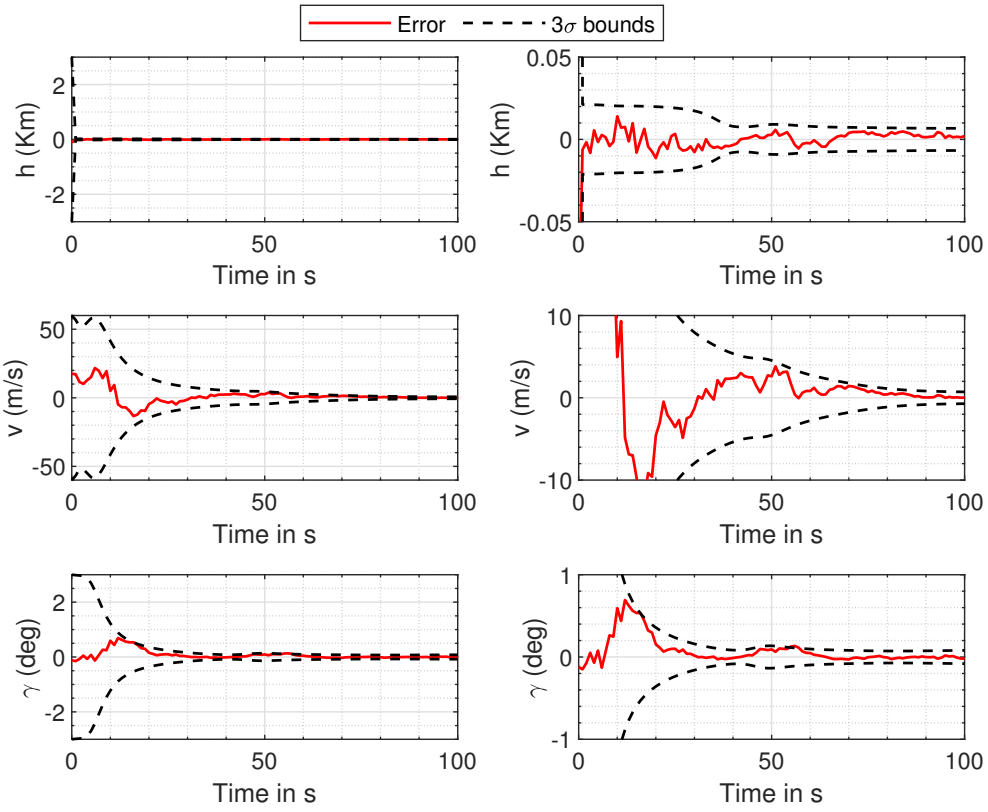

Figure 4.2: Estimation error and 3-σ outliners of states using gPC-based EnkF with $P = 3$ (with zoomed plots on the right).

The estimation results obtained from gPC-based EnKF (with third order of expansion and 2193 collocation nodes) are compared with those obtained from the UKF and bootstrap particle filter (PF) with 40000 particles. For UKF, the uncertain parameters for the estimation model are considered to be normally distributed with reasonable mean and variance in the domain of uniform uncertainty bounds. The root mean square error (RMSE) over time is considered as the comparison metric. Let $\mathbf{x}(t_j) = [x_1(t_j), \ldots, x_n(t_j)]^{\mathrm{T}}$ be the true state vector at time instant t_j and $\hat{\mathbf{x}}(t_j) =$

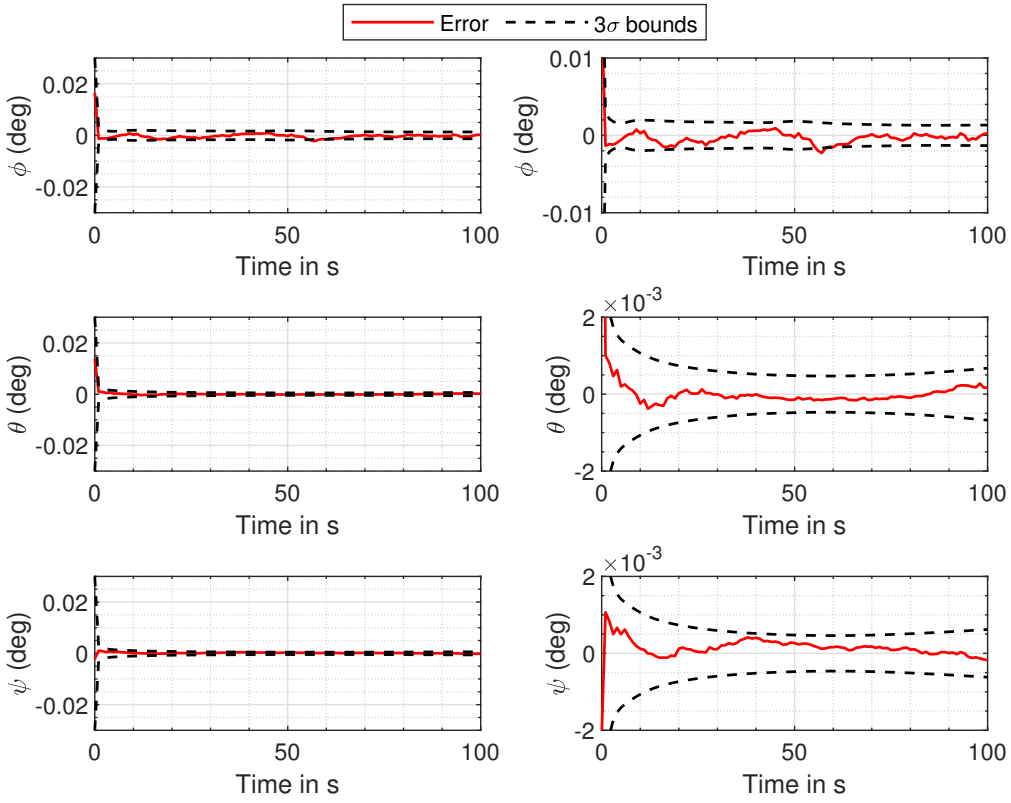

Figure 4.3: Estimation error and 3-σ outliners of states using gPC-based EnkF with $P = 3$ (with zoomed plots on the right).

$[\hat{x}_1(t_j), \ldots, \hat{x}_n(t_j)]^{\mathrm{T}}$ be the state estimate vector at time instant t_j, RMSE over time can be computed using

$$\mathrm{RMSE}_i = \sqrt{\frac{\sum_{j=1}^{n_t} \left[x_i(t_j) - \hat{x}_i(t_j)\right]^2}{n_t}} \tag{4.32}$$

where $i = 1, \ldots, n$ is the index of the state, n_t is the total number of time samples. Table 4.2 illustrates the comparison between the RMSE in the state estimates obtained from gPC-based EnKF (with third order of expansion and 2193 collocation nodes), UKF and PF (with 40000 particles). Note that UKF can produce reasonably good estimates for state estimation problem with Gaussian uncertainties in both model parameters and initial states. However, for the problem under consideration,

the uncertainties in the model parameters are uniformly distributed, which accounts for large state estimation errors (especially in the estimation of r, v, and γ) for the UKF-based approach. From Table 4.2, the RMSE in the state estimates from gPC-based EnKF and PF are approximately of the same order. Besides, for gPC-based EnKF with 2193 nodes, the computational time taken for one filtering step is about 3.6 seconds and that for PF with 40000 samples is 69.4 seconds. To that end, gPC-based EnKF produces state estimates of higher accuracy with lower computational burden as compared to the bootstrap particle filter.

Table 4.2: RMSE in estimation of states

Filter	h (m)	v (m/s)	γ (deg)	θ ($\times 10^{-4}$ deg)	ϕ ($\times 10^{-5}$ deg)	ψ ($\times 10^{-5}$ deg)
UKF	106.6905	19.8445	0.0156	1.4001	2.406	1.396
PF	54.2843	5.8622	0.0040	0.203	1.210	2.913
gPC-EnKF	12.2634	6.0945	0.0031	0.316	1.730	0.580

In addition to the RMSE comparison, the approximate posterior density of the state estimates obtained from gPC-EnKF with third order of expansion and 2193 nodes is compared with that obtained from PF with 40000 particles. The bivariate marginal PDFs among various states of the reentry vehicle at $t = 80$ s obtained from gPC-EnKF and PF are illustrated in Figs. 4.4 and 4.5. In Figs. 4.4 and 4.5, darker regions represent lower PDF value and lighter regions represent higher PDF value. It can be observed that the proposed gPC-EnKF estimator with fewer collocation nodes is able to reduce variance and capture localization of uncertainty better than the particle filter with larger number of particles.

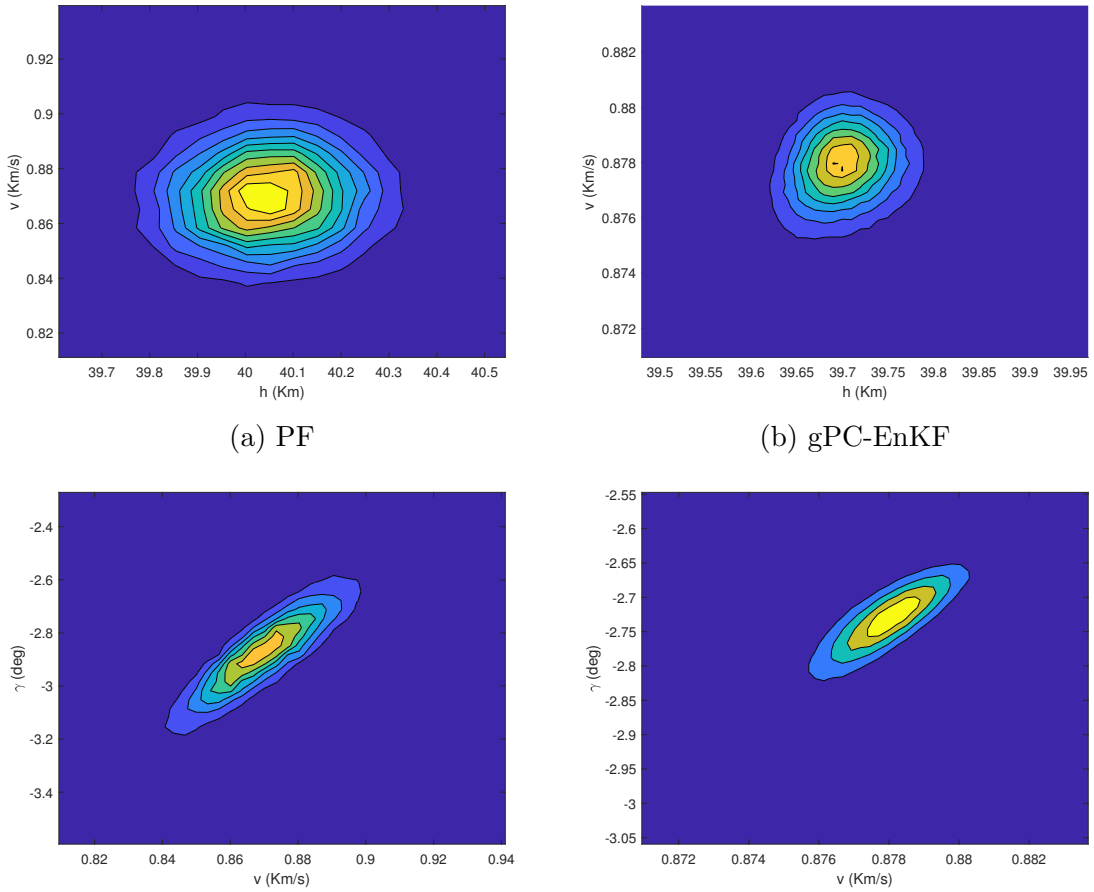

(a) PF (b) gPC-EnKF

(c) PF (d) gPC-EnKF

Figure 4.4: Final posterior bivariate marginal PDFs ($h-v$, $v-\gamma$) obtained from PF with 40000 particles and gPC-EnKF filter of order 3 with 2193 nodes.

4.4.3 Sensitivity Analysis of the Posterior Density Function of the Corrected State Estimates

As discussed in Chapter 2, global sensitivity analysis provides a measure of the contribution of each uncertain variables in the generation of the uncertainty of the quantities of interest. In the filtering problem, the sensitivity of the variance of the corrected state estimates to the state uncertainty (before the prediction step) and parametric uncertainties can be computed by calculating the total sensitivity indices.

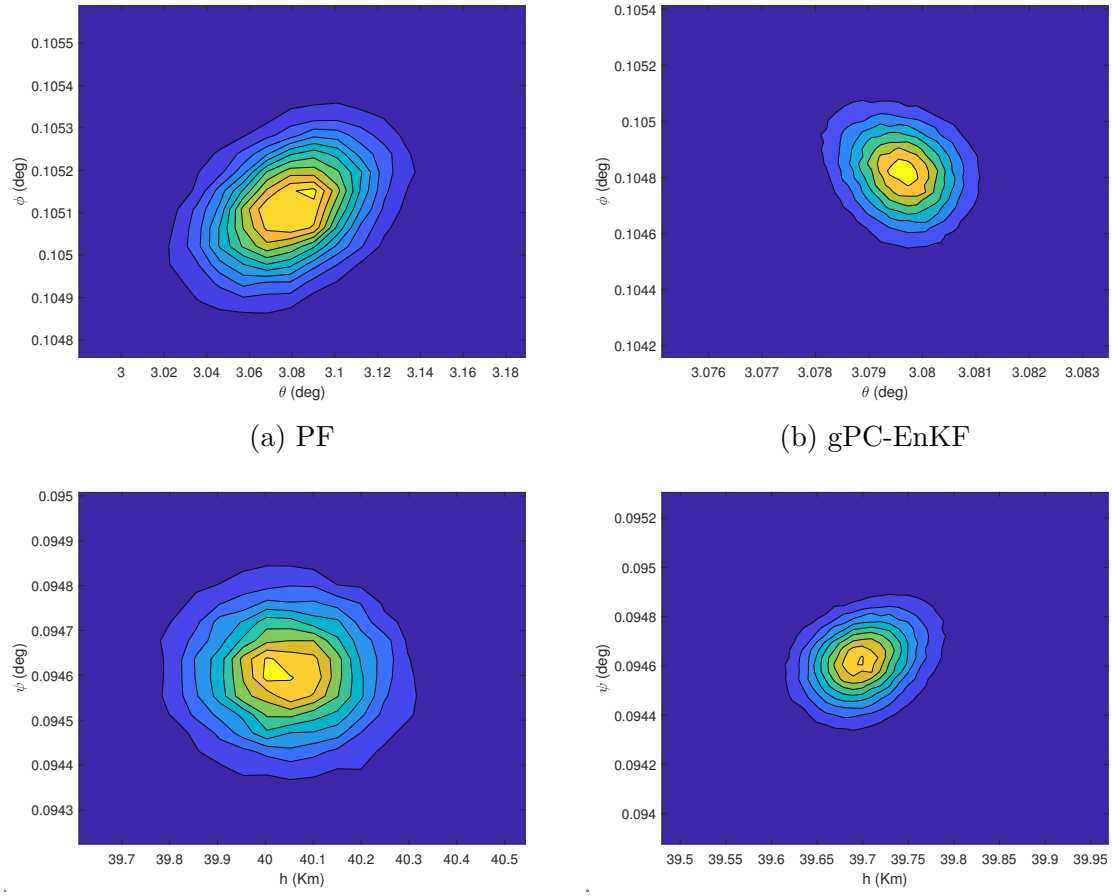

(a) PF (b) gPC-EnKF

(c) PF (d) gPC-EnKF

Figure 4.5: Final posterior bivariate marginal PDFs ($\theta - \phi$, $h - \psi$) obtained from PF with 40000 particles and gPC-EnKF filter of order 3 with 2193 nodes.

These total sensitivity indices provide a quantitative measure of the significance of a uncertain variable in the variability of the corrected state estimate.

Figure 4.6 illustrates the total sensitivity indices ($S(t)$) of the corrected estimates (after measurement update) of h, v, γ, θ, ϕ, and ψ to the uncertainties in the states (before the prediction step) and parameters. As expected, the variances of the state estimates are observed to be most sensitive to the uncertainties in their corresponding initial conditions at the initial epoch. Moreover, the variability of the estimates of the vehicle's altitude and longitude are significantly influenced by the

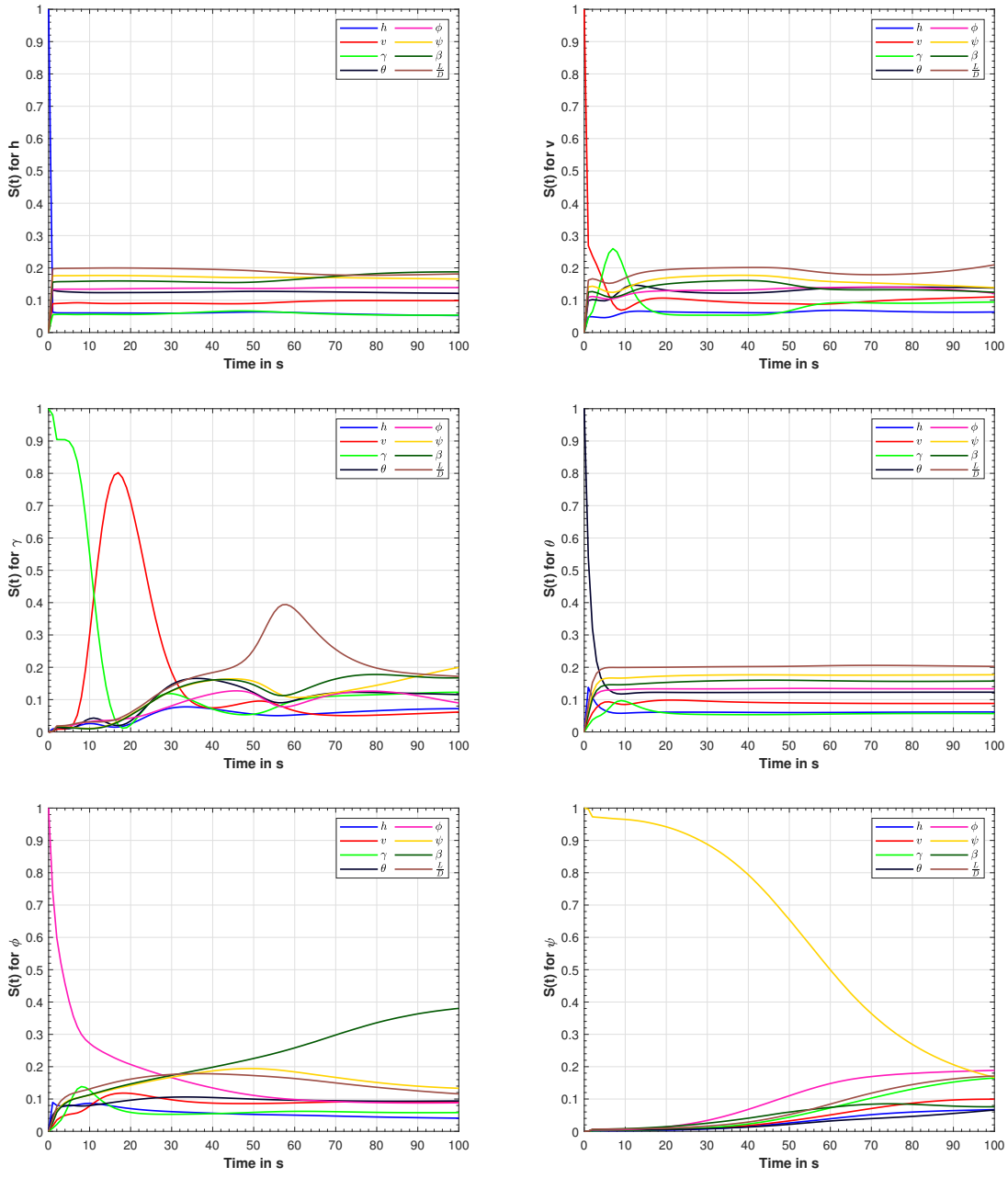

Figure 4.6: Total sensitivity indices of the state estimates to the uncertainties in the states and parameters

uncertainties in the ballistic coefficient, lift-to-drag ratio, and heading angle of the vehicle compared to the uncertainties in other states. In the early descent stage, the uncertainties in the velocity and flight-path angle are observed to affect the corrected estimates of each other significantly. However, with further propagation and decrease in the vehicle's altitude, the estimates of velocity and flight-path angle are highly sensitive to the uncertainties in the lift-to-drag ratio of the vehicle. Moreover, after around 60 seconds of descent (when the vehicle is close to the Earth's surface), the sensitivity of the corrected estimates of the flight-path angle to uncertainties in the ballistic coefficient and the heading angle is observed to be increasing and substantial. Throughout the descent phase, the uncertainty in the estimate of the latitude is observed to be significantly affected by the uncertainty in the ballistic coefficient followed by uncertainties in the heading angle and lift-to-drag ratio. The heading angle estimate is observed to be most sensitive to uncertainties in the heading angle (before the prediction step) itself. Moreover, with the decreasing altitude of the vehicle, the sensitivity of the heading angle estimate to the vehicle's latitude, lift-to-drag ratio, and flight-path angle is observed to be increasing. Clearly, for the problem under consideration, the uncertainty in the vehicle's lift-to-drag ratio is found to be the most significant in determining the variability of the state estimates during the atmospheric reentry to Earth.

4.5 Chapter Summary

In this chapter, a nonlinear filtering algorithm based on the generalized polynomial chaos expansion in the ensemble filter framework for the state estimation of a general nonlinear system has been developed. The proposed filter has been applied to the problem of atmospheric reentry of a vehicle to Earth. The estimation results obtained from gPC- based EnKF were compared with the unscented Kalman filter

and particle filter. It has been observed that gPC-based EnKF outperforms UKF in terms of state estimation accuracy for the reentry problem with uniformly distributed parametric uncertainty in the drag parameters. Moreover, gPC-based EnKF is found to be computationally more efficient than the bootstrap particle filter to obtain estimation accuracy of the same order. Besides, the global sensitivity of the posterior density function of the state estimates to the uncertainties in the system has been characterized.

Chapter 5

Probabilistic Analysis of Consensus Protocols for Uncertain Edge Weights in Multi-Agent Systems

This chapter provides probabilistic analysis of cooperative control protocols to study the effect of uncertainties in the system of multiple agents. In addition, we consider the presence of an intelligent intruder in the communication network that provides a conflicting control command. The effect of such an intruder is modeled, and its impact on the propagation of the states of the agents is analyzed. Numerical simulations based on uncertainty propagation are provided by employing sparse grid-based pseudospectral collocation in a generalized polynomial chaos expansion framework to verify the theoretical analysis. Further, variance-based sensitivity indices are computed to understand the significance of random edge weights of the graph on the response distribution of the states of the agents.

The chapter is organized as follows. In Section 5.1, we briefly review principal concepts of graph theory and formulate the problem under consideration. Section 5.2 carries out probabilistic analysis of consensus protocols for multi-agent systems. Numerical examples are presented to study the effect of uncertainties in consensus of multi-agent systems in Section 5.3. The time propagation of the states of the agents in the presence of uncertain edge weights is discussed, and a sensitivity analysis is carried out to study the influence of the edge weights on the distribution of states of the agents. Finally Section 5.4 provides concluding remarks.

5.1 Preliminaries and Problem Formulation

5.1.1 Notations

Given a matrix $\mathbf{T} \in \mathbb{R}^{n\times n}$, the operator $\|\mathbf{T}\|$ represents the induced norm of $\mathbf{T}$ such that $\|\mathbf{T}\| := \{\sup_{\|\mathbf{x}\|=1} \|\mathbf{T}\mathbf{x}\| : \mathbf{x} \in \mathbb{R}^n\}$. Further, $\sigma(\mathbf{T})$ represents the spectrum of $\mathbf{T}$ and rank($\mathbf{T}$) denotes the rank of $\mathbf{T}$. Also, $\|\mathbf{x}\|$ represents the standard Euclidean norm of the vector $\mathbf{x}$. We denote the n–dimensional identity matrix by $\mathbf{I}_n$ and $\mathbf{1}_n$ represents the n-dimensional column vector of ones.

5.1.2 Preliminaries of Algebraic Graph Theory

The interconnection among a group of N agents is encoded through communication graphs $\mathcal{G} = (\mathcal{V}, \mathcal{E})$ where $\mathcal{V} = \{1, 2, \ldots, N\}$ is a non-empty set of nodes, and $\mathcal{E} \subseteq \mathcal{V} \times \mathcal{V}$ is an edge set of ordered pairs of nodes, called edges. Each of the edges of a graph (i, k) is associated with a non-negative weight a_{ik}. Node k is the neighbor of i if $(k, i) \in \mathcal{E}$ and the set of neighbors of node i can be represented as $\mathcal{N}_i$. Directed path from node i to node k is defined as a sequence of successive edges in the form $\{(i, l), (l, m), \ldots, (n, k)\}$. The graph is connected if there is a path from every node to every other node. A root r is a node such that for each node i different from r, there is a directed path from r to i. A directed tree is a directed graph in which there is exactly one root, and every node except for this root itself has exactly one parent. A directed spanning tree is a directed tree consisting of all the nodes and some edges in $\mathcal{G}$. A graph is said to be balanced if $a_{ij} = a_{ji}$ for all $(i, j) \in \mathcal{E}_{ij}$. In the case of balanced graph, we refer the edges to be undirected.

The adjacency matrix $\mathcal{A} = [a_{ik}] \in \mathbb{R}^{N\times N}$ of a directed graph is defined such that $a_{ik} = 1$ if $(k, i) \in \mathcal{E}$ and $a_{ik} = 0$, otherwise. The in-degree of node v_i is defined as $d_i = \sum_{k=1}^{N} a_{ik}$. The diagonal matrix obtained from d_i as diagonal entries is called

diagonal in-degree matrix ($\mathcal{D}$). Finally, the graph Laplacian matrix is obtained as $\mathbf{L} = \mathcal{D} - \mathcal{A} \in \mathbb{R}^{N \times N}$.

Lemma 5.1.1. *[63] Let $\mathcal{G}$ be a connected graph with atleast one directed spanning tree. Let λ_i, $i = 1, 2, \ldots, N$ be the eigenvalues of the Laplacian matrix. Then, $\lambda_1 = 0$ is always a simple and the smallest eigenvalue of the Laplacian matrix, and $Re(\lambda_k) > 0$, for all $k = 2, \ldots, N$.*

Remark 5.1.2. *For a strongly connected and balanced graph, the graph Laplacian matrix is always symmetric. Also, $rank(\mathbf{L}) = N - 1$ and the second smallest eigenvalue of the graph Laplacian matrix (Fiedler eigenvalue) is the algebraic connectivity of the graph [97].*

5.1.3 Problem Formulation

In this chapter, the agents are modeled with single integrator dynamics over a strongly connected and balanced graph $\mathcal{G}$ as

$$\dot{x}_i = u_i, \quad i = 1, \ldots, N \tag{5.1}$$

where $x_i \in \mathbb{R}$ and $u_i \in \mathbb{R}$ are the state and control input of the agent i. The communication among the agents is modeled using a connected and balanced graph topology. It is assumed that the edge weights associated with the edges in the graph are uncertain. Although the weights a_{ij}, for all $i = 1, \ldots, N$ and $j \in \mathcal{N}_i$ are uncertain, the probability density of the edge weights are assumed to be known.

5.2 Probabilistic Analysis of Consensus Control Protocols

In this section, control protocols that solve consensus problems in a group of N autonomous agents in a fixed network topology represented by a graph $\mathcal{G}$ with edge weight uncertainties are discussed.

5.2.1 Control Protocol for Consensus

The consensus problem for a completely deterministic case can be solved considering the local control protocol for each agent i as [97]

$$u_i = -\sum_{j \in \mathcal{N}_i} a_{ij} \left(x_i - x_j \right). \tag{5.2}$$

With the control protocol in (5.2), the dynamics of each agent becomes stochastic in the presence of uncertainties in the edge weights and can now be written as following SDE

$$\dot{x}_i(\omega) = -\sum_{j \in \mathcal{N}_i} a_{ij}(\omega) \left(x_i - x_j \right). \tag{5.3}$$

Moreover, the states of the closed loop multi-agent system can be written in terms of the graph Laplacian matrix $\mathbf{L}(\omega)$ as

$$\dot{\mathbf{x}}(\omega) = -\mathbf{L}(\omega)\ \mathbf{x}(\omega) \tag{5.4}$$

where $\mathbf{x} = [x_1, x_2, \ldots, x_N]^{\mathrm{T}} \in \mathbb{R}^N$ is the global state vector of states of the agents. In the work, we shall assume that $\mathbf{L}(\omega)$ is an $N \times N$ matrix whose elements are measurable functions that are sample bounded on $[0, \infty)$ with probability 1 and further, $\mathbf{L}(\omega)$ is essentially bounded i.e. there exist $\psi > 0$ such that $\mathcal{P}(\Omega) = 1$, and $\|\mathbf{L}(\omega)\| \leq \psi$ for all $\omega \in \Omega$. The structure of the graph Laplacian matrix is preserved by restricting the uncertainties in the edge weights a_{ij} to be modeled using density functions with support $D \subset \mathbb{R}^+$. Note that, such assumption on a_{ij} preserves the property of graph Laplacian matrix, i.e. $\mathbf{L}(\omega)\ \mathbf{1} = \mathbf{0}$ and thus, $\mathbf{0}$ is a simple eigenvalue of $\mathbf{L}(\omega)$.

Here, we shall be concerned with the stochastic process

$$\mathbf{x}(t, \omega; x_0, t_0),\ t \in [t_0, \infty) \tag{5.5}$$

which is the solution of the linear SDE (5.4). Clearly, in accordance to the boundedness assumption on $\mathbf{L}(\omega)$, the stochastic process $\mathbf{x}$ defined on $[t_0, \infty) \times \Omega$ by

$\mathbf{x}(t,\omega) = e^{-\mathbf{L}(\omega)(t-t_0)}\mathbf{x}_0(\omega)$ is a solution to (5.4) almost everywhere corresponding to the initial conditions, $t_0 \in \mathbb{R}^+$ and $\mathbf{x}_0 \in L^2(\Omega)$.

Under a strongly connected and balanced graph, if there exists a consensus value c among the states of the agents with the control protocol in (5.2), $\delta = \mathbf{x} - \mathbf{1}_N c$ represents the global consensus disagreement vector. Meanwhile, the group disagreement between the states of the agents can be written as $x_i - x_j = \delta_i - \delta_j$. In reference to (5.4), it is easy to see that the dynamics of the global disagreement vector is obtained to be

$$\dot{\delta}(\omega) = -\mathbf{L}(\omega)\ \delta(\omega). \tag{5.6}$$

Definition 5.2.1. *The stationary solution $\delta = 0$ of the system (5.6) is said to be asymptotically stable in probability sense (almost surely) in the large if it is stable in probability and moreover, for all $\delta_0 \in \mathbb{R}^N$, every solution of the system (5.6) satisfies the condition*

$$\mathcal{P}\left\{\lim_{t\to\infty} \|\delta(t;\delta_0,t_0)\| = 0\right\} = 1. \tag{5.7}$$

This is equivalent to almost sure Lyapunov global asymptotic stability for the homogeneous linear systems [159].

Theorem 5.2.1. *For a strongly connected and balanced graph with any finite $\mathbf{x}(0)$, the states of the closed loop multi-agent system in (5.4) almost surely reach to an average consensus value asymptotically.*

Proof. Let $\lambda_i \in \sigma(\mathbf{L}(\omega))$ for all $i = 1,\ldots,N$ be the eigenvalues of graph Laplacian matrix. Let $\mathbf{J}(\omega) = [j_{ml}]$, for $m,l = 1,\ldots,N$, be the Jordan matrix corresponding to matrix $\mathbf{L}(\omega)$ with $j_{mm} = \lambda_m$. Using the modal decomposition, we can write

$\mathbf{L}(\omega) = \mathbf{P}(\omega)\mathbf{J}(\omega)\mathbf{P}^{-1}(\omega)$, where $\mathbf{P}$ is an $N \times N$ matrix of eigenvectors. Then, we have

$$\mathbf{x}(\omega, t) = e^{-\mathbf{L}(\omega)t}\mathbf{x}(0) = \mathbf{P}(\omega)e^{-\mathbf{J}(\omega)t}\mathbf{P}(\omega)^{-1}(\omega)\mathbf{x}(0) = \sum_{i=1}^{N} \mathbf{v}_i(\omega)e^{-\lambda_i(\omega)t}\mathbf{w}_i^{\mathrm{T}}(\omega)\mathbf{x}(0). \tag{5.8}$$

Without loss of generality, assume that $\lambda_1 < \lambda_2 < \cdots < \lambda_N$. We know that, $\lambda_1 = 0$ and λ_m is on the open right half plane for all $m = 2, \ldots, N$. For a strongly connected and balanced graph with symmetric graph Laplacian matrix, $\mathbf{v}_1(\omega) = \mathbf{1}_N$ and $\mathbf{w}_1(\omega) = (1/N)\mathbf{1}_N$ are the right and left normalized eigenvectors respectively associated to $\lambda_1 = 0$ with probability 1 [97].

As $t \to \infty$, $\mathbf{x}(\omega, t) \to (1/N)\mathbf{1}_N\mathbf{1}_N^{\mathrm{T}}\mathbf{x}(0)$. Thus, $lim_{t\to\infty}\ x_i(t, \omega) = c$, where $c = (1/N)\sum_{i=1}^{N} \mathrm{x}_i(0)$, i.e. $lim_{t\to\infty}\ \delta_i(t, \omega) = 0$. This in turn satisfies (5.7). Here, $\mathcal{P}\left\{\lim_{t\to\infty}\{x_i(\omega, t) = c\}\right. = 1$ and hence, the average consensus is achieved almost surely asymptotically. This completes the proof. □

Remark 5.2.2. *As the average consensus is achieved asymptotically, the probability density function of the states of the agents approaches a function $\bar{\delta}(x_i - c)$, where $\bar{\delta}(\cdot)$ is the unit delta function in $(\cdot)$ and c is the consensus value.*

5.2.2 Control Protocol for Constant Reference Tracking

In some applications, it is desirable that each state $x_i(t)$ approaches a reference state $x^R(t)$. If the reference state x^R is assumed to be constant, the control protocol for each agent i with deterministic edge weights is given as [160]

$$u_i = -\sum_{j\in\mathcal{N}_i} a_{ij}\left(x_i - x_j\right) - a_{iR}\left(x_i - x^R\right) \tag{5.9}$$

where the pinning gains $a_{iR} > 0$ if agent i has access to the reference state and 0 otherwise, for all $i = 1, \ldots, N$.

With the control protocol in (5.9), the dynamics of each agent in the presence of uncertainties in the edge weights and pinning gains can be written as following SDE

$$\dot{x}_i(\omega) = -\sum_{j\in\mathcal{N}_i} a_{ij}(\omega)\left(x_i - x_j\right) - a_{iR}(\omega)\left(x_i - x^R\right). \tag{5.10}$$

If $\mathbf{\Gamma}(\omega) = \mathrm{diag}(a_{1R}(\omega), \ldots, a_{nR}(\omega))$ is the diagonal matrix of the pinning gains, the global state dynamics of the agents can be expressed in terms of the graph Laplacian matrix as,

$$\dot{\mathbf{x}} = -\left(\mathbf{L}(\omega) + \mathbf{\Gamma}(\omega)\right)\mathbf{x} + \mathbf{\Gamma}(\omega)\mathbf{x}^R \tag{5.11}$$

where $\mathbf{x}^R = [x^R, \ldots, x^R]^{\mathrm{T}} \in \mathbb{R}^N$.

Definition 5.2.2. *Any matrix $\mathbf{A}(\omega)$ is said to be stable in probability if there exists $\mu > 0$ such that*

$$\mathcal{P}\left(\sup_{\lambda\in\sigma(\mathbf{A}(\omega))} Re(\lambda) < -\mu\right) = 1. \tag{5.12}$$

Remark 5.2.3. *The matrix $\mathbf{A}(\omega) = -(\mathbf{L}(\omega) + \mathbf{\Gamma}(\omega))$ is stable in probability, the proof of which is straightforward from the fact that $\lambda\left(\mathbf{L}(\omega)\right) \geq 0$ and the pinning gains $a_{iR} \geq 0$, for all $i = 1, 2, \ldots, N$.*

Theorem 5.2.4. *For a strongly connected and balanced graph with any finite $\mathbf{x}(0)$, the states of the closed loop multi-agent system in* (5.10) *attain the reference state exponentially in mean-square sense.*

Proof. Let $\delta(\omega) = \mathbf{x}(\omega) - \mathbf{x}^R$ be the global disagreement vector which is the vector of relative separation between the state of agents and the constant reference state. Hence, the local separation between the states of any two agents in the graph $\mathcal{G}$ can be written as $x_i - x_j = \delta_i - \delta_j$. The dynamics of the global disagreement for any agent i, for $i = 1, \ldots, N$ with control protocol in (5.9) can be written as

$$\dot{\delta}_i(\omega) = -\sum_{j\in\mathcal{N}_i} a_{ij}(\omega)\left(\delta_i - \delta_j\right) \; - a_{iR}(\omega)\delta_i. \tag{5.13}$$

Now, the dynamics of the disagreement vector after simplification can be expressed as

$$\dot{\delta}(\omega) = -\left(\mathbf{L}(\omega) + \mathbf{\Gamma}(\omega)\right)\delta(\omega) = \mathbf{A}(\omega)\delta(\omega). \tag{5.14}$$

The stochastic process $\delta(\omega, t) = e^{\mathbf{A}(\omega)t}\delta_0$ is the solution to the above SDE. From Remark 5.2.3, $\mathbf{A}(\omega) = -\left(\mathbf{L}(\omega) + \mathbf{\Gamma}(\omega)\right)$ is stable in probability, hence there exists $\mu > 0$ such that (5.12) holds. Moreover, from [161], there exists a $\Upsilon > 0$ such that $\|e^{\mathbf{A}(\omega)t}\| \leq \Upsilon e^{-\mu t}$ for all $\omega \in \Omega$. Thus, the mean square value (second moment) of the stochastic process $\delta(\omega, t)$ can be obtained as

$$\mathbb{E}[\delta^2(\omega,t)] = \int_\Omega \|e^{\mathbf{A}(\omega)t}\delta_0\|^2 \mathcal{P}(d\omega) \leq \Upsilon^2 e^{-2\mu t}\|\delta_0\|^2 \int_\Omega \mathcal{P}(d\omega) = \Upsilon^2 e^{-2\mu t}\|\delta_0\|^2 \tag{5.15}$$

where the last equality is obtained from the fact that integration under the probability density function (PDF) over the entire sample space Ω is unity. Clearly, the disagreement vector is mean square asymptotically stable. Hence, the states of the closed loop multi-agent system in (5.10) attain the reference state exponentially in mean-square sense. This completes the proof. □

5.2.3 Agent Dynamics in the Presence of Intelligent Intruder

Consider now, the presence of an intelligent intruder embedded in the network that provides a spurious reference signal to remain stealthy and carries out a slow "command injection" attack. While the rest of the agents in the group communicate with each other in the constrained environment subject to uncertainties in the edge weights as mentioned previously, the intruder communicates with the other agents with relatively weak strength (a significantly lower value of the edge weight) as compared to the other edge weights. Such a connection of the intruder agent with the

rest can be modeled using pinning weights associated with the edge that connects the intruder to some of the other agents. Further, more generally speaking, the pinning weights are also uncertain.

Assumption 5.2.1. *All the agents receive same strength of information from the reference node. In other words,* $a_{iR}(\omega) = a_{jR}(\omega) = \gamma(\omega)$ *for all,* $i, j = 1, \ldots, N$.

Theorem 5.2.5. *The expected value of the state of the agents in a strongly connected and balanced graph reach the* ϵ*-average consensus in finite time and approach the reference state asymptotically if* $\gamma(\omega) < \lambda_2$ *where* λ_2 *is the algebraic connectivity of the graph.*

Proof. From the assumptions on the pinning gains, we have $a_{1R}(\omega) = a_{2R}(\omega) = \cdots = a_{nR}(\omega) = \gamma(\omega)$, which leads to $\mathbf{\Gamma}(\omega) = \gamma(\omega)\mathbf{I}_N$. As $\mathbf{L}(\omega)$ and $\mathbf{\Gamma}(\omega)$ are commutative under multiplication and from (5.14) one can write

$$\delta(\omega, t) = e^{-\mathbf{L}(\omega)t} e^{-\mathbf{\Gamma}(\omega)t} \delta(0) = e^{-\mathbf{L}(\omega)t} e^{-\gamma(\omega)t} \delta(0).$$

With zero as the simple eigenvalue of the symmetric Laplacian matrix with $\mathbf{1}_N$ as the normalized right eigenvector and $(1/N)\mathbf{1}_N^{\mathrm{T}}$ as the normalized left eigenvector, the modal decomposition of $e^{-\mathbf{L}(\omega)t}$ can be written as

$$\begin{aligned} e^{-\mathbf{L}(\omega)t} &= e^{-\lambda_1(\omega)t} v_1(\omega) w_1^T(\omega) + \cdots + e^{-\lambda_N(\omega)t} v_N(\omega) w_N^T(\omega) \\ &= v_1(\omega) w_1^T(\omega) + e^{-\lambda_2(\omega)t} \Big[v_2(\omega) w_2^T(\omega) + e^{-(\lambda_3(\omega) - \lambda_2(\omega))t} v_3(\omega) w_3^T(\omega) + \ldots \\ &\quad + e^{-(\lambda_N(\omega) - \lambda_2(\omega))t} v_N(\omega) w_N^T(\omega) \Big]. \end{aligned}$$

At $t = t^* = \kappa/\lambda_2(\omega)$ for sufficiently large $\kappa > N$, we can write $\| e^{-\mathbf{L}(\omega)t^*} - v_1(\omega) w_1^T(\omega) \| \leq \epsilon^*$.

From the properties of normalized eigenvectors and using Cauchy-Schwarz inequality, one can write $\| v_i(\omega) w_i^T(\omega) \| \leq 1$ for all $i = 2, \ldots, N$, which leads to $\epsilon^* < (N-1)e^{-\kappa}$. Hence, the approximate statistics $\mathbb{E}[e^{-\mathbf{L}(\omega)t^*}] \approx \mathbb{E}[v_1(\omega) w_1^T(\omega)] =$

$(1/N)\mathbf{1}_N\mathbf{1}_N^{\mathrm{T}}$ can be readily obtained. Meanwhile, for $\gamma(\omega)$ relatively much smaller than the algebraic connectivity of the graph i.e. $\lambda_2(\omega)$, we have $e^{-\gamma(\omega)t^*} \approx 1$. Thus, the approximate statistics of the stochastic process $\delta(\omega, t)$ at $t = t^*$ can be written as $\mathbb{E}\left[\delta(\omega, t^*)\right] \approx (1/N)\mathbf{1}_N\mathbf{1}_N^{\mathrm{T}}\delta(0) = (1/N)\sum_{i=1}^{N}\delta_i(0)$. In other words, the expected values of the states of the agents approach the average consensus in finite time $t = t^*$. For, $t > t^*$, the dynamics of the global disagreement for any agent i in (5.13) reduces to $\dot{\delta}_i(\omega) = -a_{iR}(\omega)\delta_i(\omega) = -\gamma(\omega)\delta_i(\omega)$. Hence, for $t > t^*$, $\delta_i(\omega, t) = (1/N)e^{-\gamma(\omega)(t-t^*)}\sum_{i=1}^{N}\delta_i(0)$ and it can be concluded that the expected value of the disagreement vector $\delta(\omega)$ approaches $\mathbf{0}$ asymptotically. Moreover, from Theorem 5.2.4, it is known that the states of the agents reach the reference state exponentially in mean square sense. This concludes the proof. □

With Theorem 5.2.5 and the discussion pertinent to the intelligent intruder, it is evident that the agents approach the average consensus in finite time. However the agents are eventually driven to the reference state provided by the intruder while being in synchronization thereafter. Thus, control strategies for the agents to follow such reference signals needs to be monitored in applications.

5.3 Numerical Results

In this section, simulation examples are provided to support the analysis carried out in Section 5.2. Numerical simulation involves application of gPC expansion technique discussed in Chapter 2 in order to obtain the cumulative distribution function (CDF) probability levels of the states at various time instants. The gPC expansion also allows a framework to carry out sensitivity analysis of the response distribution with respect to the random variables, which may be exploited for the design and analysis of the network topology in multi-agent systems. In order to carry out gPC-based

sensitivity analysis accurately, the solution statistics obtained from gPC expansion are compared against Monte-Carlo [3] simulation-based approach.

5.3.1 Average Consensus in a Multi-Agent system With Edge Weight Uncertainties

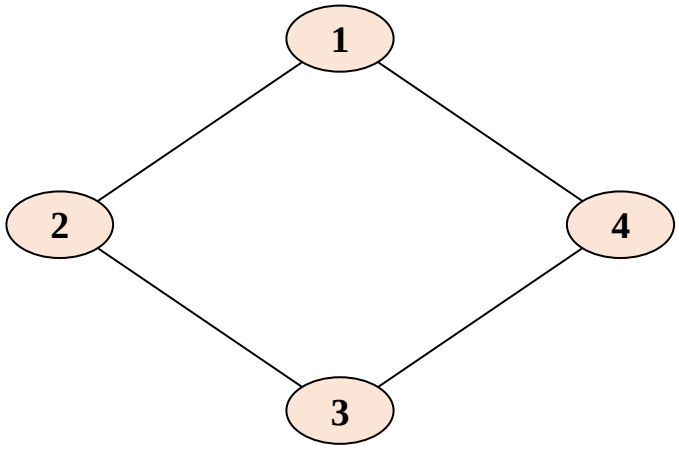

Figure 5.1: Network topology among agents

Figure 5.1 is the connected graph with $N = 4$ cooperative agents. The states of the agents are represented by $x_i \in \mathbb{R}$, $\forall i = 1, \ldots, 4$. The edge weights among the communicating agents are assumed to be uniformly distributed in the range as provided in the Table 5.1.

Table 5.1: Bounds of uncertainty

Random Variable	Distribution
$a_{12} = a_{21}$	$\mathcal{U}[0, 1]$
$a_{23} = a_{32}$	$\mathcal{U}[0, 1]$
$a_{34} = a_{43}$	$\mathcal{U}[0, 1]$
$a_{14} = a_{41}$	$\mathcal{U}[0, 1]$

The simulation is carried out with $x_{10} = 1$, $x_{20} = 3$, $x_{30} = 5$ and $x_{40} = 6$ as initial conditions for the states of the agents. The CDF obtained from repetitive simulations using 10^5 Monte Carlo samples is considered to be the reference solution. In order to obtain response CDF from gPC expansion, the coefficients of expansion are computed using sparse grid-based collocation nodes in pseudospectral framework. As all random variables are uniformly distributed, Legendre polynomial basis is used for fifth order gPC expansion.

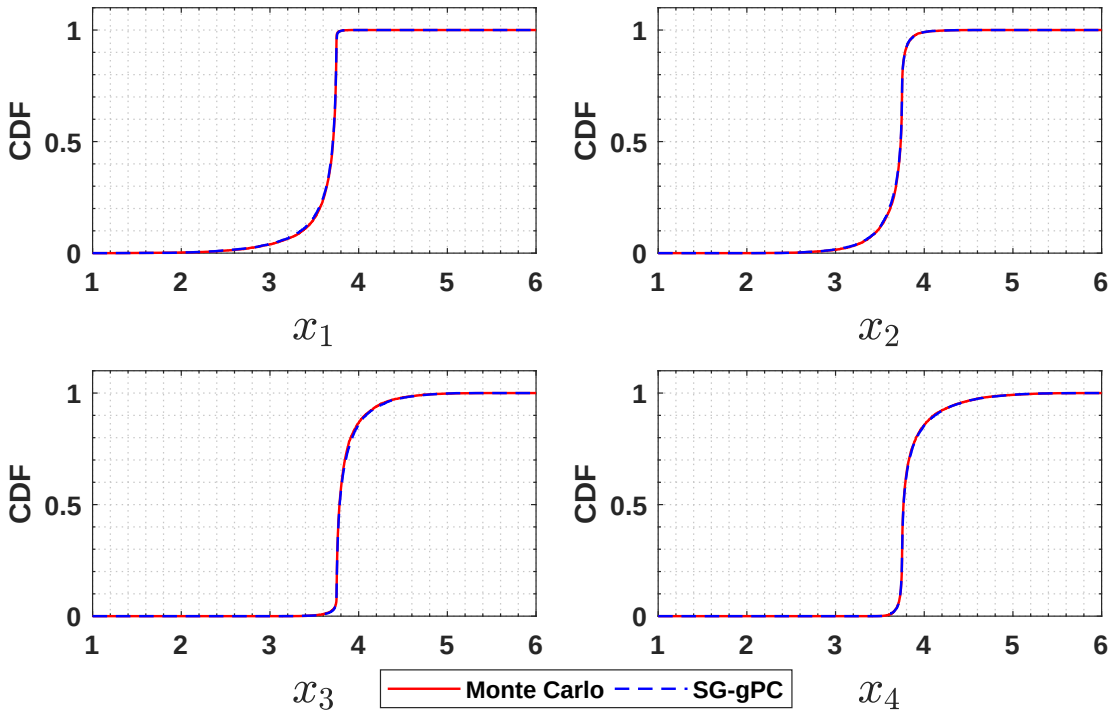

Figure 5.2: Cumulative density function of states after 5 seconds

The response CDFs for the states at three different time instants approximated using Monte Carlo simulations (MCS) and gPC expansion are shown in Figs. 5.2-5.4. The response CDFs obtained using sparse grid-based gPC expansion (SG-gPC) show a close resemblance with that obtained from the MCS. Further, this is achieved with

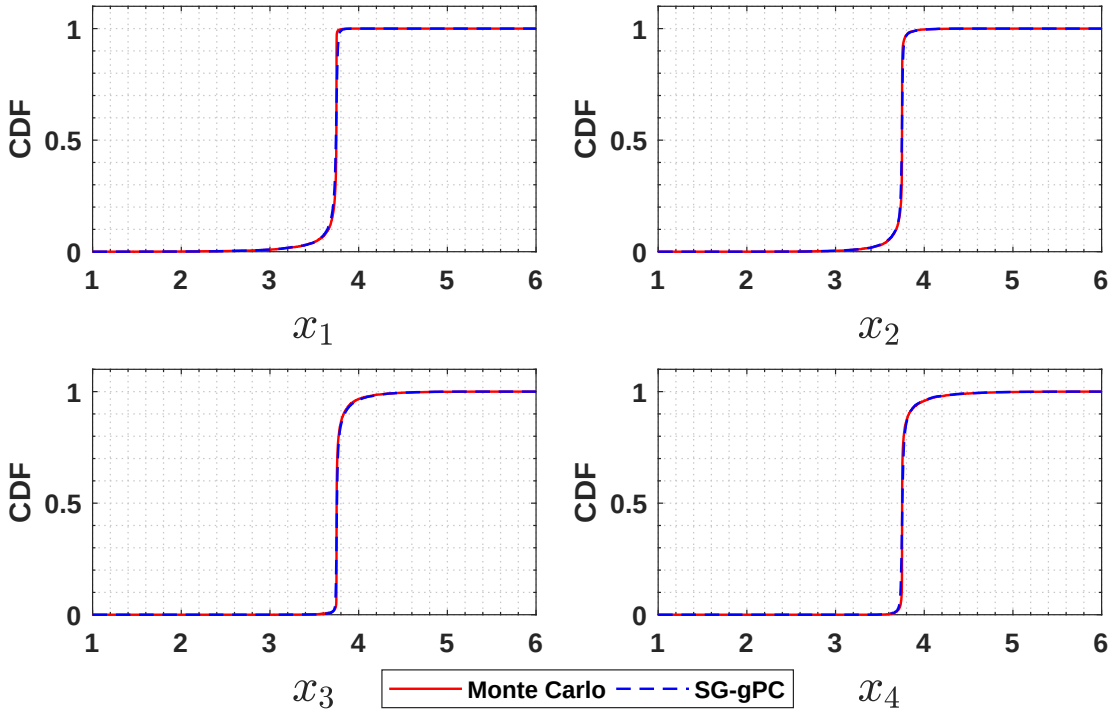

Figure 5.3: Cumulative density function of states after 10 seconds

relatively fewer nodes (10^5 MCS samples and 1217 Sg-gPC samples) which also shows the efficacy of gPC expansion as compared to MCS. It can be clearly observed that after 35 seconds, the CDF of the states of the agents becomes approximately equal to unity at $x_i = c = 3.75$, $\forall i = 1, \ldots, 4$ which is the average consensus value. Further, $\mathcal{P}\{x_i(t, \omega) \neq c\} = 0$ as proved in Theorem 5.2.1.

5.3.2 Consensus Study in the Presence of an Intelligent Intruder

A group of agents with the network topology represented by graph $\mathcal{G}$ in the presence of an intelligent intruder as shown in Fig. 5.5 is considered. As discussed in Section 5.2.3, along with the edge weights among the agents, the edge weights (known as pinning gains) linking intruder to the agents is also uncertain. The probability distribution of the edge weights and the pinning weights are known *a priori* and are

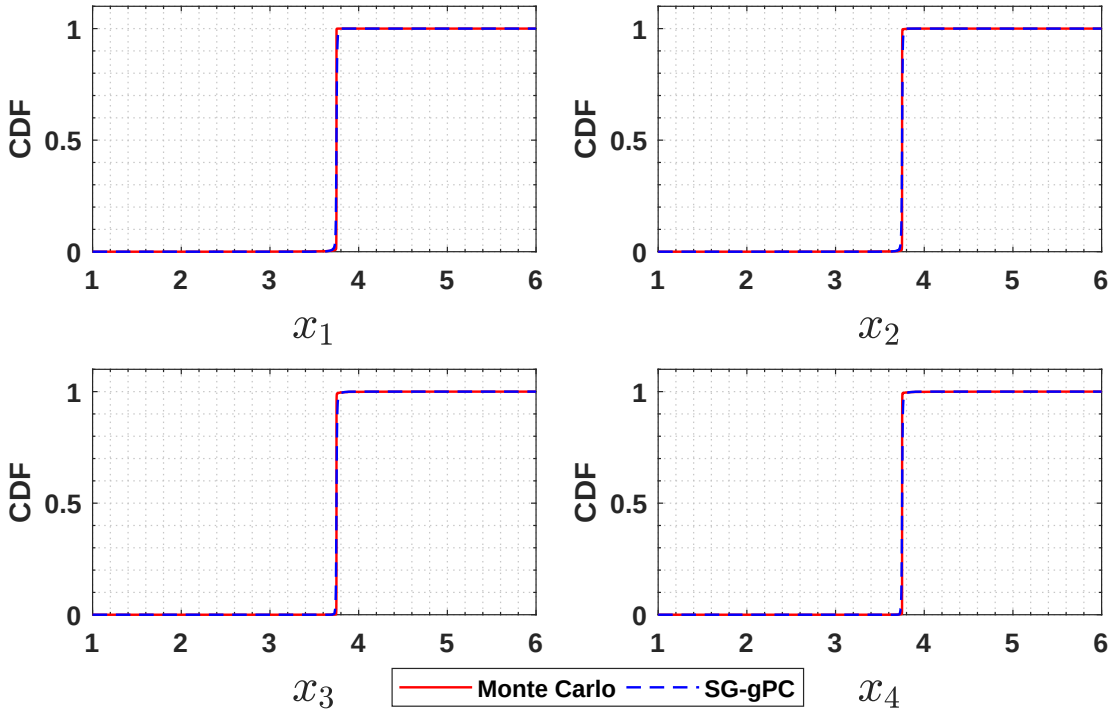

Figure 5.4: Cumulative density function of states after 35 seconds

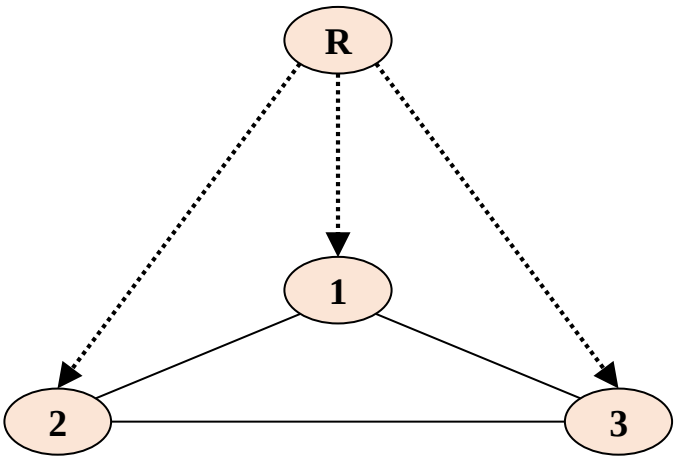

Figure 5.5: Network topology among agents with an intelligent intruder

provided in Table 5.2 which is in accordance with the assumptions made in Section 5.2.3.

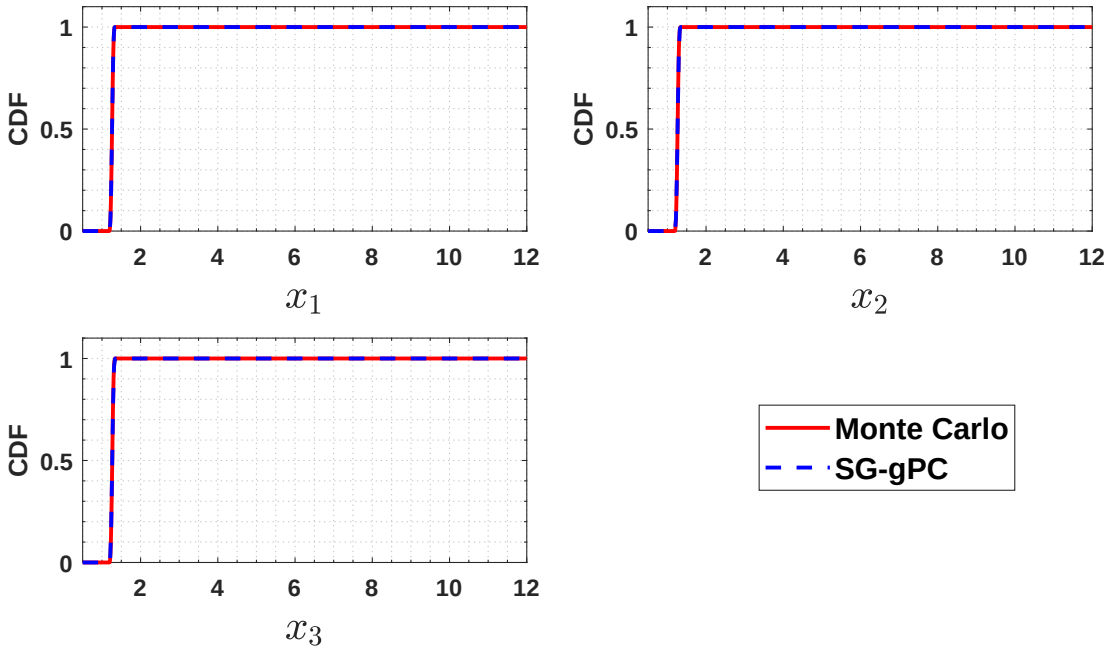

Figure 5.6: CDF of states after 2 seconds

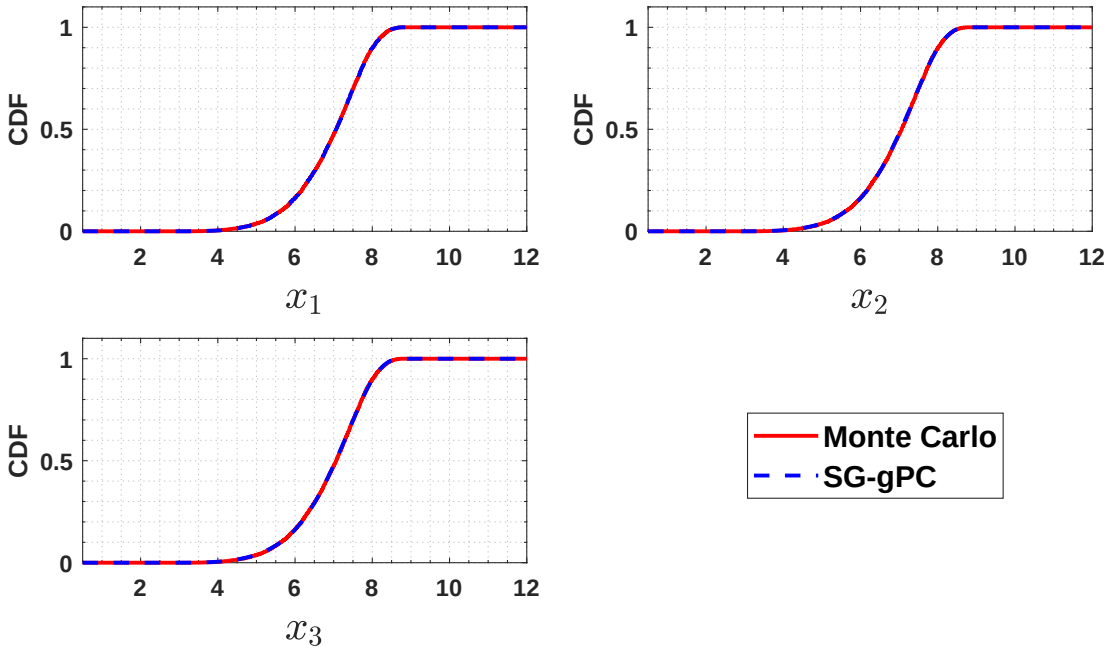

Figure 5.7: CDF of states after 200 seconds

Table 5.2: Bounds of uncertainty

Random Variable	Distribution
$a_{12} = a_{21}$	$\mathcal{U}[0, 4]$
$a_{13} = a_{31}$	$\mathcal{U}[0, 4]$
$a_{23} = a_{32}$	$\mathcal{U}[0, 4]$
a_{1R}	$\mathcal{U}[0, 0.01]$
a_{2R}	$\mathcal{U}[0, 0.01]$
a_{3R}	$\mathcal{U}[0, 0.01]$

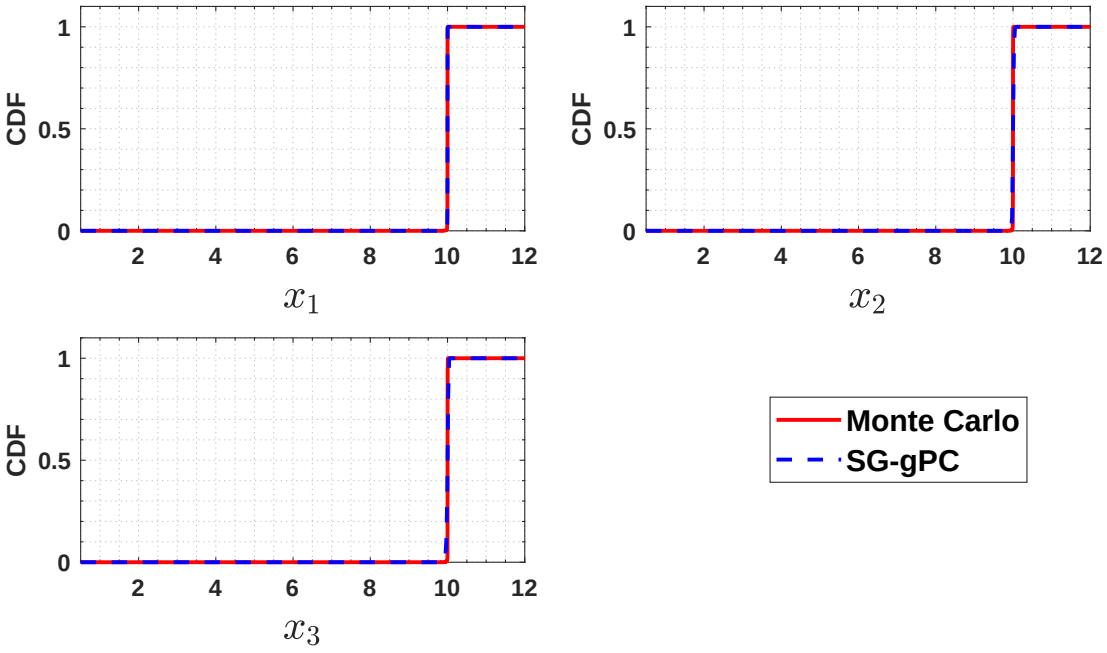

Figure 5.8: CDF of states after 2000 seconds

The initial conditions of the states of the agents are assumed as, $x_{10} = 0.5$, $x_{20} = 1$ and $x_{30} = 2$ with the constant intruder reference state as $x^R = 10$. The gPC-approximated CDFs of states of agents after 2, 200, and 2000 seconds of propagation are compared with that obtained from 10^5 MCS in Figs. 5.6, 5.7 and 5.8. Clearly, fifth order-gPC expansion is able to capture the response distribution of the states quite accurately with fewer nodes as compared to MCS (10^5 MCS samples and 1889 SG-gPC samples). Further, it can be observed that after 2 s, the CDF of the states

of the agents at around the average consensus value of $c = 1.1667$ is approximately 1. Thus, the agents reach the average consensus in finite time. However, because of the presence of the intruder which provides weak reference signal to the agents, the agents are observed to deviate from the average consensus to the constant reference state provided by the intruder after 2000 s. Though the agents stay in consensus, the intruder is able to cause the consensus value for the agents to diverge. This is in accordance with the discussion pertinent to Theorem 5.2.5.

As can be observed from Fig. 5.9, up until the time instant the agents reach the average consensus, the response distribution function of the states of the agents is significantly influenced by the edge weight associated with the edge connecting agents 1 and 3. This is in accordance with the fact that, the initial state of agent 1 is farthest from the average consensus value ($c = 1.1667$). Thus, in order to achieve the consensus, agent 1 needs to move towards agent 3 at a rate faster than it moves towards agent 2. Hence, the edge connecting agents 1 and 3 is the most significant to drive all the agents to the consensus. Further, agent 2 needs to move towards agent 3 and the edge connecting agents 2 and 3 have a significant contribution for agent 2 to reach to the consensus with other agents. Further, the undirected edges $\mathcal{E}_{23}$ and $\mathcal{E}_{12}$ have very less significance on the movement of the agents 1 and 3 for the consensus; which is in agreement with what is clearly observed in Fig. 5.9. More interestingly, it is evident that the edges connecting the intruder and the agents have reduced significance on the response distribution of the states of the agents up until they reach the average consensus. Just after the agents reach the consensus, the total sensitivity functions of the edges connecting the intruder and the agents increase drastically and that of all other edges decay to zero. Further, it can be observed that the states of the agents are most sensitive to the pinning weights associated with the edges between the intruder and the corresponding agents just after they reach the

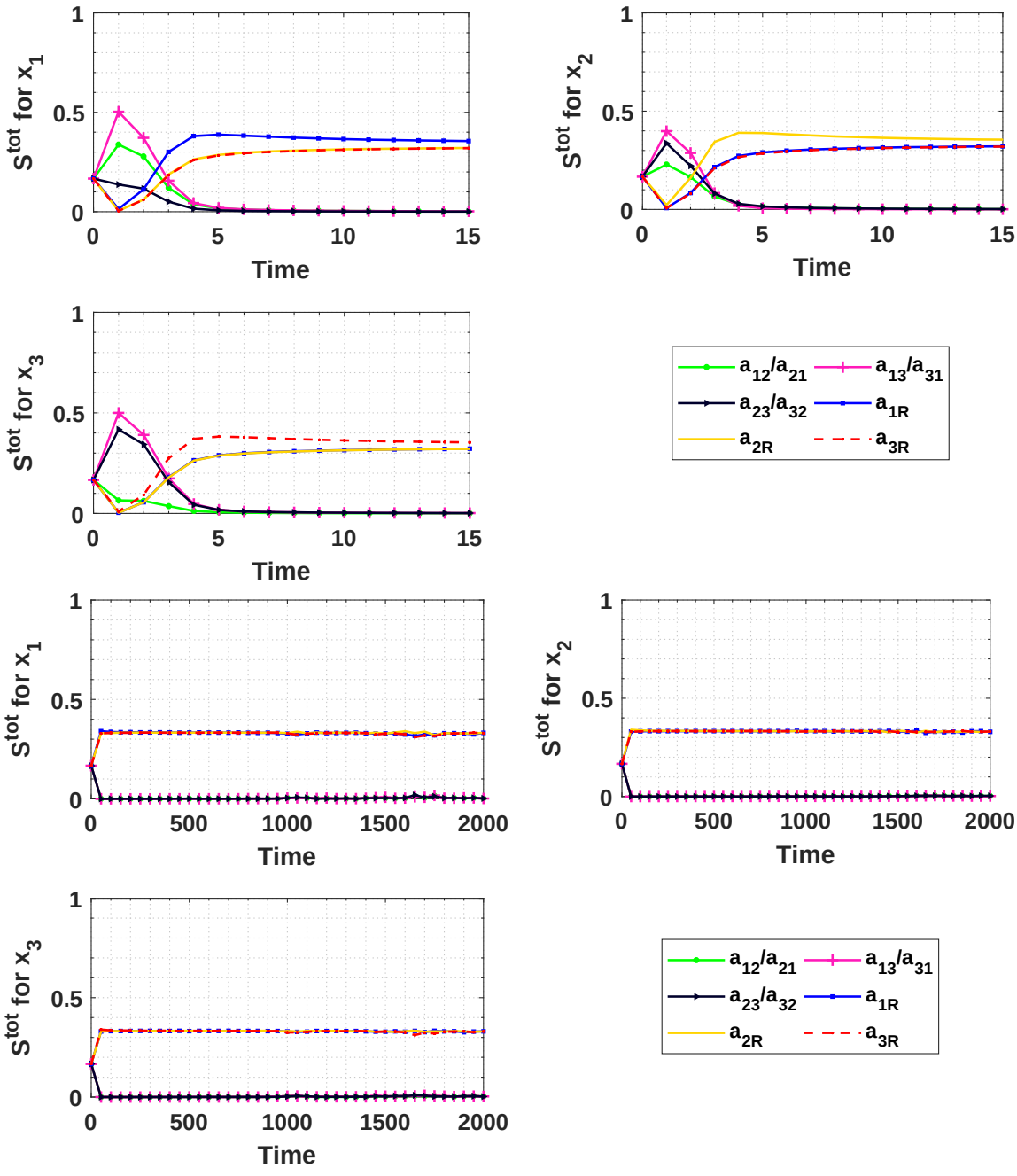

Figure 5.9: Total sensitivity of random edge weights on states of agents

consensus. After further propagation through time, it can be observed that the states of the agents are completely driven by the edges between the intruder and the agents and are insensitive to the edge connectivity amongst each other.

5.4 Chapter Summary

In this chapter, the consensus protocols are analyzed in the context of multi-agent systems where the interaction parameters (edge weights) are uncertain, however their probability density can be characterized. Sparse grid-based gPC expansion is carried out to approximate the response distribution of the states of the agents. Moreover, gPC-based sensitivity analysis is carried out to study the sensitivity of the states of the agents to the edge weights. The effect of the presence of an intelligent intruder on the consensus behavior of the multi-agent systems is analyzed from a probabilistic point of view. This work can be extended to intruder detection and network robustification for networked dynamical systems with uncertain edge weights which would aid in preventing hazardous effects from intelligent attacks.

Chapter 6

Stability Margin and Uniform Input Delay Margin of Linear Multi-Agent Systems*

This chapter provides a framework to characterize the gain and phase margins of a linear time-invariant multi-agent system where the interaction topology is described by a graph with a directed spanning tree. The stability analysis of the multi-agent system, which is based on the generalized Nyquist theorem, is converted to finding a minimum gain positive definite Hermitian perturbation and a minimum phase unitary perturbation in the feedback path of the loop transfer function. Further, we provide a framework to compute the input delay margin of the multi-agent system based on the phase perturbation of the loop transfer function. Specifically, two constrained minimization problems are solved to calculate the gain, phase, and input delay margins of the multi-agent system. We also state necessary and sufficient conditions concerning the stability of the multi-agent system independent of gain and phase perturbations and input delay.

The chapter is organized as follows. In Section 6.1, we formulate the problem under consideration. Section 6.2 discusses the stability of multi-agent systems with or without input delay in general. The main results of the chapter are presented in Section 6.3. Numerical examples are presented in Section 6.4 and the conclusions of the chapter are reported in Section 6.5.

*Part of the material reported in this chapter is reprinted with permission, from Rajnish Bhusal, Baris Taner, and Kamesh Subbarao, "On the Phase Margin of Networked Dynamical Systems and Fabricated Attacks of an Intruder," *2020 American Control Conference (ACC)*, IEEE, pp. 3279-3284, Denver, CO, July 2020, DOI: 10.23919/ACC45564.2020.9147500, Copyright © 2021, IEEE (reference [122]).

6.1 Problem Formulation

6.1.1 Multi-Agent System Without delay

Consider a group of N identical agents. The dynamics of the ith agent is described by the following linear time-invariant (LTI) system

$$\dot{\mathbf{x}}_i(t) = \mathbf{A}\mathbf{x}_i(t) + \mathbf{B}\mathbf{u}_i(t), \qquad i = 1, \ldots, N \tag{6.1}$$

where $\mathbf{A} \in \mathbb{R}^{n\times n}$, $\mathbf{B} \in \mathbb{R}^{n\times m}$ are the system matrices with $\mathbf{x}_i \in \mathbb{R}^n$ as the state and $\mathbf{u}_i \in \mathbb{R}^m$ as the input of the ith agent. The LTI continuous dynamics of each agent can also be represented by the loop transfer function in frequency domain as

$$\mathbf{P}(s) = (s\mathbf{I}_n - \mathbf{A})^{-1}\mathbf{B} \tag{6.2}$$

which is the linear mapping of Laplace transform from the input $\mathbf{u}_i(t)$ to the state $\mathbf{x}_i(t)$.

Assumption 6.1.1. $(\mathbf{A}, \mathbf{B})$ *is stabilizable.*

It is assumed that the agents share the state information among each other in a predefined graph topology. The graph theoretical framework-based multi-agent system's modeling is such that, each node in the graph represents the agents and the edge connecting the two neighboring nodes represent the communication between the agents. Further details on the algebraic graph theory can be found in Chapter 5. In this work, we make following assumption on the underlying graph topology.

Assumption 6.1.2. *Throughout the chapter, the graph is assumed to be connected with at least one directed spanning tree.*

Definition 6.1.1. *The group of agents are said to reach consensus under any control protocol* $\mathbf{u}_i$ *if for any set of initial conditions* $\{\mathbf{x}_i(0)\}$ *there exists* $\mathbf{x}^c \in \mathbb{R}^n$ *such that* $\lim_{t\to\infty} \mathbf{x}_i(t) = \mathbf{x}^c$ *for all* $i = 1, 2, \ldots, N$.

With assumption 6.1.1, let each of the agents $i = 1, 2, \ldots, N$ have identical feedback controller $\mathbf{K} \in \mathbb{R}^{m\times n}$ such that $\mathbf{A}-\mathbf{B}\mathbf{K}$ is stable. For the ith agent with plant

transfer function $\mathbf{P}(s)$ and a state feedback controller $\mathbf{K}(s)$, we define $\mathbf{H}(s) \in \mathbb{R}^{n\times n}$ to be the loop transfer function as seen when breaking the loop at the output of the plant. Thus, for each agent $i = 1, 2, \ldots, N$, we have

$$\mathbf{H}(s) = \mathbf{P}(s)\mathbf{K}(s). \tag{6.3}$$

We consider following static distributed control protocol based on the relative states between neighboring agents as discussed in [162, 163]:

$$\mathbf{u}_i(t) = c\mathbf{K}\sum_{k\in\mathcal{N}_i} a_{ik}(\mathbf{x}_k(t) - \mathbf{x}_i(t)), \qquad i = 1, 2, \ldots, N. \tag{6.4}$$

where c is the coupling gain and $\mathbf{K}$ is the feedback gain matrix. The approach to calculate c would be discussed later in Section 6.2. With control protocol in (6.4), the overall global closed-loop dynamics can be written as

$$\dot{\mathbf{x}}(t) = (\mathbf{I}_N \otimes \mathbf{A})\mathbf{x}(t) - c(\mathbf{L} \otimes \mathbf{BK})\mathbf{x}(t) \tag{6.5}$$

where $\mathbf{x} = [\mathbf{x}_1^T, \ldots, \mathbf{x}_N^T]^T \in R^{Nn}$ is the global state of multi-agent system. Now, the overall loop transfer function of multi-agent system is $\mathbf{G}(s) = \hat{\mathbf{H}}(s)\hat{\mathbf{L}}$, where $\hat{\mathbf{H}}(s) = \mathbf{I}_N \otimes \mathbf{H}(s)$ and $\hat{\mathbf{L}} = c\,(\mathbf{L} \otimes \mathbf{I}_n)$.

In this chapter, we intend to characterize the gain and phase margin of the closed-loop system in (6.5) with the state feedback controller $\mathbf{K}$ to achieve consensus.

6.1.2 Multi-Agent System With Input Delay

Let us now consider a problem of multi-agent system with N agents subjected to input delay. We assume the input delays to be uniform for all agents. The dynamics of ith agent in the presence of input delay can be written as

$$\mathbf{x}_i(t) = \mathbf{A}\mathbf{x}_i(t) + \mathbf{B}\mathbf{u}_i(t-\tau), \quad i = 1, 2, \ldots, N \tag{6.6}$$

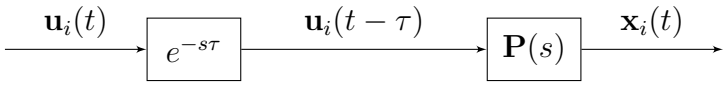

Figure 6.1: Schematic representation of input delay for ith agent

where τ is the delay in the input of the agents. Figure 6.1 illustrates the schematics of input delay for ith agent.

The presence of input delay governs the multi-agent system such that each agent i, for all $i = 1, 2, \ldots, N$ receives the state information of its neighbor and its own state information with a delay of τ. Let Assumption 6.1.1 holds for (6.6). With the distributed control protocol in (6.4), the closed loop dynamics of ith agent can be written as

$$\mathbf{x}_i(t) = \mathbf{A}\mathbf{x}_i(t) + c\mathbf{B}\mathbf{K}\left(\sum_{k\in\mathcal{N}_i} a_{ik}\left(\mathbf{x}_k(t-\tau) - \mathbf{x}_i(t-\tau)\right)\right) \tag{6.7}$$

With $\mathbf{x} = [\mathbf{x}_1^T, \ldots, \mathbf{x}_N^T]^T \in R^{Nn}$ as the global state of multi-agent system, the overall global closed-loop dynamics for input delay multi-agent system can be written as,

$$\dot{\mathbf{x}}(t) = (\mathbf{I}_N \otimes \mathbf{A})\mathbf{x}(t) - c(\mathbf{L} \otimes \mathbf{B}\mathbf{K})\mathbf{x}(t-\tau). \tag{6.8}$$

Here, we are interested in finding the input delay margin τ^* such that the multi-agent system in (6.8) achieves state consensus for any $\tau \in [0, \tau^*]$.

6.2 Stability in Multi-Agent Systems for Consensus

In this section, we discuss the stability conditions required for multi-agent systems to reach the consensus.

6.2.1 Consensus in Multi-Agent Systems Without Delay

Lemma 6.2.1. *If $\hat{\mathbf{H}}(s)\hat{\mathbf{L}}$ has p_u unstable poles, the closed loop system in* (6.5) *is stable, iff any of the following two statements hold:*

(1) The Nyquist plot of $det[\mathbf{I}_{nN} + \hat{\mathbf{H}}(s)\hat{\mathbf{L}}]$ makes p_u anti-clockwise encirclements of the origin.

(2) The Nyquist plot of $\prod_{p=2}^{N} det[\mathbf{I}_n + c\lambda_p \mathbf{H}(s)]$ makes p_u anti-clockwise encirclements of the origin; where $\{\lambda_p\}_{p=1}^{N}$ are the eigenvalues of $\mathbf{L}$.

Proof. The statement (1) is the direct consequence of generalized Nyquist Theorem for the closed loop stability of a multi-agent system. Now, the equivalence of the above two statements can be shown with the help of Schur decomposition of Laplacian matrix $\mathbf{L}$ as $\mathbf{L} = \mathbf{STS}^*$, where $\mathbf{S}$ is a unitary matrix and $\mathbf{T}$ is an upper triangular matrix. Since $\mathbf{T}$ is an upper triangular matrix with same spectrum as $\mathbf{L}$, the eigenvalues of $\mathbf{L}$ are the diagonal entries of $\mathbf{T}$. Moreover, $\mathbf{T}$ can be decomposed as,

$$\mathbf{T} = \mathbf{\Lambda} + \mathbf{\Gamma}. \tag{6.9}$$

where $\mathbf{\Lambda}$ is a diagonal matrix consisting of eigenvalues $\{\lambda_p\}_{p=1}^{N}$ of $\mathbf{L}$ and $\mathbf{\Gamma}$ is a strictly upper triangular matrix. Since, $\hat{\mathbf{L}} = c\,(\mathbf{L} \otimes \mathbf{I}_n)$, one can write

$$\begin{aligned}
\det\left[\mathbf{I}_{nN} + \hat{\mathbf{H}}(s)\hat{\mathbf{L}}\right] &= \det\left[\mathbf{I}_{nN} + c\hat{\mathbf{H}}(s)\,(\mathbf{S} \otimes \mathbf{I}_n)\,\hat{\mathbf{T}}\,(\mathbf{S}^* \otimes \mathbf{I}_n)\right] \\
&= \det\left[(\mathbf{S} \otimes \mathbf{I}_n)\,(\mathbf{I}_{nN} + c\hat{\mathbf{H}}(s)\hat{\mathbf{T}})\,(\mathbf{S}^* \otimes \mathbf{I}_n)\right] \\
&= \det[\mathbf{I}_{nN} + c\hat{\mathbf{H}}(s)\hat{\mathbf{T}}].
\end{aligned}$$

where $\hat{\mathbf{T}} = \mathbf{T} \otimes \mathbf{I}_n$. As $\hat{\mathbf{H}}(s)$ is block diagonal and $\hat{\mathbf{T}}$ is block upper triangular, one can write

$$\begin{aligned}\det[\mathbf{I}_{nN} + c\hat{\mathbf{H}}(s)\hat{\mathbf{T}}] &= \det[\mathbf{I}_{nN} + c\hat{\mathbf{H}}(s)\left(\mathbf{\Lambda} \otimes \mathbf{I}_n\right)] \\ &= \prod_{p=1}^{N} \det[\mathbf{I}_n + c\lambda_p \mathbf{H}(s)] \\ &= \prod_{p=2}^{N} \det[\mathbf{I}_n + c\lambda_p \mathbf{H}(s)]\end{aligned}$$

The last equality comes from the fact that $\lambda_1 = 0$. □

Remark 6.2.2. *Lemma 6.2.1 implies that the stability of multi-agent system is equivalent to the stability of following p transformed systems*

$$\dot{\boldsymbol{\xi}}_p(t) = \mathbf{A}\boldsymbol{\xi}_p(t) + \mathbf{B}\mathbf{u}_p(t), \quad \forall\ p = 2, 3, \ldots, N \tag{6.10}$$

where, $\boldsymbol{\xi}_p$ is the state vector and $\mathbf{u}_p(t)$ is the input of the p^{th} system which is given by $\mathbf{u}_p(t) = -\bar{\mathbf{K}}_p\boldsymbol{\xi}_p(t)$ with $\bar{\mathbf{K}}_p = c\lambda_p\mathbf{B}\mathbf{K}$. The essence of Lemma 6.2.1 is similar to the discussion carried out for formation control of multi-agent systems in [63] where the authors conclude that if the controller $\mathbf{K}$ stabilizes the transformed system for all λ_p other than the zero eigenvalue, it stabilizes the relative dynamics of formation. Alike in (6.3)*, we define the loop transfer functions of the transformed systems as*

$$\mathbf{G}_p(s) = \mathbf{P}(s)\bar{\mathbf{K}}_p(s) = (s\mathbf{I}_n - \mathbf{A})^{-1}\mathbf{B}c\lambda_p\mathbf{K}(s), \quad \forall p = 2, 3, \ldots, N. \tag{6.11}$$

6.2.1.1 Selection of $\mathbf{K}$ and $\mathbf{c}$

As stated earlier, $\mathbf{K}$ is selected such that the dynamics of the individual agent is stable before the interconnection, i.e., $\mathbf{A} - \mathbf{B}\mathbf{K}$ is Hurwitz. Now, the value of c is selected such that the consensus among the agents is achieved, i.e. $\mathbf{A} - \mathbf{B}\bar{\mathbf{K}}_p = \mathbf{A} - c\lambda_p\mathbf{B}\mathbf{K}$ for $p = 2, 3, \ldots, N$ are Hurwitz, where λ_p are the eigenvalues of Laplacian matrix. We select c based on the consensus region approach discussed in [162]. The

consensus region of a multi-agent system can be defined as $\mathcal{S}(\sigma) = \{\sigma \in \mathbb{C} \mid \mathbf{A} - \sigma\mathbf{BK}$ is Hurwitz$\}$. From [162], for the agents to reach consensus, the coupling gain c is to be selected such that $c\lambda_p \in \mathcal{S}(\sigma)$.

We make following assumption throughout the chapter for further analysis.

Assumption 6.2.1. $\mathbf{A} - \mathbf{B}\bar{\mathbf{K}}_p$ *is stable, for all* $p = 2, 3, \ldots, N$

6.2.2 Consensus in Multi-Agent Systems With Input Delay

The loop transfer function of the multi-agent system in (6.8) can be written as $\hat{\mathbf{H}}(s)\hat{\mathbf{L}}e^{-s\tau}$. Now, Lemma 6.2.1 can be extended for the multi-agent system with delay and the stability of multi-agent system with input delay in (6.8) is equivalent to the stability of following p transformed systems

$$\dot{\boldsymbol{\xi}}_p(t) = \mathbf{A}\boldsymbol{\xi}_p(t) + \mathbf{B}\mathbf{u}_p(t-\tau), \quad \forall\ p = 2, 3, \ldots, N \tag{6.12}$$

where $\boldsymbol{\xi}_p$ is the state vector and $\mathbf{u}_p(t-\tau) = -\bar{\mathbf{K}}_p\boldsymbol{\xi}_p(t-\tau)$ with $\bar{\mathbf{K}}_p = c\lambda_p\mathbf{BK}$, is the delayed input of the p^{th} system. Moreover, the loop transfer function of the transformed system in (6.12) becomes $(s\mathbf{I}_n - \mathbf{A})^{-1}\mathbf{B}c\lambda_p\mathbf{K}(s)e^{-s\tau}$.

6.3 Main Results

The stability margin serves as a robustness measure against gain and phase variations in the feedback path of the group of agents. Moreover, time delays in multi-agent systems are practically unavoidable. In this section, we provide a computational framework to characterize the stability margins, namely gain and phase margins of the delay-free system in (6.5), and input delay margin of multi-agent system with input delay in (6.8).

Definition 6.3.1. *[164] The polar decomposition of a matrix* $\mathbf{T} \in \mathbb{C}^{r\times t}$ *with* $r \geq t$ *can be written as* $\mathbf{T} = \mathbf{RU}$ *where* $\mathbf{R} \in \mathbb{C}^{r\times t}$ *is a positive semi-definite Hermitian matrix and* $\mathbf{U} \in \mathbb{C}^{t\times t}$ *is a unitary matrix.*

In this work, we calculate the stability margins and the input delay margin of the multi-agent system by assessing the characteristics of the perturbed loop transfer function $\mathbf{G}_p(j\omega_p)\mathbf{\Delta}_p$. Here, $\mathbf{\Delta}_p \in \mathbb{C}^{n\times n}$ is the multiplicative complex perturbation in the feedback path of the loop transfer function $\mathbf{G}_p(s)$. We consider different mathematical structures of $\mathbf{\Delta}_p$ depending upon the type of margin that is being computed, i.e., for computation of gain margin, phase margin and input delay margin, $\mathbf{\Delta}_p$ would be complex gain, phase and delay perturbations, respectively.

The polar decomposition is a generalization to complex matrices of the familiar polar representation $z = re^{j\phi}, r \geq 0$ of a complex number $z \in \mathbb{C}$. From Definition 6.3.1 we can polar-decompose $\mathbf{\Delta}_p$ as, $\mathbf{\Delta}_p = \mathbf{RU}$. The unitary factor $e^{j\phi}$ of z corresponds to unitary matrix $\mathbf{U} = e^{\mathbf{\Sigma}_p}$ of $\mathbf{\Delta}_p$, where $\mathbf{\Sigma}_p$ is a skew Hermitian matrix with phase information of Δ_p and $r = |z|$ of z corresponds to the Hermitian factor $\mathbf{R}$ of $\mathbf{\Delta}_p$ [165]. We assume that the complex perturbation $\mathbf{\Delta}_p$ is nonsingular and thus, the polar decomposition is unique and $\mathbf{R}$ is positive definite Hermitian.

Definition 6.3.2. *The complex perturbation* $\mathbf{\Delta}_p$ *for any* $p = 2, 3, \ldots, N$ *in the loop transfer function* $\mathbf{G}_p(s)$ *is said to be destabilizing at frequency* $\omega_p \in \mathbb{R}$ *if*

$$det(\mathbf{I} + \mathbf{G}_p(j\omega_p)\mathbf{\Delta}_p) = 0 \tag{6.13}$$

Lemma 6.3.1. *If there exists a destabilizing* $\mathbf{\Delta}_p$ *in the feedback path of* $\mathbf{G}_p(j\omega_p)$ *for any* $p = 2, 3, \ldots, N$*, the original loop transfer function* $\mathbf{G}(s) = \hat{\mathbf{H}}\hat{\mathbf{L}}$ *becomes unstable.*

Proof. From Lemma 6.2.1 and Remark 6.2.2, the stability of original loop transfer function is equivalent to the stability of p transformed loop transfer functions $\mathbf{G}_p(s)$ simultaneously. Thus, if there exists a unitary $\mathbf{\Delta}_p$ that satisfies (6.13) for any $p =$

$2, 3, \ldots, N$, it destabilizes the p^{th} transformed system and equivalently, the original loop transfer function $\mathbf{G}(s) = \hat{\mathbf{H}}\hat{\mathbf{L}}$. □

As stated earlier, input delay margin can be associated with stabilizing ranges of phase in the system, which motivates us to compute the input delay margin by considering the phase perturbations in the system. Thus, we first provide a framework to characterize phase and input delay margins consecutively and provide a framework to compute gain margin separately.

6.3.1 Phase Margin and Input Delay Margin

In order to characterize the phase margin and input delay margin, it is assumed that $\mathbf{R}$ is lumped into the loop transfer function or assumed to be an identity matrix. Thus the analysis presented in this work for characterizing phase margin and delay margin considers $\Delta_p = \mathbf{U} = e^{\mathbf{\Sigma}_p}$. Hereafter, we use Δ_p, $\mathbf{U}$, $e^{\mathbf{\Sigma}_p}$ would be used interchangeably for characterizing phase and input delay margins. The following Lemma is an extension to the work carried out by Wang et al. in [83], wherein $\mathbf{\Delta}_p$ was assumed to be structured diagonal perturbation; however in this work, we consider phase perturbations to be in the entire set of unitary matrices and not necessarily to be diagonal.

Lemma 6.3.2. *The stabilizing boundary of phase is symmetric with respect to the origin.*

Proof. Let us start by saying $(\phi_1, \phi_2, \ldots, \phi_n)$ is the point on the stabilizing boundary, then there exists some critical frequency ω_{c_p} for all $p = 2, 3, \ldots, N$ such that

$$\det[\mathbf{I} + \mathbf{G}_p(j\omega_{c_p})\Delta_p] = \det[\mathbf{I} + \mathbf{G}_p(j\omega_{c_p})e^{\mathbf{\Sigma}_p}] = 0$$

As stated before, $\mathbf{\Sigma}_p$ is a skew Hermitian matrix with $\mathbf{\Sigma}_p = -\mathbf{\Sigma}_p^*$. The eigenvalue decomposition of $\mathbf{\Sigma}_p$ can be written as $\mathbf{\Sigma}_p = \mathbf{P}\Lambda_\Delta\mathbf{P}^*$, where $\mathbf{P}$ is a unitary

matrix of eigenvectors and Λ_Δ is a diagonal matrix of eigenvalues of $\mathbf{\Sigma}_p$. As the phase information of Δ_p is contained in the unitary matrix $\mathbf{U}$ of the polar decomposition, the eigenvalues of $\mathbf{U}$ all lie on the unit circle such that, $\lambda_k(\mathbf{U}) = e^{j\phi_k}$ for all $k = 1, 2, \ldots, n$. Moreover, $\text{Im}\{\lambda_k(\mathbf{\Sigma}_p)\} = \arg\{\lambda_k(\mathbf{U})\} = \phi_k$ which implies $\Lambda_\Delta = \text{diag}(j\phi_1, j\phi_2, \ldots, j\phi_n)$. Clearly, one can write

$$\det[\mathbf{I} + \mathbf{G}_p(j\omega_{c_p})\mathbf{P}e^{\{\text{diag}(j\phi_1, j\phi_2, \ldots, j\phi_n)\}}\mathbf{P}^*] = 0 \tag{6.14}$$

On taking conjugate on the both sides of (6.14), we get

$$\det[\mathbf{I} + \mathbf{G}_p(-j\omega_{c_p})\mathbf{P}^*e^{\{\text{diag}(-j\phi_1, -j\phi_2, \ldots, -j\phi_n)\}}\mathbf{P}] = 0$$

Thus, it can be asserted that for the point $(-\phi_1, -\phi_2, \ldots, -\phi_n)$, there exists an $-\omega_{c_p}$ such that the closed-loop system is marginally stable. This implies that $(-\phi_1, -\phi_2, \ldots, -\phi_n)$ is also the point on the stabilizing boundary. □

Remark 6.3.3. *By Lemma 6.3.2, the stabilizing borders of loop phases are symmetric with respect to the origin, the values of ω_{c_p} are also symmetric with respect to the origin. This property hints that one only needs to examine the frequency response for nonnegative frequencies, while the analysis for the other half of the frequency range follows that of nonnegative frequency range due to symmetry. This simplification is analogous to the analysis of half-sectorial systems in the work of Chen et al. [166]. Further, $e^{j\phi_k}$ is a periodic function in ϕ_k with a period of $2\phi_k$ and thus, one only needs to consider $\phi_k \in (-\pi, \pi]$ and for discussing stability, it can be further narrowed to $\phi_k \in [0, \pi]$, for all $k = 1, 2, \ldots, n$. Moreover, phases of $\mathbf{\Delta}_p = \mathbf{U}$ for all $p = 2, \ldots, N$ can be calculated as $\phi_k = |Im\{\lambda_k(\mathbf{U})\}|$ for all $k = 1, 2, \ldots, n$ and in turn phase of $\mathbf{\Delta}_p$ can be defined as $\max(|Im(\lambda_k(\mathbf{U})|))$ in $[0, \pi]$.*

6.3.1.1 Stability of Multi-Agent System Independent of Unitary Phase Perturbations

We provide following necessary and sufficient conditions such that the multi-agent system is stable for any unitary phase perturbation in the feedback path. These conditions can be considered to be an extended small gain conditions in robust stability analysis.

Lemma 6.3.4. *Subject to Assumptions 6.1.2 and 6.2.1, the multi-agent system in* (6.5) *is stable independent of unitary phase perturbations* Δ_p *in the feedback path if and only if*

$$\bar{\sigma}(\mathbf{G}_p(j\omega_p)) < 1, \quad \forall \omega_p > 0, \quad \forall p = 2, \ldots, N \tag{6.15}$$

where $\sigma_i(\mathbf{G}_p)$ *are the singular values of the transfer function matrix* $\mathbf{G}_p$, $\bar{\sigma}(\mathbf{G}_p) = \max \sigma_i(\mathbf{G}_p)$ *and* $\underline{\sigma}(\mathbf{G}_p) = \min \sigma_i(\mathbf{G}_p)$.

Proof. Let us assume the condition in (6.15) holds. Now, we can write

$$\bar{\sigma}\left((j\omega_p\mathbf{I} - \mathbf{A})^{-1} c\lambda_p \mathbf{B}\mathbf{K}\right) < 1, \quad \forall \omega_p > 0. \tag{6.16}$$

For unitary phase perturbation $e^{\mathbf{\Sigma}_p}$ in the feedback path, we have

$$\bar{\sigma}\left((j\omega_p\mathbf{I} - \mathbf{A})^{-1} c\mathbf{B}\mathbf{K}\lambda_p e^{\mathbf{\Sigma}_p}\right) < 1 \tag{6.17}$$

which also can be expressed as

$$\bar{\sigma}\left((j\omega_p\mathbf{I} - \mathbf{A})^{-1} c\lambda_p \mathbf{B}\mathbf{K}\mathbf{\Delta}_p\right) < 1 \tag{6.18}$$

where, $\mathbf{\Delta}_p = e^{\mathbf{\Sigma}_p}$ is unitary. It is straightforward to see that if the condition in (6.18) holds, then

$$\det\left(\mathbf{I} + (j\omega_p\mathbf{I} - \mathbf{A})^{-1} c\lambda_p \mathbf{B}\mathbf{K}\mathbf{\Delta}_p\right) \neq 0, \quad \forall \omega_p > 0$$

or equivalently,

$$\det\left(\mathbf{I} + \mathbf{G}_p(j\omega_p)\mathbf{\Delta}_p\right) \neq 0, \quad \forall \omega_p > 0$$

i.e. the characteristic polynomial of the system in (6.10) does not intersect the imaginary axis and the system is stable independent of unitary phase perturbation. Moreover, from Lemma 6.2.1 and Remark 6.2.2, the multi-agent system in (6.5) is stable independent of unitary phase perturbations in the feedback path. The proof for the sufficiency part is completed.

To establish the necessity, assume that $\bar{\sigma}\left(\mathbf{G}_p(j\omega_{c_p})\right) = \bar{\sigma}\left((j\omega_p\mathbf{I}-\mathbf{A})^{-1}c\lambda_p\mathbf{BK}\right) = 1$, for some $\omega_{c_p} > 0$, for any $p = 2,\ldots,N$. This implies that there exists some unitary $\mathbf{\Delta}_p = e^{\mathbf{\Sigma}_p}$ such that $\det\left(\mathbf{I}+(j\omega_{c_p}\mathbf{I}-\mathbf{A})^{-1}c\lambda_p\mathbf{BK}\mathbf{\Delta}_p\right) = \det\left(\mathbf{I}+\mathbf{G}_p(j\omega_p)\mathbf{\Delta}_p\right) = 0$ and from Lemma 6.3.1 the multi-agent system in (6.5) becomes unstable. Let us now consider a case when, $\bar{\sigma}(\mathbf{G}_p(j\omega_p)) = \bar{\sigma}\left((j\omega_p\mathbf{I}-\mathbf{A})^{-1}c\lambda_p\mathbf{BK}\right) > 1$, for some $\omega_p > 0$. Since, $\bar{\sigma}\left(\mathbf{G}_p(j\omega_p)\right)$ is a continuous function of ω_p, there exists some $\omega_{c_p} \in (\omega_p,\infty)$, such that $\bar{\sigma}\left(\mathbf{G}_p(j\omega_{c_p})\right) = 1$ and the multi-agent system in (6.5) is unstable. □

Remark 6.3.5. *Note that, if $\bar{\sigma}\left(\mathbf{G}_p(j\omega_p)\right) = 1$, there exists a unit vector $\mathbf{z}_p$ such that $\|\mathbf{G_p}(j\omega_p)\mathbf{z}_p\| = 1$. The proof of which is trivial and well known.*

Now let us define a set $\Omega_p = \{\omega_p|\ \underline{\sigma}(\mathbf{G}_p(j\omega_p)) \leq 1 \leq \bar{\sigma}(\mathbf{G}_p(j\omega_p))\}$ for all $p = 2,\ldots,N$. The cardinality of set Ω_p is denoted as n_{Ω_p}.

6.3.1.2 Stability of Multi-Agent System Dependent on Unitary Phase Perturbations

If the conditions highlighted by Lemma 6.3.4 are not satisfied, then there exists a unitary perturbation which destabilizes the multi-agent system. In this section, we provide the approach to find such perturbation and a computational framework to characterize the phase margin of the system.

Lemma 6.3.6. *There exists a destabilizing unitary $\mathbf{\Delta}_p$ which is a mapping between two unit vectors, if and only if for any $p = 2,\ldots,N$ the set $\Omega_p \neq \varnothing$.*

Proof. If the set $\Omega_p \neq \varnothing$ for any $p = 2, \ldots, N$, there exists a ω_p and a unit vector $\mathbf{z}_p$ such that $\|\mathbf{G_p}(j\omega_p)\mathbf{z}_p\| = 1$ (see the proof of Lemma 6.3.4 and Remark 6.3.5). Let $\mathbf{v}_p = -\mathbf{G}_p(j\omega_p)\mathbf{z}_p$ and consider a unitary matrix Δ_p which maps $\mathbf{v}_p$ into $\mathbf{z}_p$ such that $\Delta_p\mathbf{v}_p = \mathbf{z}_p$. Since, $\mathbf{G}_p(j\omega_p)\Delta_p\mathbf{v}_p = \mathbf{G}_p(j\omega_p)\mathbf{z}_p = -\mathbf{v}_p$, one can write $(\mathbf{I}+\mathbf{G}_p(j\omega_p)\Delta_p)\mathbf{v}_p = 0$ which implies $\det(\mathbf{I}+\mathbf{G}_p(j\omega_p)\Delta_p) = 0$ and the system $\mathbf{G}_p(j\omega_p)$ is unstable. This concludes the necessity.

Now, consider a destabilizing unitary Δ_p such that, $\det(\mathbf{I} + \mathbf{G}_p(j\omega_p)\Delta_p) = 0$ and a unit vector $\mathbf{v}_p$ such that $(\mathbf{I}+\mathbf{G}_p(j\omega_p)\Delta_p)\mathbf{v}_p = 0$ and thus $\mathbf{G}_p(j\omega_p)\Delta_p\mathbf{v}_p = -\mathbf{v}_p$. Now let us assume Δ_p maps $\mathbf{v}_p$ into $\mathbf{z}_p$ such that $\mathbf{z}_p = \Delta_p\mathbf{v}_p$. As Δ_p is unitary and $\mathbf{v}_p$ is a unit vector, we have $\|\mathbf{z}_p\| = 1$. So, we can write, $\underline{\sigma}(\mathbf{G}_p) = \inf\limits_{\|\mathbf{z}_p\|=1} \|\mathbf{G}_p\mathbf{z}_p\| \leq 1$. Similarly, $1 \leq \sup\limits_{\|\mathbf{z}_p\|=1} \|\mathbf{G}_p\mathbf{z}_p\| = \bar{\sigma}(\mathbf{G}_p)$. Thus, the set $\Omega_p \neq \phi$. Hence, we have established sufficiency and necessity to the statement. □

Theorem 6.3.7. *Suppose the Assumptions 6.1.2 and 6.2.1 hold. Let $\mathbb{P}$ be the set of all $p \subset \{2, \ldots, N\}$ where $\Omega_p \neq \varnothing$. Then, the loop transfer function $\mathbf{G}_p(s)$ in (6.11) is stable if the eigenvalues $\{\lambda_k(\mathbf{\Delta}_p)\}_{k=1}^n$ of unitary perturbation $\mathbf{\Delta}_p \in \mathbb{C}^n$ in the feedback path of $\mathbf{G}_p(s)$ for all $p \in \mathbb{P}$ satisfies $\max(|Im(\lambda_k(\mathbf{\Delta}_p))|) < \phi_p$ where*

$$\phi_p = \min_{i=1,2,\ldots,n_{\Omega_p}} \{\phi_i\} \tag{6.19}$$

and $\phi_i = \min\{\cos^{-1}\{\langle \mathbf{v}_p, \mathbf{z}_p\rangle\}\}$ with unit vectors $\mathbf{v}_p$ and $\mathbf{z}_p$ satisfying $\mathbf{v}_p = -\mathbf{G}_p(j\omega_p)\mathbf{z}_p$, for all $\omega_p \in \Omega_p$. Moreover, the loop transfer function $\mathbf{G}_p(s)$ in (6.11) is stable independent of unitary perturbation $\mathbf{\Delta}_p$ if $\Omega_p = \varnothing$ for all $p = 2, \ldots, N$.

Proof. From Lemma 6.3.6, if for any $p = 2, \ldots, N$ the set $\Omega_p \neq \varnothing$, then there exists an $\omega_p \in \Omega_p$ where the system destabilizes and a set of unit vectors $\mathbf{v}_p$ and $\mathbf{z}_p$ can be calculated that satisfies $\mathbf{v}_p = -\mathbf{G}_p(j\omega_p)\mathbf{z}_p$. Moreover, there also exists a destabilizing unitary perturbation (say $\mathbf{\Delta}_p^c$) that maps $\mathbf{v}_p$ to $\mathbf{z}_p$.

For $\mathbf{G}_p(s)$ to be stable, phase of unitary Δ_p in the feedback path should be less than the smallest phase of destabilizing unitary perturbation $\mathbf{\Delta}_p^c$ that maps unit vector $\mathbf{v}_p$ to $\mathbf{z}_p$ for all $\omega_p \in \Omega_p$. Further, the angle between subspaces of $\mathbb{C}^n$ in which two unit vectors $\mathbf{v}_p$ and $\mathbf{z}_p$ lie is given by $\cos^{-1}\{\langle \mathbf{v}_p, \mathbf{z}_p \rangle\}$ [167]. Also, as $\mathbf{\Delta}_p^c$ is unitary, we can write $\langle \mathbf{v}_p, \mathbf{z}_p \rangle = \left\langle \mathbf{\Delta}_p^c \mathbf{v}_p,\ \mathbf{\Delta}_p^c \mathbf{z}_p \right\rangle$. To that end, the phase of destabilizing $\mathbf{\Delta}_p^c$ which maps the two unitary vectors $\mathbf{v}_p$ and $\mathbf{z}_p$ such that $\mathbf{z}_p = \mathbf{\Delta}_p^c \mathbf{v}_p$ is also $\cos^{-1}\{\langle \mathbf{v}_p, \mathbf{z}_p \rangle\}$. Henceforth, the smallest phase of destabilizing unitary perturbation for all $p \in \mathbb{P}$ can be obtained by minimizing $\cos^{-1}\{\langle \mathbf{v}_p, \mathbf{z}_p \rangle\}$ for all $\omega_p \in \Omega_p$ and is given by

$$\phi_p = \min_{i=1,2,\ldots,n_{\Omega_p}} \{\phi_i\}, \quad \phi_i = \min\{\cos^{-1}\{\langle \mathbf{v}_p, \mathbf{z}_p \rangle\}\}. \tag{6.20}$$

From Lemma 6.3.2 and Remark 6.3.3, one can write phase of any unitary $\mathbf{\Delta}_p$ as $\max(|\mathrm{Im}(\lambda_k(\mathbf{\Delta}_p))|)$. Therefore, for $\mathbf{G}_p(s)$ to be stable the eigenvalues of unitary perturbation $\mathbf{\Delta}_p$ in the feedback path of $\mathbf{G}_p(s)$ should satisfy $\max(|\mathrm{Im}(\lambda_k(\mathbf{\Delta}_p))|) < \phi_p$. Further, if the set $\Omega_p = \varnothing$ for all $p = 2, 3, \ldots, N$, the multi-agent system remains stable independent of phase perturbation from Lemma 6.3.4. This completes the proof. □

Remark 6.3.8. *Based on Theorem 6.3.7 and Remark 6.2.2, the phase margin of the multi-agent system can be calculated to be*

$$\phi^* = \inf_{p \in \mathbb{P}} \left\{ \min_{\omega_p \in \Omega_p} \left\{ \min\{\cos^{-1}\{\langle \mathbf{v}_p, \mathbf{z}_p \rangle\}\} \right\} \right\}. \tag{6.21}$$

Moreover, as cosine is a monotonically decreasing function in $[0, \pi]$*, minimizing* $\cos^{-1}\{\langle \mathbf{v}_p, \mathbf{z}_p \rangle\}$ *is same as maximizing the inner product* $\langle \mathbf{v}_p, \mathbf{z}_p \rangle$ *satisfying* $\mathbf{v}_p = -\mathbf{G}_p(j\omega_p)\mathbf{z}_p$*, for all* $\omega_p \in \Omega_p$*.*

6.3.1.3 Delay Independent Stability of Multi-Agent Systems

Lemma 6.3.9. *Subject to Assumptions 6.1.2 and 6.2.1, the input delay multi-agent system in* (6.8) *is stable independent of delay if and only if*

(i) $\mathbf{A}$ *is stable and*

(ii) $\bar{\sigma}(\mathbf{G}_p(j\omega_p)) < 1$, $\forall \omega_p > 0$, $\forall p = 2, \ldots, N$.

Proof. For the system to be stable independent of delay, it is necessary that it be stable for $\tau = \infty$, which requires condition (i) to hold (see [168]). Condition (ii) is neccessary and sufficient condition for the multi-agent system to be stable independent of unitary phase perturbations as discussed in Lemma 6.3.4. As input delay links to a phase change with no gain change, condition (ii) is also necessary and sufficient for the system in (6.8) to be stable independent of delay. □

6.3.1.4 Delay Dependent Stability of Multi-Agent Systems

The approach of characterizing the input delay margin of multi-agent delay system in this work bears some similarity to that of "frequency sweeping method" in the literature (see e.g., [168, 169]).

Theorem 6.3.10. *Suppose the Assumptions 6.1.2 and 6.2.1 hold. Let* $\mathbb{P}$ *be the set of all* $p \subset \{2, \ldots, N\}$ *where* $\Omega_p \neq \varnothing$. *Then, the multi-agent system with input delay in* (6.8) *is stable for any* $\tau \in [0, \tau^*)$ *where*

$$\tau^* = \begin{cases} \min\limits_{p \in \mathbb{P}} \min\limits_{1 \leq i \leq n_{\Omega_p}} \dfrac{\phi_i}{\omega_i}, & \text{if} \quad \mathbb{P} \neq \varnothing \\ \infty, & \text{if} \quad \mathbb{P} = \varnothing \end{cases} \tag{6.22}$$

and $\phi_i = \min\{\cos^{-1}\{\langle \mathbf{v}_p, \mathbf{z}_p \rangle\}\}$, $\omega_i = argmin\{\cos^{-1}\{\langle \mathbf{v}_p, \mathbf{z}_p \rangle\}\}$ *with unit vectors* $\mathbf{v}_p$ *and* $\mathbf{z}_p$ *satisfying* $\mathbf{v}_p = -\mathbf{G}_p(j\omega_p)\mathbf{z}_p$, *for all* $\omega_p \in \Omega_p$.

The proof follows from the proof of Theorem 6.3.7 and has been omitted for brevity. The sketch of the proof is as follows: since input delay can be linked to a unitary phase perturbation, once the phases ϕ_i are calculated, a set of delays can be calculated for each $\omega_p \in \Omega_p$ as $\tau_i = \dfrac{\phi_i}{\omega_i}$. Infimum of this set over all $\omega_p \in \Omega_p$ provides the upper limit of delay for the loop transfer function of p^{th} input delayed system to remain stable, i.e. $\tau_p^* = \min\limits_{1 \le i \le n_{\Omega_p}} \dfrac{\phi_i}{\omega_i}$ [170]. Moreover, from 6.1.2, one can establish $\tau^* = \min\limits_{p \in \mathbb{P}} \tau_p^*$ such that the multi-agent system with input delay in (6.8) is stable if $\tau \in [0, \tau^*)$. Further, if the set $\Omega_p = \varnothing$ for all $p = 2, 3, \ldots, N$, the system remains stable independent of delay from Lemma 6.3.9.

6.3.1.5 Computational Framework for Phase margin and Input delay margin

This section provides the computational framework to characterize the phase margin and input delay margin for multi-agent systems in (6.5) and (6.8), respectively. In order to calculate the phase margin and input delay margin, one needs to find the set Ω_p, for which it is necessary to find all $\omega_p > 0$ such that $\bar{\sigma}(\mathbf{G}_p(j\omega_p)) \ge 1$ and $\underline{\sigma}(\mathbf{G}_p(j\omega_p)) \le 1$, $\forall p = 2, \ldots, N$. The procedure to compute the set Ω_p is discussed in Procedure 2. As stated earlier, once the set Ω_p is calculated, the problem of calculating phase margin and input delay margin is equivalent to maximizing $< \mathbf{v}_p, \mathbf{z}_p >$ for all $\omega_p \in \Omega_p$ (see Remark 6.3.8) which is same as maximizing $\langle \mathbf{v}_p, \mathbf{z}_p \rangle + \langle \mathbf{z}_p, \mathbf{v}_p \rangle = \mathbf{v}_p^* \mathbf{z}_p + \mathbf{z}_p^* \mathbf{v}_p$. As $\mathbf{G}_p(j\omega_p)\mathbf{z}_p = -\mathbf{v}_p$, we can have

$$\begin{aligned} \mathbf{v}_p^* \mathbf{z}_p + \mathbf{z}_p^* \mathbf{v}_p = & -\mathbf{z}_p^* \mathbf{G}_p(j\omega_p)^* \mathbf{z}_p - \mathbf{z}_p^* \mathbf{G}_p(j\omega_p)\mathbf{z}_p \\ = & -\mathbf{z}_p^* (\mathbf{G}_p(j\omega_p)^* + \mathbf{G}_p(j\omega_p))\mathbf{z}_p. \end{aligned} \tag{6.23}$$

From (6.23), it is evident that maximizing $\mathbf{v}_p^* \mathbf{z}_p + \mathbf{z}_p^* \mathbf{v}_p$ is equivalent to minimizing $\mathbf{z}_p^* (\mathbf{G}_p(j\omega_p)^* + \mathbf{G}_p(j\omega_p))\mathbf{z}_p$. Thus the problem of calculating phase margin is

converted to a constrained minimization problem: minimize $\mathbf{z}_p^*(\mathbf{G}_p(j\omega_p)^* + \mathbf{G}_p(j\omega_p))\mathbf{z}_p$ such that $|\mathbf{v}_p| = |\mathbf{z}_p| = 1$, $-\mathbf{G}_p(j\omega_p)\mathbf{z}_p = \mathbf{v}_p$ which can be further expressed as

$$\begin{aligned} &\text{minimize} \quad [\mathbf{z}_p^*(\mathbf{G}_p(j\omega_p) + \mathbf{G}_p(j\omega_p)^*)\mathbf{z}_p] \\ \text{subject to} \quad &\mathbf{z}_p^*\mathbf{z}_p = 1, \quad \mathbf{z}_p^*\ \mathbf{G}_p(j\omega_p)^*\ \mathbf{G}_p(j\omega_p)\ \mathbf{z}_p = 1. \end{aligned} \tag{6.24}$$

With $\mathbf{U} = \mathbf{G}_p(j\omega_p) + \mathbf{G}_p(j\omega_p)^*$, $\mathbf{V} = \mathbf{G}_p(j\omega_p)^*\ \mathbf{G}_p(j\omega_p)$ and $\mathbf{w} = \mathbf{z}_p$, optimization problem in (6.24) can be rewritten as

$$\begin{aligned} &\text{minimize} \quad [\mathbf{w}^*\mathbf{U}\mathbf{w}] \\ \text{subject to} \quad &\mathbf{w}^*\mathbf{w} = 1 \\ &\mathbf{w}^*\mathbf{V}\mathbf{w} = 1 \end{aligned} \tag{6.25}$$

It is straightforward to show that the complex optimization problem in (6.25) is equivalent to the following optimization problem from the work carried out in [171]:

$$\begin{aligned} &\text{minimize} \quad \left[(\mathbf{a}^{\mathrm{T}}, \mathbf{b}^{\mathrm{T}}) \begin{pmatrix} \mathrm{Re}(\mathbf{U}) & \mathrm{Im}(\mathbf{U}) \\ -\mathrm{Im}(\mathbf{U}) & \mathrm{Re}(\mathbf{U}) \end{pmatrix} \begin{pmatrix} \mathbf{a} \\ \mathbf{b} \end{pmatrix} \right] \\ \text{subject to} \quad &\mathbf{a}_i^2 + \mathbf{b}_i^2 = 1 \quad i = 1, 2, \ldots, n \\ &(\mathbf{a}^{\mathrm{T}}, \mathbf{b}^{\mathrm{T}}) \begin{pmatrix} \mathrm{Re}(\mathbf{V}) & \mathrm{Im}(\mathbf{V}) \\ -\mathrm{Im}(\mathbf{V}) & \mathrm{Re}(\mathbf{V}) \end{pmatrix} \begin{pmatrix} \mathbf{a} \\ \mathbf{b} \end{pmatrix} = 1 \\ &\mathbf{a}, \mathbf{b} \in \mathbb{R}^n \end{aligned} \tag{6.26}$$

Let $\mathbf{Q} = \begin{pmatrix} \mathrm{Re}(\mathbf{U}) & \mathrm{Im}(\mathbf{U}) \\ -\mathrm{Im}(\mathbf{U}) & \mathrm{Re}(\mathbf{U}) \end{pmatrix}$, $\mathbf{R} = \begin{pmatrix} \mathrm{Re}(\mathbf{V}) & \mathrm{Im}(\mathbf{V}) \\ -\mathrm{Im}(\mathbf{V}) & \mathrm{Re}(\mathbf{V}) \end{pmatrix}$, $\mathbf{y} = \begin{pmatrix} \mathbf{a} \\ \mathbf{b} \end{pmatrix}$ in (6.26).
Now, the transformed optimization problem becomes

$$\begin{aligned} & \text{minimize} && \mathbf{y}^{\mathrm{T}}\mathbf{Q}\mathbf{y} \\ \text{subject to} \quad & && \mathbf{y}^{\mathrm{T}}\mathbf{y} = 1 \\ & && \mathbf{y}^{\mathrm{T}}\mathbf{R}\mathbf{y} = 1 \\ & && \mathbf{y} \in \mathbb{R}^{2n} \end{aligned} \tag{6.27}$$

The constrained optimization problem in (6.27) is a set of quadratic optimization problems with nonlinear equality constraints which can be solved by solving the Karush-Kuhn-Tucker (KKT) optimality conditions [172]. Moreover, the optimization problem in (6.27) can be equivalently written as unconstrained minimization problem by defining the *Lagrangian* as

$$\mathcal{L}(\mathbf{y}, \mu_1, \mu_2) = \mathbf{y}^{\mathrm{T}}\mathbf{Q}\mathbf{y} + \mu_1 \left(\mathbf{y}^{\mathrm{T}}\mathbf{y} - 1\right) + \mu_2 \left(\mathbf{y}^{\mathrm{T}}\mathbf{R}\mathbf{y} - 1\right) \tag{6.28}$$

where, μ_1 and μ_2 are the scalar Lagrange multipliers associated with the equality constraints [173]. Let $(\mathbf{y}^o, \mu_1^o, \mu_2^o)$ be the optimal solution to the optimization problem. Since $\mathbf{y}^*$ minimizes $\mathcal{L}(\mathbf{y}, \mu_1^o, \mu_2^o)$ over y, its gradient must vanish at $\mathbf{y}^o$. Hence, the KKT conditions which are necessary for the optimality can be written as follows:

$$\begin{aligned} \mathbf{y}^{o^{\mathrm{T}}}\mathbf{y}^{\mathbf{o}} - 1 &= 0 \\ \mathbf{y}^{o^{\mathrm{T}}}\mathbf{R}\mathbf{y}^{\mathbf{o}} - 1 &= 0 \\ \mathbf{Q}\mathbf{y}^o + \mu_1^o\mathbf{y}^o + \mu_2^o\mathbf{R}\mathbf{y}^o &= 0 \end{aligned} \tag{6.29}$$

The KKT optimality conditions are a set of $2n + 2$ equations with $2n + 2$ unknown variables. The optimal solution obtained from solving (6.29) system of equations is the global minima to the original problem in (6.27) if following KKT sufficient optimality condition holds:

$$\mathbf{Q} + \mu_1^o\mathbf{I}_{2n} + \mu_2^o\mathbf{R} \geq 0 \tag{6.30}$$

Procedure 2 Computation of ϕ^* and τ^*

1: Calculation of set Ω_p for all $p = 2, \ldots, N$:

(i) Solve $\det(\mathbf{I} - \mathbf{G}_p(j\omega_p)^*\mathbf{G}_p(j\omega_p)) = 0$ for all real roots of ω_p and calculate the eigenvalues of $\mathbf{G}_p(j\omega_p)^*\mathbf{G}_p(j\omega_p)$ at each root ω_p. Let ω_{k_p}, $k \subset \{1, 2, \ldots\}$ denote all the real roots ω_p.

(ii) Knowing the eigenvalues of $\mathbf{G}_p(j\omega_p)^*\mathbf{G}_p(j\omega_p)$ at each ω_k and at 0 will enable one to determine if there exists a $\sigma(\mathbf{G}_p(j\omega_p)) \leq 1$ and a $\sigma(\mathbf{G}_p(j\omega_p)) \geq 1$ in the region $(\omega_{(k-1)_p}, \omega_{k_p}]$ with $\omega_{0_p} = 0$.

(iii) The set Ω_p can be obtained as $\Omega_p = \cup(\omega_{(k-1)_p}, \omega_{k_p})$.

(iv) If for any $p = 2, 3, \ldots, N$, $\sigma(\mathbf{G}_p(j\omega_p))$ does not span across 1, then $\Omega_p = \varnothing$.

2: If for any $p = 2, 3, \ldots, N$, $\Omega_p \neq \varnothing$, solve optimization problem in (6.27) and compute $\mathbf{z}_p$ and $\mathbf{v}_p$ using (6.31).

3: Compute ϕ^* and τ^* using (6.21) and (6.22), respectively.

Thus, any numerical routine that can generate the local optimum ($\mathbf{y}^o$, μ_1^o, μ_2^o) by solving (6.29) and eventually satisfies (6.30) gives the global optimum $\mathbf{y}$. Further discussion on global optimization of the similar problem (quadratic objective function with quadratic equality constraints) can be found in [174, 175]. Once vector $\mathbf{y}$ is obtained by solving the optimization problem in (6.27), the vectors $\mathbf{a} \in \mathbb{R}^n$ and $\mathbf{b} \in \mathbb{R}^n$ can be calculated and, the vector $\mathbf{w} \in \mathbb{C}^n$ or equivalently $\mathbf{z}_p \in \mathbb{C}^n$ and $\mathbf{v}_p \in \mathbb{C}^n$ can be obtained as

$$\begin{aligned} \mathbf{z}_p &= \mathbf{a} + j\mathbf{b} \\ \mathbf{v}_p &= -\mathbf{G}_p(j\omega_p)\mathbf{z}_p \end{aligned} \tag{6.31}$$

The complete procedure to compute the phase margin and input delay margin of the multi-agent system is discussed in Procedure 2.

6.3.2 Gain Margin

For the gain margin calculation, the gain information of $\mathbf{\Delta}_p$ is assumed to be contained in the positive definite Hermitian part $\mathbf{R}$ of the polar decomposition of $\mathbf{\Delta}_p$. The unitary part $\mathbf{U}$ is assumed to be lumped into the loop transfer function or assumed to be an identity matrix.

6.3.2.1 Computation of Positive Definite Hermitian Matrix Mapping Two Complex Vectors

This section discusses a way to finding a positive-definite Hermitian matrix $\mathbf{R}$ mapping $\mathbf{v} \in \mathbb{C}^n$ into $\mathbf{z} \in \mathbb{C}^n$, i.e.

$$\mathbf{z} = \mathbf{R}\mathbf{v} \tag{6.32}$$

Let the set of vectors $\{\mathbf{v}, \mathbf{z}, \mathbf{u}_1, \mathbf{u}_2, \ldots, \mathbf{u}_{n-2}\}$ be a basis in $\mathbb{C}^n$. Given, a symmetric positive definite bilinear form $\langle \cdot, \cdot \rangle$ on finite-dimensional vector space, one can use the Gram-Schmidt orthogonalization process to find a orthonormal basis. Since $\langle \mathbf{v}, \mathbf{z} \rangle = \mathbf{v}^* \mathbf{z} > 0$, we can construct an orthonormal basis $\{\mathbf{q}_1, \mathbf{q}_2, \ldots, \mathbf{q}_n\}$ as

$$\begin{aligned}
\mathbf{q}_1 &= \frac{\mathbf{v}}{\sqrt{\langle \mathbf{v}, \mathbf{v} \rangle}} \\
\mathbf{q}_2 &= \frac{\hat{\mathbf{q}}_2}{\sqrt{\langle \hat{\mathbf{q}}_2, \hat{\mathbf{q}}_2 \rangle}}, \quad \hat{\mathbf{q}}_2 = \mathbf{z} - (\mathbf{q}_1^* \mathbf{z})\mathbf{q}_1; \\
\mathbf{q}_k &= \frac{\hat{\mathbf{q}}_k}{\sqrt{\langle \hat{\mathbf{q}}_k, \hat{\mathbf{q}}_k \rangle}}, \quad \hat{\mathbf{q}}_k = \mathbf{u}_{k-2} - \sum_{i=1}^{k-1} (\mathbf{q}_i^* \mathbf{u}_{k-2})\mathbf{q}_i, \quad k = 3, \ldots, n
\end{aligned} \tag{6.33}$$

Here the matrix $\mathbf{Q} = [\mathbf{q}_1 \ \mathbf{q}_2 \ \ldots \ \mathbf{q}_n]$ is such that $\mathbf{Q}\mathbf{Q}^* = \mathbf{I}$. Pre-multiplying (6.32) with $\mathbf{Q}^*$, we obtain

$$\mathbf{Q}^* \mathbf{z} = \mathbf{Q}^* \mathbf{R} \mathbf{Q} \mathbf{Q}^* \mathbf{v} \tag{6.34}$$

Let $\mathbf{Q}^*$ maps $\mathbf{v}$ into $\mathbf{e}_1$ and $\mathbf{Q}^*$ maps $\mathbf{z}$ into a linear combination of $\mathbf{e}_1$ and $\mathbf{e}_2$, such that $\mathbf{v} = \mathbf{Q}(\gamma \mathbf{e}_1)$ and $\mathbf{z} = \mathbf{Q}(\alpha \mathbf{e}_1 + \beta \mathbf{e}_2)$, where $\gamma = \sqrt{\langle \mathbf{v}, \mathbf{v} \rangle}$, $\alpha = (\mathbf{q}_1^* \mathbf{z})$ and

$\beta = \sqrt{\langle \hat{\mathbf{q}}_2, \hat{\mathbf{q}}_2 \rangle}$. Substituting for $\mathbf{z}$ and $\mathbf{v}$ in (6.34), we obtain: $\mathbf{Q}^*\mathbf{Q}(\alpha\mathbf{e}_1 + \beta\mathbf{e}_2) = (\mathbf{Q}^*\mathbf{R}\mathbf{Q})\mathbf{Q}^*\mathbf{Q}(\gamma\mathbf{e}_1)$. With $\hat{\mathbf{v}} = \gamma\mathbf{e}_1$ and $\hat{\mathbf{z}} = \alpha\mathbf{e}_1 + \beta\mathbf{e}_2$, one can write

$$\hat{\mathbf{z}} \;=\; \mathbf{P}\hat{\mathbf{v}} \tag{6.35}$$

where $\mathbf{P} = \mathbf{Q}^*\mathbf{R}\mathbf{Q}$. As $\mathbf{Q}$ is orthonormal matrix, eigenvalues of both matrices $\mathbf{R}$ and $\mathbf{P}$ are same. Since, only the upper 2×2 block of $\mathbf{Q}$ is needed to map $\hat{\mathbf{v}}$ into $\hat{\mathbf{z}}$, let us decompose $\mathbf{P}$ as $\mathbf{P} = \begin{bmatrix} \hat{\mathbf{P}} & \mathbf{0} \\ \mathbf{0} & \mathbf{I} \end{bmatrix}$, where $\hat{\mathbf{P}} \in \mathbb{C}^{2\times 2}$. Now the problem of finding a positive-definite Hermitian matrix $\mathbf{R}$ mapping $\mathbf{v}$ into $\mathbf{z}$ is reduced to the problem of finding $\hat{\mathbf{P}}$. Moreover, for $\mathbf{R}$ to be positive definite, $\hat{\mathbf{P}}$ must be positive definite and must be of the form

$$\hat{\mathbf{P}} = \begin{bmatrix} \frac{\alpha}{\gamma} & \frac{\beta}{\gamma} \\ \frac{\beta}{\gamma} & \mathbf{p}_{22} \end{bmatrix} \tag{6.36}$$

where $\mathbf{p}_{22}$ should be such that

$$\mathbf{p}_{22} > \frac{\beta^2}{\gamma\alpha} \tag{6.37}$$

Finally, $\mathbf{R}$ can be computed as $\mathbf{R} = \mathbf{Q}\mathbf{P}\mathbf{Q}^*$. It should be noted that, such a positive definite Hermitian matrix $\mathbf{R}$ is not unique.

Lemma 6.3.11. *There exists a destabilizing positive definite Hermitian $\mathbf{\Delta}_p$ if and only if there exists an ω_p and a complex vector $\mathbf{z}_p$ such that*

$$\langle \mathbf{G}_p(j\omega_p)\mathbf{z}_p, \mathbf{z}_p \rangle < 0 \tag{6.38}$$

for any $p = 2, \ldots, N$.

Proof. Let $\mathbf{v}_p = -\mathbf{G}_p(j\omega_p)\mathbf{z}_p$. Now, if for any $p = 2, \ldots, N$, $\langle \mathbf{G}_p(j\omega_p)\mathbf{z}_p, \mathbf{z}_p \rangle < 0$ implies $\mathbf{z}_p^*\mathbf{G}_p(j\omega_p)^*\mathbf{z}_p < 0$, i.e.

$$\mathbf{v}_p^*\, \mathbf{z}_p > 0 \tag{6.39}$$

Further if (6.39) holds, one can always find a positive definite Hermitian matrix Δ_p such that $\mathbf{z}_p = \Delta_p \mathbf{v}_p$, as discussed in Section 6.3.2.1. Substituting $\mathbf{z}_p$ in (6.39), we get

$$\mathbf{v}_p^* \, \Delta_p \mathbf{v}_p > 0 \tag{6.40}$$

Moreover, since $\mathbf{G}_p(j\omega_p)\Delta_p \mathbf{v}_p = \mathbf{G}_p(j\omega_p)\mathbf{z}_p = -\mathbf{v}_p$, one can write

$$(\mathbf{I} + \mathbf{G}_p(j\omega_p)\Delta_p)\mathbf{v}_p = 0 \tag{6.41}$$

which implies $\det(\mathbf{I} + \mathbf{G}_p(j\omega_p)\Delta_p) = 0$ and the system $\mathbf{G}_p(j\omega_p)$ is unstable. This concludes the necessity.

Now, consider a destabilizing positive definite Hermitian matrix Δ_p such that, $\det(\mathbf{I} + \mathbf{G}_p(j\omega_p)\Delta_p) = 0$ and a unit vector $\mathbf{v}_p$ such that $(\mathbf{I} + \mathbf{G}_p(j\omega_p)\Delta_p)\mathbf{v}_p = 0$; thus, $\mathbf{G}_p(j\omega_p)\Delta_p \mathbf{v}_p = -\mathbf{v}_p$. Let us assume Δ_p maps $\mathbf{v}_p$ into $\mathbf{z}_p$ such that $\mathbf{z}_p = \Delta_p \mathbf{v}_p$, then $\mathbf{v}_p = -\mathbf{G}_p(j\omega_p)\mathbf{z}_p$. As $\Delta_p > 0$, one can write

$$0 < \mathbf{v}_p^* \Delta_p \mathbf{v}_p = \mathbf{v}_p^* \mathbf{z}_p = -\mathbf{z}_p^* \mathbf{G}_p(j\omega_p)^* \mathbf{z}_p \tag{6.42}$$

which leads to

$$\langle \mathbf{G}_p(j\omega_p)\mathbf{z}_p, \mathbf{z}_p \rangle < 0. \tag{6.43}$$

Hence, we have established sufficiency and necessity to the statement. □

Remark 6.3.12. *For positive definite Hermitian Δ_p, $\mathbf{v}_p^* \, \Delta_p \mathbf{v}_p$ is always real and positive, i.e. $\mathbf{v}_p^* \mathbf{z}_p$ is also real and positive. Also, if $\mathbf{G}_p(j\omega_p)\mathbf{z}_p = -\mathbf{v}_p$, $\mathbf{z}_p^* \mathbf{G}_p(j\omega_p)^* \mathbf{z}_p$ is real, and thus $\mathbf{z}_p^* \mathbf{G}_p(j\omega_p)^* \mathbf{z}_p = \mathbf{z}_p^* \mathbf{G}_p(j\omega_p)\mathbf{z}_p$. Further, any positive definite Hermitian matrix $\boldsymbol{\Delta}_p$ can be written as $e^{\mathbf{S}}$. As $\lambda_k(\boldsymbol{\Delta}_p) = e^{\lambda_k(\mathbf{S})}$, for all $k = 1, 2, \ldots, n$, we define gain of $\boldsymbol{\Delta}_p$ as $\max|\lambda(\mathbf{S})| = \max|\ln(\lambda_k(\boldsymbol{\Delta}_p))|$. Note that unlike in the calculation of the phase margin, $\mathbf{v}_p$ and $\mathbf{z}_p$ need not be unit vectors.*

Now, let us define a set $\tilde{\Omega}_p = \{\omega_p|\ \langle \mathbf{G}_p(j\omega_p)\mathbf{z}_p, \mathbf{z}_p\rangle < 0\}$ for all $p = 2, \ldots, N$. The cardinality of set $\tilde{\Omega}_p$ is denoted as $n_{\tilde{\Omega}_p}$.

Corollary 6.3.13. *(Stability of multi-agent system independent of gain perturbations) If Assumptions 6.1.2 and 6.2.1 hold and the set $\tilde{\Omega}_p = \varnothing$ for all $p = 2, 3, \ldots, N$, the multi-agent system in (6.5) remains stable independent of gain perturbation in the feedback path of each agents.*

Theorem 6.3.14. *Suppose the Assumptions 6.1.2 and 6.2.1 hold. Let $\mathbb{P}$ be the set of all $p \subset \{2, \ldots, N\}$ where $\tilde{\Omega}_p \neq \varnothing$. Then, the loop transfer function $\mathbf{G}_p(s)$ in (6.11) is stable if any one of the following is satisfied:*

(i) Conditions of Corollary 6.3.13 hold, i.e., $\tilde{\Omega}_p = \varnothing$ for all $p = 2, \ldots, N$.

(ii) if the eigenvalues $\{\lambda_k(\mathbf{\Delta}_p)\}_{k=1}^{n}$ of the positive definite Hermitian perturbation $\mathbf{\Delta}_p \in C^n$ in the feedback path of loop transfer function $\mathbf{G}_p(s)$ for all $p \in \mathbb{P}$ satisfy $\max|\ln(\lambda_k(\mathbf{\Delta}_p))| < g_p$ where

$$g_p \leq \min_{1 \leq i \leq n_{\tilde{\Omega}_p}} g_i \tag{6.44}$$

and $g_i = \min\left\{\cosh^{-1}\left[\dfrac{\mathbf{v}_p^*\mathbf{v}_p + \mathbf{z}_p^*\mathbf{z}_p}{2\mathbf{v}_p^*\mathbf{z}_p}\right]\right\}$, with unit vectors $\mathbf{v}_p$ and $\mathbf{z}_p$ satisfying $\mathbf{v}_p = -\mathbf{G}_p(j\omega_p)\mathbf{z}_p$ for all $\omega_p \in \tilde{\Omega}_p$.

Proof. Statement (i) follows from Corollary 6.3.13. On the other hand, if for any $p = 2, \ldots, N$ the set $\tilde{\Omega}_p \neq \varnothing$, then there exists a $\omega_p \in \tilde{\Omega}_p$ where the system destabilizes and a set of unit vectors $\mathbf{v}_p$ and $\mathbf{z}_p$ can be calculated that satisfies $\mathbf{v}_p = -\mathbf{G}_p(j\omega_p)\mathbf{z}_p$. Moreover, from Lemma 6.3.11, there also exists a destabilizing positive definite Hermitian perturbation (say $\mathbf{\Delta}_p^c$) that maps $\mathbf{v}_p$ to $\mathbf{z}_p$.

For $\mathbf{G}_p(s)$ to be stable, gain of positive definite Hermitian Δ_p in the feedback path should be less than the smallest gain of destabilizing positive definite Hermitian perturbation $\mathbf{\Delta}_p^c$ that maps unit vector $\mathbf{v}_p$ to $\mathbf{z}_p$ for all $\omega_p \in \tilde{\Omega}_p$. Further, from [176],

the gain between two complex vectors $\mathbf{z}_p$ and $\mathbf{v}_p$ is given by $\left|\cosh^{-1}\left[\frac{\mathbf{v}_p^*\mathbf{v}_p+\mathbf{z}_p^*\mathbf{z}_p}{2\mathbf{v}_p^*\mathbf{z}_p}\right]\right|$. Moreover, gain between $\mathbf{z}_p$ and $\mathbf{v}_p$ is also the gain of the positive definite matrix that maps vectors $\mathbf{z}_p$ and $\mathbf{v}_p$. Note that $\mathbf{v}_p^*\mathbf{v}_p$ and $\mathbf{z}_p^*\mathbf{z}_p$ are positive and real, and from Remark 6.3.12, $\mathbf{v}_p^*\mathbf{z}_p$ is also real and positive. Thus, $\cosh^{-1}\left[\frac{\mathbf{v}_p^*\mathbf{v}_p+\mathbf{z}_p^*\mathbf{z}_p}{2\mathbf{v}_p^*\mathbf{z}_p}\right]$ is real and positive. Henceforth, the smallest gain of destabilizing positive definite Hermitian perturbation for all $p\in\mathbb{P}$ can be obtained by minimizing $\cosh^{-1}\left[\frac{\mathbf{v}_p^*\mathbf{v}_p+\mathbf{z}_p^*\mathbf{z}_p}{2\mathbf{v}_p^*\mathbf{z}_p}\right]$ and is given by

$$g_p=\min_{i=1,2,\ldots,n_{\tilde{\Omega}_p}}\{g_i\} \tag{6.45}$$

where

$$g_i=\min\left\{\cosh^{-1}\left[\frac{\mathbf{v}_p^*\mathbf{v}_p+\mathbf{z}_p^*\mathbf{z}_p}{2\mathbf{v}_p^*\mathbf{z}_p}\right]\right\}. \tag{6.46}$$

From Remark 6.3.12, gain of $\mathbf{\Delta}_p$ is $\max|\ln(\lambda_k(\mathbf{\Delta}_p))|$. Therefore, for $\mathbf{G}_p(s)$ to be stable the eigenvalues of positive definite Hermitian perturbation $\mathbf{\Delta}_p$ in the feedback path of $\mathbf{G}_p(s)$ should satisfy $\max|\ln(\lambda_k(\mathbf{\Delta}_p))|<g_p$. This completes the proof. □

Remark 6.3.15. *Based on Theorem 6.3.14 and Remark 6.2.2, the gain margin of the multi-agent system which is the gain of the positive definite Hermitian matrix in the feedback path of each agents can be calculated to be*

$$g^*=\begin{cases}\inf\limits_{p\in\mathbb{P}}\left\{\min\limits_{\omega_p\in\tilde{\Omega}_p}\left\{\cosh^{-1}\left[\frac{\mathbf{v}_p^*\mathbf{v}_p+\mathbf{z}_p^*\mathbf{z}_p}{2\mathbf{v}_p^*\mathbf{z}_p}\right]\right\}\right\}, & \text{if } \mathbb{P}\neq\varnothing\\ \infty, & \text{if } \mathbb{P}=\varnothing.\end{cases} \tag{6.47}$$

Further, if $\tilde{\Omega}_p=\varnothing$, it is straightforward to see that the multi-agent system is stable if the eigenvalues $\{\lambda_k\}_{k=1}^n$ of positive definite Hermitian matrix in the feedback path of all agents satisfy $\lambda_k\in\left[e^{-g^*},\ e^{g^*}\right]$. Since, eigenvalues $\{\lambda_k\}_{k=1}^n$ and singular values $\{\sigma_k\}_{k=1}^n$ of a positive definite Hermitian matrices are equivalent, we have $\sigma_k\in\left[e^{-g^*},\ e^{g^*}\right]$.

6.3.2.2 Computational Framework to Calculate Gain Margin

In order to calculate the gain margin, it is necessary to calculate the set $\tilde{\Omega}_p$. As stated in Lemma 6.3.11 and Remark 6.3.12, for a destabilizing positive definite Hermitian matrix in the feedback path of $\mathbf{G}_p(j\omega_p)$ to exist for any $p = 2, \ldots, N$, $\mathbf{v}_p^* \, \mathbf{z}_p$ must be real and positive such that $\mathbf{v}_p = -\mathbf{G}_p(j\omega_p)\mathbf{z}_p$. This leads to

$$\begin{aligned} \mathrm{Re}(\mathbf{v}_p^* \, \mathbf{z}_p) =& \frac{1}{2}(\mathbf{v}_p^* \, \mathbf{z}_p + \mathbf{z}_p^* \, \mathbf{v}_p) \\ &= \mathbf{z}_p^* \left[-\frac{1}{2} \left(\mathbf{G}_p(j\omega_p)^* + \mathbf{G}_p(j\omega_p) \right) \right] \mathbf{z}_p \\ &= \mathbf{z}_p^* \mathbf{X}_p(j\omega_p)\mathbf{z}_p > 0. \end{aligned} \tag{6.48}$$

and

$$\begin{aligned} \mathrm{Im}(\mathbf{v}_p^* \, \mathbf{z}_p) =& \; -\frac{1}{2} j(\mathbf{v}_p^* \, \mathbf{z}_p - \mathbf{z}_p^* \, \mathbf{v}_p) \\ =& \mathbf{z}_p^* \left[-\frac{1}{2} j \left(\mathbf{G}_p(j\omega_p) - \mathbf{G}_p(j\omega_p)^* \right) \right] \mathbf{z}_p \\ &= \mathbf{z}_p^* \mathbf{Y}_p(j\omega_p)\mathbf{z}_p = 0. \end{aligned} \tag{6.49}$$

Note that, both $\mathbf{X}_p(j\omega_p)$ and $\mathbf{Y}_p(j\omega_p)$ in (6.48) and (6.49) are Hermitian matrices which can be obtained by decomposing $\mathbf{G}_p(j\omega_p)$ as $\mathbf{G}_p(j\omega_p) = \mathbf{X} + j\mathbf{Y}$ such that

$$\begin{aligned} \mathbf{X} &= \frac{1}{2} \left(\mathbf{G}_p(j\omega_p) + \mathbf{G}_p(j\omega_p)^* \right), \quad \text{and} \\ \mathbf{Y} &= -\frac{1}{2} j \left(\mathbf{G}_p(j\omega_p) - \mathbf{G}_p(j\omega_p)^* \right). \end{aligned} \tag{6.50}$$

Now, for $\omega_p \in \tilde{\Omega}_p$, $\mathbf{X}_p(j\omega_p)$ needs to be positive definite and $\mathbf{Y}_p(j\omega_p)$ needs to be have an eigenvalue equal to zero simultaneously at ω_p. The detailed procedure to calculate the set $\tilde{\Omega}_p$ is discussed in Procedure 3.

Once the set $\tilde{\Omega}_p$ is computed, we need to minimize $\dfrac{\mathbf{v}_p^*\mathbf{v}_p + \mathbf{z}_p^*\mathbf{z}_p}{\mathbf{v}_p^*\mathbf{z}_p}$ at each $\omega_p \in \tilde{\Omega}_p$. It is known that cosh is a monotonically increasing function on $[0, \infty)$; therefore, minimizing $\cosh^{-1}\left[\dfrac{\mathbf{v}_p^*\mathbf{v}_p + \mathbf{z}_p^*\mathbf{z}_p}{\mathbf{v}_p^*\mathbf{z}_p}\right]$ is same as minimizing $\dfrac{\mathbf{v}_p^*\mathbf{v}_p + \mathbf{z}_p^*\mathbf{z}_p}{\mathbf{v}_p^*\mathbf{z}_p}$. Let us choose a normalization constant $\gamma^2 = \mathbf{v}_p^*\mathbf{z}_p$ such that $\tilde{\mathbf{v}}_p = \dfrac{1}{\gamma}\mathbf{v}_p$ and $\tilde{\mathbf{z}}_p = \dfrac{1}{\gamma}\mathbf{z}_p$. Note that

$\tilde{\mathbf{v}}_p^* \tilde{\mathbf{z}}_p = 1$. With necessary simplifications, the minimization problem to calculate minimum gain destabilizing Δ_i can be written as

$$\begin{aligned} \text{minimize} \quad & \tilde{\mathbf{v}}_p^* \tilde{\mathbf{v}}_p + \tilde{\mathbf{z}}_p^* \tilde{\mathbf{z}}_p \\ \text{subject to} \quad & \tilde{\mathbf{v}}_p^* \tilde{\mathbf{z}}_p = 1 \\ & \tilde{\mathbf{v}}_p = -\mathbf{G}_p(j\omega_i)\tilde{\mathbf{z}}_i. \end{aligned} \tag{6.51}$$

As $\mathbf{G}_p(j\omega_p)\mathbf{z}_p = -\mathbf{v}_p$ also implies $\mathbf{G}_p(j\omega_p)\tilde{\mathbf{z}}_p = -\tilde{\mathbf{v}}_p$, we have

$$\begin{aligned} \tilde{\mathbf{v}}_p^* \tilde{\mathbf{v}}_p + \tilde{\mathbf{z}}_p^* \tilde{\mathbf{z}}_p &= \tilde{\mathbf{z}}_p^* \mathbf{G}_p(j\omega_p)^* \mathbf{G}_p(j\omega_p)\tilde{\mathbf{z}}_p + \tilde{\mathbf{z}}_p^* \mathbf{z}_p \\ &= \tilde{\mathbf{z}}_p^* (\mathbf{G}_p(j\omega_p)^* \mathbf{G}_p(j\omega_p) + \mathbf{I}_n)\tilde{\mathbf{z}}_p \end{aligned} \tag{6.52}$$

and

$$\tilde{\mathbf{v}}_p^* \tilde{\mathbf{z}}_p = \mathbf{z}_p^* \mathbf{G}_p(j\omega_p)^* \tilde{\mathbf{z}}_p = \tilde{\mathbf{z}}_p^* \mathbf{G}_p(j\omega_p)\tilde{\mathbf{z}}_p. \tag{6.53}$$

The last equality follows from Lemma 6.3.12. Now the problem of calculating gain margin is converted to a constrained minimization problem:

$$\begin{aligned} \text{minimize} \quad & [\tilde{\mathbf{z}}_p^* (\mathbf{G}_p(j\omega_p)^* \mathbf{G}_p(j\omega_p) + \mathbf{I}_n)\tilde{\mathbf{z}}_p] \\ \text{subject to} \quad & \text{Re}[\tilde{\mathbf{z}}_p^* \mathbf{G}_p(j\omega_p)\tilde{\mathbf{z}}_p] = 1 \\ & \text{Im}[\tilde{\mathbf{z}}_p^* \mathbf{G}_p(j\omega_p)\tilde{\mathbf{z}}_p] = 0. \end{aligned} \tag{6.54}$$

With $\mathbf{U} = \mathbf{G}_p(j\omega_p)$, $\mathbf{V} = \mathbf{G}_p(j\omega_p)^*\ \mathbf{G}_p(j\omega_p)$ and $\mathbf{w} = \tilde{\mathbf{z}}_p$, optimization problem in (6.54) can be rewritten as

$$\begin{aligned} \text{minimize} \quad & [\mathbf{w}^* \mathbf{V} \mathbf{w}] \\ \text{subject to} \quad & \mathbf{w}^* \mathbf{U} \mathbf{w} = 1 \\ & \mathbf{w}^* (j\mathbf{I}) \mathbf{U} \mathbf{w} = 0. \end{aligned} \tag{6.55}$$

It is straightforward to show that the complex optimization problem in (6.55) is equivalent to the following optimization problem.

$$
\begin{aligned}
\text{minimize} \quad & \left[(\mathbf{a}^{\mathrm{T}}, \mathbf{b}^{\mathrm{T}}) \left[\begin{pmatrix} \mathrm{Re}(\mathbf{V}) & \mathrm{Im}(\mathbf{V}) \\ -\mathrm{Im}(\mathbf{V}) & \mathrm{Re}(\mathbf{V}) \end{pmatrix} + \mathbf{I}_{2n} \right] \begin{pmatrix} \mathbf{a} \\ \mathbf{b} \end{pmatrix} \right] \\
\text{subject to} \quad & \\
& (\mathbf{a}^{\mathrm{T}}, \mathbf{b}^{\mathrm{T}}) \begin{pmatrix} \mathrm{Re}(\mathbf{U}) & \mathrm{Im}(\mathbf{U}) \\ -\mathrm{Im}(\mathbf{U}) & \mathrm{Re}(\mathbf{U}) \end{pmatrix} \begin{pmatrix} \mathbf{a} \\ \mathbf{b} \end{pmatrix} = 1 \\
& (\mathbf{a}^{\mathrm{T}}, \mathbf{b}^{\mathrm{T}}) \begin{pmatrix} \mathrm{Re}(j\mathbf{I}) & \mathrm{Im}(j\mathbf{I}) \\ -\mathrm{Im}(j\mathbf{I}) & \mathrm{Re}(j\mathbf{I}) \end{pmatrix} \begin{pmatrix} \mathrm{Re}(\mathbf{U}) & \mathrm{Im}(\mathbf{U}) \\ -\mathrm{Im}(\mathbf{U}) & \mathrm{Re}(\mathbf{U}) \end{pmatrix} \begin{pmatrix} \mathbf{a} \\ \mathbf{b} \end{pmatrix} = 0 \\
& \mathbf{a}, \mathbf{b} \in \mathbb{R}^n \, .
\end{aligned}
\tag{6.56}
$$

Now, to further simplify (6.56), let us define the following

$$
\begin{aligned}
\mathbf{Q} &= \begin{pmatrix} \mathrm{Re}(\mathbf{U}) & \mathrm{Im}(\mathbf{U}) \\ -\mathrm{Im}(\mathbf{U}) & \mathrm{Re}(\mathbf{U}) \end{pmatrix}, \quad \mathbf{R} = \begin{pmatrix} \mathrm{Re}(\mathbf{V}) & \mathrm{Im}(\mathbf{V}) \\ -\mathrm{Im}(\mathbf{V}) & \mathrm{Re}(\mathbf{V}) \end{pmatrix} \\
\mathbf{y} &= \begin{pmatrix} \mathbf{a} \\ \mathbf{b} \end{pmatrix}, \quad \mathbf{J} = \begin{pmatrix} \mathrm{Re}(j\mathbf{I}) & \mathrm{Im}(j\mathbf{I}) \\ -\mathrm{Im}(j\mathbf{I}) & \mathrm{Re}(j\mathbf{I}) \end{pmatrix}.
\end{aligned}
\tag{6.57}
$$

To that end, the optimization problem in (6.56) becomes

$$
\begin{aligned}
& \text{minimize} \quad \mathbf{y}^{\mathrm{T}} \left(\mathbf{R} + \mathbf{I}_{2n} \right) \mathbf{y} \\
\text{subject to} \quad & \mathbf{y}^{\mathrm{T}} \mathbf{Q} \mathbf{y} = 1 \\
& \mathbf{y}^{\mathrm{T}} \mathbf{J} \mathbf{Q} \mathbf{y} = 0 \\
& \mathbf{y} \in \mathbb{R}^{2n} \, .
\end{aligned}
\tag{6.58}
$$

The optimization problem in (6.58) can be equivalently written as unconstrained minimization problem by defining the *Lagrangian* as in (6.28) and similar KKT conditions as in (6.29) and (6.30) can be derived. Once vector $\mathbf{y}$ is obtained by solving

Procedure 3 Computation of g^*

1: Calculation of set $\tilde{\Omega}_p$ for all $p = 2, \ldots, N$:

(i) Find $\mathbf{X}(j\omega_p)$ and $\mathbf{Y}(j\omega_p)$ from (6.50) Solve $\det(\mathbf{Y}(j\omega_p)) = 0$ for all real roots of ω_p. Let ω_k, $k \subset \{1, 2, \ldots\}$ denote all real roots ω_p.

(ii) Calculate the eigenvalues of $\mathbf{Y}(j\omega_p)$ at each ω_k and at 0.

(iii) If for any $\omega \in (\omega_{(k-1)_p}, \omega_{k_p}]$ with $\omega_{0_p} = 0$, $\lambda_{\max}(\mathbf{Y}(j\omega))\lambda_{\min}(\mathbf{Y}(j\omega)) \leq 0$ and $\mathbf{X}_p(j\omega)$ is positive semidefinite, then $(\omega_{(k-1)_p}, \omega_{k_p}] \subset \tilde{\Omega}_p$.

(iii) The set $\tilde{\Omega}_p$ can be obtained as $\tilde{\Omega}_p = \cup(\omega_{(k-1)_p}, \omega_k)$.

(iv) If for any $p = 2, 3, \ldots, N$, condition (iii) does not hold, then $\tilde{\Omega}_p = \varnothing$.

2: If for any $p = 2, 3, \ldots, N$, $\tilde{\Omega}_p \neq \varnothing$, solve optimization problem in (6.58) and compute $\tilde{\mathbf{z}}_p$ and $\tilde{\mathbf{v}}_p$ using (6.59).

3: Compute g^* using (6.47).

the optimization problem in (6.58), the vectors $\mathbf{a} \in \mathbb{R}^n$ and $\mathbf{b} \in \mathbb{R}^n$ can be calculated. Finally, the vector $\mathbf{w} \in \mathbb{C}^n$ or equivalently $\tilde{\mathbf{z}}_p \in \mathbb{C}^n$ and $\tilde{\mathbf{v}}_p \in \mathbb{C}^n$ can be obtained as

$$\begin{aligned} \tilde{\mathbf{z}}_p &= \mathbf{a} + j\mathbf{b} \\ \tilde{\mathbf{v}}_p &= -\mathbf{G}_p(j\omega_p)\tilde{\mathbf{z}}_p. \end{aligned} \tag{6.59}$$

The procedure to compute the gain margin of the multi-agent system is discussed in Procedure 3.

6.4 Simulation Results

6.4.1 Example 1

To demonstrate the preceeding analysis, we consider a multi-agent system with following system matrices [177]:

$$\mathbf{A} = \begin{bmatrix} -2 & 2 \\ -1 & 1 \end{bmatrix}, \qquad \mathbf{B} = \begin{bmatrix} 1 \\ 0 \end{bmatrix}. \tag{6.60}$$

The choice of $\mathbf{A}$ and $\mathbf{B}$ satisfies Assumption 6.1.1. Let us now choose a stabilizing feedback gain, $\mathbf{K} = \begin{bmatrix} -2 & -0.5 \end{bmatrix}$ such that $\mathbf{A} - \mathbf{BK}$ is Hurwitz. We consider a network of 3 agents with following graph Laplacian matrix,

$$\mathbf{L} = \begin{bmatrix} 0 & 0 & 0 \\ -1 & 2 & -1 \\ 0 & -1 & 1 \end{bmatrix}. \tag{6.61}$$

In order to calculate the value of coupling gain c we follow the procedure described in 6.1.1 which is taken from [162, 177]. The characteristic polynomial of $\mathbf{A} - \sigma\mathbf{BK}$ is calculated to be $p(s) = s^2 + (1 - 2x - j2y)s + (5/2)x + j(5/2)y$ with $\sigma = x + jy$. From Lemma 4 of [177], $\mathbf{A} - \sigma\mathbf{BK}$ is stable if and only if $1 - 2x > 0$ and $(25/2)(1 - 2x)^2x^2 - 5y^2(1 - 2x) - (25/4)y^2 > 0$; which describes the consensus region $\mathcal{S}(x, y) = \{x + jy \mid x < 0.5; (25/2)(1 - 2x)^2x^2 - 5y^2(1 - 2x) - (25/4)y^2 > 0\}$. From [162], for the agents to reach consensus, the coupling gain c is to be selected such that $c\lambda_p$, $p = 2, 3, \ldots, N$ belong to the consensus region $\mathcal{S}(x, y)$ where λ_p are eigenvalues of Laplacian matrix. The non-zero eigenvalues of the Laplacian matrix are calculated to be: $\lambda_2 = 0.3820$ and $\lambda_3 = 2.6180$. Thus, $c < 0.1910$ guarantees the consensus. For the simulation, we consider c to be 0.15.

Based on the framework provided in Sections 6.3.1 and 6.3.2, the phase and gain margins are calculated to be $\phi^* = 0.1820$ radians and $g^* = 0.4025$, respectively.

In other words, any unitary matrix whose phase is less than 0.1820 radians in the feedback path will not destabilize the system. From Lemma 6.3.2 the stabilizing boundary of phase is symmetric about the origin; thus the overall phase margin of the multi-agent system is calculated to be $[-0.1820, 0.1820]$ radians. Moreover, as stated in Remark 6.3.15, any positive definite Hermitian matrix in the feedback path of loop transfer function of each agents whose singular values lie within $\sigma^* = \left[e^{-g^*}, e^{g^*}\right] = [0.6686, 1.4956]$ would guarantee the stability of multi-agent system.

Further, we compare our results with the conventional *disk-based gain* and *disk-based phase margins* that have been widely utilized in the literature as robustness measure of a general MIMO system and can be obtained from the sensitivity and complimentary sensitivity functions of the system [113, 114, 178]. To compare the conservativeness and accuracy, the obtained gain and phase margins from the proposed approach are compared with the disk-based gain and disk-based phase margins obtained from sensitivity and complimentary sensitivity functions of the multi-agent system. The disk-based gain margin in terms of singular values of perturbation matrix is calculated to be $\tilde{\sigma}^* = [0.5143, 1.0820]$ and the disk-based phase margin is calculated to be $[-0.0788, 0.0788]$ radians.

To verify the accuracy of the proposed framework, we construct a matrix $\mathbf{\Delta} \in \mathbb{C}^2$ which can be polar decomposed as follows

$$\mathbf{\Delta} = \mathbf{R}\mathbf{U} \tag{6.62}$$

where $\mathbf{R}$ is the positive definite Hermitian and $\mathbf{U}$ is a unitary matrix. As discussed in Lemma 6.3.2, we can construct $\mathbf{U}$ as

$$\mathbf{U} = \mathbf{P}e^{\{\text{diag}(j\phi_1,\ j\phi_2)\}}\mathbf{P}^* \tag{6.63}$$

where $\mathbf{P}$ is any unitary matrix. To construct $\mathbf{U}$, we choose the following unitary $\mathbf{P}$ matrix

$$\mathbf{P} = \begin{bmatrix} \cos(0.2) & -\sin(0.2) \\ \sin(0.2) & \cos(0.2) \end{bmatrix} \tag{6.64}$$

and the phases of the unitary matrix are chosen to be $\phi_1 = 0.18$ radians and $\phi_2 = 0.16$ radians.

On the other hand the positive definite Hermitian matrix $\mathbf{R}$ is chosen to be

$$\mathbf{R} = \begin{bmatrix} 1 & -0.15 \\ -0.15 & 1 \end{bmatrix} \tag{6.65}$$

whose singular values are $\sigma = [0.85, 1.15]$. This yields

$$\mathbf{\Delta} = \begin{bmatrix} 0.9841 + j0.1777 & -0.1487 - j0.0202 \\ -0.1483 - j0.0229 & 0.9872 + j0.1595 \end{bmatrix}. \tag{6.66}$$

Note that $\sigma^* \ni \sigma \notin \tilde{\sigma}^*$, and $\phi^* > \phi_1 > \tilde{\phi}^*$ and $\phi^* > \phi_2 > \tilde{\phi}^*$. Figure 6.3 shows the states of agents with $\mathbf{\Delta}$ from (6.66) whose gain and phase are within the margins provided by the proposed approach but not within the margins provided by the disk-based margin.

Moreover, for the multi-agent system with input delay and with same system matrices as in (6.60) and graph Laplacian as in (6.61), the time delay margin is calculated to be $\tau^* = 0.1978$ seconds. Figure 6.3 shows the states of agents with a delay of $\tau = 0.18$ seconds in the inputs of three agents.

To illustrate the effectiveness of the proposed approach, we use different graph structures for the agents with the same system matrices as in (6.60) and with feedback

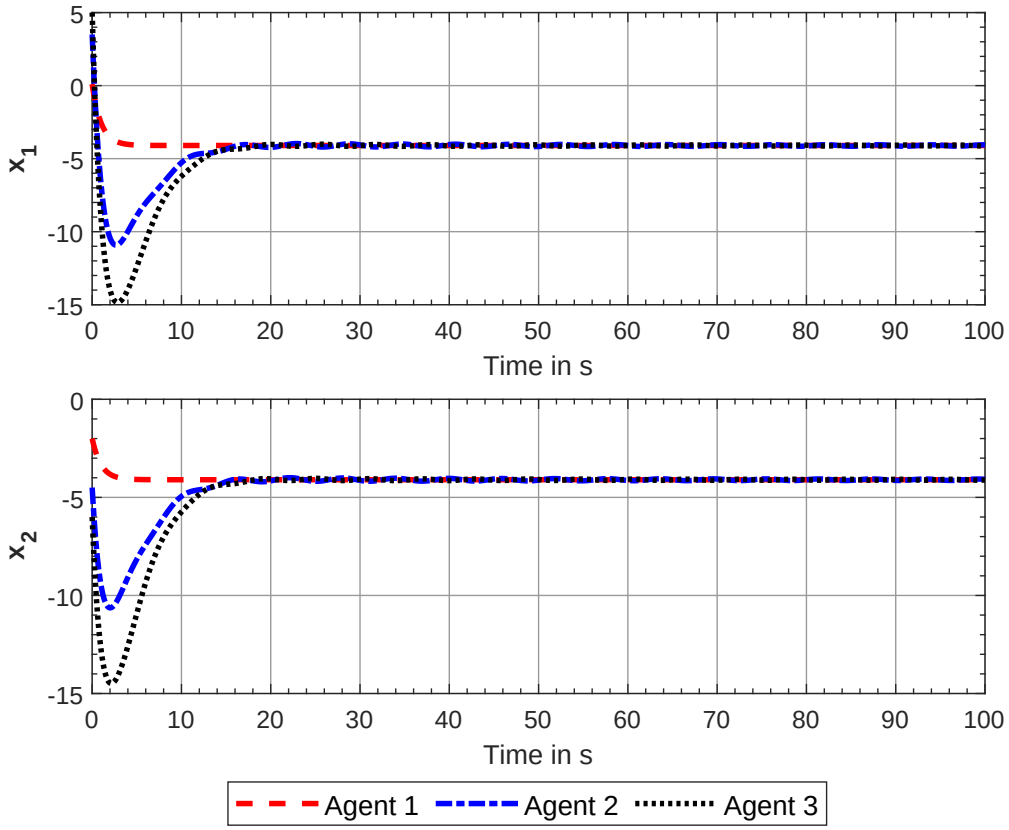

Figure 6.2: State trajectories of agents with feedback perturbation $\mathbf{\Delta}$ from (6.66)

gain matrix $\mathbf{K} = \begin{bmatrix} -2 & -0.5 \end{bmatrix}$. For a directed cycle among 4 agents with the graph Laplacian matrix as

$$\mathbf{L} = \begin{bmatrix} 1 & 0 & 0 & -1 \\ -1 & 1 & 0 & 0 \\ 0 & -1 & 1 & 0 \\ 0 & 0 & -1 & 1 \end{bmatrix} \tag{6.67}$$

, the distributed consensus protocol achieves consensus for any $c < 0.5$. With $c = 0.15$, we compute gain margin and phase margin from the proposed approach to be $[0.3355, 2.9805]$ and $[-0.7995, 0.7995]$ radians, respectively. On the other hand, the disk-based gain and disk-based phase margins are computed to be $[0.676, 1.4792]$ and

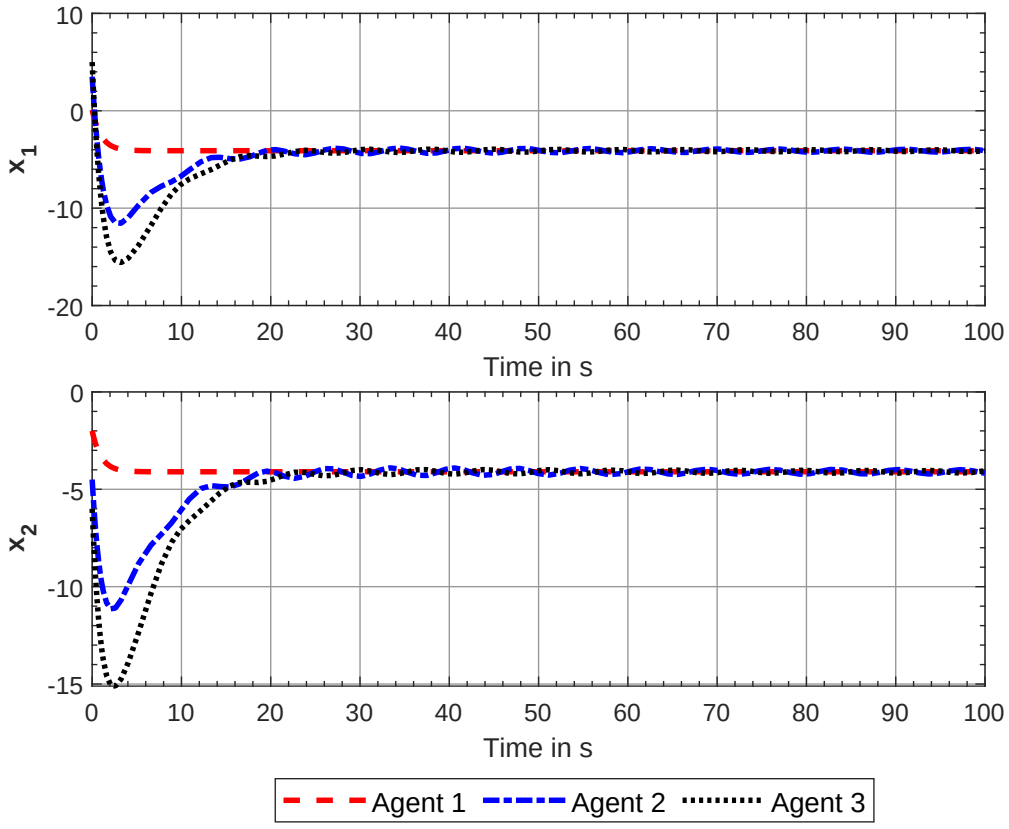

Figure 6.3: State trajectories of agents with $\tau = 0.18$ seconds

$[-0.3819, 0.3819]$ radians, respectively. Moreover, the input delay margin from the proposed approach is computed to be 2.05091 seconds.

Further, for an undirected cycle among 5 agents with the graph Laplacian matrix

$$\mathbf{L} = \begin{bmatrix} 2 & -1 & 0 & 0 & -1 \\ -1 & 2 & -1 & 0 & 0 \\ 0 & -1 & 2 & -1 & 0 \\ 0 & 0 & -1 & 2 & -1 \\ -1 & 0 & 0 & -1 & 2 \end{bmatrix}, \tag{6.68}$$

the distributed consensus protocol achieves consensus for any $c < 0.1382$. With $c = 0.12$, the gain margin and phase margin from the proposed approach is calculated to be $[0.6673, 1.4986]$ and $[-0.1066, 0.1066]$ radians, respectively. On the other hand, the disk-based gain and disk-based phase margins are computed to be $[0.6980, 1.0472]$ and $[-0.0461, 0.0461]$ radians, respectively. Moreover, the input delay margin from the proposed approach is computed to be 0.1066 seconds. To that end, the proposed approach provides less conservative and accurate gain and phase margins within which the multi-agent system remains stable and achieves consensus, compared to disk-based gain and phase margins.

6.4.2 Example 2

In order to test the methodology for the delay margin, we consider the example presented in [106,115]. Consider a multi-agent system with following system matrices

$$\mathbf{A} = \begin{bmatrix} 0.2 & 0 & 0 \\ 0 & 0 & 1 \\ 1 & -1 & 0 \end{bmatrix}, \qquad \mathbf{B} = \begin{bmatrix} 1 & 0 \\ 0 & 1 \\ 1 & 0 \end{bmatrix}, \tag{6.69}$$

and the state feedback controller given by

$$\mathbf{K} = -\begin{bmatrix} -0.2694 & 0.0402 & -0.0899 \\ 0.0386 & -0.2857 & -0.1238 \end{bmatrix}. \tag{6.70}$$

A group of five agents is considered with following graph Laplacian matrix

$$\mathbf{L} = \begin{bmatrix} 2 & -1 & 0 & 0 & -1 \\ -1 & 2 & -1 & 0 & 0 \\ 0 & -1 & 2 & -1 & 0 \\ 0 & 0 & -1 & 2 & -1 \\ -1 & 0 & 0 & -1 & 2 \end{bmatrix}. \tag{6.71}$$

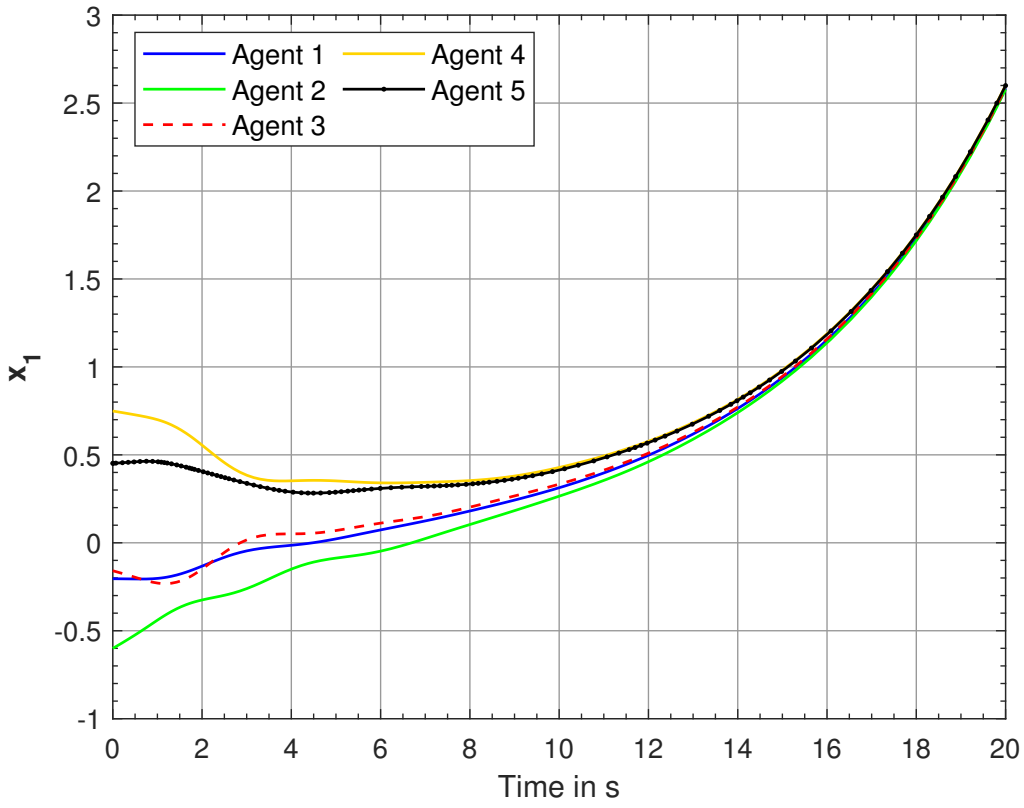

Figure 6.4: State (x_1) trajectories of agents with $\tau = 0.61$ seconds

The results are summarized as follows:

(i) By applying Theorem 6.3.10, we obtain the delay margin to be $\tau^* = 0.62$ seconds. This is almost 1.7 times the value of 0.35 seconds reported in [115]. To verify the accuracy of the obtained delay margin, we present simulation results with $\tau = 0.61$ seconds in Figs. 6.4 and 6.5. The framework provided in [115] uses Lyapunov-Krasovskii approach and the delay margin is obtained as the solution of a linear matrix inequality which results in a conservative delay margin.

(ii) For the multi-agent system in consideration, the delay margin of 0.901 seconds is reported in [106]. The framework presented in [106] uses cluster treatment

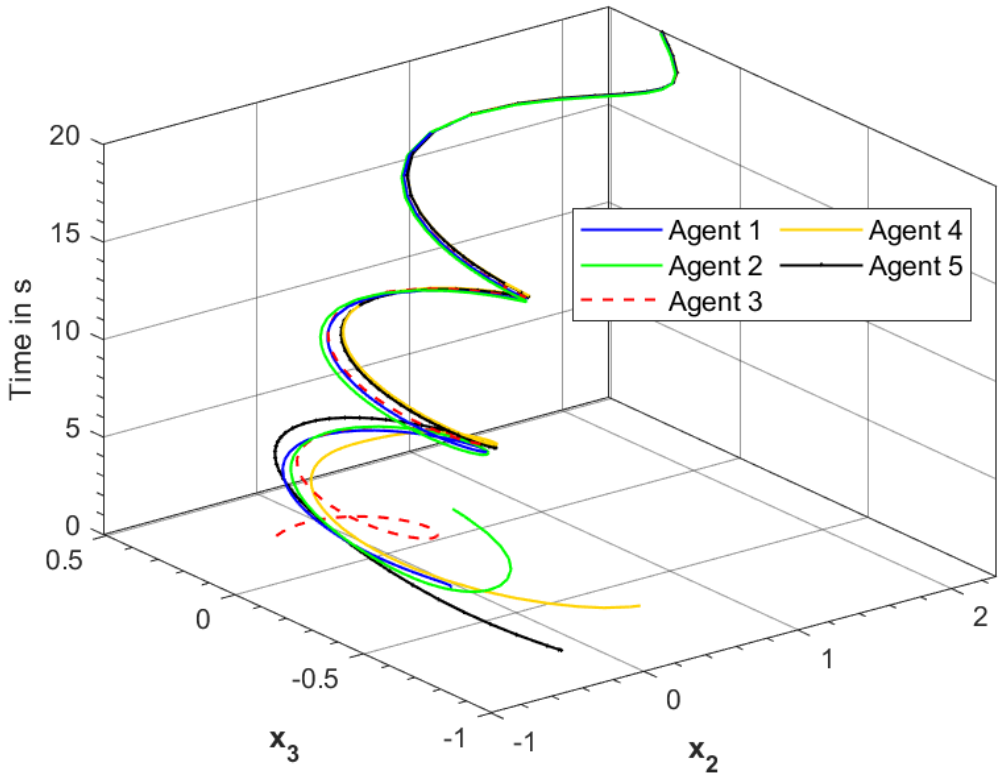

Figure 6.5: State (x_2 and x_3) trajectories of agents with $\tau = 0.61$ seconds

of characteristic roots which provides exact delay margin. Although the result obtained from the proposed methodology in this work is more conservative than that presented in [106], it should be noted that, the approach in [106] is only suitable for the multi-agent systems in an undirected graph topology (with symmetric graph Laplacian matrix). On the other hand, the framework to compute delay margin proposed in this work is applicable to multi-agent systems in both directed (see Example 1) and undirected graph topology. In addition to that, we provide a unified framework to compute gain margin, phase margin and input delay margin of multi-agent systems.

6.5 Chapter Summary

In this chapter, we have studied the stability of the multi-agent system under gain, phase, and input delay perturbations where each agent in the graph-based interconnection network is a linear time-invariant multi-input multi-output system. Based on the consensus protocol under a static graph communication topology, we provide a computational strategy to compute the gain, phase and input delay margins for multi-agent systems using the approach of multiplicative perturbation. Conditions for the gain, phase and delay independent stability of multi-agent system are discussed. To illustrate the effectiveness of the proposed framework, a numerical example with various graph structures was presented which depicted the lower conservativeness of the proposed approach as compared to disk-based gain and phase margins.

Chapter 7

Delay Margin for Linear Multi-Agent Systems With Non-Uniform Time-Varying Communication Delays

In this chapter we study the consensus problem of high-order linear multi-agent systems subject to non-uniform time-varying delays. We first design a distributed control protocol for the agents in directed graph topology and provide an equivalent stability problem to be solved that guarantees the state consensus in the group of agents. Next, a delay-dependent consensus criterion is provided in the form of a matrix inequality by exploiting the Lyapunov-Krasovskii approach. The solution to the matrix inequality provides the upper bound of the multiple delays that ensure the consensus in the multi-agent system. The obtained theoretical result is then applied to achieve synchronization in the angle of attack and pitch rate of multiple F-16 VISTA aircraft subject to time-varying non-uniform delays.

The chapter is organized as follows. Section 7.1 describes the preliminaries and formulates the problem in consideration. Section 7.2 discusses the control protocol for multi-agent systems with non-uniform time-varying delays. The main results concerning the delay-margin characterization for the multi-agent system are presented in Section 7.3. A numerical example is presented in Section 7.4 and Section 7.5 provides the concluding remarks.

7.1 Preliminaries and Problem Formulation

7.1.1 Preliminaries

Lemma 7.1.1. *[179] For any constant matrix $\mathbb{X} \in \mathbb{R}^{n\times n}$, $\mathbb{X} = \mathbb{X}^T > 0$, a scalar $\gamma > 0$, and a vector function $\dot{\mathbf{z}} : [-\gamma, 0] \to \mathbb{R}^n$, following integral inequality holds*

$$-\gamma \int_{t-\gamma}^{t} \dot{\mathbf{z}}(t+\theta)^T \mathbb{X} \dot{\mathbf{z}}(t+\theta) d\theta \;\leq \begin{bmatrix} \mathbf{z}(t) \\ \mathbf{z}(t-\gamma) \end{bmatrix}^T \begin{bmatrix} -\mathbb{X} & \mathbb{X} \\ * & -\mathbb{X} \end{bmatrix} \begin{bmatrix} \mathbf{z}(t) \\ \mathbf{z}(t-\gamma) \end{bmatrix}. \tag{7.1}$$

Lemma 7.1.2. *[180] For any constant matrix $\mathbb{Y} \in \mathbb{R}^{n\times n}$, $\mathbb{Y} = \mathbb{Y}^T > 0$, scalars $h_1 \leq \tau(t) \leq h_2$ and a vector function $\dot{\mathbf{z}} : [-h_2, -h_1] \to \mathbb{R}^n$, following integral inequality holds*

$$-\big(h_2 - h_1\big) \int_{t-h_2}^{t-h_1} \dot{\mathbf{z}}^T(s)\ \mathbb{Y}\ \dot{\mathbf{z}}(s)\ ds \leq \begin{bmatrix} \mathbf{z}\,(t-h_1) \\ \mathbf{z}(t-\tau(t)) \\ \mathbf{z}\,(t-h_2) \end{bmatrix}^T \begin{bmatrix} -\mathbb{Y} & \mathbb{Y} & \mathbf{0} \\ * & -2\mathbb{Y} & \mathbb{Y} \\ * & * & \mathbb{Y} \end{bmatrix} \begin{bmatrix} \mathbf{z}\,(t-h_1) \\ \mathbf{z}(t-\tau(t)) \\ \mathbf{z}\,(t-h_2) \end{bmatrix}. \tag{7.2}$$

Lemma 7.1.3. *(Lyapunov-Krasovskii Stability Theorem) [168] Consider the following time-delay system*

$$\begin{aligned} \dot{x}(t) &= f\left(t, x(t)\right),\ \forall t \geq t_0 \\ x(t_0+\theta) &= \phi(\theta),\ \theta \in [-h, 0] \end{aligned} \tag{7.3}$$

where $f : \mathbb{R} \in \mathcal{C}([-h,0],\mathbb{R}^n) \to \mathbb{R}^n$ is continuous and is bounded for all bounded values of its arguments, $h > 0$ is the delay, and $\phi \in \mathcal{C}([-h,0],\mathbb{R}^n)$ is the functional of initial conditions. Assume $f(t,0) = 0$ such that (7.3) has a trivial solution $x(t) = 0$. Let u, v, and $w : \mathbb{R}_+ \to \mathbb{R}_+$ be continuous and increasing functions such that $u(\theta)$ and $v(\theta)$ are strictly positive for all $\theta > 0$, and $u(0) = v(0) = 0$. If there exists a continuous and differentiable functional $V : \mathbb{R} \times \mathcal{C}([-h,0],\mathbb{R}^n) \to \mathbb{R}_+$ such that :

a) $u(\|\phi(0)\|) \leq V(t,\phi) \leq v(\|\phi\|_c)$,

b) $\dot{V}(t,\phi) \leq -w(\|\phi(0)\|)$.

Then the trivial solution $x(t) = 0$ *is uniformly stable. If* $w(\theta) > 0$ *for* $\theta > 0$*, the the trivial solution is uniformly asymptotically stable. In addition, if* $\lim_{\theta\to\infty} u(\theta) = \infty$*, then the trivial solution is globally uniformly asymptotically stable.*

7.1.2 Problem Formulation

Let us consider a multi-agent system comprising of N agents with identical dynamics. The dynamics of the ith agent is considered to be as follows:

$$\dot{\mathbf{x}}_i(t) = \mathbf{A}\mathbf{x}_i(t) + \mathbf{B}\mathbf{u}_i(t), \qquad i = 1, \ldots, N \tag{7.4}$$

where $\mathbf{A} \in \mathbb{R}^{n\times n}$ and $\mathbf{B} \in \mathbb{R}^{n\times m}$ are the system matrices with $\mathbf{x}_i \in \mathbb{R}^n$ as the state and $\mathbf{u}_i \in \mathbb{R}^m$ as the input of the ith agent.

Assumption 7.1.1. $(\mathbf{A}, \mathbf{B})$ *is stabilizable.*

It is assumed that the agents share the state information among each other in a predefined graph topology. The graph theoretical framework-based multi-agent system's modeling is such that, each node in the graph represents the agents and the edge connecting the two neighboring nodes represent the communication between the agents. In this work, we make following assumption on the underlying graph topology.

Assumption 7.1.2. *Throughout the chapter, the graph is assumed to be connected with at least one directed spanning tree.*

The objective of this chapter is to design a distributed consensus control protocol for the multi-agent system in (7.4) subject to *non-uniform time-varying delays*. For clarity, we define *non-uniform delays* in the context of multi-agent systems as follows.

Definition 7.1.1. *(Non-uniform delays)*

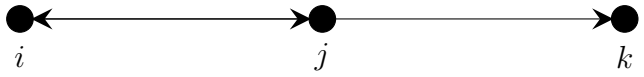

Figure 7.1: Communication graph

Consider a multi-agent system of three agents (i, j and k) with a graph topology as shown in Fig. 7.1. Let τ_{ij}, τ_{ji} and τ_{jk} be the delays in sharing the state information from agent i to j, j to i and j to k, respectively. The delays in sharing the state information among the agents with the underlying graph topology in Fig. 7.1 are said to be non-uniform if $\tau_{ij} \neq \tau_{ji} \neq \tau_{jk}$.

7.2 Distributed Control Protocol

With Assumption 7.1.1, let each of the agents $i = 1, \ldots, N$ have identical feedback controller $\mathbf{K} \in \mathbb{R}^{m \times n}$ such that $\mathbf{A} - \mathbf{BK}$ is Hurwitz. We consider following distributed control protocol based on the relative states between neighboring agents:

$$\mathbf{u}_i(t) = c\mathbf{K}\left[\sum_{j \in \mathcal{N}_i} a_{ij}(\mathbf{x}_j(t - \tau_{ij}(t)) - \mathbf{x}_i(t - \tau_{ij}(t))\right] \tag{7.5}$$

where $\tau_{ij}(t)$ is the time-delay in the communication between agents i and j and $c > 0$ is the coupling gain. Let $\mathbf{L} \in \mathbb{R}^{N \times N}$ be the Laplacian matrix associated with the underlying graph topology between the agents. In (7.5), the value of c is chosen such that the consensus among the agents is achieved for delay-free multi-agent system, i.e. $\mathbf{A} - c\lambda_p\mathbf{BK}$ for $p = 2, 3, \ldots, N$ are Hurwitz, where λ_p are the eigenvalues of the Laplacian matrix. In this chapter, we select c based on the consensus region approach discussed in [162].

We assume the time delay $\tau_{ij}(t)$ and the delay derivatives $\dot{\tau}_{ij}(t)$ to be bounded for all $i, j = 1, \ldots, N$ and for all $t > 0$ such that $\tau_{ij}(t) \leq \bar{\tau}_{ij}$, and $\dot{\tau}_{ij}(t) \leq \mu_{ij} < 1$. Moreover, in reference to the Definition 7.1.1, the time delay is dependent on the

direction of the information flow, i.e, $\tau_{ij} \neq \tau_{ji}$. Therefore, a unique time-delay is associated with each edge in the graph. Let $r \leq N(N-1)$ be the total number of edges in the graph and $\tau_k(t)$, $k = 1, \ldots r$ be the delay associated with the kth edge. Let $\mathbf{L}_k \in \mathbb{R}^N$ be the Laplacian matrix of the subgraph associated with the time delay τ_k such that $\mathbf{L} = \sum_{k=1}^{r} \mathbf{L}_k$. In order to compute the single index k for time-delay τ_{ij} with double indices, Procedure 4 is used.

Procedure 4 Computation of k

1: **Initialize:** $k = 0$
2: **for** $i = \{1, 2, \ldots, N\}$ **do**
3: **for** $j \in \mathcal{N}_i$ **do**
4: $k = k + 1$
5: $\tau_k = \tau_{ij}$
6: **end for**
7: **end for**

Now, with the distributed control protocol in (7.5), the closed-loop dynamics of agent i, for all $i = 1, \ldots, N$ can be written as

$$\dot{\mathbf{x}}_i(t) = \mathbf{A}\mathbf{x}_i(t) + c\mathbf{B}\mathbf{K}\left[\sum_{j\in\mathcal{N}_i} a_{ij}(\mathbf{x}_j(t-\tau_{ij}(t)) - \mathbf{x}_i(t-\tau_{ij}(t))\right] \tag{7.6}$$

Denote $\mathbf{x} = \text{col}(\mathbf{x}_1, \mathbf{x}_2, \ldots, \mathbf{x}_N) \in \mathbb{R}^{Nn}$ as the global state vector. Now the global state dynamics can be written as

$$\dot{\mathbf{x}}(t) = (\mathbf{I}_N \otimes \mathbf{A})\,\mathbf{x}(t) - \sum_{k=1}^{r} (\mathbf{L}_k \otimes \mathbf{B}\mathbf{K})\,\mathbf{x}(t-\tau_k(t)). \tag{7.7}$$

7.3 Main Results

This section provides the delay-dependent stability conditions for the consensus in the multi-agent system in (7.7). In order to derive the stability conditions, the consensus problem is transformed to an equivalent stability problem using the following Lemma.

Lemma 7.3.1. *Suppose the graph topology of N agents satisfy Assumption 7.1.2. Then, the multi-agent system in* (7.7) *reaches consensus asymptotically if the following equivalent system is asymptotically stable*

$$\dot{\mathbf{z}}(t) = (\mathbf{I}_{N-1} \otimes \mathbf{A})\, \mathbf{z}(t) - \sum_{k=1}^{r} \left(\bar{\mathbf{L}}_k \otimes \mathbf{BK}\right) \mathbf{z}\left(t - \tau_k(t)\right) \tag{7.8}$$

where $\mathbf{z} = col(\mathbf{z}_1, \mathbf{z}_2, \ldots, \mathbf{z}_{N-1}) \in \mathbb{R}^{(N-1)n}$ *is the global consensus error such that* $\mathbf{z}_i = \mathbf{x}_1 - \mathbf{x}_{i+1} \in \mathbb{R}^n$, *(*$i = 1, \cdots, N-1$*). Moreover,* $\bar{\mathbf{L}}_k = c\mathbf{U}\mathbf{L}_k\mathbf{W} \in \mathbb{R}^{(N-1)\times(N-1)}$ *with* $\mathbf{U} = \begin{bmatrix} \mathbf{1}_{N-1} & -\mathbf{I}_{N-1} \end{bmatrix} \in \mathbb{R}^{(N-1)\times N}$, *and* $\mathbf{W} = \begin{bmatrix} \mathbf{0}_{N-1}^T \\ -\mathbf{I}_{N-1} \end{bmatrix} \in \mathbb{R}^{N\times(N-1)}$.

Proof. Since $\mathbf{z}_i = \mathbf{x}_1 - \mathbf{x}_{i+1}$, $(i = 1, \cdots, N-1)$. $\mathbf{z} = \mathrm{col}(\mathbf{z}_1, \mathbf{z}_2, \ldots, \mathbf{z}_N)$, and $\mathbf{U} = \begin{bmatrix} \mathbf{1}_{N-1} & -\mathbf{I}_{N-1} \end{bmatrix}$, one can write

$$\mathbf{z}(t) = (\mathbf{U} \otimes \mathbf{I}_n)\, \mathbf{x}(t). \tag{7.9}$$

Also with $\mathbf{W} = \begin{bmatrix} \mathbf{0}_{N-1}^{\mathrm{T}} \\ -\mathbf{I}_{N-1} \end{bmatrix}$, we have $\mathbf{UW} = \mathbf{I}_{N-1}$; therefore, the global state vector of the multi-agent system in (7.7) can be written as $\mathbf{x}(t) = (\mathbf{W} \otimes \mathbf{I}_n)\, \mathbf{z}(t)$. Differentiating (7.9) with respect to time, we obtain

$$\dot{\mathbf{z}}(t) = (\mathbf{U} \otimes \mathbf{I}_n) \left[(\mathbf{I}_N \otimes \mathbf{A})\, (\mathbf{W} \otimes \mathbf{I}_n)\, \mathbf{z}(t) - \sum_{k=1}^{r} c\, (\mathbf{L}_k \otimes \mathbf{BK})\, (\mathbf{W} \otimes \mathbf{I}_n)\, \mathbf{z}(t - \tau_k) \right] \tag{7.10}$$

Using the Kronecker identities, (7.10) can be rewritten as

$$\dot{\mathbf{z}}(t) = (\mathbf{UW} \otimes \mathbf{A})\, \mathbf{z}(t) - \sum_{k=1}^{r} \left[c\, (\mathbf{U}\mathbf{L}_k\mathbf{W}) \otimes \mathbf{BK}\right] \mathbf{z}(t - \tau_k) \tag{7.11}$$

With $\mathbf{UW} = \mathbf{I}_{N-1}$ and $\bar{\mathbf{L}}_k = c\mathbf{U}\mathbf{L}_k\mathbf{W}$, we obtain (7.8). Note that, as $\mathbf{z}(t) \to 0$, $\mathbf{x}_i \to \mathbf{x}_1$, $i = 2, \ldots, N$. □

In order to derive the delay-dependent stability conditions of the consensus error system in (7.8), we introduce Theorem 7.3.2 using the Lyapunov-Krasovskii approach. For notational simplicity, we denote identity matrix $\mathbf{I}_{N-1}$ with $\mathbf{I}$.

Theorem 7.3.2. *Suppose the graph topology of N agents satisfy Assumption 7.1.2. Then, the multi-agent system in* (7.7) *reaches consensus asymptotically for any $\tau_k(t)$ satisfying $\tau_k(t) \leq \bar{\tau}_k$, and $\dot{\tau}_k(t) \leq \mu_k < 1$ $(k = 1, \ldots, r)$ if there exists $\mathbf{P} = \mathbf{P}^T > 0 \in \mathbb{R}^{n\times n}$, $\mathbf{Q}_k = \mathbf{Q}_k^T > 0 \in \mathbb{R}^{n\times n}$, $\mathbf{R}_k = \mathbf{R}_k^T > 0 \in \mathbb{R}^{n\times n}$, $k = 1, \ldots, r$ and $\mathbf{S}_{kj} = \mathbf{S}_{kj}^T > 0 \in \mathbb{R}^{n\times n}$, $k = 1, \ldots, r-1$, $j = k+1, k+2, \ldots, r$ such that the following matrix inequality holds*

$$\mathbf{\Pi} + \boldsymbol{\xi}^T \mathbf{\Gamma} \boldsymbol{\xi} < 0 \tag{7.12}$$

where $\mathbf{\Pi} \in \mathbb{R}^{(N-1)n(1+2r)\times(N-1)n(1+2r)}$ is defined as

$$\mathbf{\Pi} = \begin{bmatrix} \mathbf{\Pi}_{1,1} & \mathbf{\Pi}_{1,2} & \mathbf{0} & \mathbf{\Pi}_{1,4} & \mathbf{0} & \cdots & \mathbf{\Pi}_{1,2r} & \mathbf{0} \\ * & \mathbf{\Pi}_{2,2} & \mathbf{I}\otimes\mathbf{R}_1 & \mathbf{I}\otimes\mathbf{S}_{12} & \mathbf{0} & \cdots & \mathbf{I}\otimes\mathbf{S}_{1r} & \mathbf{0} \\ * & * & -\mathbf{I}\otimes\mathbf{R}_1 & \mathbf{0} & \mathbf{0} & \cdots & \mathbf{0} & \mathbf{0} \\ * & * & * & \mathbf{\Pi}_{4,4} & \mathbf{I}\otimes\mathbf{R}_2 & \cdots & \mathbf{I}\otimes\mathbf{S}_{2r} & \mathbf{0} \\ * & * & * & * & -\mathbf{I}\otimes\mathbf{R}_2 & \cdots & \mathbf{0} & \mathbf{0} \\ \vdots & \vdots & \vdots & \vdots & \vdots & \vdots & \vdots & \vdots \\ * & * & * & * & * & \cdots & \mathbf{\Pi}_{2k,2k} & \mathbf{I}\otimes\mathbf{R}_r \\ * & * & * & * & * & \cdots & * & -\mathbf{I}\otimes\mathbf{R}_r \end{bmatrix}. \tag{7.13}$$

such that

$$
\begin{aligned}
\mathbf{\Pi}_{1,1} &= \mathbf{I} \otimes \left[\mathbf{A}^T\mathbf{P} + \mathbf{P}\mathbf{A} + \sum_{k=1}^{r} \left(\mathbf{Q}_k - \mathbf{R}_k \right) \right], \\
\mathbf{\Pi}_{1,2k} &= \left(\mathbf{I} \otimes \mathbf{R}_k \right) - \left(\bar{\mathbf{L}}_k \otimes \mathbf{P}\mathbf{B}\mathbf{K} \right), \\
\mathbf{\Pi}_{2k,2k} &= -\mathbf{I} \otimes \left[\alpha_k \mathbf{Q}_k + 2\mathbf{R}_k + \sum_{j=1}^{k-1} \mathbf{S}_{jk} + \sum_{j=k+1}^{r} \mathbf{S}_{kj} \right] \\
\alpha_k &= 1 - \mu_k.
\end{aligned}
\tag{7.14}
$$

Moreover, the matrices $\mathbf{\Gamma} \in \mathbb{R}^{n(N-1)\times n(N-1)}$ *and* $\boldsymbol{\xi} \in \mathbb{R}^{n(N-1)\times(N-1)n(1+2r)}$ *are defined as follows*

$$
\begin{aligned}
\mathbf{\Gamma} &= \mathbf{I} \otimes \left[\sum_{k=1}^{r} \bar{\tau}_k^2 \mathbf{R}_k + \sum_{k=1}^{r-1} \sum_{j=k+1}^{r} \left(\bar{\tau}_k - \bar{\tau}_j \right)^2 \mathbf{S}_{kj} \right] \\
\boldsymbol{\xi} &= \begin{bmatrix} (\mathbf{I} \otimes \mathbf{A}) & -(\bar{\mathbf{L}}_1 \otimes \mathbf{B}\mathbf{K}) & \mathbf{0} & \cdots & -(\bar{\mathbf{L}}_r \otimes \mathbf{B}\mathbf{K}) & \mathbf{0} \end{bmatrix}.
\end{aligned}
\tag{7.15}
$$

Proof. Let us consider the following Lyapunov-Krasovskii functional

$$
V\left(\mathbf{z}_t, t \right) = V_1\left(\mathbf{z}_t, t \right) + V_2\left(\mathbf{z}_t, t \right) + V_3\left(\mathbf{z}_t, t \right) + V_4\left(\mathbf{z}_t, t \right) \tag{7.16}
$$

such that

$$
\begin{aligned}
V_1\left(\mathbf{z}_t, t \right) &= \mathbf{z}^{\mathrm{T}}(t) \left(\mathbf{I} \otimes \mathbf{P} \right) \mathbf{z}(t), \\
V_2\left(\mathbf{z}_t, t \right) &= \sum_{k=1}^{r} \left[\int_{t-\tau_k(t)}^{t} \mathbf{z}^{\mathrm{T}}(s) \left(\mathbf{I} \otimes \mathbf{Q}_k \right) \mathbf{z}(s) ds \right], \\
V_3\left(\mathbf{z}_t, t \right) &= \sum_{k=1}^{r} \left[\bar{\tau}_k \int_{-\bar{\tau}_k}^{0} \int_{t+\theta}^{t} \dot{\mathbf{z}}^{\mathrm{T}}(s) \left(\mathbf{I} \otimes \mathbf{R}_k \right) \dot{\mathbf{z}}(s) ds d\theta \right], \\
V_4\left(\mathbf{z}_t, t \right) &= \sum_{k=1}^{r-1} \sum_{j=k+1}^{r} \left[\left(\bar{\tau}_k - \bar{\tau}_j \right) \int_{-\bar{\tau}_k}^{-\bar{\tau}_j} \int_{t+\theta}^{t} \dot{\mathbf{z}}^{\mathrm{T}}(s) \left(\mathbf{I} \otimes \mathbf{S}_{kj} \right) \dot{\mathbf{z}}(s) ds d\theta \right]
\end{aligned}
\tag{7.17}
$$

where $\mathbf{z}_t = \mathbf{z}(t)$, $\mathbf{P} = \mathbf{P}^{\mathrm{T}} > 0 \in \mathbb{R}^{n\times n}$, $\mathbf{Q}_k = \mathbf{Q}_k^{\mathrm{T}} > 0 \in \mathbb{R}^{n\times n}$, $\mathbf{R}_k = \mathbf{R}_k^{\mathrm{T}} > 0 \in \mathbb{R}^{n\times n}$, $k = 1, \ldots, r$ and $\mathbf{S}_{kj} = \mathbf{S}_{kj}^{\mathrm{T}} > 0 \in \mathbb{R}^{n\times n}$, $k = 1, \ldots, r-1$, $j = k+1, k+2, \ldots, r$. It can be easily verified that, the given Lyapunov-Krasovskii functional satisfies condition (a) in Lemma 7.1.3. The time-derivative of the components of the Lyapunov-Krasovskii functional along the trajectory of (7.8) can be written as

$$
\begin{aligned}
\dot{V}_1(\mathbf{z}_t,t) &= 2\mathbf{z}^{\mathrm{T}}(t)\left(\mathbf{I}\otimes\mathbf{P}\right)\left[\left(\mathbf{I}\otimes\mathbf{A}\right)\mathbf{z}(t)-\sum_{k=1}^{r}\left(\bar{\mathbf{L}}_k\otimes\mathbf{BK}\right)\mathbf{z}\left(t-\tau_k(t)\right)\right]\\
\dot{V}_2(\mathbf{z}_t,t) &= \sum_{k=1}^{r}\left[\mathbf{z}^{\mathrm{T}}(t)\left(\mathbf{I}\otimes\mathbf{Q}_k\right)\mathbf{z}(t)-\left(1-\dot{\tau}_k(t)\right)\mathbf{z}^{\mathrm{T}}\left(t-\tau_k(t)\right)\left(\mathbf{I}\otimes\mathbf{Q}_k\right)\mathbf{z}\left(t-\tau_k(t)\right)\right]\\
\dot{V}_3(\mathbf{z}_t,t) &= \sum_{k=1}^{r}\left[\bar{\tau}_k\int_{t-\bar{\tau}_k}^{t}\dot{\mathbf{z}}^{\mathrm{T}}(t)\left(\mathbf{I}\otimes\mathbf{R}_k\right)\dot{\mathbf{z}}(t)d\theta\right]\\
&\quad-\sum_{k=1}^{r}\left[\bar{\tau}_k\int_{t-\bar{\tau}_k}^{t}\dot{\mathbf{z}}^{\mathrm{T}}(t+\theta)\left(\mathbf{I}\otimes\mathbf{R}_k\right)\dot{\mathbf{z}}(t+\theta)d\theta\right]\\
&= \dot{\mathbf{z}}^{\mathrm{T}}(t)\left[\sum_{k=1}^{r}\bar{\tau}_k^2\left(\mathbf{I}\otimes\mathbf{R}_k\right)\right]\dot{\mathbf{z}}(t)-\sum_{k=1}^{r}\left[\bar{\tau}_k\int_{t-\bar{\tau}_k}^{t}\dot{\mathbf{z}}^{\mathrm{T}}(t+\theta)\left(\mathbf{I}\otimes\mathbf{R}_k\right)\dot{\mathbf{z}}(t+\theta)d\theta\right]\\
\dot{V}_4(\mathbf{z}_t,t) &= \sum_{k=1}^{r-1}\sum_{j=k+1}^{r}\left[\left(\bar{\tau}_k-\bar{\tau}_j\right)\int_{t-\bar{\tau}_k}^{t-\bar{\tau}_j}\dot{\mathbf{z}}^{\mathrm{T}}(t)\left(\mathbf{I}\otimes\mathbf{S}_{kj}\right)\dot{\mathbf{z}}(t)d\theta\right]\\
&\quad-\sum_{k=1}^{r-1}\sum_{j=k+1}^{r}\left[\left(\bar{\tau}_k-\bar{\tau}_j\right)\int_{t-\bar{\tau}_k}^{t-\bar{\tau}_j}\dot{\mathbf{z}}^{\mathrm{T}}(t+\theta)\left(\mathbf{I}\otimes\mathbf{S}_{kj}\right)\dot{\mathbf{z}}(t+\theta)d\theta\right]\\
&= \dot{\mathbf{z}}^{\mathrm{T}}(t)\sum_{k=1}^{r-1}\sum_{j=k+1}^{r}\left[\left(\bar{\tau}_k-\bar{\tau}_j\right)^2\left(\mathbf{I}\otimes\mathbf{S}_{kj}\right)\right]\dot{\mathbf{z}}(t)\\
&\quad-\sum_{k=1}^{r-1}\sum_{j=k+1}^{r}\left[\left(\bar{\tau}_k-\bar{\tau}_j\right)\int_{t-\bar{\tau}_k}^{t-\bar{\tau}_j}\dot{\mathbf{z}}^{\mathrm{T}}(t+\theta)\left(\mathbf{I}\otimes\mathbf{S}_{kj}\right)\dot{\mathbf{z}}(t+\theta)d\theta\right]
\end{aligned}
\tag{7.18}
$$

With $\mathbf{\Gamma}$ as defined in (7.15), the derivative of the Lyapunov-Krasovskii functional can be written as

$$
\begin{aligned}
\dot{V}(\mathbf{z}_t,t) &= 2\mathbf{z}^{\mathrm{T}}(t)\left(\mathbf{I}\otimes\mathbf{P}\right)\left[\left(\mathbf{I}\otimes\mathbf{A}\right)\mathbf{z}(t)-\sum_{k=1}^{r}\left(\bar{\mathbf{L}}_k\otimes\mathbf{BK}\right)\mathbf{z}\left(t-\tau_k(t)\right)\right]\\
&\quad+\sum_{k=1}^{r}\left[\mathbf{z}^{\mathrm{T}}(t)\left(\mathbf{I}\otimes\mathbf{Q}_k\right)\mathbf{z}(t)-\left(1-\dot{\tau}_k(t)\right)\mathbf{z}^{\mathrm{T}}\left(t-\tau_k(t)\right)\left(\mathbf{I}\otimes\mathbf{Q}_k\right)\mathbf{z}\left(t-\tau_k(t)\right)\right]\\
&\quad+\dot{\mathbf{z}}^{\mathrm{T}}(t)\mathbf{\Gamma}\dot{\mathbf{z}}(t)-\sum_{k=1}^{r}\left[\bar{\tau}_k\int_{t-\bar{\tau}_k}^{t}\dot{\mathbf{z}}^{\mathrm{T}}(t+\theta)\left(\mathbf{I}\otimes\mathbf{R}_k\right)\dot{\mathbf{z}}(t+\theta)d\theta\right]\\
&\quad-\sum_{k=1}^{r-1}\sum_{j=k+1}^{r}\left[\left(\bar{\tau}_k-\bar{\tau}_j\right)\int_{t-\bar{\tau}_k}^{t-\bar{\tau}_j}\dot{\mathbf{z}}^{\mathrm{T}}(t+\theta)\left(\mathbf{I}\otimes\mathbf{S}_{kj}\right)\dot{\mathbf{z}}(t+\theta)d\theta\right].
\end{aligned}
\tag{7.19}
$$

Since the delays and the delay derivatives are assumed to be bounded such that $\tau_k(t) \leq \bar{\tau}_k$ for all t and k, $\dot{\tau}_k(t) \leq \mu_k < 1$, for all k, the derivative of the Lyapunov-Krasovskii functional in (7.19) can be recast as following inequality

$$\begin{aligned}\dot{V}\left(\mathbf{z}_t, t\right) \leq 2\mathbf{z}^{\mathrm{T}}(t)\left(\mathbf{I}\otimes\mathbf{P}\right)\Bigg[\left(\mathbf{I}\otimes\mathbf{A}\right)\mathbf{z}(t) - \sum_{k=1}^{r}\left(\bar{\mathbf{L}}_k\otimes\mathbf{BK}\right)\mathbf{z}\left(t-\tau_k(t)\right)\Bigg] \\ + \sum_{k=1}^{r}\Bigg[\mathbf{z}^{\mathrm{T}}(t)\left(\mathbf{I}\otimes\mathbf{Q}_k\right)\mathbf{z}(t) - \alpha_k\mathbf{z}^{\mathrm{T}}\left(t-\tau_k(t)\right)\left(\mathbf{I}\otimes\mathbf{Q}_k\right)\mathbf{z}\left(t-\tau_k(t)\right)\Bigg] \\ + \dot{\mathbf{z}}^{\mathrm{T}}(t)\mathbf{\Gamma}\dot{\mathbf{z}}(t) - \sum_{k=1}^{r}\Bigg[\bar{\tau}_k\int_{t-\bar{\tau}_k}^{t}\dot{\mathbf{z}}^{\mathrm{T}}(t+\theta)\left(\mathbf{I}\otimes\mathbf{R}_k\right)\dot{\mathbf{z}}(t+\theta)d\theta\Bigg] \\ - \sum_{k=1}^{r-1}\sum_{j=k+1}^{r}\Bigg[\left(\tau_k(t)-\tau_j(t)\right)\int_{t-\tau_k(t)}^{t-\tau_j(t)}\dot{\mathbf{z}}^{\mathrm{T}}(t+\theta)\left(\mathbf{I}\otimes\mathbf{S}_{kj}\right)\dot{\mathbf{z}}(t+\theta)d\theta\Bigg].\end{aligned} \tag{7.20}$$

Further, using Kronecker identities, we can express the derivative of the Lyapunov-Krasovskii functional as

$$\begin{aligned}\dot{V}\left(\mathbf{z}_t, t\right) \leq \mathbf{z}^{\mathrm{T}}(t)\Bigg[\mathbf{I}\otimes\left(\mathbf{PA}+\mathbf{A}^{\mathrm{T}}\mathbf{P}+\sum_{k=1}^{r}\mathbf{Q}_k\right)\Bigg]\mathbf{z}(t) - 2\mathbf{z}^{\mathrm{T}}(t)\Bigg[\sum_{k=1}^{r}\left(\bar{\mathbf{L}}_k\otimes\mathbf{PBK}\right) \\ \mathbf{z}\left(t-\tau_k(t)\right)\Bigg] - \sum_{k=1}^{r}\Bigg[\mathbf{z}^{\mathrm{T}}\left(t-\tau_k(t)\right)\left(\mathbf{I}\otimes\alpha_k\mathbf{Q}_k\right)\mathbf{z}\left(t-\tau_k(t)\right)\Bigg] + \dot{\mathbf{z}}^{\mathrm{T}}(t)\mathbf{\Gamma}\dot{\mathbf{z}}(t) \\ - \sum_{k=1}^{r}\Bigg[\bar{\tau}_k\int_{t-\bar{\tau}_k}^{t}\dot{\mathbf{z}}^{\mathrm{T}}(t+\theta)\left(\mathbf{I}\otimes\mathbf{R}_k\right)\dot{\mathbf{z}}(t+\theta)d\theta\Bigg] \\ - \sum_{k=1}^{r-1}\sum_{j=k+1}^{r}\Bigg[\left(\tau_k(t)-\tau_j(t)\right)\int_{t-\tau_k(t)}^{t-\tau_j(t)}\dot{\mathbf{z}}^{\mathrm{T}}(t+\theta)\left(\mathbf{I}\otimes\mathbf{S}_{kj}\right)\dot{\mathbf{z}}(t+\theta)d\theta\Bigg].\end{aligned} \tag{7.21}$$

Using (7.8), $\dot{\mathbf{z}}^{\mathrm{T}}(t)\mathbf{\Gamma}\dot{\mathbf{z}}(t)$ in (7.21) can be written as

$$\begin{aligned}\dot{\mathbf{z}}^{\mathrm{T}}(t)\mathbf{\Gamma}\dot{\mathbf{z}}(t) = \mathbf{z}^{\mathrm{T}}(t)(\mathbf{I}\otimes\mathbf{A})^{\mathrm{T}}\mathbf{\Gamma}(\mathbf{I}\otimes\mathbf{A})\mathbf{z}(t) - \mathbf{z}^{\mathrm{T}}(t)(\mathbf{I}\otimes\mathbf{A})^{\mathrm{T}}\sum_{k=1}^{r}\Bigg[\left(\bar{\mathbf{L}}_k\otimes\mathbf{BK}\right) \\ \mathbf{z}\left(t-\tau_k(t)\right)\Bigg] - \sum_{k=1}^{r}\Bigg[\mathbf{z}^{\mathrm{T}}(t-\tau_k)\left(\bar{\mathbf{L}}_k\otimes\mathbf{BK}\right)^{\mathrm{T}}\Bigg]\ \mathbf{\Gamma}\ (\mathbf{I}\otimes\mathbf{A})\mathbf{z}(t) \\ + \sum_{k=1}^{r}\Bigg[\mathbf{z}^{\mathrm{T}}(t-\tau_k)\left(\bar{\mathbf{L}}_k\otimes\mathbf{BK}\right)^{\mathrm{T}}\Bigg]\mathbf{\Gamma}\sum_{k=1}^{r}\Bigg[\left(\bar{\mathbf{L}}_k\otimes\mathbf{BK}\right)\mathbf{z}(t-\tau_k)\Bigg]\end{aligned} \tag{7.22}$$

Now, using Lemma 7.1.1 with $\mathbb{X}$=$\mathbf{I}\otimes\mathbf{S}_{kj}$, one can obtain the following integral inequality

$$-\left(\tau_k(t)-\tau_j(t)\right)\int_{t-\tau_k(t)}^{t-\tau_j(t)}\dot{\mathbf{z}}^{\mathrm{T}}(t+\theta)\left(\mathbf{I}\otimes\mathbf{S}_{kj}\right)\dot{\mathbf{z}}(t+\theta)d\theta \leq \begin{bmatrix}\mathbf{z}\left(t-\tau_j(t)\right)\\ \mathbf{z}\left(t-\tau_k(t)\right)\end{bmatrix}^{\mathrm{T}}\begin{bmatrix}-\left(\mathbf{I}\otimes\mathbf{S}_{kj}\right) & \left(\mathbf{I}\otimes\mathbf{S}_{kj}\right)\\ * & -\left(\mathbf{I}\otimes\mathbf{S}_{kj}\right)\end{bmatrix}\begin{bmatrix}\mathbf{z}\left(t-\tau_j(t)\right)\\ \mathbf{z}\left(t-\tau_k(t)\right)\end{bmatrix}. \tag{7.23}$$

Further, using Lemma 7.1.2 with $\mathbb{Y}=\mathbf{I}\otimes\mathbf{R}_k$, following integral inequality can be obtained

$$-\bar{\tau}_k\int_{t-\bar{\tau}_k}^{t}\dot{\mathbf{z}}^{\mathrm{T}}(t+\theta)\left(\mathbf{I}\otimes\mathbf{R}_k\right)\dot{\mathbf{z}}(t+\theta)d\theta \leq \begin{bmatrix}\mathbf{z}(t)\\ \mathbf{z}\left(t-\tau_k(t)\right)\\ \mathbf{z}\left(t-\bar{\tau}_k\right)\end{bmatrix}^{\mathrm{T}}\begin{bmatrix}-\left(\mathbf{I}\otimes\mathbf{R}_k\right) & \left(\mathbf{I}\otimes\mathbf{R}_k\right) & \mathbf{0}\\ * & -2\left(\mathbf{I}\otimes\mathbf{R}_k\right) & \left(\mathbf{I}\otimes\mathbf{R}_k\right)\\ * & * & -\left(\mathbf{I}\otimes\mathbf{R}_k\right)\end{bmatrix}\begin{bmatrix}\mathbf{z}(t)\\ \mathbf{z}\left(t-\tau_k(t)\right)\\ \mathbf{z}\left(t-\bar{\tau}_k\right)\end{bmatrix}. \tag{7.24}$$

By defining the following augmented error vector,

$$\Sigma(t)=\mathrm{col}\big(\mathbf{z}(t),\ \mathbf{z}\left(t-\tau_1(t)\right),\ \mathbf{z}\left(t-\bar{\tau}_1\right),\ \cdots,\ \mathbf{z}\left(t-\tau_r(t)\right),\ \mathbf{z}\left(t-\bar{\tau}_r\right)\big), \tag{7.25}$$

and substituting (7.23), (7.24) and (7.22) in (7.21), one can express the derivative of the Lyapunov-Krasovskii functional in a compact form as follows

$$\dot{V}\left(\mathbf{z}_t,t\right)\leq\Sigma^T(t)\left[\mathbf{\Pi}+\boldsymbol{\xi}^T\mathbf{\Gamma}\boldsymbol{\xi}\right]\Sigma(t) \tag{7.26}$$

where $\boldsymbol{\xi}$ and $\mathbf{\Pi}$ are as defined in (7.15) and (7.13), respectively. Using the Lyapunov-Krasovskii stability theorem (Lemma 7.1.3), we can conclude that the system in (7.8) achieves asymptotic stability for $\tau_k\leq\bar{\tau}_k$, for all $k=1,\ldots,r$ if the inequality $\left[\mathbf{\Pi}+\boldsymbol{\xi}^T\mathbf{\Gamma}\boldsymbol{\xi}\right]<\mathbf{0}$ holds. Moreover, using Lemma 7.3.1, the multi-agent system in (7.7) achieves consensus asymptotically. This concludes the proof. □

Remark 7.3.3. *The bilinear matrix inequality (BMI) in* (7.12) *does not have any analytical solution and must be solved numerically to obtain the delay bounds* τ_k, $k = 1, \ldots, r$ *and the weighting matrices. The BMI can be solved using local BMI solvers such as PENBMI [181] from PENOPT.*

7.4 Simulation Results

To demonstrate the preceeding analysis, we consider a group of multiple F-16 VISTA aircraft with short-period dynamics. The states of the vehicles are represented by $\mathbf{x} = [\alpha \;\; q]^{\mathrm{T}}$, where α is the angle of attack and q is the pitch rate. The control, $\mathbf{u} = \delta_e$ is the elevator deflection. The standard short period equations of motion of the plant can be modeled as [182],

$$\begin{bmatrix} \dot{\alpha} \\ \dot{q} \end{bmatrix} = \begin{bmatrix} Z_\alpha & 1 \\ M_\alpha & M_q \end{bmatrix} \begin{bmatrix} \alpha \\ q \end{bmatrix} + \begin{bmatrix} Z_{\delta_e} \\ M_{\delta_e} \end{bmatrix} \delta_e \implies \dot{\mathbf{x}} = \mathbf{A}\mathbf{x} + \mathbf{B}\mathbf{u} \tag{7.27}$$

where Z_α, M_α, and M_q are the dimensional stability derivatives; Z_{δ_e} and M_{δ_e} are the dimensional control derivatives for the longitudinal motion of the aircraft. It is assumed that α is a surrogate for the flight speed, and minor adjustments to the speed at trim can be made using the elevator input.

The aircraft are assumed to be operating at an altitude of 25000 ft. with Mach number of 0.45. At this flight condition, the dimensional derivatives of the aircraft are obtained to be $Z_\alpha = -0.3809$, $M_\alpha = -0.0195$, $M_q = -0.4587$, $Z_{\delta_e} = -0.0624$, and $M_{\delta_e} = -3.5020$ [182].

The choice of $\mathbf{A}$ and $\mathbf{B}$ satisfies Assumption 7.1.1. The standard LQR controller is designed for each vehicle using weighting matrices $\mathbf{Q} = \mathbf{I}_2$ and $\mathbf{R} = 1$ such that $\mathbf{A} - \mathbf{B}\mathbf{K}$ is Hurwitz. We consider a network of 4 agents in a directed path topology

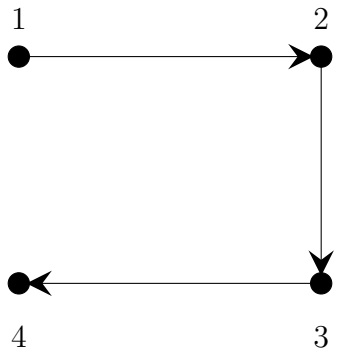

Figure 7.2: Communication graph among the agents

as depicted in Fig. 7.2. The graph Laplacian matrix of the communication graph can be written as follows

$$\mathbf{L} = \begin{bmatrix} 0 & 0 & 0 & 0 \\ -1 & 1 & 0 & 0 \\ 0 & -1 & 1 & 0 \\ 0 & 0 & -1 & 1 \end{bmatrix}. \tag{7.28}$$

The distributed control protocol is designed as discussed in Section 7.2. In order to calculate the value of coupling gain c, we follow the procedure described in [162, 177]. For the simulation, we consider $c = 0.1$ which guarantees the consensus in the delay-free multi-agent system.

For the graph topology in Fig. 7.2, the total number of edges $r = 3$ and the three Laplacian matrices of the subgraph associated with the time delay τ_k, $k = 1, 2, 3$ are computed as

$$\mathbf{L}_1 = \begin{bmatrix} 0 & 0 & 0 & 0 \\ -1 & 1 & 0 & 0 \\ 0 & 0 & 0 & 0 \\ 0 & 0 & 0 & 0 \end{bmatrix}, \ \mathbf{L}_2 = \begin{bmatrix} 0 & 0 & 0 & 0 \\ 0 & 0 & 0 & 0 \\ 0 & -1 & 1 & 0 \\ 0 & 0 & 0 & 0 \end{bmatrix}, \text{ and } \mathbf{L}_3 = \begin{bmatrix} 0 & 0 & 0 & 0 \\ 0 & 0 & 0 & 0 \\ 0 & 0 & 0 & 0 \\ 0 & 0 & -1 & 1 \end{bmatrix}. \tag{7.29}$$

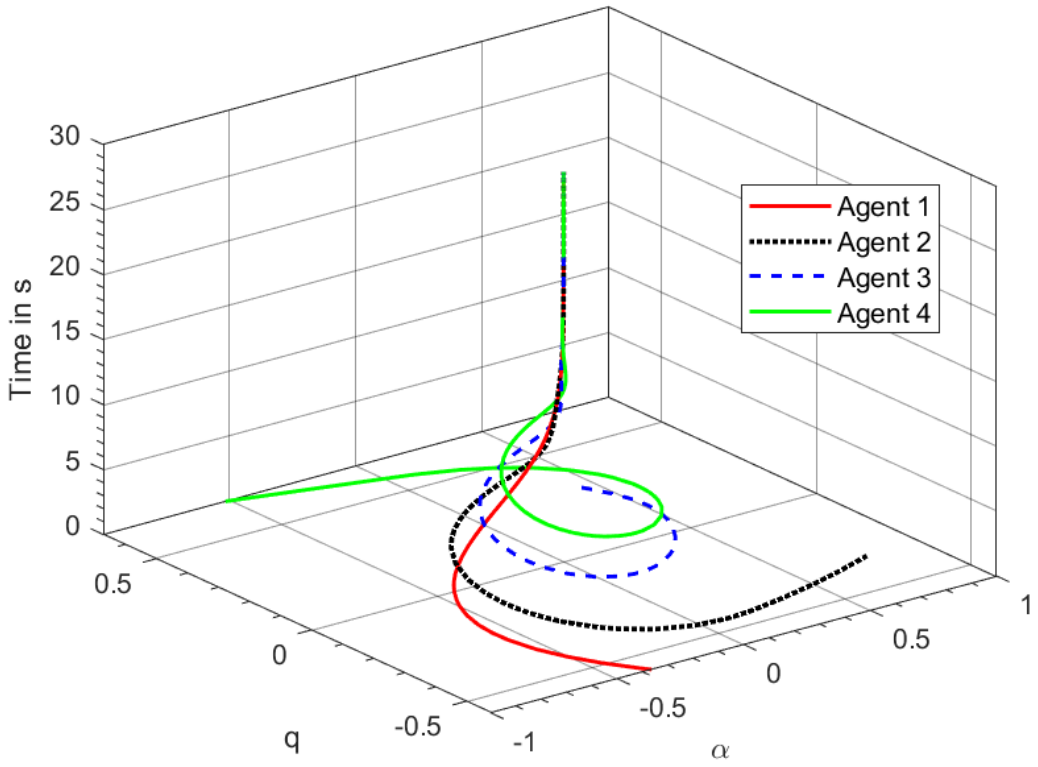

Figure 7.3: State trajectories of agents with $\tau_1 = 1.09$ s, $\tau_2 = 0.76$ s, and $\tau_3 = 0.76$ s.

For the simulation, the maximum bounds on the delay derivatives are assumed to be: $\mu_1 = 0.7$, $\mu_2 = 0.8$, and $\mu_3 = 0.9$. Upon solving the matrix inequality in (7.12), we obtain maximum delay bounds to be $\bar{\tau}_1 = 1.0935$ s, $\bar{\tau}_2 = 0.7682$ s, and $\bar{\tau}_3 = 0.7677$ s for the angle of attack and pitch rate consensus among the four F-16 VISTA aircraft.

To demonstrate the accuracy of the proposed approach, we simulate the trajectories of the four agents with proposed control protocol and delay values of $\tau_1 = 1.09$ s, $\tau_2 = 0.76$ s, and $\tau_3 = 0.76$ s. Figure 7.3 depicts the angle of attack and pitch rate trajectories of the four F-16 VISTA agents. Clearly, the agents have achieved

Table 7.1: Delay margin associated with each edge of various graph topologies

Type	r	$\bar{\tau}_{21}$	$\bar{\tau}_{31}$	$\bar{\tau}_{12}$	$\bar{\tau}_{32}$	$\bar{\tau}_{13}$	$\bar{\tau}_{23}$
Directed path	2	-	-	0.9972	-	-	1.0122
Directed Cycle	3	-	0.5022	0.5864	-	-	0.5264
Undirected Path	4	0.2760	-	0.2928	0.2825	-	0.2829
Undirected Cycle	6	0.1008	0.1008	0.1012	0.1012	0.1012	0.1012

consensus in the angle of attack and pitch rate with proposed control protocol and with delay values lower than the delay bounds.

Further, we also compute the maximum consensuable delay bounds for the multi-agent system with 3 agents communicating in various graph topologies (directed path, directed cycle, undirected path, and undirected cycle). The maximum bounds on the delay derivatives are assumed to be $\mu_i = 0.6$, for all $i = 1, \ldots, r$. The delay bounds (for consensus) associated with each edge of various graph topologies are reported in the Table 7.1 (the delay bounds are presented in double indexed notation to maintain notational uniformity among all the graph structures) . It can be inferred that the edges in the directed path have higher delay robustness as compared to the edges in directed cycle, undirected path, and directed cycle. The undirected cycle is observed to have edges with smallest delay robustness as compared to other graph structures listed in Table 7.1.

7.5 Chapter Summary

In this chapter, we have studied the consensus condition for high-order linear multi-agent system with non-uniform, time-varying delays among the agents. First, a distributed control protocol was designed for the multi-agent system with delay and subsequently, the problem of state consensus among the agents was transformed to an equivalent problem of stability of the consensus error. Then, using Lyapunov-

Krasovskii approach, we derive delay dependent stability criteria to characterize the delay margin for multi-agent system with non-uniform time-varying delays. Numerical results demonstrated that, the edges in the directed path have higher delay robustness as compared to the edges in directed cycle, undirected path, and directed cycle.

Chapter 8

Summary, Future Work, and Closing Remarks

In this dissertation, we have studied the uncertainty propagation in dynamical systems subject to initial condition and parametric uncertainties governed by different distribution types. The uncertainty propagation was carried out in the framework of generalized polynomial chaos expansion in Chapter 2. We proposed the mixed sparse grid sampling technique in the pseudospectral collocation scheme to employ generalized polynomial chaos expansion for stochastic dynamical systems. Further, we compared the computational efficacy of the proposed technique to various other sampling techniques in the existing literature by studying the uncertainty propagation in various benchmark problems. In addition to that, sensitivity of the system output to the input uncertainties was studied using the generalized polynomial chaos expansion framework.

In Chapter 3, novel robust control algorithms were developed for stochastic linear systems subject to parametric uncertainties. The controllers have been designed to minimize finite horizon and infinite horizon expectation performance indices. In particular, feedback control laws were developed using generalized polynomial expansion technique to stabilize the stochastic plant for all variations of the random variable within the domain of its probability density function. Subsequently, in Chapter 4, a filtering algorithm based on the generalized polynomial chaos expansion in the ensemble filter framework was developed for the state estimation of a general nonlinear system. The proposed filter can carry out state estimation for a nonlinear system with non-Gaussian uncertainties in the parameters and was applied to the problem

of atmospheric reentry of a vehicle to Earth. Besides, the global sensitivity of the posterior density function of the state estimates to the uncertainties in the system was characterized.

Further, this dissertation conducted probabilistic analysis of the consensus control protocols in the scenario where the interaction parameters in a system of interconnected cooperative agents are susceptible to uncertainties in Chapter 5. The framework of generalized polynomial chaos expansion was utilized to obtain numerical solution of the stochastic multi-agent system. Finally, sensitivity analysis based on gPC expansion was carried out to study the significance of edge weights on response distribution of the states of agents to answer the following question: "Who is the weakest link?" In addition to that, we examined the impact of cyber attacks from malicious intruders on the consensus performance of the agents using the probabilistic analysis framework.

In Chapter 6, the robust stability margin (gain and phase margins) of the multi-agent systems subject to multiplicative uncertainties in the feedback path was characterized. Moreover, the consensuability criterion for multi-agent systems with uniform input delays was computed. The problem of calculating the stability margins and input delay margin was converted into finding eigenvalues of multiplicative perturbation in the feedback paths of a set of MIMO loop transfer functions and it involved solving a constrained minimization problem. Additionally, necessary and sufficient conditions for gain-independent, phase-independent and delay-independent stability of multi-agent systems were developed.

Finally, the consensus criterion for multi-agent systems subject to non-uniform time-varying communication delays was developed in Chapter 7. The problem of consensus in multi-agent systems with non-uniform time-varying delays was converted

to an equivalent MIMO stability problem. Using the Lyapunov-Krasovskii theorem, novel delay-dependent stability criterion is derived in the form of an LMI.

In essence, this dissertation dealt with the development of computationally efficient solutions to problems of uncertainty propagation, optimal control, and state estimation of stochastic systems with probabilistic uncertainties. In addition, computational approaches were designed to characterize robust stability margins and delay margins in the coordinated group of agents with multiplicative uncertainties and delays. Though the proposed approaches in this dissertation address a wide range of issues in analysis and control of dynamical systems, we suggest following extensions to the techniques developed.

In general, the gPC expansion technique can be used to carry out uncertainty propagation in stochastic systems with both discrete and continuous distribution functions. In this dissertation, the efficacy of the mixed sparse grid quadrature technique has been studied for stochastic systems subject to uncertainties governed only by normal and uniform probability distributions (both of which are continuous). To that end, the accuracy and computational efficiency of the proposed quadrature rule can be studied for various other benchmark problems with distribution functions other than normal and uniform.

Further, the work related to stochastic control carried out in this dissertation assumes the system dynamics to be linear. The methodology can be extended to develop robust control strategies for stochastic nonlinear systems. Further, one can investigate the gPC expansion-based distributed model predictive control for unmanned cooperative systems subject to stochastic uncertainties in the parameters.

Additionally, the framework of gPC expansion can be used to analyze the region of attraction of stochastic nonlinear systems with uncertainty dependent equilibrium points. To that end, the stochastic nonlinear system can be converted to a deter-

ministic system in terms of coefficients of gPC expansion and a set of uncertainty-dependent equilibrium points of the stochastic system can be computed. Afterwards, the region of attraction of the gPC expanded deterministic system can be used to extract information about the attractive behavior of the original stochastic system.

In this dissertation, we have studied the consensus problems in multi-agent systems, wherein the information exchange among the agents is governed by a fixed graph topology. In the future, the proposed framework to compute the stability margins can be extended to the case where the multi-agent systems are modeled using switching network topologies.

APPENDIX A

Examples of Probability Density Functions: Gaussian and Uniform Density Functions

Here we provide a brief overview of Gaussian and Uniform density functions, which are prevalent throughout this dissertation.

A.1 Gaussian Probability Density Function

The Gaussian or normal PDF is one of the most widely used PDFs in the probability theory to characterize a real-valued random variable. The Gaussian PDF characterizing a random variable Z has the following form:

$$f_Z(z) = \frac{1}{\sqrt{2\pi}\sigma}\exp\left(-\frac{(z-\mu)^2}{2\sigma^2}\right), \quad -\infty < z < \infty \tag{A.1}$$

where μ and σ are the two parameters that completely characterize the Gaussian PDF $f_Z(z)$, and are called as the mean and the standard deviation of the random variable z, respectively. Consequently, the Gaussian PDF of Z is usually represented by

$$Z \sim \mathcal{N}(\mu, \sigma^2) \tag{A.2}$$

where σ^2 is known as the variance of Z. The Gaussian distribution with a mean of 0 and variance of 1, i.e. $\mathcal{N}(0, 1^2)$ is known as standard Gaussian distribution.

Geometrically, the Gaussian or normal PDF is a bell-shaped curve that is symmetric about the mean μ and attains its maximum value of $\frac{1}{\sqrt{2\pi}\sigma}$ at $x = \mu$. Figure A.1 represents a Gaussian PDF for a random variable z with $\mu = 1$ and $\sigma = 2$.

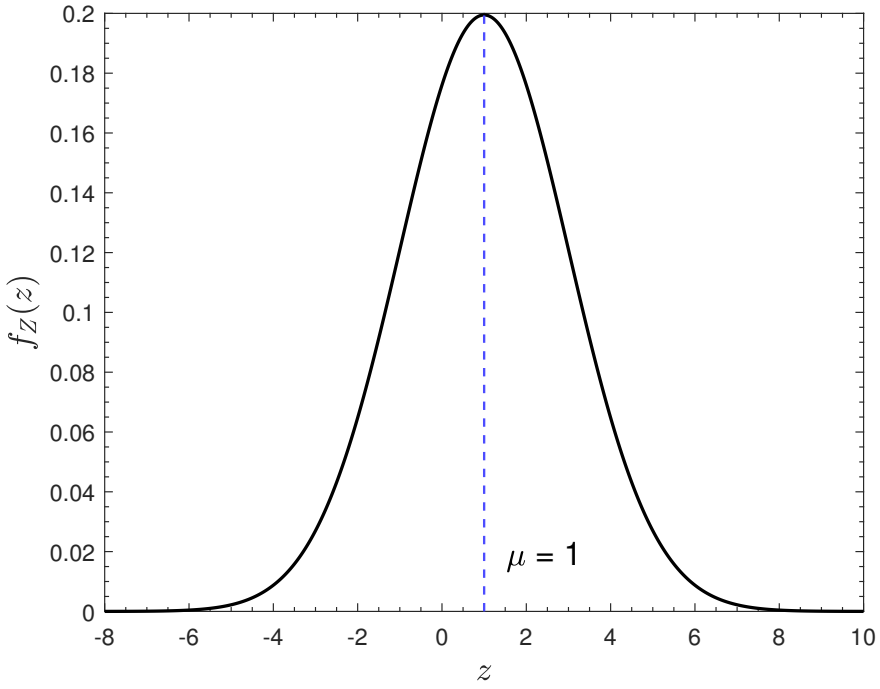

Figure A.1: Gaussian PDF $\mathcal{N}(1, 2^2)$ of the random variable Z.

A.2 Uniform Probability Density Function

The uniform probability distribution is another commonly used distribution in probability theory and it describes an experiment where there is an arbitrary outcome that lies between certain bounds. The uniform PDF characterizing a random variable z has the following form:

$$f_Z(z) = \frac{1}{b-a}, \quad a \leq z \leq b \tag{A.3}$$

where the two constants a and b completely characterize the uniform PDF $f_Z(z)$, and are the minimum and maximum values of the random variable z, respectively. The uniform PDF is often abbreviated as

$$Z \sim \mathcal{U}[a, b]. \tag{A.4}$$

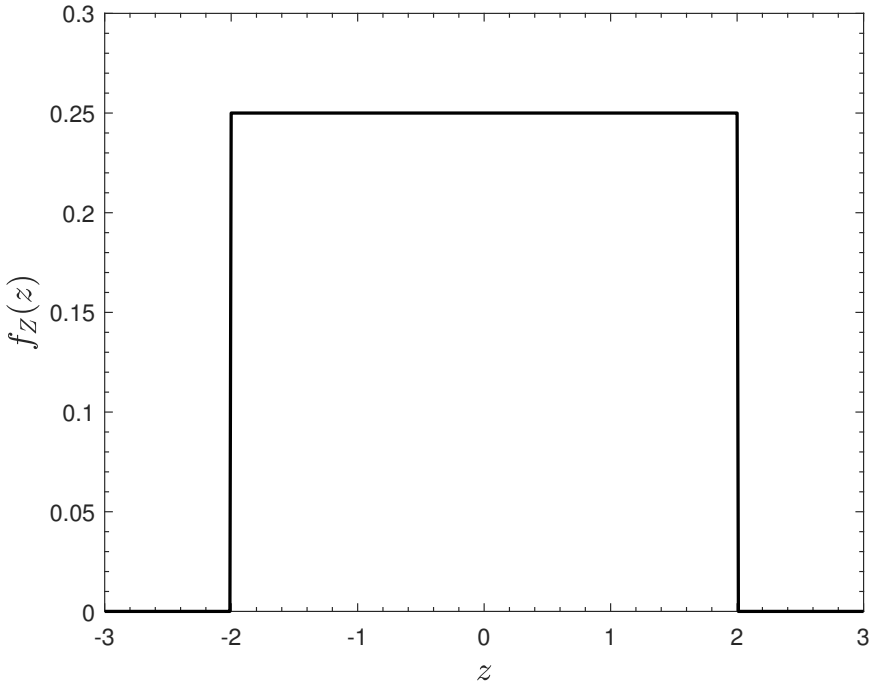

Figure A.2: Uniform PDF $\mathcal{U}[-2, 2]$ of the random variable Z.

The standard uniform distribution is where $a = -1$ and $b = 1$ and is commonly used for random number generation. Geometrically, the uniform PDF is a rectangular curve with a base of $(b - a)$ and a height of $\frac{1}{b-a}$. Figure A.1 represents a Uniform PDF for a random variable z with $a = -2$ and $b = 2$.

APPENDIX B

Hermite and Legendre Polynomials

Here we present two of the widely used orthogonal polynomials, namely Hermite and Legendre polynomials. These two polynomials have been extensively used in this dissertation.

B.1 Hermite Polynomials

The Hermite polynomials $H_n(x)$ are set of orthogonal polynomials over the domain $(-\infty, \infty)$ and are defined by following orthogonality relation

$$\int_{-\infty}^{\infty} H_m(x) H_n(x) w(x) dx = n! \delta_{mn} \tag{B.1}$$

where the weighting function $w(x)$ is defined as

$$w(x) = \frac{1}{\sqrt{2\pi}} e^{-x^2/2}. \tag{B.2}$$

Table B.1 lists first few Hermite polynomials. The Rodrigues formula for the Hermite polynomial is,

$$H_n(x) = (-1)^n e^{-x^2/2} \frac{d^n}{dx^n} \left(e^{-x^2/2} \right) \tag{B.3}$$

The system of Hermite Polynomials $\{H_n(x), n \in \mathbb{N}\}$ satisfy the following three-term recurrence relation

$$H_{n+1}(x) = x H_n(x) - n H_{n-1}(x). \tag{B.4}$$

Table B.1: One-dimensional Hermite Polynomials

Order (n)	$H_n(x)$
0	1
1	x
2	$x^2 - 1$
3	$x^3 - 3x$
4	$x^4 - 6x^2 + 3$
5	$x^5 - 10x^3 + 15x$
6	$x^6 - 15x^4 + 45x^2 - 15$

B.2 Legendre Polynomials

The Legendre polynomials $P_n(x)$ are set of orthogonal polynomials over the domain $(-1, 1)$ and are defined by following orthogonality relation

$$\int_{-1}^{1} P_m(x)P_n(x)w(x)dx = \frac{2}{2n+1}\delta_{mn} \tag{B.5}$$

where the weighting function $w(x) = 1$. Table B.2 lists first few Legendre polynomials. The Rodrigues formula for the Legendre polynomial is,

$$P_n(x) = \frac{1}{2^n n!}\frac{d^n}{dx^n}\left((x^2-1)^n\right). \tag{B.6}$$

The system of Legendre Polynomials $\{P_n(x), n \in \mathbb{N}\}$ satisfy the following three-term recurrence relation

$$P_{n+1}(x) = \frac{2n+1}{n+1}xP_n(x) - \frac{n}{n+1}P_{n-1}(x). \tag{B.7}$$

Table B.2: One-dimensional Legendre Polynomials

Order (n)	$P_n(x)$
0	1
1	x
2	$\frac{3}{2}x^2 - \frac{1}{2}$
3	$\frac{5}{2}x^3 - \frac{3}{2}x$
4	$\frac{35}{8}x^4 - \frac{30}{8}x^2 + \frac{3}{8}$
5	$\frac{63}{8}x^5 - \frac{70}{8}x^3 + \frac{15}{8}x$
6	$\frac{231}{16}x^6 - \frac{315}{16}x^4 + \frac{105}{16}x^2 - \frac{5}{16}$

APPENDIX C

Kronecker Product and Related Identities

C.1 Kronecker Product

The Kronecker product denoted as $\mathbf{A} \otimes \mathbf{B}$ of a matrix $\mathbf{A} = [\mathbf{A}_{ij}] \in \mathbb{R}^{m \times n}$, $i = 1, 2, \ldots, m$, $j = 1, 2, \ldots, n$ with a matrix $\mathbf{B} == [\mathbf{B}_{kl}] \in \mathbb{R}^{p \times q}$, $k = 1, 2, \ldots, p$, $l = 1, 2, \ldots, q$ is defined as

$$\mathbf{A} \otimes \mathbf{B} = \begin{bmatrix} \mathbf{A}_{11}\mathbf{B} & \mathbf{A}_{12}\mathbf{B} & \cdots & \mathbf{A}_{1n}\mathbf{B} \\ \mathbf{A}_{21}\mathbf{B} & \mathbf{A}_{22}\mathbf{B} & \cdots & \mathbf{A}_{2n}\mathbf{B} \\ \vdots & \vdots & \vdots & \vdots \\ \mathbf{A}_{m1}\mathbf{B} & \mathbf{A}_{m2}\mathbf{B} & \cdots & \mathbf{A}_{mn}\mathbf{B} \end{bmatrix} \tag{C.1}$$

C.2 Some Important Kronecker Product Identities

Following is the list of some identities related to Kronecker product of matrices, which has been used throughout this dissertation. In the following list, $\mathbf{A}$, $\mathbf{B}$, $\mathbf{C}$, and $\mathbf{D}$ are matrices of suitable dimensions.

(i) $\mathbf{A} \otimes (\mathbf{B} + \mathbf{C}) = \mathbf{A} \otimes \mathbf{B} + \mathbf{A} \otimes \mathbf{C}$

(ii) $(\mathbf{A} \otimes \mathbf{B}) \otimes \mathbf{C} = \mathbf{A} \otimes (\mathbf{B} \otimes \mathbf{C})$

(iii) $(\mathbf{A} \otimes \mathbf{B}) \otimes (\mathbf{C} \otimes \mathbf{D}) = (\mathbf{AC}) \otimes (\mathbf{BD})$

(iv) $(\mathbf{A} \otimes \mathbf{B})^{\mathrm{T}} = \mathbf{A}^{\mathrm{T}} \otimes \mathbf{B}^{\mathrm{T}}$

(v) $(\mathbf{A} \otimes \mathbf{B})^{-1} = \mathbf{A}^{-1} \otimes \mathbf{B}^{-1}$

APPENDIX D

Expressions of Coefficients and Forcing Functions in Modified Equations of Motion of Nonlinear Aeroelastic System in (2.49)

D.1 Coefficients c_i, $i = 0, 1, \ldots, 10$

$$
\begin{aligned}
c_0 &= 1 + \frac{1}{\mu} \\
c_1 &= x_\alpha - \frac{a_h}{\mu} \\
c_2 &= 2\zeta_\xi \frac{\omega_r}{V_r} + \frac{2}{\mu}\left(1 - \psi_1 - \psi_2\right) \\
c_3 &= \frac{1 + 2\left(1/2 - a_h\right)\left(1 - \psi_1 - \psi_2\right)}{\mu} \\
c_4 &= \left(\frac{\omega_r}{V_r}\right)^2 + \frac{2}{\mu}\left(\psi_1\epsilon_1 + \psi_2\epsilon_2\right) \\
c_5 &= \left(\frac{\omega_r}{V_r}\right)^2 \beta_\xi \\
c_6 &= \frac{2}{\mu}\left\{\left(1 - \psi_1 - \psi_2\right) + \left(\frac{1}{2} - a_h\right)\left(\psi_1\epsilon_1 + \psi_2\epsilon_2\right)\right\} \\
c_7 &= \frac{2}{\mu}\psi_1\epsilon_1\left\{\left(1 - \left(\frac{1}{2} - a_h\right)\epsilon_1\right)\right\} \\
c_8 &= \frac{2}{\mu}\psi_2\epsilon_2\left\{\left(1 - \left(\frac{1}{2} - a_h\right)\epsilon_2\right)\right\} \\
c_9 &= -\frac{2}{\mu}\psi_1\epsilon_1^2 \\
c_{10} &= -\frac{2}{\mu}\psi_2\epsilon_2^2
\end{aligned}
$$

D.2 Coefficients d_i, $i = 0, 1, \ldots, 10$

$$
\begin{aligned}
d_0 &= \frac{x_\alpha}{r_\alpha^2} - \frac{a_h}{\mu r_\alpha^2} \\
d_1 &= 1 + \frac{1 + 8a_h^2}{8\mu r_\alpha^2} \\
d_2 &= 2\frac{\zeta_\alpha}{V_r} + \frac{1 - 2a_h}{2\mu r_\alpha^2} - \frac{\left(1 + 2a_h\right)\left(1 - 2a_h\right)\left(1 - \psi_1 - \psi_2\right)}{2\mu r_\alpha^2} \\
d_3 &= \frac{1}{V_r^2} - \frac{1 + 2a_h}{2\mu r_\alpha^2} - \frac{\left(1 + 2a_h\right)\left(1 - 2a_h\right)\left(\psi_1\epsilon_1 + \psi_2\epsilon_2\right)}{2\mu r_\alpha^2} \\
d_4 &= \frac{\beta_\alpha}{V_r^2}
\end{aligned}
$$

$$
\begin{aligned}
d_5 &= -\frac{(1+2a_h)\,(1-\psi_1-\psi_2)}{\mu r_\alpha^2} \\
d_6 &= -\frac{(1+2a_h)\,(\psi_1\epsilon_1+\psi_2\epsilon_2)}{\mu r_\alpha^2} \\
d_7 &= -\frac{(1+2a_h)\,\psi_1\epsilon_1\,[1-(1/2-a_h)\,\epsilon_1]}{\mu r_\alpha^2} \\
d_8 &= -\frac{(1+2a_h)\,\psi_2\epsilon_2\,[1-(1/2-a_h)\,\epsilon_2]}{\mu r_\alpha^2} \\
d_9 &= \frac{(1+2a_h)\,\psi_1\epsilon_1^2}{\mu r_\alpha^2} \\
d_{10} &= \frac{(1+2a_h)\,\psi_2\epsilon_2^2}{\mu r_\alpha^2}
\end{aligned}
$$

D.3 Forcing Functions $f(\tau)$ and $g(\tau)$

$$
\begin{aligned}
f(\tau) &= \frac{2}{\mu}\left[\left(\frac{1}{2}-a_h\right)\alpha(0)+\xi(0)\right]\left(\Psi_1\varepsilon_1 \mathrm{e}^{-\varepsilon_1\tau}+\Psi_2\varepsilon_2\mathrm{e}^{-\varepsilon_2\tau}\right) \\
g(\tau) &= -\frac{(1+2a_h)\,f(\tau)}{2r_\alpha^2}
\end{aligned}
$$

References

[1] N. R. Council, *Assessing the reliability of complex models: mathematical and statistical foundations of verification, validation, and uncertainty quantification*. National Academies Press, Jun. 2012. [Online]. Available: https://doi.org/10.17226/13395

[2] T. Sauer, "Numerical solution of stochastic differential equations in finance," in *Handbook of Computational Finance*. Springer Berlin Heidelberg, Jul. 2011, pp. 529–550. [Online]. Available: https://doi.org/10.1007/978-3-642-17254-0_19

[3] G. Fishman, *Monte Carlo: concepts, algorithms, and applications*. Springer Science & Business Media, 2013.

[4] J. Duan, *An introduction to stochastic dynamics*. Cambridge University Press, 2015, vol. 51.

[5] T. Gao, J. Duan, and X. Li, "Fokker–planck equations for stochastic dynamical systems with symmetric lévy motions," *Applied Mathematics and Computation*, vol. 278, pp. 1–20, Mar. 2016. [Online]. Available: https://doi.org/10.1016/j.amc.2016.01.010

[6] B. Sudret, "Uncertainty propagation and sensitivity analysis in mechanical models–contributions to structural reliability and stochastic spectral methods," *Habilitationa diriger des recherches, Université Blaise Pascal, Clermont-Ferrand, France*, 2007.

[7] D. Zhang, *Stochastic methods for flow in porous media: coping with uncertainties*. Elsevier, 2001.

[8] A. Prabhakar, J. Fisher, and R. Bhattacharya, "Polynomial chaos-based analysis of probabilistic uncertainty in hypersonic flight dynamics," *Journal of Guidance, Control, and Dynamics*, vol. 33, no. 1, pp. 222–234, Jan. 2010. [Online]. Available: https://doi.org/10.2514/1.41551

[9] R. Madankan, P. Singla, T. Singh, and P. D. Scott, "Polynomial-chaos-based bayesian approach for state and parameter estimations," *Journal of Guidance, Control, and Dynamics*, vol. 36, no. 4, pp. 1058–1074, Jul. 2013. [Online]. Available: https://doi.org/10.2514/1.58377

[10] S. Hosder and R. Walters, "Non-intrusive polynomial chaos methods for uncertainty quantification in fluid dynamics," in *48th AIAA Aerospace Sciences Meeting Including the New Horizons Forum and Aerospace Exposition*. American Institute of Aeronautics and Astronautics, Jan. 2010. [Online]. Available: https://doi.org/10.2514/6.2010-129

[11] N. Wiener, "The homogeneous chaos," *American Journal of Mathematics*, vol. 60, no. 4, p. 897, Oct. 1938. [Online]. Available: https://doi.org/10.2307/2371268

[12] R. H. Cameron and W. T. Martin, "The orthogonal development of non-linear functionals in series of fourier-hermite functionals," *The Annals of Mathematics*, vol. 48, no. 2, p. 385, Apr. 1947. [Online]. Available: https://doi.org/10.2307/1969178

[13] K. ITO, "Multiple wiener integral," *Journal of the Mathematical Society of Japan*, vol. 3, no. 1, May 1951. [Online]. Available: https://doi.org/10.2969/jmsj/00310157

[14] R. G. Ghanem and P. D. Spanos, "Stochastic finite element method: Response statistics," in *Stochastic finite elements: a spectral approach*. Springer, 1991, pp. 101–119.

[15] D. Xiu and G. E. Karniadakis, "The wiener–askey polynomial chaos for stochastic differential equations," *SIAM Journal on Scientific Computing*, vol. 24, no. 2, pp. 619–644, Jan. 2002. [Online]. Available: https://doi.org/10.1137/s1064827501387826

[16] D. Xiu and J. S. Hesthaven, "High-order collocation methods for differential equations with random inputs," *SIAM Journal on Scientific Computing*, vol. 27, no. 3, pp. 1118–1139, Jan. 2005. [Online]. Available: https://doi.org/10.1137/040615201

[17] A. H. Stroud and D. Secrest, *Gaussian quadrature formulas*, ser. Prentice-Hall series in automatic computation. Englewood Cliffs, NJ: Prentice-Hall, 1966. [Online]. Available: http://cds.cern.ch/record/104292

[18] S. A. Smolyak, "Quadrature and interpolation formulas for tensor products of certain classes of functions," *Dokl. Akad. Nauk SSSR*, vol. 148, no. 5, p. 1042–1045, 1963.

[19] P. M. Congedo, R. Abgrall, and G. Geraci, "On the Use of the Sparse Grid Techniques Coupled with Polynomial Chaos," INRIA, Research Report RR-7579, Mar. 2011. [Online]. Available: https://hal.inria.fr/inria-00579205

[20] B. A. Jones, A. Doostan, and G. H. Born, "Nonlinear propagation of orbit uncertainty using non-intrusive polynomial chaos," *Journal of Guidance, Control, and Dynamics*, vol. 36, no. 2, pp. 430–444, Mar. 2013. [Online]. Available: https://doi.org/10.2514/1.57599

[21] L. Dell'Elce and G. Kerschen, "Probabilistic assessment of lifetime of low-earth-orbit spacecraft: Uncertainty propagation and sensitivity analysis," *Journal of Guidance, Control, and Dynamics*, vol. 38, no. 5, pp. 886–899, May 2015. [Online]. Available: https://doi.org/10.2514/1.g000149

[22] N. Adurthi, P. Singla, and T. Singh, "Conjugate unscented transformation: Applications to estimation and control," *Journal of Dynamic Systems, Measurement, and Control*, vol. 140, no. 3, Nov. 2017. [Online]. Available: https://doi.org/10.1115/1.4037783

[23] R. Madankan, P. Singla, and T. Singh, "Application of conjugate unscented transform in source parameters estimation," in *2013 American Control Conference*. IEEE, Jun. 2013. [Online]. Available: https://doi.org/10.1109/acc.2013.6580201

[24] J. R. Fisher, "Stability analysis and control of stochastic dynamic systems using polynomial chaos," Ph.D. dissertation, 2008.

[25] H. Scheffe, *The analysis of variance*. John Wiley & Sons, 1999, vol. 72.

[26] B. Sudret, "Global sensitivity analysis using polynomial chaos expansions," *Reliability Engineering & System Safety*, vol. 93, no. 7, pp. 964–979, Jul. 2008. [Online]. Available: https://doi.org/10.1016/j.ress.2007.04.002

[27] I. M. Sobol, "Sensitivity estimates for nonlinear mathematical models," *Mathematical modelling and computational experiments*, vol. 1, no. 4, pp. 407–414, 1993.

[28] S. Bhattacharyya, "Robust control under parametric uncertainty: An overview and recent results," *Annual Reviews in Control*, vol. 44, pp. 45–77, 2017. [Online]. Available: https://doi.org/10.1016/j.arcontrol.2017.05.001

[29] I. R. Petersen and R. Tempo, "Robust control of uncertain systems: Classical results and recent developments," *Automatica*, vol. 50, no. 5, pp. 1315–1335, May 2014. [Online]. Available: https://doi.org/10.1016/j.automatica.2014.02.042

[30] K.-K. K. Kim and R. D. Braatz, "Generalised polynomial chaos expansion approaches to approximate stochastic model predictive control†," *International*

Journal of Control, vol. 86, no. 8, pp. 1324–1337, Aug. 2013. [Online]. Available: https://doi.org/10.1080/00207179.2013.801082

[31] J. A. Paulson, S. Streif, and A. Mesbah, "Stability for receding-horizon stochastic model predictive control," in *2015 American Control Conference (ACC)*. IEEE, Jul. 2015. [Online]. Available: https://doi.org/10.1109/acc.2015.7170854

[32] J. Moon and T. E. Duncan, "A simple proof of indefinite linear-quadratic stochastic optimal control with random coefficients," *IEEE Transactions on Automatic Control*, vol. 65, no. 12, pp. 5422–5428, Dec. 2020. [Online]. Available: https://doi.org/10.1109/tac.2020.2970982

[33] E. Bakolas, "Constrained minimum variance control for discrete-time stochastic linear systems," *Systems & Control Letters*, vol. 113, pp. 109–116, Mar. 2018. [Online]. Available: https://doi.org/10.1016/j.sysconle.2018.02.001

[34] B. Lu and F. Wu, "Probabilistic robust control design for an f-16 aircraft," in *AIAA Guidance, Navigation, and Control Conference and Exhibit*. American Institute of Aeronautics and Astronautics, Jun. 2005. [Online]. Available: https://doi.org/10.2514/6.2005-6080

[35] R. Tempo, G. Calafiore, and F. Dabbene, *Randomized Algorithms for Analysis and Control of Uncertain Systems*. Springer London, 2013. [Online]. Available: https://doi.org/10.1007/978-1-4471-4610-0

[36] J. Fisher and R. Bhattacharya, "Linear quadratic regulation of systems with stochastic parameter uncertainties," *Automatica*, vol. 45, no. 12, pp. 2831–2841, Dec. 2009. [Online]. Available: https://doi.org/10.1016/j.automatica.2009.10.001

[37] R. Bhattacharya, "Robust LQR design for systems with probabilistic uncertainty," *International Journal of Robust and Nonlinear Control*,

vol. 29, no. 10, pp. 3217–3237, Apr. 2019. [Online]. Available: https://doi.org/10.1002/rnc.4548

[38] D. E. Shen, S. Lucia, Y. Wan, R. Findeisen, and R. D. Braatz, "Polynomial chaos-based h2-optimal static output feedback control of systems with probabilistic parametric uncertainties," *IFAC-PapersOnLine*, vol. 50, no. 1, pp. 3536–3541, Jul. 2017. [Online]. Available: https://doi.org/10.1016/j.ifacol.2017.08.949

[39] S.-C. Hsu and R. Bhattacharya, "Design of linear parameter varying quadratic regulator in polynomial chaos framework," *International Journal of Robust and Nonlinear Control*, vol. 30, no. 16, pp. 6661–6682, Aug. 2020. [Online]. Available: https://doi.org/10.1002/rnc.5128

[40] P. M. Blok, K. van Boheemen, F. K. van Evert, J. IJsselmuiden, and G.-H. Kim, "Robot navigation in orchards with localization based on particle filter and kalman filter," *Computers and Electronics in Agriculture*, vol. 157, pp. 261–269, Feb. 2019. [Online]. Available: https://doi.org/10.1016/j.compag.2018.12.046

[41] Z. Guang, B. Xingzi, Z. Hanyu, and L. Bin, "Non-cooperative maneuvering spacecraft tracking via a variable structure estimator," *Aerospace Science and Technology*, vol. 79, pp. 352–363, Aug. 2018. [Online]. Available: https://doi.org/10.1016/j.ast.2018.05.052

[42] S. Yin, S. X. Ding, X. Xie, and H. Luo, "A review on basic data-driven approaches for industrial process monitoring," *IEEE Transactions on Industrial Electronics*, vol. 61, no. 11, pp. 6418–6428, Nov. 2014. [Online]. Available: https://doi.org/10.1109/tie.2014.2301773

[43] D. Bhattacharjee and K. Subbarao, "Set-membership filter for discrete-time nonlinear systems using state dependent coefficient parameterization," *IEEE*

Transactions on Automatic Control, pp. 1–1, 2021. [Online]. Available: https://doi.org/10.1109/tac.2021.3082504

[44] C. Yang, W. Shi, and W. Chen, "Comparison of unscented and extended kalman filters with application in vehicle navigation," *Journal of Navigation*, vol. 70, no. 2, pp. 411–431, Sep. 2016. [Online]. Available: https://doi.org/10.1017/s0373463316000655

[45] P. L. Houtekamer and F. Zhang, "Review of the ensemble kalman filter for atmospheric data assimilation," *Monthly Weather Review*, vol. 144, no. 12, pp. 4489–4532, Nov. 2016. [Online]. Available: https://doi.org/10.1175/mwr-d-15-0440.1

[46] S. Yun and R. Zanetti, "Sequential monte carlo filtering with gaussian mixture sampling," *Journal of Guidance, Control, and Dynamics*, vol. 42, no. 9, pp. 2069–2077, Sep. 2019. [Online]. Available: https://doi.org/10.2514/1.g004403

[47] J. Li and D. Xiu, "A generalized polynomial chaos based ensemble kalman filter with high accuracy," *Journal of Computational Physics*, vol. 228, no. 15, pp. 5454–5469, Aug. 2009. [Online]. Available: https://doi.org/10.1016/j.jcp.2009.04.029

[48] M. L. Psiaki, "Gaussian-mixture kalman filter for orbit determination using angles-only data," *Journal of Guidance, Control, and Dynamics*, vol. 40, no. 9, pp. 2341–2347, Sep. 2017. [Online]. Available: https://doi.org/10.2514/1.g002812

[49] D. Goswami and D. A. Paley, "Non-gaussian estimation and dynamic output feedback using the gaussian mixture kalman filter," *Journal of Guidance, Control, and Dynamics*, vol. 44, no. 1, pp. 15–24, Jan. 2021. [Online]. Available: https://doi.org/10.2514/1.g005005

[50] G. Terejanu, P. Singla, T. Singh, and P. D. Scott, "Adaptive gaussian sum filter for nonlinear bayesian estimation," *IEEE Transactions on Automatic Control*, vol. 56, no. 9, pp. 2151–2156, Sep. 2011. [Online]. Available: https://doi.org/10.1109/tac.2011.2141550

[51] H. Wang and C. Li, "An improved gaussian mixture CKF algorithm under non-gaussian observation noise," *Discrete Dynamics in Nature and Society*, vol. 2016, pp. 1–10, 2016. [Online]. Available: https://doi.org/10.1155/2016/1082837

[52] P. Fearnhead and H. R. Künsch, "Particle filters and data assimilation," *Annual Review of Statistics and Its Application*, vol. 5, no. 1, pp. 421–449, Mar. 2018. [Online]. Available: https://doi.org/10.1146/annurev-statistics-031017-100232

[53] C. Snyder, T. Bengtsson, P. Bickel, and J. Anderson, "Obstacles to high-dimensional particle filtering," *Monthly Weather Review*, vol. 136, no. 12, pp. 4629–4640, Dec. 2008. [Online]. Available: https://doi.org/10.1175/2008mwr2529.1

[54] P. Dutta and R. Bhattacharya, "Hypersonic state estimation using the frobenius-perron operator," *Journal of Guidance, Control, and Dynamics*, vol. 34, no. 2, pp. 325–344, Mar. 2011. [Online]. Available: https://doi.org/10.2514/1.52184

[55] E. D. Blanchard, A. Sandu, and C. Sandu, "A polynomial chaos-based kalman filter approach for parameter estimation of mechanical systems," *Journal of Dynamic Systems, Measurement, and Control*, vol. 132, no. 6, Nov. 2010. [Online]. Available: https://doi.org/10.1115/1.4002481

[56] P. Dutta and R. Bhattacharya, "Nonlinear estimation of hypersonic state trajectories in bayesian framework with polynomial chaos," *Journal of Guidance, Control, and Dynamics*, vol. 33, no. 6, pp. 1765–1778, Nov. 2010. [Online]. Available: https://doi.org/10.2514/1.49743

[57] Y. Yang, H. Cai, B. Gong, and R. Norman, "Schmidt-kalman filter with polynomial chaos expansion for state estimation," in *2019 22th International Conference on Information Fusion (FUSION)*. IEEE, 2019, pp. 1–8.

[58] Y. Yang, H. Cai, and K. Zhang, "Schmidt-kalman filter with polynomial chaos expansion for orbit determination of space objects," in *Advanced Maui Optical and Space Surveillance Technologies Conference*, 2016.

[59] L. Sanchez, S. Infante, J. Marcano, and V. Griffin, "Polynomial chaos based on the parallelized ensemble kalman filter to estimate precipitation states," *Statistics, Optimization & Information Computing*, vol. 3, no. 1, Feb. 2015. [Online]. Available: https://doi.org/10.19139/soic.v3i1.113

[60] Z. Yu, P. Cui, and M. Ni, "A polynomial chaos based square-root kalman filter for mars entry navigation," *Aerospace Science and Technology*, vol. 51, pp. 192–202, Apr. 2016. [Online]. Available: https://doi.org/10.1016/j.ast.2016.02.009

[61] R. Bhusal and K. Subbarao, "Uncertainty quantification using generalized polynomial chaos expansion for nonlinear dynamical systems with mixed state and parameter uncertainties," *ASME Journal of Computational and Nonlinear Dynamics*, vol. 14, no. 2, Jan. 2019. [Online]. Available: https://doi.org/10.1115/1.4041473

[62] Y. Cao, W. Yu, W. Ren, and G. Chen, "An overview of recent progress in the study of distributed multi-agent coordination," *IEEE Transactions on Industrial Informatics*, vol. 9, no. 1, pp. 427–438, Feb. 2013. [Online]. Available: https://doi.org/10.1109/tii.2012.2219061

[63] R. Olfati-Saber, J. A. Fax, and R. M. Murray, "Consensus and cooperation in networked multi-agent systems," *Proceedings of the IEEE*, vol. 95, no. 1, pp. 215–233, Jan. 2007. [Online]. Available: https://doi.org/10.1109/jproc.2006.887293

[64] W. Ren, R. Beard, and E. Atkins, "A survey of consensus problems in multi-agent coordination," in *Proceedings of the 2005, American Control Conference, 2005.* IEEE. [Online]. Available: https://doi.org/10.1109/acc.2005.1470239

[65] K.-K. Oh, M.-C. Park, and H.-S. Ahn, "A survey of multi-agent formation control," *Automatica*, vol. 53, pp. 424–440, Mar. 2015. [Online]. Available: https://doi.org/10.1016/j.automatica.2014.10.022

[66] F. Xiao, L. Wang, J. Chen, and Y. Gao, "Finite-time formation control for multi-agent systems," *Automatica*, vol. 45, no. 11, pp. 2605–2611, Nov. 2009. [Online]. Available: https://doi.org/10.1016/j.automatica.2009.07.012

[67] W. Yu, G. Chen, and M. Cao, "Distributed leader–follower flocking control for multi-agent dynamical systems with time-varying velocities," *Systems & Control Letters*, vol. 59, no. 9, pp. 543–552, Sep. 2010. [Online]. Available: https://doi.org/10.1016/j.sysconle.2010.06.014

[68] D. Kingston, W. Ren, and R. Beard, "Consensus algorithms are input-to-state stable," in *Proceedings of the 2005, American Control Conference, 2005.* IEEE. [Online]. Available: https://doi.org/10.1109/acc.2005.1470210

[69] H. Du and S. Li, "Attitude synchronization control for a group of flexible spacecraft," *Automatica*, vol. 50, no. 2, pp. 646–651, Feb. 2014. [Online]. Available: https://doi.org/10.1016/j.automatica.2013.11.022

[70] M. Huang and J. H. Manton, "Coordination and consensus of networked agents with noisy measurements: Stochastic algorithms and asymptotic behavior," *SIAM Journal on Control and Optimization*, vol. 48, no. 1, pp. 134–161, Jan. 2009. [Online]. Available: https://doi.org/10.1137/06067359x

[71] D. Bhattacharjee and K. Subbarao, "Set-membership filtering-based leader–follower synchronization of discrete-time linear multi-agent sys-

tems," *Journal of Dynamic Systems, Measurement, and Control*, vol. 143, no. 6, Feb. 2021. [Online]. Available: https://doi.org/10.1115/1.4049553

[72] J. Mei, W. Ren, and G. Ma, "Distributed containment control for lagrangian networks with parametric uncertainties under a directed graph," *Automatica*, vol. 48, no. 4, pp. 653–659, Apr. 2012. [Online]. Available: https://doi.org/10.1016/j.automatica.2012.01.020

[73] Y. Hatano and M. Mesbahi, "Agreement over random networks," *IEEE Transactions on Automatic Control*, vol. 50, no. 11, pp. 1867–1872, Nov. 2005. [Online]. Available: https://doi.org/10.1109/tac.2005.858670

[74] Z. Kan, J. M. Shea, and W. E. Dixon, "Leader–follower containment control over directed random graphs," *Automatica*, vol. 66, pp. 56–62, Apr. 2016. [Online]. Available: https://doi.org/10.1016/j.automatica.2015.12.016

[75] I. Matei, J. S. Baras, and C. Somarakis, "Convergence results for the linear consensus problem under markovian random graphs," *SIAM Journal on Control and Optimization*, vol. 51, no. 2, pp. 1574–1591, Jan. 2013. [Online]. Available: https://doi.org/10.1137/100816870

[76] K. You, Z. Li, and L. Xie, "Consensus condition for linear multi-agent systems over randomly switching topologies," *Automatica*, vol. 49, no. 10, pp. 3125–3132, Oct. 2013. [Online]. Available: https://doi.org/10.1016/j.automatica.2013.07.024

[77] A. Teixeira, H. Sandberg, and K. H. Johansson, "Networked control systems under cyber attacks with applications to power networks," in *Proceedings of the 2010 American Control Conference*. IEEE, Jun. 2010. [Online]. Available: https://doi.org/10.1109/acc.2010.5530638

[78] Z. Feng and G. Hu, "Distributed tracking control for multi-agent systems under two types of attacks," *IFAC Proceedings Volumes*, vol. 47, no. 3, pp. 5790–5795, 2014. [Online]. Available: https://doi.org/10.3182/20140824-6-za-1003.01511

[79] W. Haddad, E. Collins, and D. Bernstein, "Robust stability analysis using the small gain, circle, positivity, and popov theorems: a comparative study," *IEEE Transactions on Control Systems Technology*, vol. 1, no. 4, pp. 290–293, 1993. [Online]. Available: https://doi.org/10.1109/87.260275

[80] M. Safonov and M. Athans, "A multiloop generalization of the circle criterion for stability margin analysis," *IEEE Transactions on Automatic Control*, vol. 26, no. 2, pp. 415–422, Apr. 1981. [Online]. Available: https://doi.org/10.1109/tac.1981.1102595

[81] N. Lehtomaki, N. Sandell, and M. Athans, "Robustness results in linear-quadratic gaussian based multivariable control designs," *IEEE Transactions on Automatic Control*, vol. 26, no. 1, pp. 75–93, Feb. 1981. [Online]. Available: https://doi.org/10.1109/tac.1981.1102565

[82] Z.-Y. Nie, Q.-G. Wang, M. Wu, and Y. He, "Exact computation of loop gain margins of multivariable feedback systems," *Journal of Process Control*, vol. 20, no. 6, pp. 762–768, Jul. 2010. [Online]. Available: https://doi.org/10.1016/j.jprocont.2010.04.006

[83] Q.-G. Wang, Y. He, Z. Ye, C. Lin, and C. C. Hang, "On loop phase margins of multivariable control systems," *Journal of Process Control*, vol. 18, no. 2, pp. 202–211, Feb. 2008. [Online]. Available: https://doi.org/10.1016/j.jprocont.2007.06.004

[84] Y. Kim, "On the stability margin of networked dynamical systems," *IEEE Transactions on Automatic Control*, vol. 62, no. 10, pp. 5451–5456, Oct. 2017. [Online]. Available: https://doi.org/10.1109/tac.2017.2697312

[85] A. Raza, M. Iqbal, and J. Moon, "Robustness of hierarchical schemes for multi-agent systems," in *2019 12th Asian Control Conference (ASCC)*. IEEE, 2019, pp. 1167–1172.

[86] Z. P. Jiang, A. R. Teel, and L. Praly, "Small-gain theorem for ISS systems and applications," *Mathematics of Control, Signals, and Systems*, vol. 7, no. 2, pp. 95–120, Jun. 1994. [Online]. Available: https://doi.org/10.1007/bf01211469

[87] S. Tonetti and R. M. Murray, "Limits on the network sensitivity function for homogeneous multi-agent systems on a graph," in *Proceedings of the 2010 American Control Conference*. IEEE, Jun. 2010. [Online]. Available: https://doi.org/10.1109/acc.2010.5530753

[88] V. Hamdipoor and Y. Kim, "Partitioning of relative sensing networks: A stability margin perspective," *Automatica*, vol. 106, pp. 294–300, Aug. 2019. [Online]. Available: https://doi.org/10.1016/j.automatica.2019.04.042

[89] T. Qi, L. Qiu, and J. Chen, "Consensus over directed graph: Output feedback and topological constraints," in *2013 9th Asian Control Conference (ASCC)*. IEEE, Jun. 2013. [Online]. Available: https://doi.org/10.1109/ascc.2013.6606016

[90] Y. Chen and Y. Shi, "Distributed consensus of linear multiagent systems: Laplacian spectra-based method," *IEEE Transactions on Systems, Man, and Cybernetics: Systems*, vol. 50, no. 2, pp. 700–706, Feb. 2020. [Online]. Available: https://doi.org/10.1109/tsmc.2017.2774841

[91] J. Cockburn, Y. Sidar, and A. Tannenbaum, "Stability margin optimization via interpolation and conformal mappings," *IEEE Transactions on Automatic Control*, vol. 40, no. 6, pp. 1066–1070, Jun. 1995. [Online]. Available: https://doi.org/10.1109/9.388685

[92] J. Lee, J.-S. Kim, and H. Shim, "Disc margins of the discrete-time LQR and its application to consensus problem," *International Journal of Systems Science*, vol. 43, no. 10, pp. 1891–1900, Oct. 2012. [Online]. Available: https://doi.org/10.1080/00207721.2011.555012

[93] H. Zhang, T. Feng, H. Liang, and Y. Luo, "LQR-based optimal distributed cooperative design for linear discrete-time multiagent systems," *IEEE Transactions on Neural Networks and Learning Systems*, vol. 28, no. 3, pp. 599–611, Mar. 2017. [Online]. Available: https://doi.org/10.1109/tnnls.2015.2490072

[94] Y.-P. Tian and C.-L. Liu, "Consensus of multi-agent systems with diverse input and communication delays," *IEEE Transactions on Automatic Control*, vol. 53, no. 9, pp. 2122–2128, Oct. 2008. [Online]. Available: https://doi.org/10.1109/tac.2008.930184

[95] J. Xu, H. Zhang, and L. Xie, "Input delay margin for consensusability of multi-agent systems," *Automatica*, vol. 49, no. 6, pp. 1816–1820, Jun. 2013. [Online]. Available: https://doi.org/10.1016/j.automatica.2013.02.044

[96] M. Zhang, A. Saberi, and A. A. Stoorvogel, "Synchronization in a network of identical continuous- or discrete-time agents with unknown nonuniform constant input delay," *International Journal of Robust and Nonlinear Control*, vol. 28, no. 13, pp. 3959–3973, May 2018. [Online]. Available: https://doi.org/10.1002/rnc.4115

[97] R. Olfati-Saber and R. Murray, "Consensus problems in networks of agents with switching topology and time-delays," *IEEE Transactions on Automatic Control*, vol. 49, no. 9, pp. 1520–1533, Sep. 2004. [Online]. Available: https://doi.org/10.1109/tac.2004.834113

[98] P. Lin and Y. Jia, "Average consensus in networks of multi-agents with both switching topology and coupling time-delay," *Physica A: Statistical Mechanics and its Applications*, vol. 387, no. 1, pp. 303–313, Jan. 2008. [Online]. Available: https://doi.org/10.1016/j.physa.2007.08.040

[99] D. Ma, J. Chen, R. Lu, J. Chen, and T. Chai, "Delay consensus margin of first-order multi-agent systems with undirected graphs and PD protocols," *IEEE Transactions on Automatic Control*, pp. 1–1, 2020. [Online]. Available: https://doi.org/10.1109/tac.2020.3035556

[100] U. Münz, A. Papachristodoulou, and F. Allgöwer, "Delay robustness in consensus problems," *Automatica*, vol. 46, no. 8, pp. 1252–1265, Aug. 2010. [Online]. Available: https://doi.org/10.1016/j.automatica.2010.04.008

[101] M. Zhang, A. Saberi, A. A. Stoorvogel, and Z. Liu, "State synchronization of a class of homogeneous linear multi-agent systems in the presence of unknown input delays via static protocols," *European Journal of Control*, vol. 47, pp. 20–29, May 2019. [Online]. Available: https://doi.org/10.1016/j.ejcon.2018.08.002

[102] H. Zhang, D. Yue, W. Zhao, S. Hu, and C. Dou, "Distributed optimal consensus control for multiagent systems with input delay," *IEEE Transactions on Cybernetics*, vol. 48, no. 6, pp. 1747–1759, Jun. 2018. [Online]. Available: https://doi.org/10.1109/tcyb.2017.2714173

[103] Y. Zhao and W. Zhang, "Guaranteed cost consensus protocol design for linear multi-agent systems with sampled-data information: An input delay approach," *ISA Transactions*, vol. 67, pp. 87–97, Mar. 2017. [Online]. Available: https://doi.org/10.1016/j.isatra.2016.12.003

[104] D. Ma, J. Chen, and T. Chai, "Exact computation of maximal allowable delay for general second-order multi-agents consensus," *International*

Journal of Robust and Nonlinear Control, Mar. 2021. [Online]. Available: https://doi.org/10.1002/rnc.5488

[105] W. Hou, M. Fu, H. Zhang, and Z. Wu, "Consensus conditions for general second-order multi-agent systems with communication delay," *Automatica*, vol. 75, pp. 293–298, Jan. 2017. [Online]. Available: https://doi.org/10.1016/j.automatica.2016.09.042

[106] R. Cepeda-Gomez, "Finding the exact delay bound for consensus of linear multi-agent systems," *International Journal of Systems Science*, vol. 47, no. 11, pp. 2598–2606, 2016. [Online]. Available: https://doi.org/10.1080/00207721.2015.1005194

[107] L. Li, M. Fu, H. Zhang, and R. Lu, "Consensus control for a network of high order continuous-time agents with communication delays," *Automatica*, vol. 89, pp. 144–150, Mar. 2018. [Online]. Available: https://doi.org/10.1016/j.automatica.2017.12.006

[108] M. Zhang, A. Saberi, and A. A. Stoorvogel, "Synchronization for a network of identical discrete-time agents with unknown, nonuniform constant input delay," in *2015 54th IEEE Conference on Decision and Control (CDC)*. IEEE, Dec. 2015. [Online]. Available: https://doi.org/10.1109/cdc.2015.7403331

[109] Z. Wang, "Consensus analysis for high-order discrete-time agents with time-varying delay," *International Journal of Systems Science*, vol. 52, no. 5, pp. 1003–1013, 2021. [Online]. Available: https://doi.org/10.1080/00207721.2020.1852626

[110] Z.-J. Tang, T.-Z. Huang, J.-L. Shao, and J.-P. Hu, "Consensus of second-order multi-agent systems with nonuniform time-varying delays," *Neurocomputing*, vol. 97, pp. 410–414, Nov. 2012. [Online]. Available: https://doi.org/10.1016/j.neucom.2012.05.025

[111] A. Petrillo, A. Salvi, S. Santini, and A. S. Valente, "Adaptive synchronization of linear multi-agent systems with time-varying multiple delays," *Journal of the Franklin Institute*, vol. 354, no. 18, pp. 8586–8605, Dec. 2017. [Online]. Available: https://doi.org/10.1016/j.jfranklin.2017.10.015

[112] A. Desai, J. A. S. Witteveen, and S. Sarkar, "Uncertainty quantification of a nonlinear aeroelastic system using polynomial chaos expansion with constant phase interpolation," *Journal of Vibration and Acoustics*, vol. 135, no. 5, Jul. 2013. [Online]. Available: https://doi.org/10.1115/1.4024794

[113] J. D. Blight, R. L. Dailey, and D. Gangsaas, "Practical control law design for aircraft using multivariable techniques," *International Journal of Control*, vol. 59, no. 1, pp. 93–137, Jan. 1994. [Online]. Available: https://doi.org/10.1080/00207179408923071

[114] A.-K. Schug, P. Seiler, and H. Pfifer, "Robustness margins for linear parameter varying systems," *AerospaceLab Journal*, vol. Issue 13, pp. December 2017; ISSN: 2107–6596, 2017. [Online]. Available: https://aerospacelab.onera.fr/sites/www.aerospacelab-journal.org/files/AL13-06_0.pdf

[115] Y. Zhang and Y.-P. Tian, "Allowable delay bound for consensus of linear multi-agent systems with communication delay," *International Journal of Systems Science*, vol. 45, no. 10, pp. 2172–2181, 2014. [Online]. Available: https://doi.org/10.1080/00207721.2013.763303

[116] X.-L. Zhu and G.-H. Yang, "Jensen integral inequality approach to stability analysis of continuous-time systems with time-varying delay," *IET Control Theory & Applications*, vol. 2, no. 6, pp. 524–534, Jun. 2008. [Online]. Available: https://doi.org/10.1049/iet-cta:20070298

[117] R. Bhusal and K. Subbarao, "Generalized polynomial chaos expansion approach for uncertainty quantification in small satellite orbital debris problems," *The*

Journal of the Astronautical Sciences, vol. 67, no. 1, pp. 225–253, May 2019. [Online]. Available: https://doi.org/10.1007/s40295-019-00176-1

[118] B. Taner, R. Bhusal, and K. Subbarao, "Nested robust controller design for interconnected linear parameter varying aerial vehicles," *AIAA Journal of Guidance, Control, and Dynamics*, vol. 44, no. 8, pp. 1454–1468, Aug. 2021. [Online]. Available: https://doi.org/10.2514/1.g005323

[119] R. Bhusal and K. Subbarao, "Sensitivity analysis of cooperating multi-agent systems with uncertain connection weights," in *2019 American Control Conference (ACC)*. IEEE, Jul. 2019. [Online]. Available: https://doi.org/10.23919/acc.2019.8815336

[120] R. Bhusal, B. Taner, and K. Subbarao, "Performance analysis of a team of highly capable individual unmanned aerial systems," in *AIAA Scitech 2020 Forum*. American Institute of Aeronautics and Astronautics, Jan. 2020. [Online]. Available: https://doi.org/10.2514/6.2020-2070

[121] B. Taner, R. Bhusal, and K. Subbarao, "A nested robust controller design for interconnected vehicles," in *AIAA Scitech 2020 Forum*. American Institute of Aeronautics and Astronautics, Jan. 2020. [Online]. Available: https://doi.org/10.2514/6.2020-0602

[122] R. Bhusal, B. Taner, and K. Subbarao, "On the phase margin of networked dynamical systems and fabricated attacks of an intruder," in *2020 American Control Conference (ACC)*. IEEE, Jul. 2020. [Online]. Available: https://doi.org/10.23919/acc45564.2020.9147500

[123] R. Bhusal and K. Subbarao, "Generalized polynomial chaos expansion-based stochastic linear quadratic regulator for multi-agent systems," in *AIAA Scitech 2021 Forum*. American Institute of Aeronautics and Astronautics, Jan. 2021. [Online]. Available: https://doi.org/10.2514/6.2021-0979

[124] ——, "Generalized polynomial chaos-based ensemble kalman filtering for orbit estimation," in *2021 American Control Conference (ACC)*. IEEE, May 2021. [Online]. Available: https://doi.org/10.23919/acc50511.2021.9482961

[125] F. C. Klebaner, *Introduction to Stochastic Calculus with Applications*. IMPERIAL COLLEGE PRESS, Mar. 2012. [Online]. Available: https://doi.org/10.1142/p821

[126] J. A. Gubner, *Probability and Random Processes for Electrical and Computer Engineers*. Cambridge University Press, 2006. [Online]. Available: https://doi.org/10.1017/cbo9780511813610

[127] T. S. Chihara, "The three term recurrence relation and spectral properties of orthogonal polynomials," in *Orthogonal Polynomials*. Springer Netherlands, 1990, pp. 99–114. [Online]. Available: https://doi.org/10.1007/978-94-009-0501-6_4

[128] D. Xiu, *Numerical methods for stochastic computations: a spectral method approach*. Princeton University Press, 2010, ISBN: 978-0-691-14212-8.

[129] R. Askey and J. Wilson, "Some basic hypergeometric orthogonal polynomials that generalize jacobi polynomials," *Memoirs of the American Mathematical Society*, vol. 54, no. 319, pp. 0–0, 1985. [Online]. Available: https://doi.org/10.1090/memo/0319

[130] A. Desai and S. Sarkar, "Analysis of a nonlinear aeroelastic system with parametric uncertainties using polynomial chaos expansion," *Mathematical Problems in Engineering*, vol. 2010, pp. 1–21, 2010. [Online]. Available: https://doi.org/10.1155/2010/379472

[131] F. Heiss and V. Winschel, "Likelihood approximation by numerical integration on sparse grids," *Journal of Econometrics*, vol. 144, no. 1, pp. 62–80, May 2008. [Online]. Available: https://doi.org/10.1016/j.jeconom.2007.12.004

[132] G. Wasilkowski and H. Wozniakowski, "Explicit cost bounds of algorithms for multivariate tensor product problems," *Journal of Complexity*, vol. 11, no. 1, pp. 1–56, Mar. 1995. [Online]. Available: https://doi.org/10.1006/jcom.1995.1001

[133] B. Jia, M. Xin, and Y. Cheng, "Sparse gauss-hermite quadrature filter with application to spacecraft attitude estimation," *Journal of Guidance, Control, and Dynamics*, vol. 34, no. 2, pp. 367–379, Mar. 2011. [Online]. Available: https://doi.org/10.2514/1.52016

[134] S. J. Julier and J. K. Uhlmann, "New extension of the kalman filter to nonlinear systems," in *Signal Processing, Sensor Fusion, and Target Recognition VI*, I. Kadar, Ed. SPIE, Jul. 1997. [Online]. Available: https://doi.org/10.1117/12.280797

[135] A. H. Stroud, "Some fifth degree integration formulas for symmetric regions," *Mathematics of Computation*, vol. 20, no. 93, pp. 90–90, Jan. 1966. [Online]. Available: https://doi.org/10.1090/s0025-5718-1966-0191094-8

[136] ——, "Some seventh degree integration formulas for symmetric regions," *SIAM Journal on Numerical Analysis*, vol. 4, no. 1, pp. 37–44, 1967. [Online]. Available: https://www.jstor.org/stable/2949733

[137] B. Jia, M. Xin, and Y. Cheng, "High-degree cubature kalman filter," *Automatica*, vol. 49, no. 2, pp. 510–518, Feb. 2013. [Online]. Available: https://doi.org/10.1016/j.automatica.2012.11.014

[138] H. H. Rosenbrock, "An automatic method for finding the greatest or least value of a function," *The Computer Journal*, vol. 3, no. 3, pp. 175–184, Mar. 1960. [Online]. Available: https://doi.org/10.1093/comjnl/3.3.175

[139] M. Eldred, C. Webster, and P. Constantine, "Evaluation of non-intrusive approaches for wiener-askey generalized polynomial chaos," in *49th AIAA/ASME/ASCE/AHS/ASC Structures, Structural Dynamics, and*

Materials Conference, 16th AIAA/ASME/AHS Adaptive Structures Conference,10th AIAA Non-Deterministic Approaches Conference, 9th AIAA Gossamer Spacecraft Forum, 4th AIAA Multidisciplinary Design Optimization Specialists Conference. American Institute of Aeronautics and Astronautics, Apr. 2008. [Online]. Available: https://doi.org/10.2514/6.2008-1892

[140] H. Peter D, "Kernel estimation of a distribution function," *Communications in Statistics - Theory and Methods*, vol. 14, no. 3, pp. 605–620, Jan. 1985. [Online]. Available: https://doi.org/10.1080/03610928508828937

[141] B. A. Jones, D. S. Bryant, B.-T. Vo, and B.-N. Vo, "Challenges of multi-target tracking for space situational awareness," in *18th International Conference on Information Fusion (FUSION)*. IEEE, 2015, pp. 1278–1285.

[142] R. G. Gottlieb, "Fast gravity, gravity partials, normalized gravity, gravity gradient torque and magnetic field: derivation, code and data," *NASA Contractor Report 188243*, 1993.

[143] B. Tapley, J. Ries, S. Bettadpur, D. Chambers, M. Cheng, F. Condi, B. Gunter, Z. Kang, P. Nagel, R. Pastor, T. Pekker, S. Poole, and F. Wang, "GGM02 – an improved earth gravity field model from GRACE," *Journal of Geodesy*, vol. 79, no. 8, pp. 467–478, Sep. 2005. [Online]. Available: https://doi.org/10.1007/s00190-005-0480-z

[144] H. D. Curtis, "Orbital mechanics for engineering students." Elsevier, 2014. [Online]. Available: https://doi.org/10.1016/c2011-0-69685-1

[145] D. J. Scheeres, F.-Y. Hsiao, R. S. Park, B. F. Villac, and J. M. Maruskin, "Fundamental limits on spacecraft orbit uncertainty and distribution propagation," *The Journal of the Astronautical Sciences*, vol. 54, no. 3-4, pp. 505–523, Dec. 2006. [Online]. Available: https://doi.org/10.1007/bf03256503

[146] S. Kullback and R. A. Leibler, "On information and sufficiency," *The Annals of Mathematical Statistics*, vol. 22, no. 1, pp. 79–86, Mar. 1951. [Online]. Available: https://doi.org/10.1214/aoms/1177729694

[147] K. Petras, *Advances in Computational Mathematics*, vol. 12, no. 1, pp. 71–93, 2000. [Online]. Available: https://doi.org/10.1023/a:1018904816230

[148] E. Doornbos, *Thermospheric density and wind determination from satellite dynamics*. Springer Science & Business Media, 2012.

[149] K. Moe, M. M. Moe, and E. Doornbos, "Outstanding issues related to thermospheric measurements and modelling," in *38th COSPAR Scientific Assembly*, vol. 38, 2010, p. 4.

[150] Y. C. Fung, *An introduction to the theory of aeroelasticity*. Courier Dover Publications, 2008.

[151] B. Lee, L. Gong, and Y. Wong, "Analysis and computation of nonlinear dynamic response of a two-degree-of-freedom system and its application in aeroelasticity," *Journal of Fluids and Structures*, vol. 11, no. 3, pp. 225–246, Apr. 1997. [Online]. Available: https://doi.org/10.1006/jfls.1996.0075

[152] R. T. Jones, "The unsteady lift of a wing of finite aspect ratio," *NACA*, vol. TR-681, 1940.

[153] D. Millman, P. King, R. Maple, and P. Beran, "Predicting uncertainty propagation in a highly nonlinear system with a stochastic projection method," in *45th AIAA/ASME/ASCE/AHS/ASC Structures, Structural Dynamics & Materials Conference*. American Institute of Aeronautics and Astronautics, Apr. 2004. [Online]. Available: https://doi.org/10.2514/6.2004-1613

[154] B. Lee, L. Jiang, and Y. Wong, "Flutter of an airfoil with a cubic restoring force," *Journal of Fluids and Structures*, vol. 13, no. 1, pp. 75–101, Jan. 1999. [Online]. Available: https://doi.org/10.1006/jfls.1998.0190

[155] M. Thanusha and S. Sarkar, "Uncertainty quantification of subcritical nonlinear aeroelastic system using integrated interpolation method and polynomial chaos expansion," *Procedia Engineering*, vol. 144, pp. 982–989, 2016. [Online]. Available: https://doi.org/10.1016/j.proeng.2016.05.128

[156] G. A. F. Seber and A. J. Lee, *Linear Regression Analysis*. Wiley, Jan. 2003. [Online]. Available: https://doi.org/10.1002/9780471722199

[157] J. L. Crassidis and J. L. Junkins, *Optimal Estimation of Dynamic Systems*. Chapman and Hall/CRC, 2011.

[158] J.-S. Chern and N. X. Vinh, "Optimum reentry trajectories of a lifting vehicle," *NASA-CR-3236*, 1980.

[159] F. Kozin, "On almost sure stability of linear systems with random coefficients," *Journal of Mathematics and Physics*, vol. 42, no. 1-4, pp. 59–67, 1963.

[160] W. Ren and R. W. Beard, *Distributed consensus in multi-vehicle cooperative control*. Springer, 2008.

[161] J. Levin and N. Levinson, "Singular perturbations of non-linear systems of differential equations and an associated boundary layer equation," *Journal of rational mechanics and analysis*, vol. 3, pp. 247–270, 1954. [Online]. Available: https://www.jstor.org/stable/24900288

[162] Z. Li and Z. Duan, "Distributed consensus protocol design for general linear multi-agent systems: a consensus region approach," *IET Control Theory & Applications*, vol. 8, no. 18, pp. 2145–2161, Dec. 2014. [Online]. Available: https://doi.org/10.1049/iet-cta.2014.0012

[163] H. Zhang, F. L. Lewis, and A. Das, "Optimal design for synchronization of cooperative systems: State feedback, observer and output feedback," *IEEE Transactions on Automatic Control*, vol. 56, no. 8, pp. 1948–1952, Aug. 2011. [Online]. Available: https://doi.org/10.1109/tac.2011.2139510

[164] F. R. Gantmakher, *The theory of matrices*. AMS Chelsea Publishing, 1959, vol. 1.

[165] P. Zielinski and K. Zietak, "The polar decomposition— properties, applications and algorithms," *Mathematica Applicanda*, vol. 24, no. 38, Jul. 1995. [Online]. Available: https://doi.org/10.14708/ma.v24i38.1833

[166] W. Chen, D. Wang, S. Z. Khong, and L. Qiu, "Phase analysis of MIMO LTI systems," in *2019 IEEE 58th Conference on Decision and Control (CDC)*. IEEE, 2019, pp. 6062–6067.

[167] A. Galántai and C. J. Hegedűs, "Jordan's principal angles in complex vector spaces," *Numerical Linear Algebra with Applications*, vol. 13, no. 7, pp. 589–598, 2006. [Online]. Available: https://doi.org/10.1002/nla.491

[168] K. Gu, J. Chen, and V. L. Kharitonov, *Stability of time-delay systems*. Springer Science & Business Media, 2003.

[169] J. Chen and H. Latchman, "Frequency sweeping tests for stability independent of delay," *IEEE Transactions on Automatic Control*, vol. 40, no. 9, pp. 1640–1645, 1995. [Online]. Available: https://doi.org/10.1109/9.412637

[170] R. H. Middleton and D. E. Miller, "On the achievable delay margin using LTI control for unstable plants," *IEEE Transactions on Automatic Control*, vol. 52, no. 7, pp. 1194–1207, Jul. 2007. [Online]. Available: https://doi.org/10.1109/tac.2007.900824

[171] A. M.-C. So, J. Zhang, and Y. Ye, "On approximating complex quadratic optimization problems via semidefinite programming relaxations,"

Mathematical Programming, vol. 110, no. 1, pp. 93–110, Dec. 2006. [Online]. Available: https://doi.org/10.1007/s10107-006-0064-6

[172] H. W. Kuhn and A. W. Tucker, "Nonlinear programming," in *Traces and emergence of nonlinear programming*. Springer, 2014, pp. 247–258.

[173] S. Boyd and L. Vandenberghe, *Convex optimization*. Cambridge university press, 2004.

[174] S. M. Guu and Y. C. Liou, "On a quadratic optimization problem with equality constraints," *Journal of Optimization Theory and Applications*, vol. 98, no. 3, pp. 733–741, Sep. 1998. [Online]. Available: https://doi.org/10.1023/a:1022688416335

[175] J. R. Bar-On and K. A. Grasse, "Global optimization of a quadratic functional with quadratic equality constraints, part 2," *Journal of Optimization Theory and Applications*, vol. 93, no. 3, pp. 547–556, Jun. 1997. [Online]. Available: https://doi.org/10.1023/a:1022691012894

[176] J. R. Bar-On and E. A. Jonckheere, "Multivariable gain margin," *International Journal of Control*, vol. 54, no. 2, pp. 337–365, Aug. 1991. [Online]. Available: https://doi.org/10.1080/00207179108934164

[177] Z. Li, Z. Duan, G. Chen, and L. Huang, "Consensus of multiagent systems and synchronization of complex networks: A unified viewpoint," *IEEE Transactions on Circuits and Systems I: Regular Papers*, vol. 57, no. 1, pp. 213–224, Jan. 2010. [Online]. Available: https://doi.org/10.1109/tcsi.2009.2023937

[178] K. Furuta and S. Kim, "Pole assignment in a specified disk," *IEEE Transactions on Automatic Control*, vol. 32, no. 5, pp. 423–427, May 1987. [Online]. Available: https://doi.org/10.1109/tac.1987.1104624

[179] Q.-L. Han, "Absolute stability of time-delay systems with sector-bounded nonlinearity," *Automatica*, vol. 41, no. 12, pp. 2171–2176, Dec. 2005. [Online]. Available: https://doi.org/10.1016/j.automatica.2005.08.005

[180] C. Peng and Y.-C. Tian, "Improved delay-dependent robust stability criteria for uncertain systems with interval time-varying delay," *IET Control Theory & Applications*, vol. 2, no. 9, pp. 752–761, Sep. 2008. [Online]. Available: https://doi.org/10.1049/iet-cta:20070362

[181] M. Kocvara, M. Stingl, and P. GbR, "Penbmi user's guide (version 2.0)," *Software Manual, PENOPT GbR*, 2005. [Online]. Available: http://penopt.com

[182] J. Ackermann, *Robust Control: The Parameter Space Approach*, ser. Communications and Control Engineering. Springer-Verlag London, 2002. [Online]. Available: https://doi.org/10.1007/978-1-4471-0207-6

Biographical Statement

Rajnish Bhusal was born in Chitwan, Nepal, in 1992. He received his Bachelor of Engineering in mechanical engineering from Visvesvaraya Technological University, India, in 2015. After graduation, he worked as a mechanical engineer for Bata India Ltd. until April 2016. He then came to the United States in Fall 2016 to pursue Ph.D. in Aerospace Engineering at the University of Texas at Arlington (UTA). During his graduate studies, Rajnish worked as a graduate research assistant at the Aerospace Systems Laboratory in UTA. He also worked as a graduate teaching assistant for multiple courses at the mechanical and aerospace engineering department in UTA. Rajnish was awarded the summer 2021 Dissertation Fellowship from the University of Texas at Arlington. He mainly works in the areas of dynamical systems, control theory, uncertainty quantification, and estimation theory as applied to unmanned systems.

Upon completion of his Ph.D., Rajnish will be joining the Department of Mechanical and Aerospace Engineering at the University of Texas at Arlington as a Postdoctoral Researcher.